CONTROLLING MOLECULAR INTERACTIONS TO DEFINE INTERFACIAL PHENOMENA AND STRUCTURE

OMAR TAREK MANSOUR

A thesis submitted in partial fulfilment of the requirements of the University of Greenwich for the Degree of Doctor of Philosophy

July 2016

DECLARATION

I certify that this work has not been accepted in any substance for any degree, and is not concurrently being submitted for any degree other than that of Doctor of Philosophy being studied at the University of Greenwich. I also declare that this work is the result of my own investigations except where otherwise identified by references and that I have not plagiarised the work of the others.

…………………………………………….. Omar T. Mansour (Candidate)

…………………………………………….. Date

…………………………………………….. Professor P.C.Griffiths (Supervisor)

…………………………………………….. Date

…………………………………………….. Dr B.D.Alexander (Supervisor)

…………………………………………….. Date

ACKNOWLEDGEMENTS

ABSTRACT

Polymers and surfactants are often employed together in a wide range of formulations, such as paints, foodstuffs, pharmaceuticals and in detergency. Using the polymers and the surfactants together in a formulation provides additional or modulated physicochemical properties required for certain applications. Therefore, a good knowledge of the properties of these components and the interactions between each in mixtures ensures that formulation is more of an engineered approach than a "black" art.

In this thesis, the interactions between polymers and small molecules were probed in various states: solution, gel and foam. The main techniques used were tensiometry, diffusion NMR and small-angle neutron scattering (SANS).

The experiments involved investigating the competitive interactions between Pluronic P123 and small molecule surfactants, SMS, (sodium dodecylsulfate, SDS or $C_{12}SO_4Na$, dodecyltrimethylammonium bromide, $C_{12}TAB$ and polyoxyethylene (23) lauryl ether, Brij 35) in the presence of alcohols (ethanol, hexanol and decanol). The composition of the mixed micelles formed was found to be sensitive to the nature of the alcohol present in the system.

Gelation from Pluronic P123, F108 and their mixtures was also investigated. P123 showed very interesting changes in its phase behaviour as both temperature and polymer concentration were varied. Whilst for F108, the phase behaviour remained largely unchanged, insensitive to any variation in concentration and temperature. The phase behaviour of gels from mixtures of both Pluronics showed dependence on the Pluronic ratio in the mixture and the temperature.

Finally, in-situ investigations of wet and dry foams stabilised by SMS (alkyl sulfates and alkyl bromides) and mixtures of polymers (P123, poly(vinylpyrrolidone), PVP) with the SMS were performed using SANS. SANS was deployed to probe the structure of the surfactant and/or polymer at the foam air/water interface. Data analysis and modelling suggested the presence of an interfacial structure comprising paracrystalline stacks (around five layers) of adsorbed surfactant and/or polymer layers interspersed with water layers. The thickness of these layers was found to be sensitive to the SMS architecture (hydrocarbon chain length) and to the strength of the interactions between the polymers and the SMS in the mixtures case.

CONTENTS

List of Figures

List of Tables

List of Abbreviations and Symbols

This a comprehensive list of the most commonly used abbreviations in this thesis, followed by a list of the symbols used (with Greek letters at the end).

AOT	aerosol OT
bcc	body-centred cubic
C_8SO_4	sodium octylsulfate
C_8TAB	trimethyloctylammonium bromide
$C_{10}SO_4$	sodium decylsulfate
$C_{10}TAB$	decyltrimethylammonium bromide
$C_{12}SO_4$	sodium dodecylsulfate
$C_{12}TAB$	dodecyltrimethylammonium bromide
$C_{14}SO_4$	sodium tetradecylsulfate
$C_{14}TAB$	tetradecyltrimethylammonium bromide
$C_{16}SO_4$	sodium hexadecylsulfate
$C_{16}TAB$	hexadecyltrimethylammoium bromide
CAC	critical aggregation concentration
CGC	critical gelation concentration
CGT	critical gelation temperature
CMC	critical micelle concentration
CMT	critical micelle temperature
CORE	component resolved
DLS	dynamic light scattering
DSC	differential scanning calorimetry
fcc	face-centred cubic
FT	Fourier transform
hcp	hexagonally close packed
HLB	hydrophilic-lipophilic balance
ITC	isothermal calorimetry
N_{agg}	aggregation number
NMR	nuclear magnetic resonance
NR	neutron reflectivity

PEO	poly(ethylene oxide)
PGSE	pulsed gradient spin echo
PPO	poly(propylene oxide)
PS-PI	polystyrene-polyisoprene
PVA	poly(vinyl amine)
PVFA	poly-*N*-vinyl formamide
PVP	poly(vinyl pyrrolidone)
RF	radio frequency
RMSA	rescaled mean spherical approximation
SANS	small-angle neutron scattering
SAS	small angle scattering
SAXS	small-angle X-ray scattering
SDS	sodium dodecylsulfate
SLD	scattering length density
SMS	small molecule surfactant
UV	ultra-violet

a	crystal lattice parameter
B_{inc}	incoherent background scattering
D	separation between layers
D_{HS}	spacing between adjacent micelles
G	gradient
$I(Q)$	scattering intensity
L	thickness of layer
M	number of layers
N	number of particles per unit volume
N_m	number of micelles per unit volume
$P(Q)$	form factor
Q	SANS scattering vector
R_A	radius of the core
R_B	radius of the shell
$S(Q)$	structure factor

T	interface diffuseness
α	SMS fraction in the mixed micelle
δ	gradient pulse duration
Δ	diffusion time
$\Delta\rho$	difference in SLD of the micelle and the solvent
θ	scattering angle
λ	wavelength

Chapter 1

1. Introduction

1.1 Polymer and surfactants in formulation

Formulation is an important aspect of many industrial and technological products, and the driver of the "nanotechnology revolution". There is an ever-increasing need for tailored formulations and products with special properties for controlled release and delivery. In formulation science, surfactants are often employed for emulsion stabilisation, detergency, solubilisation, thickening and emolliency, while polymers are used for better control over the system viscosity and consistency. In many cases, mixed polymer and surfactant systems perform much better than single surfactants or polymers due to the interactions between the components.

One main class of studies has been to focus on understanding the interactions between polymers and surfactants in solution. Techniques like surface tension,[1–3] viscosity[4–6] and conductivity[7,8] have been used to quantify the amounts of surfactant associating or interacting with the polymer. A more detailed understanding of the structure and the morphology of the mixed systems in solution was obtained by neutron scattering,[9–12] nuclear magnetic resonance[13–15] and fluorescence spectroscopy.[16–18] Most of these studies have concluded that some surfactants do not interact at all with the polymers while others interact significantly.

To illustrate the complexity of these systems, Barbosa *et al.*[19] studied the interactions between polyethylene oxide (PEO) and $C_{12}SO_4Na$ in bulk as a function of different simple ionic cosolutes, such as, NaCl, Na_2SO_4 and Li_2SO_4 and more complex ones as $Na_2[Fe(CN_3)NO]$ and $Na_3[Co(NO)_6]$ using isothermal titration calorimetry (ITC) and small-angle X-ray scattering (SAXS).

The authors showed that at low surfactant concentrations, there are no significant interactions between the surfactant and the polymer. This was not the case at higher surfactant concentrations, where it was shown that the interactions yielded more stable micelles in which the EO groups are solubilized in the headgroup region of the micelle. The addition of the simple cosolutes had no impact on the interactions, however, the addition of the more complex ones led to the absence of any interactions between the polymer and the surfactant.

Nambam *et al.*[20] have investigated the effect of adding non-ionic (nonylphenolethoxylate, NP 9) and ionic surfactants (sodium dodecylsulfate, $C_{12}SO_4Na$ and cetyltrimethylammonium bromide, $C_{16}TAB$) on the self-assembly of PEO-PPO-PEO triblock copolymers (F108, PEO_{128}-PPO_{54}-PEO_{128}) and consequently its rheological behaviour. The authors concluded that the addition of $C_{12}SO_4Na$ has significantly reduced the viscoelastic properties of F108, where no changes were recorded in the presence of NP 9 and CTAB. This strong effect of the $C_{12}SO_4Na$ was related to the strong electrostatic barrier induced by the $C_{12}SO_4Na$ at the micellar interface which restricts the self-assembly and the growth of the F108 micelles.

The interactions between the triblock copolymer Pluronic® P123 (PEO_{20}-PPO_{70}-PEO_{20}) micelles and $C_{12}SO_4Na$ have been investigated by Kumar *et al.*[21] using tensiometry and diffusion NMR. The authors observed $C_{12}SO_4Na$ concentration dependant interactions between both components. At low and intermediate concentrations of $C_{12}SO_4Na$, strong interactions between P123 micelles and $C_{12}SO_4Na$. However, in the presence of high concentrations of $C_{12}SO_4Na$, weaker interactions were observed. This was attributed to the disruption of the polymer network caused by the high concentration of $C_{12}SO_4Na$.

Surface tension and viscosity measurements were utilised by Banipal *et al.*[22] to study the interactions between the mixed micelles of Pluronic® F68 (PEO_{76}-PPO_{29}-PEO_{76}), P123 and the cationic surfactants; dodecyltrimethylammonium bromide, $C_{12}TAB$, tetradecyltrimethylammonium bromide, $C_{14}TAB$ and $C_{16}TAB$. The authors have concluded that both P123 and F68 showed weak interactions with all the cationic surfactants mentioned earlier. These weak interactions could be accounted for by two possible explanations. The first being the large size of the head group where it shields the hydrophobic core, and suppress the presence of the polymer at the hydrocarbon-water interface. The second explanation is related to the electrostatic repulsion as a result of a slight positive charge present on the polymer, originating from the protonation of the ether oxygen in the PEO chains.[23,24]

Chapter 1. Introduction

The nature of the interactions between polymers and surfactants has shown to be of importance for potential drug delivery mechanisms by Mondal *et al.*[25] by using dynamic light scattering (DLS), isothermal titration calorimetry (ITC) and fluorescence spectroscopy. A cationic phenazinium dye, phenosafranin, was used as a model drug with Pluronic® F127 (PEO-PPO-PEO) without and with $C_{12}SO_4Na$, where the latter formed mixed micelles with F127. It was found that in the presence of $C_{12}SO_4Na$ at low concentrations, the fraction of the dye bound to F127 is significantly increased, up to 58 %. Furthermore, the binding constant estimated from the ITC measurements supports this finding. The explanation behind this was attributed to the penetration of the dye to the more hydrophobic core of the mixed micelle system, if compared to the F127 micelles alone.

It is then critical to understand the driving mechanisms behind these interactions, this would allow formulators to optimise any synergies if present and also understand the effect of any other additives to the formulation on its overall performance. For example, while formulating personal care products such as shampoos and shower gels, controlling the key properties such as appearance, ease of application, distribution on the skin or hair, shear thinning behaviour of the liquid is often achieved by mixing several polymers and surfactants.

The interactions between polymers and surfactants have been widely studied in solution, however the literature concerned with drawing a detailed understanding of the interactions between polymers and surfactants in other challenging, yet very relevant environments, such as foams and gels, is less developed.

Petkova *et al.*[26,27] have investigated the interactions between the cationic poly(vinylamine) PVA, the non-ionic poly(*N*-vinyl-formamide) PVFA and the anionic $C_{12}SO_4Na$, the cationic $C_{12}TAB$ and the non-ionic Brij 35 ($C_{12}EO_{23}$) on foam stability (time taken for the foam to collapse) and "foaminess" (measured height of the foam) . The authors showed that the systems composed of $C_{12}SO_4Na$ and PVA demonstrated strong interactions illustrated by a significant decrease in the foamability but higher foam stability when compared to the $C_{12}SO_4Na$ foam in the absence of the polymer. This decrease in foamability was related to the synergistic interactions between the polymer and the surfactant which resulted in a decrease in the concentration of the unbound $C_{12}SO_4Na$ monomer, due to its strong binding to the polymer.

3

Chapter 1. Introduction

The effect of the interactions between polymers and surfactants on the structures formed at a dynamic air/water interface has been studied by Angus-Smyth *et al.*[28] The systems investigated comprised PEO, $C_{12}SO_4Na$ and $C_{14}TAB$ and were studied using ellipsometry and neutron reflectivity (NR).The authors co-modeled the NR and ellipsometry data to elucidate the mechanism by which the polymer, the surfactants and their mixtures adsorb at the air/water interface. It was concluded that for PEO/$C_{14}TAB$ systems, the polymer adsorption drops significantly (to zero) over a narrow range of $C_{14}TAB$, while for PEO/$C_{12}SO_4Na$ systems, the inhibition of the polymer adsorption was more gradual.

Pluronic gels are known to be very versatile and possess a possibility of wide range of applications especially in drug delivery, hence the importance of understanding their concentration and temperature dependence. By using rheology and small-angle scattering (SAS), Newby *et al.*[29] studied the structure and the shear alignment of mixtures of P123 and P85 (PEO_{25}-PPO_{40}-PEO_{25}) at different temperatures and concentrations. Gel structures from these polymers and their mixtures showed a range of structures as face-centred cubic (fcc) and hexagonally close packed (hcp). The authors also reported that the cubic gels from these Pluronic mixtures have an enhanced stability in the high concentration region, in contrast to lesser stable systems; P123/F127.[30]

.

.

1.2 Aims

The aim of this project is to help optimise formulations by understanding the synergistic and the competitive interactions between polymers and surfactants in solution and in more complex formulations such as foams and gels.

1.3 Project overview

A wide range of systems comprising mainly the polymeric surfactant Pluronic® and small molecule surfactants have been studied in this thesis. A more specific introduction of the relevant literature is given at the beginning of every chapter. The chapters are structured as research papers, and they have been either published[31], submitted for publication[32] or in preparation to be submitted to journals.

Chapter 2 explores the interactions between the widely used triblock copolymer Pluronic® P123 and small molecule surfactants (SMS) such as the anionic sodium dodecylsulfate ($C_{12}SO_4Na$), the cationic dodecyltrimethylammonium bromide ($C_{12}TAB$) and the non-ionic Brij 35 ($C_{12}EO_{23}$) in the presence of short, medium and long -chain alcohols. A number of techniques was used. Tensiometry was used to determine critical micelle and aggregate concentrations along with understanding the surface properties of the single systems and the mixtures. Pulsed gradient spin-echo nuclear magnetic resonance (PGSE-NMR) was used to understand the partitioning of the alcohols and how perturbation of the local structure could drive or control the interactions. Finally, small-angle neutron scattering (SANS) was used to derive detailed structural and morphological information of the mixed micelles from P123, SMS and the alcohols.

Chapter 3 investigates the same class of polymers but at higher concentrations, specifically gelation from Pluronic® P123 (30% PEO), F108 (PEO_{128}-PPO_{54}-PEO_{128}, 80% PEO) and their mixtures. SANS was used to probe the gel structures as a function of both polymer concentrations/ratio and temperature. To our knowledge, this was the first time gels from Pluronic® F108 and P123 mixtures have been investigated extensively by neutron scattering. Most of the previous studies have focused on gels from mixtures of Pluronics with medium and high lipophilicity due to the stabilised gel structures obtained. In this chapter, several gel structures were observed (body centred cubic, face centred cubic, hexagonally closed packed and lamellar). These structures showed interesting stabilisation/destabilisation dependant on the Pluronic ratio and temperature changed.

In Chapter 4, we extend the work to include more challenging systems: foams stabilised by SMS. In this study, foams were stabilised by a homologous series of surfactants; alkyl sulfate and alkyl bromide based surfactants. It is well-established that the architecture of the surfactant has a significant contribution to the foam performance (foamability, foam stability, etc.). However, a better understanding of the self-assembly of these surfactants at the foam air/water interface is needed. Tensiometry was used again to determine the CMC of the surfactants and surface activity in solution while SANS was employed to probe the surfactant structure at the foam air/water interface. Here, one of the main challenges of investigating these systems beside the complexity of the foam as a system, was the SANS sample environment needed to study these foams. A Perspex foam column was used instead of the usual SANS sample environment as sample changer.

As foams in practical applications are often stabilised by mixtures of polymers and surfactants, the interactions between polymers and SMS in foams have been explored in Chapter 5. Tensiometry was once more used to determine surface characterises in P123, poly(vinyl pyrrolidone) (PVP), C_8 and C_{12} SMS systems, while SANS was used to probe the effect of these interactions on the polymer/surfactant structure at the foam air/water interface.

Conclusions drawn from these studies and recommendations for future work for areas that has shown to be interesting have been summarised in Chapter 6. Extra data and figures have been included in this thesis under several Appendices (A to C). Tensiometry, PGSE-NMR and SANS techniques have been described in Appendix D. Finally, the manuscripts of the published work have been included in Appendix E.

Chapter 1. Introduction

Bibliography

(1)   Nakashima, K.; Bahadur, P. Aggregation of Water-Soluble Block Copolymers in Aqueous Solutions: Recent Trends. *Adv. Colloid Interface Sci.* **2006**, *123-126*, 75–96.

(2)   Hooshyar, H.; Sadeghi, R. Influence of Sodium Salts on the Micellization and Interfacial Behavior of Cationic Surfactant Dodecyltrimethylammonium Bromide in Aqueous Solution. *J. Chem. Eng. Data* **2015**, *60*, 983–992.

(3)   Griffiths, P. C.; Hirst, N.; Paul, A.; King, S. M. Effect of Ethanol on the Interaction between Poly (Vinylpyrrolidone) and Sodium Dodecyl Sulfate. *Langmuir* **2004**, *20*, 6904–6913.

(4)   Anthony, O.; Zana, R. Interactions between Water-Soluble Polymers and Surfactants: Effect of the Polymer Hydrophobicity. 1. Hydrophilic Polyelectrolytes. *Langmuir* **1996**, *12*, 1967–1975.

(5)   Pham Trong, L. C.; Djabourov, M.; Ponton, A. Mechanisms of Micellization and Rheology of PEO-PPO-PEO Triblock Copolymers with Various Architectures. *J. Colloid Interface Sci.* **2008**, *328*, 278–287.

(6)   Clasen, C.; Kulicke, W. M. Determination of Viscoelastic and Rheo-Optical Material Functions of Water-Soluble Cellulose Derivatives. *Prog. Polym. Sci.* **2001**, *26*, 1839–1919.

(7)   Tang, B.; White, S. P.; Frisbie, C. D.; Lodge, T. P. Synergistic Increase in Ionic Conductivity and Modulus of Triblock Copolymer Ion Gels. *Macromolecules* **2015**, *48*, 4942–4950.

(8)   Rodríguez, A.; Junquera, E.; Del Burgo, P.; Aicart, E. Conductometric and Spectrofluorimetric Characterization of the Mixed Micelles Constituted by Dodecyltrimethylammonium Bromide and a Tricyclic Antidepressant Drug in Aqueous Solution. *J. Colloid Interface Sci.* **2004**, *269*, 476–483.

(9)   Hammouda, B. SANS from Pluronic P85 in D-Water. *Eur. Polym. J.* **2010**, *46*, 2275–2281.

(10) Shibayama, M.; Karino, T.; Domon, Y.; Ito, K. Complementary Use of Small-Angle Neutron Scattering and Dynamic Light Scattering Studies for Structure Analysis and Dynamics of Polymer Gels. *J. Appl. Crystallogr.* **2007**, *40*, 43–47.

(11) Et-Tarhouni, Z. O.; Carter, E.; Murphy, D. M.; Griffiths, P. C.; Mansour, O. T.; King, S. M.; Paul, A. Quantifying the Micellar Structure Formed from Hydrocarbon-Fluorocarbon Surfactants. *Colloids Surfaces A Physicochem. Eng. Asp.* **2015**, *492*, 255–262.

(12) Mortensent, K.; Talrnon, Y. Cryo-TEM and SANS Microstructural Study of Pluronic Polymer Solutions. *Macromolecules* **1995**, *28*, 8829–8834.

(13) Jansson, J.; Schillén, K. Small-Angle X-Ray Scattering, Light Scattering, and NMR Study of PEO-PPO-PEO Triblock Copolymer/cationic Surfactant Complexes in Aqueous Solution. *J. Phys. Chem. B* **2005**, *109*, 7073–7083.

(14) Cooper, C. L.; Cosgrove, T.; van Duijneveldt, J. S.; Murray, M.; Prescott, S. W. The Use of Solvent Relaxation NMR to Study Colloidal Suspensions. *Soft Matter* **2013**, *9*, 7211-7228.

(15) Becker, B. A.; Morris, K. F.; Larive, C. K. An Improved Method for Suppressing Protein Background in PFG NMR Experiments to Determine Ligand Diffusion Coefficients in the Presence of Receptor. *J. Magn. Reson.* **2006**, *181*, 327–330.

(16) Zahid, N. I.; Abou-Zied, O. K.; Hashim, R.; Heidelberg, T. Fluorescence Probing of the Temperature-Induced Phase Transition in a Glycolipid Self-Assembly: Hexagonal ↔ Micellar and Cubic ↔ Lamellar. *Langmuir* **2012**, *28*, 4989–4995.

(17) Bales, B. L.; Zana, R. Characterization of Micelles of Quaternary Ammonium Surfactants as Reaction Media I: Dodecyltrimethylammonium Bromide and Chloride. *J. Phys. Chem. B* **2002**, *106*, 1926–1939.

(18) Jangher, A.; Griffiths, P. C.; Paul, A.; King, S. M.; Heenan, R. K.; Schweins, R. Polymeric Micelle Disruption by Cosolvents and Anionic Surfactants. *Colloids Surfaces A Physicochem. Eng. Asp.* **2011**, *391*, 88–94.

(19) Barbosa, A. M.; Santos, I. J. B.; Ferreira, G. M. D.; Hespanhol Da Silva, M. D. C.; Teixeira, Á. V. N. D. C.; Da Silva, L. H. M. Microcalorimetric and SAXS Determination of PEO-SDS Interactions: The Effect of Cosolutes Formed by Ions. *J. Phys. Chem. B* **2010**, *114*, 11967–11974.

(20) Nambam, J. S.; Philip, J. Effects of Interaction of Ionic and Nonionic Surfactants on Self-Assembly of PEO–PPO–PEO Triblock Copolymer in Aqueous Solution. *J. Phys. Chem. B* **2012**, *116*, 1499–1507.

(21) Kumar, B. V. N. P.; Priyadharsini, S. U.; Prameela, G. K. S.; Mandal, A. B. NMR Investigations of Self-Aggregation Characteristics of SDS in a Model Assembled Tri-Block Copolymer Solution. *J. Colloid Interface Sci.* **2011**, *360*, 154–162.

(22) Banipal, T. S.; Sood, A. K. Effect of Hydrophobicity and Temperature on the Interactions in the Mixed Micelles of Triblock Polymers [(EO76PO29EO76) and (EO19PO69EO19)] with Monomeric and Gemini Surfactants. *J. Surfactants Deterg.* **2014**, *17*, 1169–1180.

(23) Schwuger, M. J. Mechanism of Interaction between Ionic Surfactants and Polyglycol Ethers in Water. *J. Colloid Interface Sci.* **1973**, *43*, 491–498.

(24) Mata, J.; Joshi, T.; Varade, D.; Ghosh, G.; Bahadur, P. Aggregation Behavior of a PEO–PPO–PEO Block Copolymer + Ionic Surfactants Mixed Systems in Water and Aqueous Salt Solutions. *Colloids Surfaces A Physicochem. Eng. Asp.* **2004**, *247*, 1–7.

(25) Mondal, R.; Ghosh, N.; Mukherjee, S. Enhanced Binding of Phenosafranin to Triblock Copolymer F127 Induced by Sodium Dodecyl Sulfate: A Mixed Micellar System as an Efficient Drug Delivery Vehicle. *J. Phys. Chem. B* **2016**, *120*, 2968–2976.

(26) Petkova, R.; Tcholakova, S.; Denkov, N. D. Foaming and Foam Stability for Mixed Polymer-Surfactant Solutions: Effects of Surfactant Type and Polymer Charge. *Langmuir* **2012**, *28*, 4996–5009.

(27) Petkova, R.; Tcholakova, S.; Denkov, N. D. Role of Polymer–surfactant Interactions in Foams: Effects of pH and Surfactant Head Group for Cationic Polyvinylamine and Anionic Surfactants. *Colloids Surfaces A Physicochem. Eng. Asp.* **2013**, 1–12.

(28) Angus-Smyth, A.; Campbell, R. A.; Bain, C. D. Dynamic Adsorption of Weakly Interacting Polymer/surfactant Mixtures at the Air/water Interface. *Langmuir* **2012**, *28*, 12479–12492.

(29) Newby, G. E.; Hamley, I. W.; King, S. M.; Martin, C. M.; Terrill, N. J. Structure, Rheology and Shear Alignment of Pluronic Block Copolymer Mixtures. *J. Colloid Interface Sci.* **2009**, *329*, 54–61.

(30) Chaibundit, C.; Ricardo, N. M. P. S.; Costa, F. D. M. L. L.; Yeates, S. G.; Booth, C. Micellization and Gelation of Mixed Copolymers P123 and F127 in Aqueous Solution. *Langmuir* **2007**, *23*, 9229–9236.

(31) Mansour, O. T.; Cattoz, B.; Heenan, R. K.; King, S. M.; Griffiths, P. C. Probing Competitive Interactions in Quaternary Formulations. *J. Colloid Interface Sci.* **2015**, *454*, 35–43.

(32) Mansour, O. T.; Cattoz, B.; Montagnnon, M.; Heenan, R. K.; King, S. M.; Schweins, R.; Griffiths, P. C. Probing the Interfactial Structure of Small Molecule Surfactants Air-in-Water Stabilised Foams. submitted to *Langmuir* **2016**.

Chapter 2

2. Probing competitive interactions in quaternary formulations

2.1 Abstract

The interaction of amphiphilic block copolymers of the poly(ethylene oxide)–poly(propylene oxide)-poly(ethylene oxide) (PEO–PPO-PEO) group with small molecule surfactants may be "tuned" by the presence of selected alcohols, with strong interactions leading to substantial changes in (mixed) micelle morphology, whilst weaker interactions lead to coexisting micelle types. The nature and the strength of the interactions between Pluronic P123 ($EO_{20}PO_{70}EO_{20}$) and small molecule surfactants (anionic sodium dodecylsulfate, SDS, $C_{12}SO_4Na$), (cationic dodecyltrimethylammonium bromide, $C_{12}TAB$) and (non-ionic polyoxyethylene (23) lauryl ether, Brij 35, $C_{12}EO_{23}OH$) is expected to depend on the partitioning of the short, medium and long chain alcohols (ethanol, hexanol and decanol ,respectively) and was probed using tensiometry, pulsed-gradient spin-echo nuclear magnetic resonance (PGSE-NMR) and small-angle neutron scattering (SANS).

The SANS data for aqueous P123 solutions with added alcohols were well described by a charged spherical core/shell model for the micelle morphology. The addition of the surfactants led to significantly smaller, oblate elliptical mixed micelles in the absence of alcohols. Addition of ethanol to these systems led to a decrease in the micelle size, whereas larger micelles were observed upon addition of the longer chain alcohols. PGSE-NMR studies provided complementary estimates of the micelle composition, and the partitioning of the various components into the micelle.

2.2 Introduction

Amphiphilic molecules, commonly known as surfactants, form discrete aggregates, called micelles above the critical micelle concentration (CMC). A widely studied and practically relevant series of surfactants is the water soluble triblock copolymer group made up of poly(ethylene oxide) (PEO) and poly(propylene oxide) (PPO), denoted as $(PEO_n-PPO_m-PEO_n)$, commercially known as Pluronic (BASF), Synperonic (Croda) or Poloxamers (ICI).[1–7] The CMC is sensitive to the composition of the Pluronic and various grades are available. It has been well established that Pluronics form temperature sensitive micelles that adopt a core-shell morphology, where the more hydrophobic domain (PPO) forms the core and the hydrophilic domain (PEO) forms the hydrophilic corona, *i.e.* the shell.[8–12]

In practical applications, it is usual that polymer-surfactant mixtures are employed as these often have improved properties derived by complex formulation; the addition of ionic/non-ionic surfactants to such polymeric surfactant solutions. The improvement in performance arises due to the synergistic (or antagonistic) interactions between the various surfactants.[13] A considerable number of studies have focused on determining the onset of the micellization process and the composition/morphology of the mixed micelles formed,[9,14–16] though theoretical modelling is limited to systems that are considerably more simple than generally encountered in "real-life' formulations.[17,18]

The interactions of small molecule surfactants with Pluronics are of relevance to their numerous pharmaceutical, domestic, technological and industrial applications. Mixtures of small molecules surfactant with Pluronic have previously been examined[9,19,20] as has the effect of alcohols.[11,13,21] To our knowledge, there have been far fewer studies of the quaternary systems, Pluronic/small molecule surfactants/alcohol/water, at least in non (micro) emulsion systems.

Previously, the interaction between the homopolymer polyvinylpyrrolidone (PVP) and SDS in the presence of ethanol was quantified,[13] and subsequently Pluronic P123 and sodium dodecylsulfate (SDS) in the presence of ethanol.[11] A range of techniques were employed including small-angle neutron scattering (SANS), surface tension and spectrofluorometry. Synergistic interactions between the SDS and P123 were observed, these interactions were characterised by the adsorption of the SDS into the

PPO core. It was also observed that addition of ethanol to both P123 and SDS solubilized the PPO core, increasing the CMC of P123, and that reducing the dielectric constant of the solvent led to the formation of smaller micelles in both cases.[6,11,19]

Against this background, the present study was undertaken to quantify the effect of short (ethanol), medium (hexanol) and long (decanol) chain alcohols, ionic/non-ionic surfactants comprising dodecyl chain and different head group sizes (anionic SDS, cationic $C_{12}TAB$ and non-ionic Brij 35) on the micellar structure of one specific Pluronic, P123. These effects were investigated using SANS, pulsed-gradient spin-echo nuclear magnetic resonance spectroscopy (PGSE-NMR) and surface tension measurements. The aim is to quantify the interactions between the Pluronic and the small molecule and to elaborate the dependence on the presence of the added alcohol, and demonstrate how the partitioning of the alcohol will drive the interaction between the surfactants.

2.3 Experimental

2.3.1 Materials

Pluronic P123, PEO_{20}-PPO_{70}-PEO_{20}, average $M_n \sim 5800$ g mol^{-1} (Sigma Aldrich) was used as received. Sodium dodecylsulfate (SDS) (Sigma Aldrich, purity 98.5%), dodecyltrimethylammonium bromide ($C_{12}TAB$) (Aldrich, purity 98%), polyoxyethylene (23) lauryl ether (Brij 35) (Aldrich, 98.5%) were all used as received. Deuterated SDS (d-SDS) and $C_{12}TAB$ (d-$C_{12}TAB$) for SANS experiments were purchased from Sigma Aldrich (99.9%) and used as received. Ethanol, hexanol and decanol, all protonated (Fisher Scientific), deuterium oxide (Sigma Aldrich, 99.9%) were used as received. Regarding materials purity, there was no evidence of any impurity in surface tension data (manifest as pre-CMC minima or incorrect CMC values). Furthermore, PGSE-NMR measurements showed no cause to suggest that there were impurities present.

2.3.2 Methods

2.3.2.1 Surface Tension

The surface tension measurements of pure and the mixed systems were carried out using a maximum bubble pressure tensiometer (SITA science on-line t60, Germany), calibrated by reference to deionized water. Surface tension was recorded at a bubble life time of value 10 s. All measurements were taken at 25 ± 1°C.

2.3.2.2 Small-angle neutron scattering (SANS)

SANS measurements were performed at 25°C on the fixed-geometry, time of flight LOQ diffractometer (ISIS Spallation Neutron Source, Oxfordshire, UK). Neutron wavelengths spanning 2.2-10 Å were used to access a *Q* range (*Q = 4π sin (θ/2)/λ*) of approximately 0.008-0.25 Å^{-1} (25 Hz), with a fixed sample-detector distance of 4.1 m.

The samples were contained in 1 mm path length, UV-spectrophotometer grade, quartz cuvettes (Hellma) and mounted in aluminium holders on top of an enclosed, computer-controlled, sample chamber. Temperature control was achieved through the use of a thermostatted circulating bath pumping fluid through the base of the sample chamber. Under these conditions a temperature stability of better than ± 0.5°C can be achieved. Experimental measuring times were approximately 40 min.

All scattering data were normalised for the sample transmission and the incident wavelength distribution, corrected for instrumental and sample backgrounds using a quartz cell filled with D_2O (this also removes the incoherent instrumental background arising from vacuum windows, *etc.*), and corrected for the linearity and efficiency of the detector response using the instrument specific software package. The data were put onto an absolute scale using a well-characterized partially deuterated polystyrene blend standard sample.

The intensity of the scattered radiation, *I*(*Q*), as a function of the wavevector, is given by :

$$I(Q) = N_m V_m^2 (\Delta\rho)^2 P(Q)S(Q) + B_{inc}$$ (2.1)

where *P*(*Q*) describes the morphology of the scattering species, *S*(*Q*) describes the spatial arrangement of the micelles in solution, N_m is the number of micelles per unit volume, V_m is the volume of the micelle, $\Delta\rho$ is the difference between the neutron scattering length density of the micelle and the solvent and B_{inc} is the incoherent background scattering.

Assuming there are three discrete regions; core, shell and the continuous solvent, the macroscopic scattering cross section is given as the particle number density multiplied by the square of the single-particle form factor, *P*(*Q*):

$$P(Q) = N\left[(\rho_A - \rho_C)V_A \frac{3j_1(QR_A)}{QR_A} + (\rho_B - \rho_C)V_{A+B}\left(\frac{3j_1(QR_B)}{QR_B} - \frac{3j_1(QR_A)}{QR_A}\right)\right]^2 \qquad (2.2)$$

where N is the number of core-shell particles per unit volume of solution, ρ_A is the scattering length density for the core, ρ_B is the scattering length density for the shell, ρ_C is the scattering length density for the solvent, V_A is the specific volume in the core, V_B is the specific volume in the shell and V_{A+B} is the volumes of the core and that of the shell.[22]

The first part of the equation is the contribution to the differential cross section from the core with the relevant scattering length density difference between the core and the solvent. The second part of the equation is the shell contribution (R_A and R_B) to the scattering (j_1 is the first order spherical Bessel function of the first kind).[22]

The $S(Q)$ used in the fitting routine is the rescaled mean spherical approximation (RMSA) provided by Hayter *et al.*[23,24] for spheres of given micellar concentration, charge and ionic strength, incorporating refinements for low-volume fractions and a penetrating ionic background.

The data were fitted using the SasView analysis program.[25] The software is open source and has been developed by major neutron scattering facilities; ISIS, ILL and NIST. The morphology of the micelle adopted for P123 here follows a model for that of a charged particle with core-shell morphology. The shell may also contain solvent and/or the added surfactant or alcohol, so an intermediate scattering length density (SLD) between that of the core and solvent could be used. In some cases *e.g.*, P123/small molecule surfactant mixed micelles, we invoke a slightly simpler model of a charged solid ellipsoidal micelle *(i.e.* no shell) as there are no signature of the shell (a bump at high Q) in the data. A detailed structure of the core-shell micelle is not required as it will be difficult to extract meaningful information without over parameterising the fit.

It should be also noted that for anisotropic particles such as ellipsoids, there is a numerical integration over the particle orientation. Given that Pluronic micelles are known to be slightly polydisperse,[26,27] a polydispersity parameter was included in the fitting routine and for most of the samples, it was set at 0.15.

The mixed micelle has been treated as a two-component (P123 and small molecule surfactant, SMS) surfactant system.[28] The volume of this mixed micelle having aggregation number, N, is calculated by:

$$V_m = N(x_1 \; v_{SMS} + (1 - x_1)v_{P123})$$ (2.3)

where x_1 is the mole fraction of SMS in the mixed micelle. V_{SMS} and V_{P123} are the molecular volumes of SMS and P123, respectively.

The micelle composition was extracted from the SANS data without any data fitting,[6] from the ratio of the intensities of scattering $R(Q)$ obtained with h- and d-SMS at the same composition via:

$$Vf_{SMS} = \left(\frac{(\sqrt{R(Q)}-1)(\rho_{P123}-\rho_{D2O})}{(\rho_{h-SMS}-\rho_{P123})-\sqrt{R(Q)}(\rho_{d-SMS}-\rho_{P123})} \right)$$ (2.4)

where

$$R(Q) = \frac{I(Q)^{h-SMS.P123}-B_{inc}^{h-SMS.P123}}{I(Q)^{d-SMS.P123}-B_{inc}^{d-SMS.P123}}$$ (2.5)

For the P123-Brij 35 mixed micelles, the micelle composition was not extracted using the same method as it was not possible to obtain deuterated Brij 35.

2.3.2.3 Pulsed-gradient spin echo nuclear magnetic resonance (PGSE-NMR)
PGSE-NMR (diffusion NMR) experiments were carried out at 25°C on a 400MHz Bruker FT NMR spectrometer. The gradient pulse duration (δ) was set to 1 ms and the magnetic field gradient (G) was varied from 5 to 500 G/cm. The diffusion time (Δ) was set to 300 ms. Further information on PGSE-NMR may be found in reference 29. Eight scans were accumulated over sixteen gradient steps. The self-diffusion coefficient was extracted by using CORE.[30]

The partitioning of the alcohol and small molecule surfactant may be easily quantified by diffusion NMR measurements since the measured self-diffusion coefficient is an average value containing contributions from the monomeric and micellized surfactant, weighted by the respective concentrations. This is equivalent to the fractional time spent by each molecule in a given environment, and is frequently expressed in terms of the fractional micelle composition, $p_{micelle}^{P123}$ [31]:

$$\bar{D}^{P123} = p_{micelle}^{P123} D_{micelle}^{P123} + (1 - p_{micelle}^{p123}) D_{monomer}^{P123} \qquad (2.6)$$

Where $\bar{D}^{P123}$ is the measured self-diffusion coefficient, $D_{micelle}^{P123}$ is the micelle self-diffusion coefficient and $D_{monomer}^{P123}$ is the self-diffusion coefficient of P123 monomers.

A similar analysis[31] to extract the partitioning of the alcohol (p_{free}^{R-OH}) and the small molecule surfactant, may be conducted as shown in equation 2.7, where $D_{micelle}$ is the measured self-diffusion coefficient, $D_{micelle}^{R-OH}$ is the micelle self-diffusion coefficient after alcohol solubilisation and D_{free}^{R-OH} is the free alcohol self-diffusion coefficient.

$$p_{free}^{R-OH} = \frac{D_{free}^{R-OH} - D_{micelle}^{R-OH}}{D_{free}^{R-OH} - D_{micelle}} \qquad (2.7)$$

Hence from a single PGSE-NMR measurement, p_{free}^{R-OH} and $p_{micelle}^{P123}$ can be obtained.

2.4 Results and Discussion

2.4.1 Onset of Micellization

Surface tension is a particularly convenient experimental technique to determine the onset of micellization. However, for complex systems *e.g.* mixtures of surfactants/water, the discontinuities in the surface tension may be at least initially counterintuitive. For example, when one dilutes a binary surfactant/water system through its CMC, does the experimental design maintain a fixed ratio of two surfactants or a fixed concentration of one of the materials? The surface tension curves would be quite different, as the system would evolve from mixed micelles to none or mixed to pure. This is especially important when there is a hydrophobic component present. It should also be noted that surface tension is a measure of the surface properties, hence, the difficulty of designing an experiment investigating bulk characteristics and competitive interactions. Accordingly, selections of behaviours are presented in Figure 2.1.

Figure 2.1, compiles several approaches we have used to design surface tension experiments. If we dilute P123 in simple aqueous solvent (open circles), there is clearly one break point in the curve yielding CMC ≈ 0.1 wt%. In the presence of SDS, keeping [P123] = 0.5 wt% (filled grey circles), several behaviours that are insensitive to the presence of ethanol can be noticed. Three different SDS concentration regions can be distinguished, for low SDS concentrations, (up to 1 mM), the surface tension remains unaffected by the SDS concentration and remains dominantly controlled by the P123; over an intermediate SDS concentration, (1 mM to 10 mM), the surface tension increases sharply to a plateau, upon further increase of SDS concentration, the surface tension again decreases.

As outlined in Table 2.1, the CMC of pure SDS is 7.9 mM which agrees well with earlier reported data.[32–34] In the presence of 0.5 wt% of the polymer, the CMC of SDS is significantly lowered from 7.9 mM to 1.2 mM as shown in Table 2.1, such decrease in the CMC could be understood as the aggregation of the SDS on the polymer. Outlined in Table 2.2, is the surface tension data from $C_{12}TAB$ based systems.

In the presence of ethanol, the CMC and the surface tension of SDS (filled squares, Figure 2.1) is also remarkably reduced, confirming that the micellization is promoted by the presence of ethanol: the cosurfactant effect. In the presence of 10 wt% ethanol, the P123 surface tension curve (filled circles, Figure 2.1), shows one break in the curve yielding a CMC of ≈ 0.6 wt%, which in comparison to the CMC of the simpler P123 solution, ≈ 0.1 wt%, confirms that the micellization process is unfavoured (the CMC increases) as the solvent is less hydrophobic.

System Description	CMC or CAC
SDS/water	7.9 mM
SDS/0.5 wt% P123-water	1.2 mM
SDS/10 wt% ethanol	4.5 mM
P123/water	0.1 wt%
P123/10 wt% ethanol	0.6 wt%
P123/50 mM SDS-water	0.3 wt%
P123/50 mM SDS/10 wt% ethanol	0.6 wt%

Table 2.1 Surface tension derived CMC/critical aggregate concentration (CAC) values as a function of P123, SDS and ethanol concentration in water.

System Description	CMC or CAC
C_{12}TAB/water	15.0 mM
C_{12}TAB/0.5 wt% P123-water	3.70 mM
C_{12}TAB/10 wt% ethanol	12.0 mM
P123/water	0.10 wt%
P123/10 wt% ethanol	0.60 wt%
P123/50 mM C_{12}TAB-water	0.04 wt%
P123/50mM C_{12}TAB/10 wt% ethanol	0.10 wt%

Table 2.2 Surface tension derived CMC/critical aggregate concentration (CAC) values as a function of P123, C_{12}TAB and ethanol concentration in water.

When the concentration of SDS/ethanol is kept constant (open diamonds, Figure 2.1), a decrease in surface tension is observed by increasing the P123 concentration as the less surface active species (small molecule surfactant and ethanol) are being stripped from the surface and it is being replaced with more active ones, P123.

While if we keep a fixed SDS/hexanol concentration, the surface tension increases by increasing the P123 concentration as it has a lower surface activity compared to the SDS/hexanol and water mixture (Appendix A).
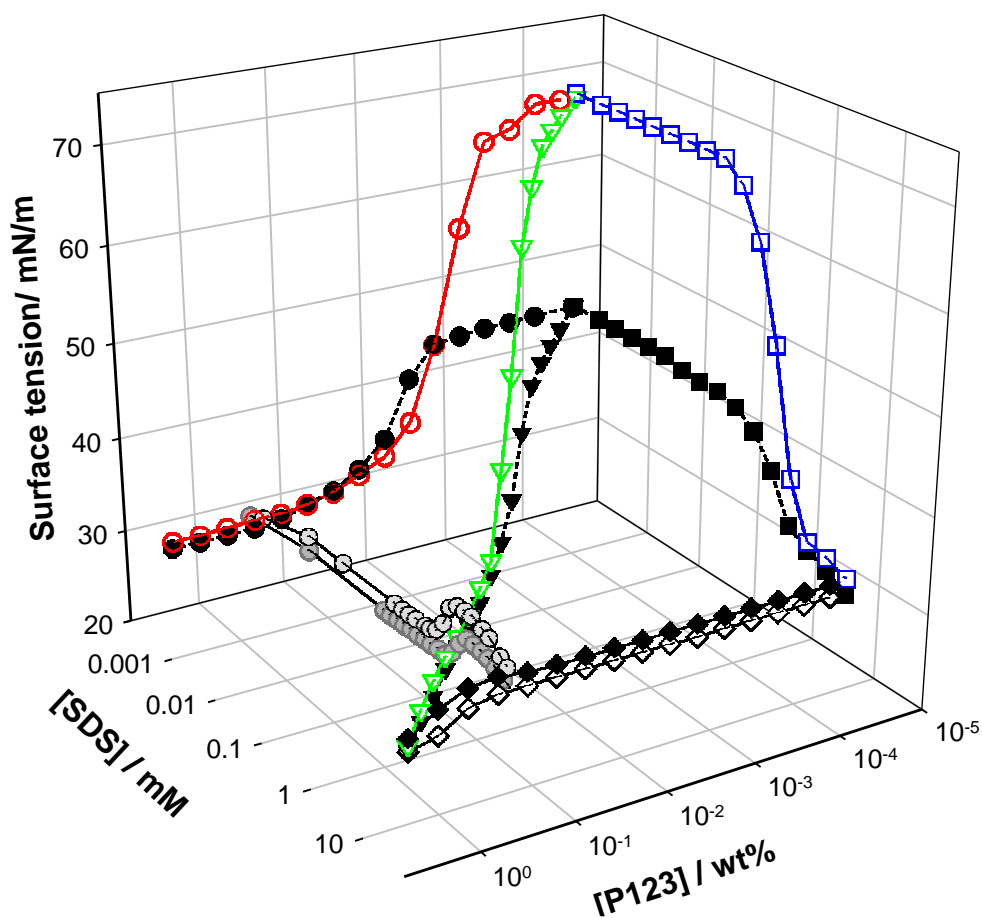
Figure 2.1 Surface tension as a function of surfactant concentration: open squares = [SDS/water], filled squares = [SDS + constant ethanol concentration of 10 wt% in water].

Open diamonds = [P123 + constant SDS and ethanol concentration of 50 mM & 10 wt% in water], filled diamonds = [P123 + constant SDS concentration of 50 mM in water].

Open triangles = [P123 + SDS in water], filled triangles = [P123 + SDS + constant ethanol concentration, 10 wt% in water].

Grey open circles across the SDS axis = [SDS + constant P123 concentration of 0.5wt% in water], grey filled circles across the SDS axis = [SDS + constant P123 and ethanol concentration of 0.5 wt% & 10 wt% ethanol in water].

Open circles = [P123/water], filled circles = [P123 + constant ethanol concentration of 10 wt% in water].

Changes in the system along the concentration range of ternary mixtures of P123 or small molecule surfactant and the hydrophobic alcohols (hexanol and decanol) in water, where the alcohol is kept constant, are quite significant. Below the CMC, where surfactant monomers only are present, the alcohol solubilisation is lower and the alcohol phase separates out of the solution. This phase behaviour and the maximum solubilisation of the alcohol, within the context of previously published SANS data[11,35,36] were the defining rules for the alcohol concentration selection in the P123 in the aqueous P123 and P123-small molecule surfactant mixtures.

The interactions contributing to the formation of the mixed micelles can be described as synergistic or antagonistic in terms of the change in the CMC. We use the terms in a more general sense. In these quaternary systems investigated, interactions with varying strengths between the surfactants were observed for SDS-P123, C_{12}TAB-P123 and Brij 35-P123 in water and water/alcohol mixtures. These interactions are observed as the small surfactant molecules are being included between the Pluronic molecules. The size and shape of the self- assembled structure is dictated by these interactions. SANS has been used to quantify these structures, and again only illustrative data are presented.

2.4.2 Effect of alcohol on Pluronic micelle structure

Scattering profiles for 5 wt% Pluronic P123 above the CMC are shown in Figure 2.2. The scattering profile of 5 wt% P123 in D_2O yields considerable scattering intensity with a noticeable "bump" around $Q = 0.09$ Å^{-1} , reflecting a sharp discontinuity in the scattering length density profile across the micelle indicative of the well-defined core and corona regions. Fitting the data to the core-shell model described earlier shows that the P123 micelles are slightly polydisperse with a spherical core of 57 Å ± 1 and corona of 14 Å ± 0.5 with the latter adopting Gaussian statistics.[26]

Given that the CMC of P123 increases in the presence of ethanol, it is more likely that this decreasing intensity at low Q after the addition of 10 wt% ethanol, Figure 2.2, is due to the reduction of the number and/or the volume of the micelle and/or a change in the interaction between the micelles *via* the structure factor. This could be simply attributed to the fact that the ethanol/water mixture solubilises the hydrophobic PPO core more than pure water [36,37], changing the effective HLB of the surfactant. Support (albeit indirect) arises from an interpretation of the micellar volume fraction parameter

extracted from the Hayter-Penfold fit, in that all attempts to describe the data with a volume fraction greater than 0.05 (in essence, the mass fractions of the Pluronic plus the solubilised alcohol) led to poor fits. It was concluded therefore, that the ethanol displaces the water in the EO-rich shell, thereby not significantly increasing the fraction of the micelle bounded material.

Figure 2.2 SANS from 5 wt% P123 solutions as a function of alcohol concentration; circles [alcohol] = 0 wt%, squares [ethanol] = 10 wt%, triangles [hexanol] = 1 wt% and diamonds [decanol] = 0.1 wt%. The inset shows the structure factor $S(Q)$ extracted from the fit of the same data in the same symbols order of the main graph. Solid lines are fits to the core-shell model, see Table 2.3.

By contrast, in the case of 1 wt% hexanol and 0.1 wt% decanol, the scattering intensity at low Q increases reflecting the presence of more and/or larger micelles as the hydrophobic alcohol is incorporated into the micellar core. Making the reasonable assumption that the hydroxyl group is present at the core/corona interface to maintain its hydration, the modelling shows that this drives the formation of a larger micelle. The slight shift of the structure factor, extracted from the fit (inset in Figure 2.2) towards higher Q values is indicative of the decreasing distance between the micelles associated with the increase in the micelle size. The key parameters, extracted from the fitting, are listed in Table 2.3.

The SLD for the solvent (D_2O) was kept constant in the fitting routine for most of the samples at 6.39×10^{-6} $Å^{-2}$, but was adjusted accordingly using the partitioning values extracted from PGSE-NMR data analysis. For example, the samples containing 10 wt% ethanol, where PGSE-NMR has shown that 2.5 % only remains unbound in the solvent, the SLD of the solvent (D_2O and some fraction of the h-ethanol) and the core (PPO and the remaining fraction of h-ethanol) were included in the fitting routine based on some simple assumptions: (i) all the ethanol partitions into the core (ii) all the ethanol partitions into the shell and (iii) some distribution of the ethanol between the core and the shell. For each simulation, the SLD of the appropriate region was estimated based on the composition, and this value is used as an input parameter ("as a best guess") or occasionally held constant in the fitting routine. Based on this analysis, we conclude that the majority of the ethanol is located in the shell of the micelle. PGSE-NMR has also shown that both hexanol and decanol partition into the micelle, but in these cases, due to their low concentration, the change in the solvent SLD was negligible.

Figure 2.2 also shows the effect of hexanol on the aggregation behaviour of the P123 micelle. Addition of 1 wt% hexanol resulted in a large increase in the scattering intensity at low Q. The linearity observed in the low Q region is suggestive of ellipsoidal micelles.[35,38] Data fitting suggests the formation of prolate ellipsoidal micelles with major axis of 160 Å and a minor axis of 55 Å. Key fitting parameters are listed in Table 2.3.

The material-balance equations, described by Slawecki *et al.*[39] allow us to quantify the composition of the core and shell of the P123 micelle in D_2O using the SANS data. There were 5-6 D_2O molecules per EO monomer in the shell. The aggregation number, 110 ± 5, is in good agreement with other reported values from data previously fitted to the Pedersen model for Pluronics in solution[40] at the same polymer concentration and temperature, 5 wt% and 25°C.[11,36] Percentage of EO monomers inside the PO core was found to be ≈ 3 % which agrees with the simple understanding of a core shell model, where both regions are well defined.

Self-diffusion coefficients obtained by PGSE-NMR were used to determine values of $p_{\text{free}}^{\text{OH}}$, (free fraction of alcohol not solubilised the micelles) as shown in equation 2.7. Applying the values obtained for $p_{\text{free}}^{\text{OH}}$ to the mass balance equation, one may correct to a first assumption that 50 %, 15 % and 3 % of these micelle volumes are the solubilized alcohols, giving an estimate of the aggregation number of 60, 200 and 160 for micelles with ethanol, hexanol and decanol, respectively. These estimates of the aggregation numbers are entirely consistent with the measured P123 diffusion rates.

Alcohol concentration	0 wt%	10 wt% Ethanol	1 wt% Hexanol	0.1 wt% Decanol
Core radius (±1, Å)	57	50	a:166/b:55	60
Shell thickness (±0.5, Å)	14	13.5	--	13
Volume fraction of hard spheres (±0.001)	0.05	0.05	0.05	0.05
Volume of the micelles (nm^3), V_{mic}	1500	1100	2100	1600
Free alcohol fraction, $p_{\text{free}}^{\text{OH}}$, from NMR	-----	0.25	0.03	0
Aggregation number, N_{agg} (± 5)	110	60[i]	200	160
Micelles number density, n, 10^{16} cm^{-3}	3.5[ii]	4.7	2.0	3.2

i: Similar aggregation numbers for P123 with ethanol have been reported by Jangher *et al.*[11], Alexander *et al.*[36] and Soni *et al.*[41].
ii: Micelles number density value is in good agreement with the values reported by Manet *et al.*[42].

Table 2.3 Fitting parameters for 5 wt% P123 as a function of alcohol concentration at 25°C (from SANS and PGSE-NMR).

Significant changes in micelle morphology are observed when small molecule surfactants are added to the P123/alcohol systems. Take for example the SDS case, on addition of 50 mM SDS to the 5 wt% P123 aqueous and alcohol/aqueous solutions, in Figure 2.3, SANS data show significant loss in the scattering intensity and the emergence of correlation peaks at higher Q values which together indicates the formation of smaller, mixed, charged micelles.

Adding the SDS resulted in the loss of the "bump" at ≈ 0.09 Å^{-1}. The addition of the ethanol to the P123/SDS mixed micelle led to a slight decrease in the scattering intensity with no significant change in the position of the correlation peak. As shown previously in Figure 2.2, the hydrophobicity of the micellar core increases by increasing the hydrophobicity of the alcohols, evident by the increase in the scattering intensity, along with a shift in the correlation peak toward the lower Q region indicating the formation of larger aggregates, Table 2.4. The scattering from these mixed micelles were fitted using a form factor describing the micelle as an oblate ellipsoid with a charged structure factor as calculated by Hayter and Penfold. The key parameters are listed in Table 2.4.

It is widely accepted that SDS absorbs into the PPO core as the interaction between SDS and the hydrophobic PPO block of P123 is stronger than that between SDS and the hydrophilic PEO block where it renders the core less hydrophobic.[15,16] Jansson *et al.*[43] showed that at low SDS/P123 mole ratios, the principle structure is a P123 micelle with co-micellised SDS. At higher SDS/P123 mole ratios, P123 micelles are broken up, forming SDS-rich micelles co-micellised with few P123 molecules.

Alcohol concentration	0 wt%	10 wt% Ethanol	1 wt% Hexanol	0.1 wt% Decanol
Radius A, polar (±0.5,Å)	17	17	21	19
Radius B, equatorial (±1, Å)	39	37	46	39
Volume fraction of hard spheres (±0.001)	0.05	0.05	0.06	0.06
Volume of the micelles (nm^3), V_{mic}	110	95	185	120
Mixed micelle aggregation number, N_{agg} (± 5)	12	10	20	13
Micelles number density, n, 10^{17} cm^{-3}	5.9	5.2	3.2	5.0

Table 2.4 SANS parameters for 5 wt% P123- 50 mM h-SDS as a function of alcohol concentration at 25°C.
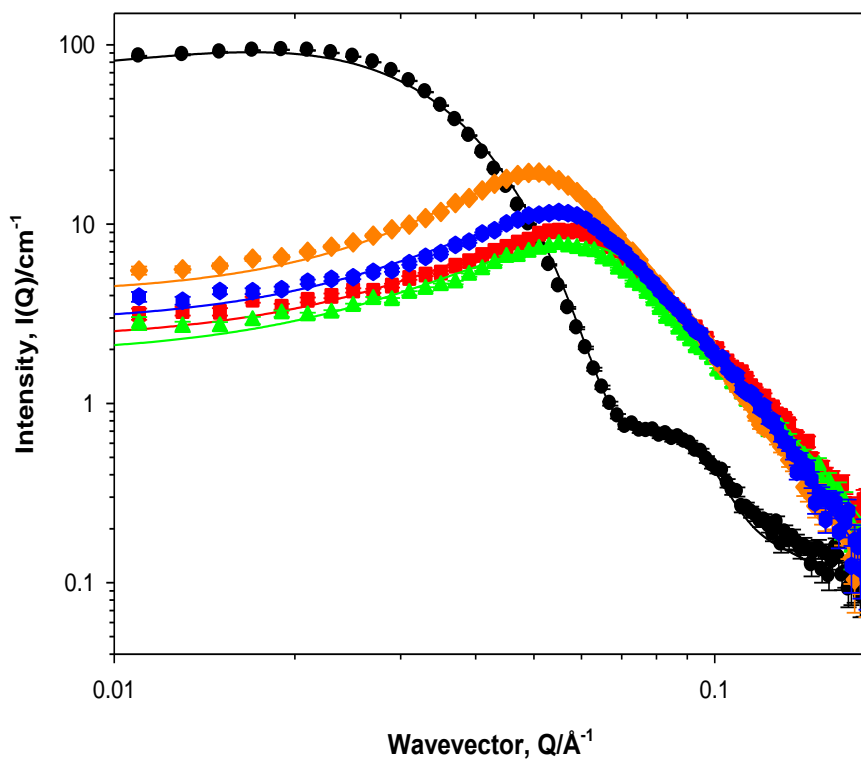
Figure 2.3 SANS from 5 wt% P123 solutions + 50 mM h-SDS as a function of alcohol chain length; circles [alcohol] = 0 wt% and [h-SDS] = 0 mM, squares [alcohol] = 0 wt% , triangles [ethanol] = 10 wt%, diamonds [hexanol] = 1 wt% and hexagons, [decanol] = 0.1 wt%. Solid lines correspond to model fits as discussed in the text.
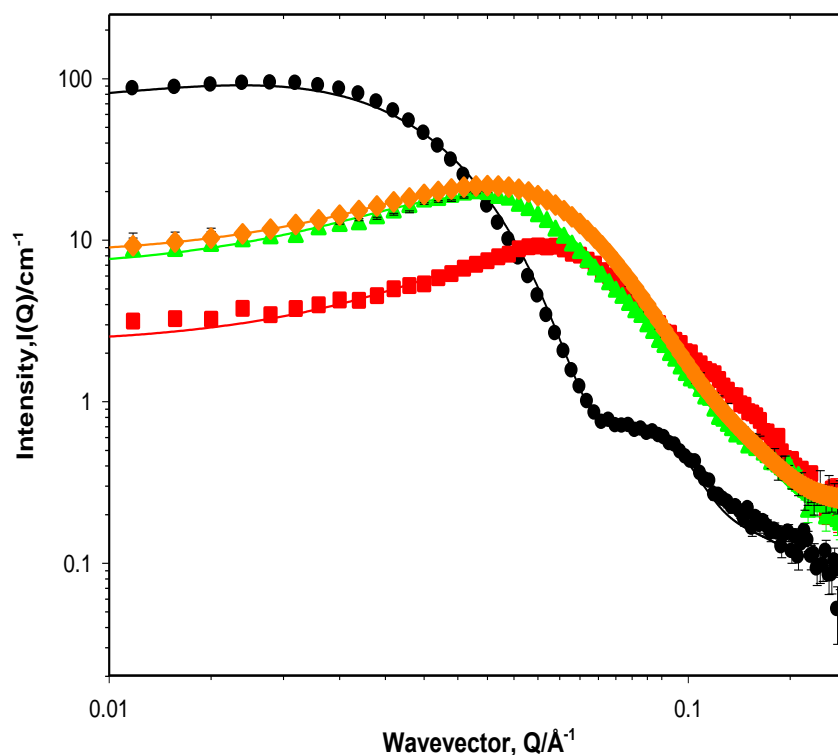
Figure 2.4 SANS from 5 wt% P123 solutions as a function of small molecule surfactant head group size; circles [SMS] = 0 mM, squares [h-SDS] = 50 mM, triangles [h-C_{12}TAB] = 50 mM, and diamonds [Brij 35] = 50 mM.

One could envisage a situation where the bulkiness of the head group of the small molecule or its charge density would control the size and the hydration level of the mixed micelle, summarised in Table 2.5. SANS data shown in Figure 2.4, shows the effect of the head group size on the scattering intensity. The mixed micelle aggregation number shows variations with changing the small molecule surfactant charge. For the P123/SDS system, the aggregation number decreases after adding SDS to the block copolymer (N_{agg} = 12 ± 5),[11,15,16,44] which is expected as the head group (SO_4Na^+) forms small curved surfaces, whereas in the P123/C_{12}TAB system, the C_{12}TAB ($N(CH_3)_3Br^-$) is likely to be less charged where the degree of counterion dissociation is less, hence the decrease in the curvature and the formation of larger structures (N_{agg} = 20 ± 5). Upon introducing a non-ionic surfactant, Brij 35, there is a further decrease in the charge which forms even larger structures (N_{agg} = 25 ± 5). For comparison, the dimensions expressed in terms of the volume of the pure components micelles are; SDS[19] – 35 nm^3, C_{12}TAB[45] – 40 nm^3, Brij 35[46] – 275 nm^3 whilst P123 – 1500 nm^3 (See Table 2.5).

Surfactant	SDS	$C_{12}TAB$	Brij 35
Radius A, polar (±0.5,Å)	17	23	26
Radius B, equatorial (±1, Å)	39	45	45
Volume fraction of hard spheres(±0.001)	0.06	0.06	0.09
Volume of the micelles (nm³), V_{mic}	110	195	210
Mixed micelle aggregation number,(± 5)	12	20	25
Micelles number density,n,10^{17} cm^{-3}	5.9	3.1	4.3

Table 2.5 SANS parameters for 5 wt% P123 as a function of 50 mM h-surfactants in D$_2$O at 25°C.

Figure 2.5 shows the variations in the scattering data at lower P123 and small molecule surfactant concentrations but at identical P123/surfactant ratio and above CMC$_{mixed}$. Studying these systems at lower concentrations yields more insight about the shape of the aggregates formed and the nature of the interactions between the surfactants. At low SDS concentrations, 5 mM, there is significantly less scattering intensity indicating the presence of small, charged micelles as a result of the strong adsorption of the SDS into the PPO core and the synergistic interaction between SDS and P123. On increasing the head group size of the surfactant, *i.e.* C$_{12}$TAB, the scattering intensity is recovered where the micelle also regains its core-shell morphology demonstrating antagonistic interactions between both surfactants. Upon a further increase in the head group size; Brij 35, the scattering pattern adopts a slope of −2 at high *Q* confirming the formation of a mixed oblate elliptical micelle. The synergistic interactions between P123 and Brij 35 as reported earlier,[47,48] occurs as both surfactants have hydrated EO chains when in contact with water, which results in a full miscibility of both surfactants in the mixed micelle. The antagonistic interactions between P123 and C$_{12}$TAB could be accounted for by two possible explanations. The first being the large size of the head group where it shields the hydrophobic core, and suppress the presence of the polymer at the hydrocarbon-water interface. The second explanation is related to the electrostatic repulsion as a result of a slight positive charge present on the polymer, originating from the protonation of the ether oxygen in the PEO chains.[49,50] Significant SANS parameters are presented in Table 2.6.
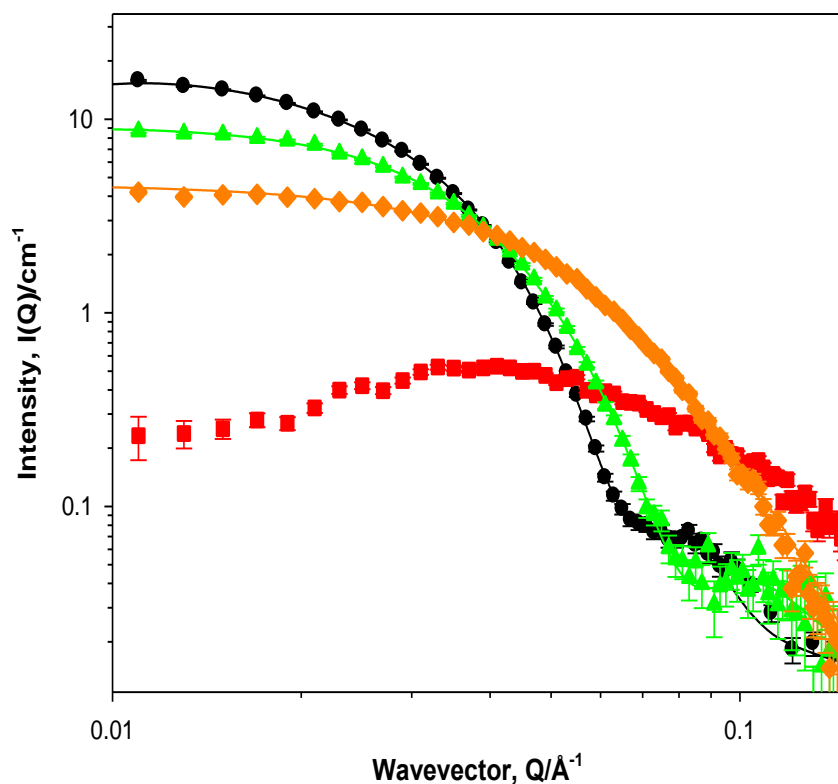
Figure 2.5 SANS from 0.5 wt% P123 solutions as a function of SMS head group size; circles [surfactant] = 0 mM, squares [h-SDS] = 5mM, triangles [h-C$_{12}$TAB] = 5 mM, and diamonds [Brij 35] = 5 mM.

Surfactant	No SMS added	C$_{12}$TAB	Brij 35
Radius A (±1, Å)	57	42	23
Thickness/Radius B (±1, Å)	17	12	51
Volume fraction of hard spheres (±0.001)	0.005	0.005	0.01
Volume of the micelles (nm^3)	1500	860	250
Micelles number density, n, 10^{15} cm^{-3}	3.3	5.8	40
Mixed micelle aggregation number (± 5)	130[iii]	88	26

iii: Results in good agreement with Jangher *et al.*[11] and Bhattacharjee *et al.*[26]

Table 2.6 SANS parameters for 0.5 wt% P123 as a function of 5 mM h-surfactants in D$_2$O at 25°C.

2.4.3 Determination of micelle composition

Contrast variation experiments have also been used to separate the scattering from the P123 and the small molecule surfactants; the use of d-surfactants in D_2O renders them invisible. In the case of h-P123/d-SDS/D_2O, shown in Figure 2.6, SDS is invisible and the scattering intensity observed arises predominantly from P123. In the h-P123/h-SDS/D_2O case, both surfactants are visible and hence the stronger scattering intensity observed. h-P123/h-C_{12}TAB/D_2O system, Figure 2.7, shows higher intensity profiles than the h-SDS case and a signature of a structure adopting core-shell morphology.

A crude estimate of the SDS and C_{12}TAB fraction (Vf_{SMS}) presented as α, within the aggregate could be extracted from the SANS measurements without any data fitting from the ratio of the scattering intensities, R(Q), obtained with h and d-surfactants at the same composition, equation 2.4. For 0.5 wt% P123-5 mM SDS, α(SDS) = 31 ($\pm$ 5) %,[11] and for 0.5 wt% P123-5 mM C_{12}TAB, α(C_{12}TAB) = 11 ($\pm$ 5) %.

These findings agree with the data extracted from the fitting where SDS had the strongest interaction with P123 as discussed earlier, and it forms up to 30% of the mixed micelle structure, where in the weakest interaction case (P123-C_{12}TAB), the small molecule surfactant makes up 11% only of the mixed micelle structure.

Figure 2.6 SANS from 0.5 wt% P123 and 5 mM [h-SDS] = empty circles, 5 mM [d-SDS] = filled circles in D$_2$O. Error bars have been removed for clarity.
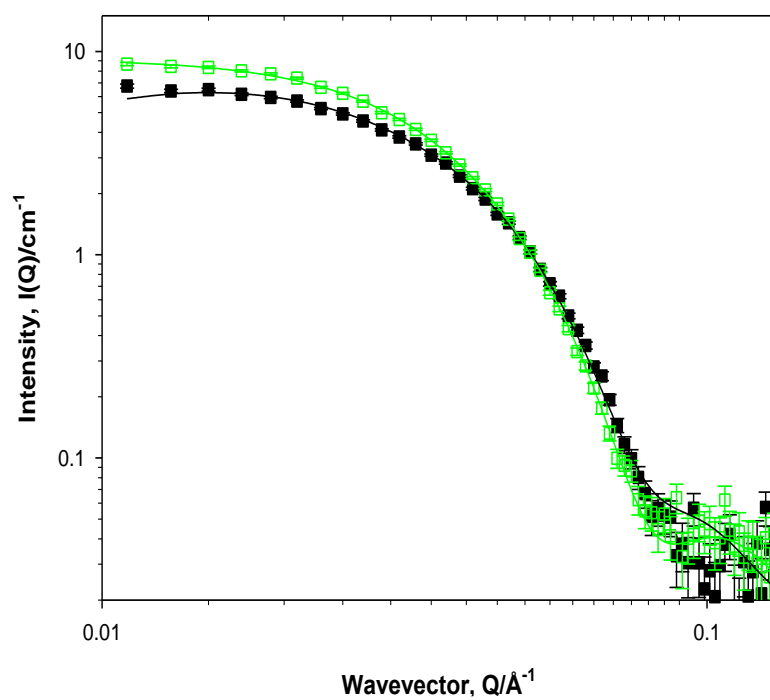
Figure 2.7 SANS from 0.5 wt % P123 and 5 mM [h-C$_{12}$TAB] = empty squares, 5 mM [d-C$_{12}$TAB] = filled squares in D$_2$O.

Applying the same analysis to these systems in the presence of alcohols, provides a further understanding to the role of the solvent partitioning in controlling the interactions, Table 2.7. When 1 wt% ethanol is added to the mixed system of $C_{12}TAB$ and P123, the subtle effect of ethanol becomes greater, yielding a higher $C_{12}TAB$ fraction ($\alpha(C_{12}TAB)$ =35($\pm$ 5) %) in comparison to the P123-$C_{12}TAB$ in D_2O case, α ($C_{12}TAB$) = 11($\pm$ 5) %.

Adding 1 wt% ethanol to the P123-SDS system, ($\alpha(SDS)$ = 28($\pm$ 5) %), the P123-SDS effect wins over the effect of the ethanol, without showing any significant changes in the SDS fraction.

The P123-SDS effect still wins over the further increase in the hydrophobicity of the alcohol, as the fraction of SDS does not change significantly. However, the alcohols effect still wins over the P123-$C_{12}TAB$ effect, where the fraction of $C_{12}TAB$ shows a noticeable change, Table 2.7.

System description	0 wt%	1 wt% ethanol	0.1 wt% hexanol	0.01 wt% decanol
0.5wt% P123/5 mM SDS	31	28	30	31
0.5wt% P123/5 mM $C_{12}TAB$	11	35	31	14

Table 2.7 Mixed micelle composition in terms of small molecule surfactant fraction, α ($\pm$5) %, as a function of alcohol concentration.

The model developed by Nagarajan[51] and Nikas *et al.*[52] for mixed, charged surfactant micelles allows us to frame the discussion on the effect of the added alcohol on the mechanisms driving the interactions in these systems. The model states that the free energy of formation for mixed aggregates has a number of contributing terms: the deformation of the surfactant tail as it conforms to packing requirements within the micellar core; the energy of forming the aggregate core/solvent interface which depends on the aggregation number and the presence of any alcohol; and a term that accounts for the headgroup interactions over the micellar surface, again defined by the composition of this region. Further terms must be included to account for the free energy of the polymer, including any change in entropy induced by the different packing of the polymer within the mixed micelle compared to the pure micelle, plus any changes induced in the interfacial energy terms due to the displacement of solvent by polymer in the micellar shell.

Making the assumption that the interfacial tension of the aggregate core/continuous phase follows the same trend as the surface tension of the bulk solution, the energy required to produce the interface decreases on addition of alcohol, favouring micelle formation: the CMCs of SDS and C_{12}TAB decrease with added alcohols. The term which considers the ionic headgroup interactions is a complex one, which cannot be estimated simply. A number of factors come into play in determining the energies of the headgroup interactions, including the dielectric constant, Debye length, the radius of the micelle and the presence of the polymer. For instance, the dielectric constant of the solution decreases in the presence of alcohol, which in turn influences the various charge effects such as counterion dissociation (hence the size and shape of the micelle), changes in the level of hydration of the ethylene oxide (EO) groups, as well as composition dependent micelle/solvent interfacial tension. Work is on-going to identify and model the magnitudes of these various effects, but a first step in this process is the determination of the polymer/small molecule surfactant micelle dimensions. It is hoped that this work will stimulate further effort on this area.

2.5 Conclusions

The effect of small molecule surfactants and alcohols on the aggregation behaviour of Pluronic P123 has been widely studied due to their extensive use in industry.[1–7] Aqueous/alcohol mixtures comprising the polymeric (Pluronic) surfactant P123, anionic SDS, cationic $C_{12}TAB$ and non-ionic Brij 35 have been characterised by using tensiometry, PGSE-NMR and SANS. The results are presented firstly in terms of the ternary systems: (i) interaction between P123 in the presence of alcohols; (ii) interaction between P123 in the presence of surfactants; and (iii) the quaternary system.

The partitioning in the micelle has been quantified by PGSE-NMR where it also shows that larger aggregates with slow diffusion rates were formed after adding hexanol and decanol and faster diffusing aggregates were formed after the addition of ethanol. The partitioning is in good agreement with the literature values.[35,41]

The micelle size decreases with the addition of ethanol, but increases with both hexanol and decanol. The micelle shape is spherical in the absence of any alcohol, and interestingly, remains so in the presence of ethanol and decanol, but forms prolate micelles in the presence of hexanol. We suggest this is a balance between the site and degree of alcohol solubilisation: ethanol is located in the outer shell of the Pluronic micelle, the more hydrophobic hexanol and decanol are solubilised into the core.

The scattering data clearly report on micelle disruption by the small molecule surfactants. By comparing the relative changes in the scattering profiles, we found that SDS has the strongest interaction with P123,[11,43] followed by Brij 35 and then $C_{12}TAB$ which showed the weakest interaction.[49,50]

The addition of the alcohols to the Pluronic/small molecule surfactant solution has introduced further changes to the mixed micelle composition. The effects of the alcohol have been compared with the effect of mixing the pure surfactants, in terms of the micelle composition. For (the dilute) Pluronic/SDS cases, adding the different alcohols has little effect on the micelle composition, suggesting that there is a strong interaction between SDS and P123. For systems comprising P123 and $C_{12}TAB$, the $C_{12}TAB$ micelle mole fraction increases for all cases of alcohol, indicative of a weaker interaction between the small molecule surfactant and the Pluronic (consistent with the relative changes in CMC). This work has allowed us to extend our understanding of the interactions between different surfactants and will direct the design of further experiments where more complex systems will be investigated.

Bibliography

(1) Kaur, R.; Kumar, S.; Aswal, V. K.; Mahajan, R. K. Influence of Headgroup on the Aggregation and Interactional Behavior of Twin-Tailed Cationic Surfactants with Pluronics. *Langmuir* **2013**, *29*, 11821–11833.

(2) Booth, C.; Attwood, D. Effects of Block Architecture and Composition on the Association Properties of Poly (Oxyalkylene) Copolymers in Aqueous Solution. *Macromol. Rapid Commun.* **2000**, *527*, 501–527.

(3) Alexandridis, P.; Holzwarthf, J. F.; Hatton, T. A. Micellization of Poly (Ethylene Oxide) -Poly (Propylene Oxide) -Poly (Ethylene Oxide) Triblock Copolymers in Aqueous Solutions : Thermodynamics of Copolymer Association. *Macromolecules* **1994**, *27*, 2414–2425.

(4) Marinov, G.; Michels, B.; Zana, R. Study of the State of the Triblock Copolymer Poly (Ethylene Oxide)-Poly (Propylene Oxide)-Poly (Ethylene Oxide) L64 in Aqueous Solution. *Langmuir* **1998**, *14*, 2639–2644.

(5) Alexandridis, P.; Hatton, T. A. Block Copolymer Surfactants in Aqueous Solutions and at Interface: Thermodynamics , Structure , Dynamics , and Modeling. *Colloids Surfaces A Physicochem. Eng. Asp.* **1995**, *96*, 1–46.

(6) Griffiths, P. C.; Cheung, A. Y. F.; Finney, G. J.; Farley, C.; King, S. M.; Heenan, R. K.; Bales, B. L. Electron Paramagnetic Resonance and Small-Angle Neutron Scattering Studies of Mixed Sodium Dodecyl Sulfate and (Tetradecylmalono) Bis (N-Methylglucamide) Surfactant Micelles. *Langmuir* **2002**, *18*, 1065–1072.

(7) Nambam, J. S.; Philip, J. Effects of Interaction of Ionic and Nonionic Surfactants on Self-Assembly of PEO–PPO–PEO Triblock Copolymer in Aqueous Solution. *J. Phys. Chem. B* **2012**, *116*, 1499–1507.

(8) Li, Y.; Xu, R.; Bloor, D. M.; Holzwarth, J. F.; Wyn-Jones, E.; Couderc, S. The Binding of Sodium Dodecyl Sulfate to the ABA Block Copolymer Pluronic F127 (EO97 PO69 EO97): An Electromotive Force, Microcalorimetry, and Light Scattering Investigation. *Langmuir* **2000**, *16*, 10515–10520.

(9) Ivanova, R.; Lindman, B.; Alexandridis, P. Modification of the Lyotropic Liquid Crystalline Microstructure of Amphiphilic Block Copolymers in the Presence of Cosolvents. *Adv. Colloid Interface Sci.* **2001**, *89-90*, 351–382.

(10) Kabanov, A. V.; Batrakova, E. V.; Alakhov, V. Y. Pluronic® Block Copolymers as Novel Polymer Therapeutics for Drug and Gene Delivery. *J. Control. Release* **2002**, *82*, 189–212.

(11) Jangher, A.; Griffiths, P. C.; Paul, A.; King, S. M.; Heenan, R. K.; Schweins, R. Polymeric Micelle Disruption by Cosolvents and Anionic Surfactants. *Colloids Surfaces A Physicochem. Eng. Asp.* **2011**, *391*, 88–94.

(12) Linse, P.; Malmsten, M. Temperature-Dependent Micellization in Aqueous Block Copolymer Solutions. *Macromolecules* **1992**, *25*, 5434–5439.

(13) Griffiths, P. C.; Hirst, N.; Paul, A.; King, S. M. Effect of Ethanol on the Interaction between Poly (Vinylpyrrolidone) and Sodium Dodecyl Sulfate. *Langmuir* **2004**, *20*, 6904–6913.

(14) Nakashima, K.; Bahadur, P. Aggregation of Water-Soluble Block Copolymers in Aqueous Solutions: Recent Trends. *Adv. Colloid Interface Sci.* **2006**, *123-126*, 75–96.

(15) Ganguly, R.; Aswal, V. K.; Hassen, P. A.; Gopalakrishnan, I. K.; Kulshreshtha, S. K. Effect of SDS on the Self-Assembly Behavior of the PEO-PPO-PEO Triblock Copolymer (EO)20 (PO)70 (EO)20. *Langmuir* **2006**, *20*, 9843–9849.

(16) Hecht, E.; Mortensen, K. Interaction of ABA Block Copolymers with Ionic Surfactants: Influence on Micellization and Gelation. *J. Phys. Chem. B* **1995**, *88*, 4866–4874.

(17) Sarmoria, C.; Puvvada, S.; Blankschtein, D. Predicition of Critical Micelle Concentrations of Nonideal Binary Surfactant Mixtures. *Langmuir* **1992**, *8*, 2690–2697.

(18) Puvvada, S.; Blankschtein.D. Surfactants in Solutions. *Surfactants Solut.* **1991**, *11*, 95–111.

(19) Griffiths, P. C.; Paul, A.; Heenan, R. K. Role of Counterion Concentration in Determining Micelle Aggregation: Evaluation of the Combination of Constraints from Small-Angle Neutron Scattering, Electron. *J. Phys. Chem. B* **2004**, *108*, 3810–3816.

(20)   Desai, P. R.; Jain, N. J.; Sharma, R. K.; Bahadur, P. Effect of Additives on the Micellization of PEO/PPO/PEO Block Copolymer F127 in Aqueous Solution. *Colloids Surfaces A Physicochem. Eng. Asp.* **2001**, *178*, 57–69.

(21)   Sarkar, B.; Ravi, V.; Alexandridis, P. Micellization of Amphiphilic Block Copolymers in Binary and Ternary Solvent Mixtures. *J. Colloid Interface Sci.* **2013**, *390*, 137–146.

(22)   Hammouda, B. SANS from Pluronic P85 in D-Water. *Eur. Polym. J.* **2010**, *46*, 2275–2281.

(23)   Hansen, J.; Hayter, J. B. An Analytic Structure Factor for Macroion Solutions. *Mol. Phys.* **1981**, *42*, 109–118.

(24)   Hansen, J.; Hayter, J. B. A Rescaled MSA Structure Factor for Dilute Charged Colloidal Dispersions. *Mol. Phys.* **1982**, *46*, 651–656.

(25)   SasView. SasView. *http://www.sasview.org/* version 2.1, **2012**.

(26)   Bhattacharjee, J.; Verma, G.; Aswal, V. K.; Patravale, V.; Hassan, P. A. Microstructure, Drug Binding and Cytotoxicity of Pluronic P123–aerosol OT Mixed Micelles. *RSC Adv.* **2013**, *3*, 23080-23089.

(27)   Foster, B.; Cosgrove, T.; Hammouda, B. Pluronic Triblock Copolymer Systems and Their Interactions with Ibuprofen. *Langmuir* **2009**, *25*, 6760–6766.

(28)   Joshi, J. V.; Aswal, V. K.; Goyal, P. S. Small Angle Neutron Scattering Study of Mixed Micelles of Oppositely Charged Surfactants. *Pramana* **2008**, *71*, 1039–1043.

(29)   Occhipinti, P.; Griffiths, P. C. Quantifying Diffusion in Mucosal Systems by Pulsed-Gradient Spin-Echo NMR. *Adv. Drug Deliv. Rev.* **2008**, *60*, 1570–1582.

(30)   Stilbs, P.; Paulsen, K.; Griffiths, P. C. Global Least-Squares Analysis of Large, Correlated Spectral Data Sets: Application to Component-Resolved FT-PGSE NMR Spectroscopy. *J. Phys. Chem. B* **1996**, *3654*, 8180–8189.

(31)   Stilbs, P. Micellar Breakdown by Short-Chain Alcohols. A Multicomponent FT-PGSE-NMR Self-Diffusion Study. *J. Colloid Interface Sci.* **1982**, *89*, 547–554.

(32) Cifuentes, A.; Bernal, J. L.; Diez-Masa, J. C. Determination of Critical Micelle Concentration Values Using Capillary Electrophoresis Instrumentation. *Anal. Chem.* **1997**, *69*, 4271–4274.

(33) Lin, S.; Lin, Y.; Chen, E.; Hsu, C.; Kwan, C. A Study of the Equilibrium Surface Tension and the Critical Micelle Concentration of Mixed Surfactant Solutions. *Langmuir* **1999**, *15*, 4370–4376.

(34) Flockhart, B. D. The Critical Micelle Concentration of Sodium Dodecylsulfate in Ethanol-Water Mixtures. *J. Colloid Interface Sci.* **1957**, *565*, 557–565.

(35) Patel, V.; Dey, J.; Ganguly, R.; Kumar, S.; Nath, S.; Aswal, V. K.; Bahadur, P. Solubilization of Hydrophobic Alcohols in Aqueous Pluronic Solutions: Investigating the Role of Dehydration of the Micellar Core in Tuning the Restructuring and Growth of Pluronic Micelles. *Soft Matter* **2013**, *9*, 7583–7591.

(36) Alexander, S.; Cosgrove, T.; Castle, T. C.; Grillo, I.; Prescott, S. W. Effect of Temperature , Cosolvent , and Added Drug on Pluronic − Flurbiprofen Micellization. *J. Phys. Chem. B* **2012**, *116*, 11545–11551.

(37) Alexandridis, P.; Yang, L. SANS Investigation of Polyether Block Copolymer Micelle Structure in Mixed Solvents of Water and Formamide, Ethanol, or Glycerol. *Macromolecules* **2000**, *33*, 5574–5587.

(38) Kumar, S.; Aswal, V. K. Tuning of Nanoparticle-Surfactant Interactions in Aqueous System. *J. Phys. Condens. Matter* **2011**, *23*, 1–8.

(39) Slawecki, T.; Glinka, C.; Hammouda, B. Shear-Induced Micellar Crystal Structures in an Aqueous Triblock Copolymer Solution. *Phys. Rev. E* **1998**, *58*, 4084–4087.

(40) Pedersen, J. S.; Svaneborg, C. Scattering from Block Copolymer Micelles. *Curr. Opin. Colloid Interface Sci.* **2002**, *7*, 158–166.

(41) Soni, S. S.; Brotons, G. Quantitative SAXS Analysis of the P123/water/ethanol Ternary Phase Diagram. *J. Phys. Chem. B* **2006**, *110*, 15157–15165.

(42) Manet, S.; Lecchi, A. Structure of Micelles of a Nonionic Block Copolymer Determined by SANS and SAXS. *J. Phys. Chem. B* **2011**, *115*, 11318–11329.

(43) Jansson, J.; Schillén, K. Small-Angle X-Ray Scattering, Light Scattering, and NMR Study of PEO-PPO-PEO Triblock Copolymer/cationic Surfactant Complexes in Aqueous Solution. *J. Phys. Chem. B* **2005**, *109*, 7073–7083.

(44) Hecht, E.; Hoffmann, H. Interaction of ABA Block Copolymers with Ionic Surfactants in Aqueous Solution. *Langmuir* **1994**, *14*, 86–91.

(45) Bales, B. L.; Zana, R. Characterization of Micelles of Quaternary Ammonium Surfactants as Reaction Media I: Dodeclytrimethylammonium Bromide and Chloride. *J. Phys. Chem. B* **2002**, *106*, 1926–1939.

(46) Tomšič, M.; Bešter-Rogač, M.; Jamnik, A.; Kunz, W.; Touraud, D.; Bergmann, A.; Glatter, O. Ternary Systems of Nonionic Surfactant Brij 35, Water and Various Simple Alcohols: Structural Investigations by Small-Angle X-Ray Scattering and Dynamic Light Scattering. *J. Colloid Interface Sci.* **2006**, *294*, 194–211.

(47) Couderc, S.; Li, Y.; Bloor, D. M.; Holzwarth, J. F. Interaction between the Nonionic Surfactant Hexaethylene Glycol Mono- N -Dodecyl Ether (C12EO6) and the Surface Active Nonionic ABA Block Copolymer Pluronic F127 (EO97 PO69 EO97) Formation of Mixed Micelles Studied Using Isothermal Titration Calorimetry. *Langmuir* **2001**, *77*, 4818–4824.

(48) Löf, D.; Tomšič, M. Structural Characterization of Nonionic Mixed Micelles Formed by C12EO6 Surfactant and P123 Triblock Copolymer. *J. Phys. Chem. B* **2009**, *113*, 5478–5486.

(49) Schwuger, M. J. Mechanism of Interaction between Ionic Surfactants and Polyglycol Ethers in Water. *J. Colloid Interface Sci.* **1973**, *43*, 491–498.

(50) Mata, J.; Joshi, T.; Varade, D.; Ghosh, G.; Bahadur, P. Aggregation Behavior of a PEO–PPO–PEO Block Copolymer + Ionic Surfactants Mixed Systems in Water and Aqueous Salt Solutions. *Colloids Surfaces A Physicochem. Eng. Asp.* **2004**, *247*, 1–7.

(51) Nagarajan, R. In: Structure-Performance Relationships in Surfactants. In *Structure-Performance Relationships in Surfactants*; Chapters 1 and 12, MarcelDekker: New York, 1997.

(52) Nikas, Y.; Blankschtein, D. Complexation of Nonionic Polymers and Surfactants in Dilute Aqueous Solutions. *Langmuir* **1994**, *10*, 3512–3528.

Chapter 3

3. Temperature and concentration induced gelation of triblock copolymers as viewed by SANS

3.1 Abstract

The structure and the phase behaviour of gels from triblock copolymers Pluronic P123 and F108 and their mixtures in deuterium oxide have been studied using small-angle neutron scattering (SANS) as a function of temperature and concentration. SANS data showed that for systems below the critical gelation concentration/temperature (CGC and CGT), significant inter-particle interactions were present, represented by strong structure factor peaks. When gels were formed (above the CGC and the CGT), diffraction peaks were observed, indicating ordering of the micelles. P123 gel structure was found to be dominated by multiple phases, but for some of the conditions studied, body centred cubic (bcc), hexagonally close packed (hcp) and lamellar structures were observed. F108 structure stayed largely of a bcc nature and did not show any changes as the temperature increased. The addition of small amounts of F108 (25%) to P123 systems, resulted in the destabilisation of lamellar phases, and hcp structures were favoured. As the relative amount of F108 was increased (50% and 75%), face centred cubic (fcc) and bcc structures were observed.

Chapter 3. Temperature and concentration induced gelation of triblock copolymers as viewed by SANS

3.2 Introduction

Amphiphilic block copolymers of the poly (ethylene oxide)–poly (propylene oxide)-poly (ethylene oxide) (PEO–PPO-PEO) group, commonly known as Pluronic® (BASF) or Poloxamer (ICI), are widely used in numerous formulations, especially the pharmaceutical, consumer and technological areas. These polymers have received considerable interest due to their low toxicity profiles and colloidal behaviour.[1–4] Pluronic solubility has shown sensitivity to temperature changes via the critical micelle temperature (CMT), which consequently affects its self-assembly, micelle size and structure.[5–7]

We have previously probed the interactions between P123 micelles, small molecule surfactants (SMS) and alcohols, where we demonstrated that the partitioning of both the SMS and the alcohol between the hydrophilic PEO corona and the hydrophobic PPO core, plays a significant role in controlling the P123 micelle size and shape (Chapter 2). Furthermore, the charge and the size of the headgroup of the SMS affects the size and the shape of the mixed micelle.[8,9]

At sufficiently high concentrations, Pluronics have been reported to form lyotropic liquid crystal phases, evidenced by a high viscosity hydrogel type behaviour.[10–14] Hydrogels formed by these polymers have been the focus of many studies due to their sol-gel transition induced by several stimuli as temperature, pH and light. This makes them attractive for applications in drug delivery systems, bio-adhesives manufacturing and personal care products given their high biocompatibility.[15,16]

Most hydrogels are formed as a result of the swelling of a network of covalently cross-linked polymer chains above a so called critical gelation concentration (CGC). The mechanism of gelation of triblock copolymers investigated here is through the formation of reversible entanglements between the coronae of neighbouring micelles.[17] These reversible entanglements are due to the absence of the previously mentioned covalent cross linking between the micelles, and as a result of these reversible mechanisms, the systems are quite versatile and could interchange from simple structures such as spherical micelles into more complex thermosensitive structures (cubic, lamellar, *etc.*).[12,13,18,19]

43

Chapter 3. Temperature and concentration induced gelation of triblock copolymers as viewed by SANS

Most of the Pluronic gel applications, especially the pharmaceutical and pharmacological applications, are temperature sensitive and it is very important to be able to "tune" and quantify the CMT and the critical gelation temperature (CGT). Such tuning could be achieved with more than one approach. Pragatheeswaran et al.[20] and Gilbert et al.[21] have reported changes in the CMT and the CGC of Pluronic F127 in the presence of the homopolymer poly(ethylene oxide) (PEO) with different chain lengths and concentrations. The authors demonstrated that the CMT of F127 always decreases in the presence of PEO irrespective of the homopolymer chain length. While a loss or a delay in the gelation for the same Pluronic was observed in the presence of high molecular weight PEO due to the formation of micellar clusters with heterogeneity of size, leading to a hindering effect on the micellar ordering.

Jiang et al.[22] investigated the effect of the physiologically relevant additives such as the inorganic salts sodium chloride (NaCl) and calcium chloride (CaCl$_2$) on F127 gel. The authors have shown that as the salt concentration increases, a slight decrease in the CGT was observed. They attributed this to the higher affinity of the water molecules to the salt ions, if compared with the affinity of the water molecules to the polymer.

Pluronic gels have been extensively studied before, but far fewer studies have focused on the changes observed in the structure and the gelation behaviour of Pluronic binary mixtures as a function of temperature. Artzner et al.[18] have investigated the interactions between P85 and F88 (both with similar PPO block, but different PEO chains, (Appendix B) in solution and gel state by differential scanning calorimetry (DSC), small-angle X-ray scattering (SAXS) and rheology. For P85 gels, a multiple phase of face-centred cubic phase (fcc) and hexagonally close packed (hcp) was observed at the CGT, while for F88, a single phase of body-centred cube (bcc) was reported. Mixtures from both polymers at different ratios yielded phases that were mainly dominated by the structure of F88 (bcc). A cartoon presentation of these phases is shown in Figure 3.1.
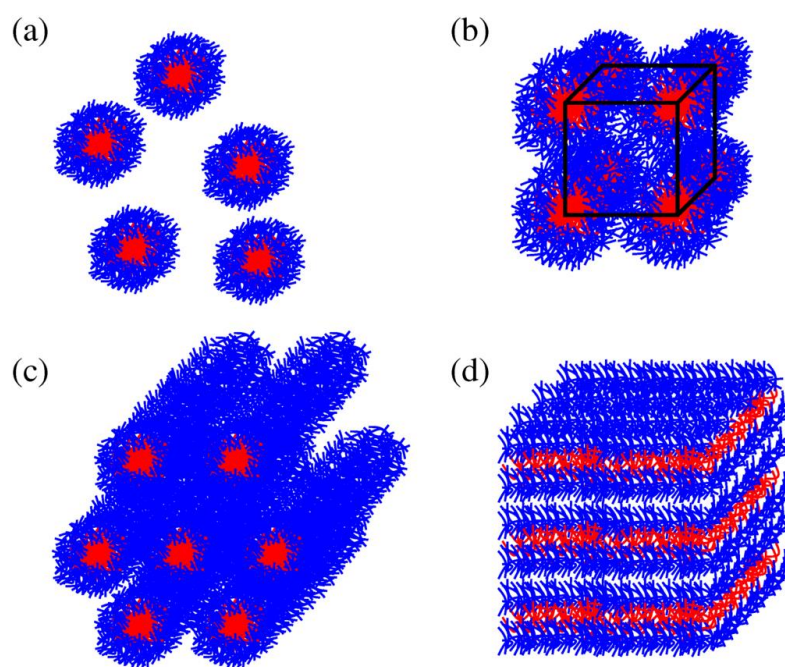
Figure 3.1 Schematic drawings of the (a) micellar, (b) cubic, (c) hexagonal and (d) lamellar structures from triblock copolymers in water.[23]

Gels formed by mixtures of P123 and F127 with different ratios have been studied by Chaibundit et al.[24] by light scattering, polarised microscopy and rheology at different temperatures. The authors concluded that the CGC increases as the P123 ratio increases. They also reported some insight into the structures formed by the gels, where mainly two structures were observed (cubic and hexagonal) verified by the presence of birefringence (for hexagonal sturctures) when examined by polarized light microscopy as a function of temperature.

Newby et al.[13] have used rheo-SAS (combined rheology and small-angle scattering) to study the structure and the shear alignment of P123 and P85 mixtures at different temperatures. The authors investigated the gel structures from these polymers and their mixtures at 50/50 ratio; 50/50 mixtures at 35 wt% showed a crystalline structure of fcc at 36°C and upon increasing the temperature to 70°C, the structure observed changed to hcp. This behaviour was also observed for other concentrations of the 50/50 mixtures, however the temperature at which fcc structure was observed varied with concentration. The authors also reported that the cubic gels from these Pluronic mixtures have an enhanced stability in the high concentration region, in contrast to lesser stable systems; P123/F127.[24]

More recently, Oshiro *et al.*[25] studied the gelation behaviour of Pluronic F127 (PPO: PEO is 1:3) and L81 (intermediate lyophilicty, PPO: PEO is 7:1) single systems and binary mixtures, where the mixtures showed a decrease in the CGT compared to the single components. They also reported on the structure of gel, where for F127, the structure was found to be lamellar at 25°C and for all the mixture ratios with L81, the structure of the gel remained lamellar at this temperature, while changes in the structure (lamellar to hexagonal) were observed for systems at 37°C.

Against this background, a series of gels formed from P123 and F108 and their mixtures at different ratios of P123:F108, concentrations and temperatures were studied by SANS. In contrast to the conclusions reported in previous studies of gels from Pluronics with similar PPO blocks, but different PEO chains *e.g.* P123 and F127, where it was found that longer PEO chain destabilises the cubic phase,[13,24] we have observed the opposite for the majority of our systems in terms of the structures formed and the stability of the phases, however similarities in the gelation temperature changes as the system composition changes were noted. To our knowledge, there has been no other study on the properties and the structure of the gels from mixtures of P123 and F108.

3.3 Experimental

3.3.1 Materials

Pluronic P123 (30% PEO), PEO_{20}-PPO_{70}-$PEO_{20,}$ average molecular weight of 5800 $gmol^{-1}$ and Pluronic F108 (80% PEO), PEO_{128}-PPO_{54}-PEO_{128}, average molecular weight of 14800 g mol^{-1} (Aldrich) were used as received.

3.3.1.1 Sample preparation

All samples were prepared in D_2O at concentrations 20-40 wt%. Polymers were dissolved in D_2O using a rotary mixer placed in a cold room at 4°C and were then left to equilibrate for at least 24 hours at the same temperature. Three hybrids (H) of P123:F108 were prepared at three different ratios (75:25, 50:50 and 25:75) and concentrations (20, 30 and 40 wt %).

3.3.2 Methods

3.3.2.1 Small-angle neutron scattering (SANS)

SANS measurements were performed on the fixed-geometry, time of flight LOQ diffractometer (ISIS Spallation Neutron Source, Oxfordshire, UK). Neutron wavelengths spanning 2.2-10 Å were used to access a Q range ($Q = 4\pi \sin (\theta/2)/\lambda$) of approximately 0.008-0.25 Å^{-1} (25 Hz), with a fixed sample-detector distance of 4.1 m.

The samples were contained in 1 mm path length, UV-spectrophotometer grade, quartz cuvettes (Hellma) and then kept at 4°C (below the CGT) overnight in order to remove any shear induced crystalline structural changes (sample loading in the cell was done using syringes). The samples were then mounted in standard aluminium holders on top of an enclosed, computer-controlled, sample chamber. Scattering was recorded at temperatures spanning 10-70°C with equilibration time of at least 2 hours before the scattering was recorded at a specified temperature. Temperature control was achieved through the use of a thermostatted circulating bath pumping fluid through the base of the sample chamber. Under these conditions a temperature stability of better than ± 0.5°C can be achieved. Experimental measuring times were approximately 20 min.

All scattering data were normalised for the sample transmission and the incident wavelength distribution, corrected for instrumental and sample backgrounds using a quartz cell filled with D$_2$O (this also removes the incoherent instrumental background arising from vacuum windows, *etc.*), and corrected for the linearity and efficiency of the detector response using the instrument specific software package. The data were put onto an absolute scale using a well characterized partially deuterated polystyrene blend standard sample.

3.4 Results and Discussion

3.4.1 Analysis of SANS data

As mentioned earlier, it is well established that Pluronic gels can adopt several ordered phases such as hexagonal, lamellar and cubic structures. Table 3.1 shows the theoretical peak positions for most of these common structures along with the related positions to the main scattering peak. The relevant *d*-spacing, could be calculated from $d = 2\pi/Q$, where Q is the position of the first peak. The crystal lattice parameter, *a*, for cubic phases, where $a = b = c$, for fcc and bcc, could be calculated from the *d*-spacing related to the first scattering peak (d_{hkl}) as shown in equation 3.1.[26] In addition, the term representing the distance between adjacent micelles centres (D_{HS}) in cubic phases could be estimated from the first peak position using equation 3.2.[27]

The *a* parameter however is treated differently in the hcp systems and is equal to 2*r*, *r* being the radius of the micelle. Also for hcp structures, another important parameter is *c*, which is the distance between the centres of two micelles in the structure. Both parameters *a* and *c*, could be related by equation 3.3. The *c/a* ratio determines the origin of the hcp phase, *e.g.* if the value is equal to $\sqrt{(8/3)}$, this means that the hcp phase is derived from the organization of the spherical micelles.[18]

$$a = (h^2 + k^2 + l^2)^{1/2} d_{hkl} \tag{3.1}$$

$$D_{HS} = \frac{\pi\sqrt{6}}{Q} \tag{3.2}$$

$$2r = a = \left(\frac{a^2}{3} + \frac{c^2}{4}\right)^{1/2} \tag{3.3}$$

Unit all	Order of diffraction peak							
	1	2	3	4	5	6	7	8
Simple cubic	1.000 (100)	1.414 (110)	1.733 (111)	2.000 (200)	2.237 (210)	2.450 (211)	2.832 (220)	3.000 (221)
Face centred cubic	1.000 (111)	1.154 (200)	1.631 (220)	1.919 (311)	2.000 (222)	2.304 (400)	2.638 (331)	2.583 (420)
Body centred cubic	1.000 (110)	1.414 (200)	1.733 (211)	2.000 (200)	2.450 (222)	2.652 (321)	2.832 (400)	3.000 (330)
Hexagonally close-packed	1.000 (10)	1.733 (11)	2.000 (20)	2.645 (21)	3.000 (30)	3.460 (22)	3.703 (31)	4.000 (40)
Lamellae	1.000	2.000	3.000	4.000	5.000	6.000	7.000	8.000

Table 3.1 The relative peak positions, allowing for systematic absences, characterising some selected unit cells. The figures in brackets are the *hkl* indices of the reflection.

3.4.2 Phase behaviour of 20 wt% P123

For the measurements performed at 10°C, the data, Figure 3.2, shows typical scattering behaviour from core-shell systems that has been observed before by small-angle scattering from Pluronic micelles in solution.[8,28–31] The core-shell structure typically presents itself in the data in the form of the "bump" at mid Q, as a result of the difference in the contrast terms between the core and the shell. Between 20-50°C, the phase behaviour is largely micellar and the scattering data suggests the presence of significant inter-micelle interactions characterised by the strong presence of the structure factor peak at ≈ 0.03 Å^{-1}. The data at temperatures > 50°C show a different scattering behaviour *i.e.* very strong scattering intensity if compared with measurements performed at lower temperatures indicative of a phase change/transition.

The data at 70°C, is characterised by the emergence of a maximum at very low Q (0.013 Å^{-1}, *d*-spacing of ≈ 475 Å). The most compelling explanation to these significant changes in the scattering behaviour is that the higher temperatures, at least for these systems, induces a significant change in the structure. This may be attributed to a transition from spherical micelles to large cylindrical structures that are filling all the available volume. At 60°C, the peaks observed are not as well defined if compared with the case at 70°C; as the temperature increases, they become well defined.

That said, none of these peaks at both 60°C and 70°C are as well defined as a typical Bragg peak, hence indexing it to a certain structure, Table 3.1, was not possible which indicates the absence of any micellar ordering.

.
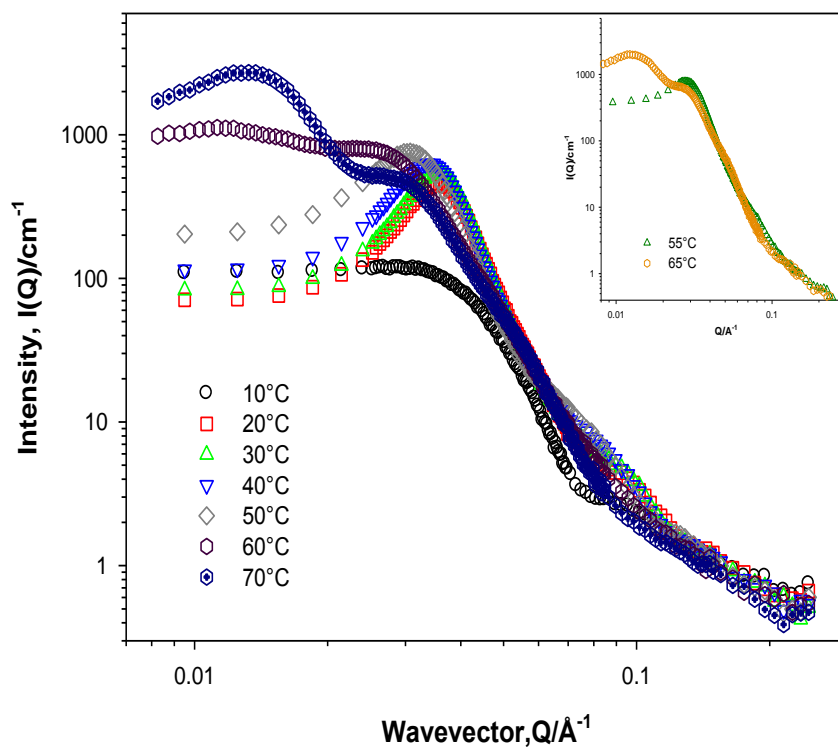
Figure 3.2 SANS from 20 wt% P123 as a function of temperature in D$_2$O. The inset shows the transition in the structure observed at 55°C and 65°C.

3.4.3 Phase behaviour of 30 wt% P123

At 30 wt% P123, the micellar phase is only observed at 10°C. For samples studied between 15-55°C, the data is characterised by the presence of strong Bragg peaks that slightly change position across the wavevector as a function of temperature (0.0423-0.0357 Å^{-1}) corresponding to d-spacing values of 150 Å and 175 Å respectively, Figure 3.3. The presence of these Bragg peaks is a signature of the macroscopic formation of the gel occurring as a result of the hard-sphere crystallisation of micelles.[32] At mid and high Q, the data shows up to two and occasionally three more orders of diffraction peaks that also change positions across the wavevector. It was not possible to observe more order of peaks at higher Q values due to the limited Q range of the instrument.

The peaks observed for 30 wt % P123 at 18°C, 20°C and 22°C are consistent with a bcc structure (1(*110*), 1.733(*211*), 2.000(*220*), 2.450(*222*)), similar to what have been reported for P123 previously at similar concentrations and temperatures.[13,14] However, the expected 1.414 (*200*) peak from a bcc structure could not be identified in this case, this is most probably due to defects in the crystalline structure. The parameters of the bcc phase (volume, micelle size, D_{HS} and *d*-spacing) did not vary, which is possibly due to the small difference in the temperature range at which the structure was observed, Table 3.2.

Between 22°C and 45°C, the structure remains largely multiphasic. This agrees with the previous work done by Wanka *et al.*[33] where multiple phases from P123 gels have been reported at 20 and 30 wt% P123 at temperatures above 40°C. At 50°C and 55°C, the peaks were attributed to lamellar structures (1.000, 2.000*)*. Lamellar ordering from Pluronics have been reported before for F127 and P123 but at higher concentrations, ≥ 60 wt%, for the latter.[25,33] At temperatures ≥ 60°C, there is now less defined, weaker Bragg peaks at mid and high *Q,* indicative of the presence of a less ordered structure but with a strong structure factor. This could be attributed to the thermal breakdown of the gel as the temperature increases, as a result, the periodic ordering observed at lower temperatures is lost.
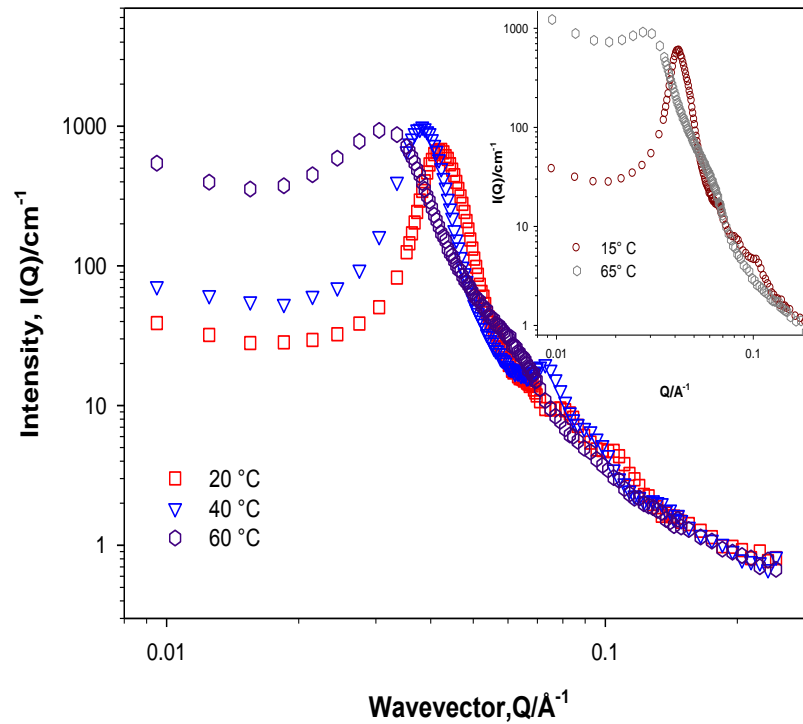
Figure 3.3 SANS from 30 wt% P123 as a function of temperature in D_2O. The inset shows the transition in the structure observed between 15°C and 65°C.

System	d (Å)	a (Å)	c (Å)	Volume(x 10^3 $\mathring{A}^3$)
30 wt%, 18°C	148	210	210	925
30 wt%, 20°C	148	210	210	925
30 wt%, 22°C	148	210	210	925

Table 3.2 bcc structure parameters of gels from P123 at 30 wt% as a function of temperature in D_2O.

3.4.4 Phase behaviour of 40 wt% P123

At 40 wt% P123, the micellar phase observed previously at lower temperatures, 10°C, is no longer seen. Bragg peaks were observed over all the temperature range (10°C to 70°C), Figure 3.4. In contrast to the 30 wt% case, the Bragg peaks do not lose their intensity or their definition as the temperature increases, indicating an enhanced resistance of the structure to temperature. The change in the Bragg peak positions and intensity as a function of temperature is however more pronounced in this case compared to the 30 wt% P123 case. This shift in the peak positions towards lower Q is indicative of larger structures. The Bragg peaks correspond to a d-spacing range between 130 Å and 195 Å for gels at 10°C and 70°C, respectively.

Pluronics are known to show an increase in micellar size with temperature.[34] This explains the observed increase in the d-spacing values. These changes in d-spacing cannot however be interpreted without relating them to the sharp changes in the structure of the gel; the structure starts with a multiple phase with fractions of bcc between 10°C and 25°C, and as the temperature increases (30°C to 50°C), it changes to hcp with d-spacing of 146 Å and 158 Å,respectively. The multiple phase/bcc to hcp transition is most probably related to the changes in the micelle shape from spherical to elongated.

In order to determine the volume of the hcp, one would need an estimate of the radius of the micelle at the relevant temperatures, this is indeed possible using SANS or dynamic light scattering (DLS). However, this is an unrealistic approach in the case of gels, the concentration being very high, it is not possible to perform these measurements on DLS, as for SANS, fitting the data to a core shell model will not be suitable, given also the significant inter-particle interaction, which renders the structure factor, $S(Q)$, term significant. The $S(Q)$ used in the core-shell model is valid only for solutions with low volume fraction of particles.

Chapter 3. Temperature and concentration induced gelation of triblock copolymers as viewed by SANS

At temperatures > 50°C, the structure now shows lamellar behaviour as seen with the 30 wt% P123 case, with a strong increase in the *d*-spacing values ≈195 Å. A phase diagram of P123 is shown in Figure 3.5. The dynamics behind the transition from one phase to another as the temperature, concentration and system composition are varied will be discussed in detail in a later section.
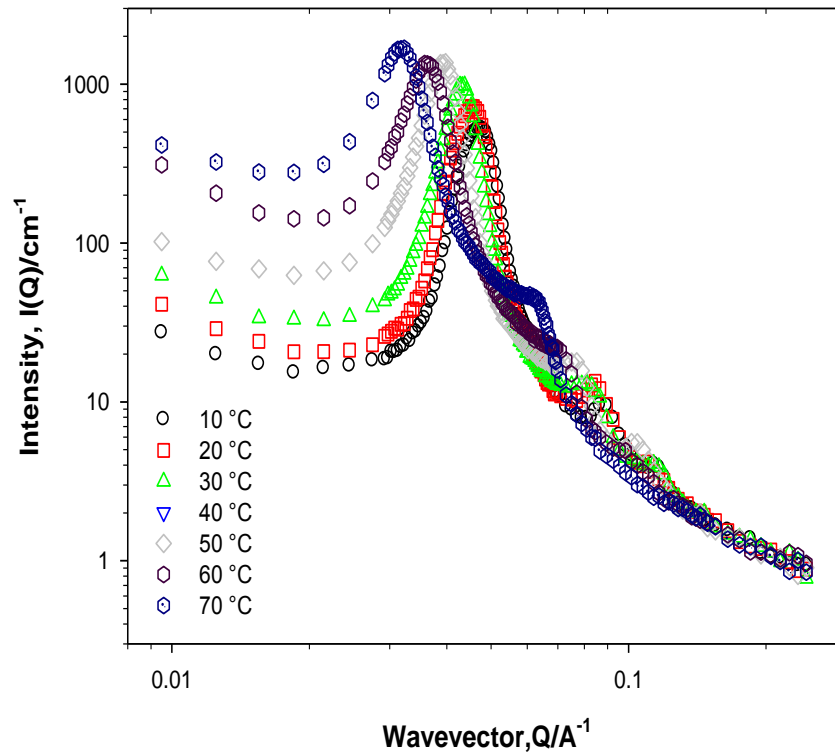
Figure 3.4 SANS from 40 wt% P123 as a function of temperature in D$_2$O.
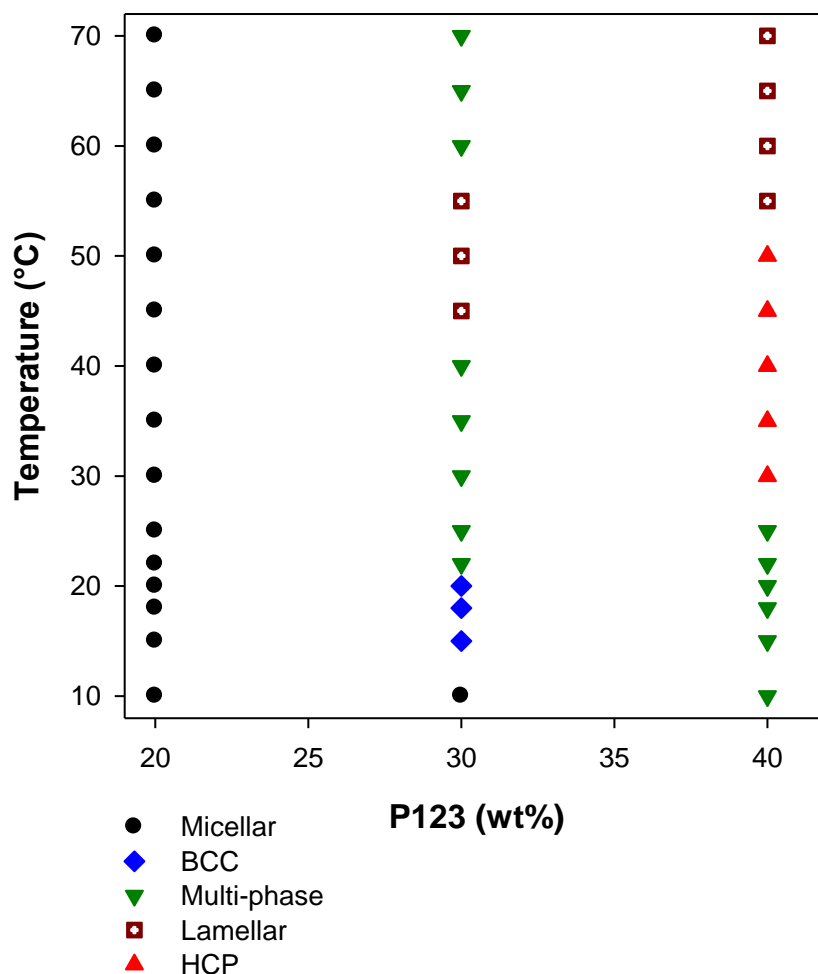
Figure 3.5 Phase diagram of P123

3.4.5 Phase behaviour of F108

In contrast to P123, F108 gels possess mainly two structures, micellar (above the CMT) and cubic gels. For 20 wt% F108 at 10-20°C, the scattering shows that no micelles are present, as those temperatures are below the CMT for F108, Figure 3.6. As the temperature increases, 20-25°C, typical scattering behaviours from surfactant micelles are observed. However, they do not seem to be well defined core-shell systems as P123 based micelles. At temperatures > 25°C, gels with cubic structures are formed and interestingly the structure remains largely so, regardless of any temperature variations up to 70°C. bcc/fcc structures have been previously reported from F127,[35] however, no previous SANS studies have focused on the structures of the gels from F108.
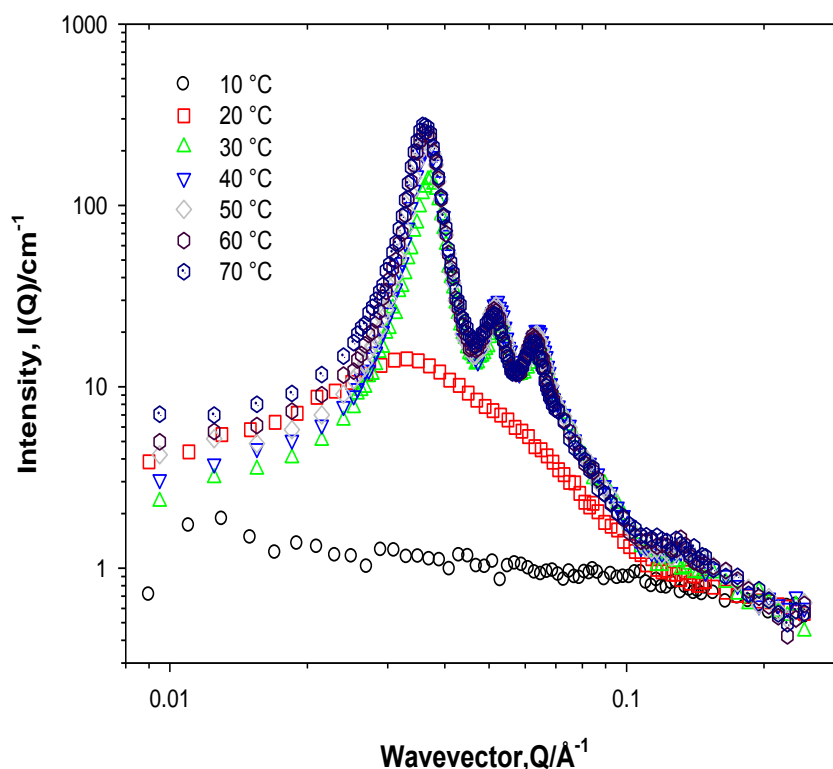
Figure 3.6 SANS from 20 wt% F108 as a function of temperature in D$_2$O.

At 30 wt% F108, between 10°C and 22°C, scattering from micelles is observed with similar features as in the 20 wt% case, Figure 3.7. Above 22°C, cubic gels are observed. At 40 wt%, the only difference noticed from the previous concentrations, is that scattering from micelles in solution is no longer observed at any temperatures, Figure 3.8. This is similar to the scattering behaviour from 40 wt% P123 and quite expected, given that the concentration of the polymer is now very high. A phase diagram summarising the structures observed is shown in Figure 3.9.

In regards to the nature of the gel structure, it is worth mentioning that the slight shift of the Bragg peak towards lower Q has yielded subtle changes in the lattice parameters, especially in the 20 wt% case, which eventually had some impact on the volume of the lattice. The changes in these parameters are shown in Table 3.3.
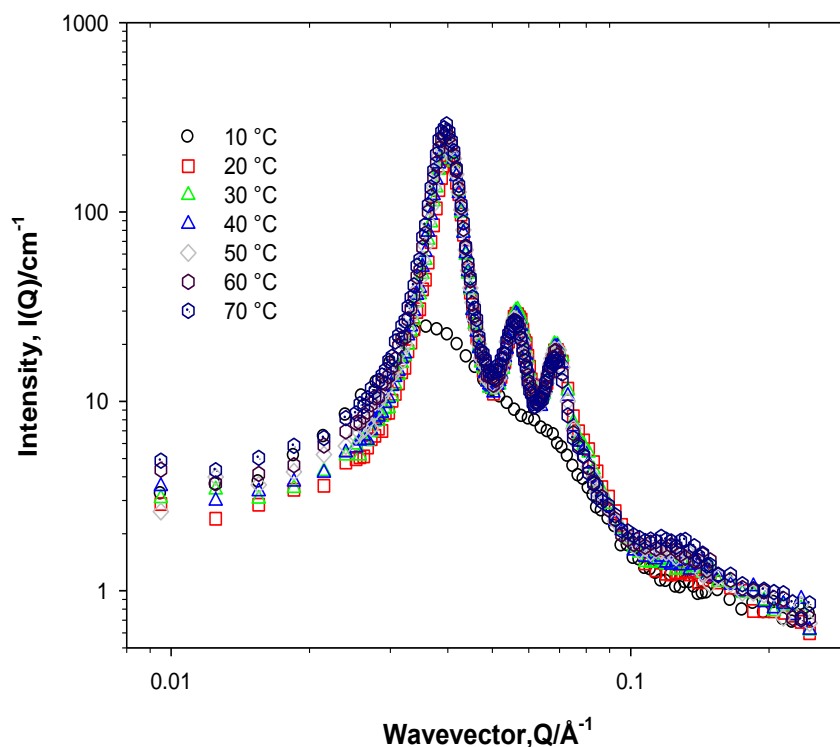
Figure 3.7 SANS from 30 wt% F108 as a function of temperature in D$_2$O.

If compared with the parameters obtained for P123 systems, Table 3.2, gels from F108 show quite a different behaviour. In pure P123 systems, where bcc was observed, no change in either the lattice parameter *a* or in the volume of the lattice as a function of temperature (18-22°C) or the concentration was observed. However, the effect of temperature/concentration variations is evident in F108 gels. This could be analysed by several approaches. (i) For 20 wt% F108 systems, the *a* parameter is directly affected by the temperature, and as the temperature increases, the parameter value increases with a subsequent increase in the volume of the lattice. This is accompanied by an expected increase in the D_{HS}. (ii) The *a* parameter decreases as the concentration of the Pluronic increases, for instance, at 30°C, 20 wt% F108 shows an *a* parameter of 238 Å, for 30 wt % it shows 220 Å and 215 Å for 40 wt %.

This decrease in the *a* parameter could be attributed to the relation between the concentration of the polymer and the space available in the lattice to accommodate more micelles. (iii) Finally, the space availability and the difference in the structure geometry can also be observed through the changes in D_{HS}. For 20 wt% F108 at 30°C, the D_{HS} starts at 206 Å, and as the temperature increases, the D_{HS} increases as expected for Pluronics which are very sensitive to temperature.

What is more interesting however, is the change in the same parameter as the concentration of the same Pluronic increases at a constant temperature (30°C), *e.g.* 30 wt%. The D_{HS} is now at smaller value (193 Å), the value further decreases as the concentration goes to 40 wt% (185 Å). This again could be related to the space constrain and to the presence of more ordered lattices at higher concentrations, not allowing the micelle to retain its full dimensions.

The effect of the concentration on packing capacity is more obvious in the F108 case than the P123 case is possibly due to the difference in the thickness of the PEO corona between both Pluronics, which is larger for F108. One would expect that as the number of the F108 micelles increases, the PEO chains cannot be fully extended, and the overall dimension of the micellar structure would change leading decrease in the micelle radius.
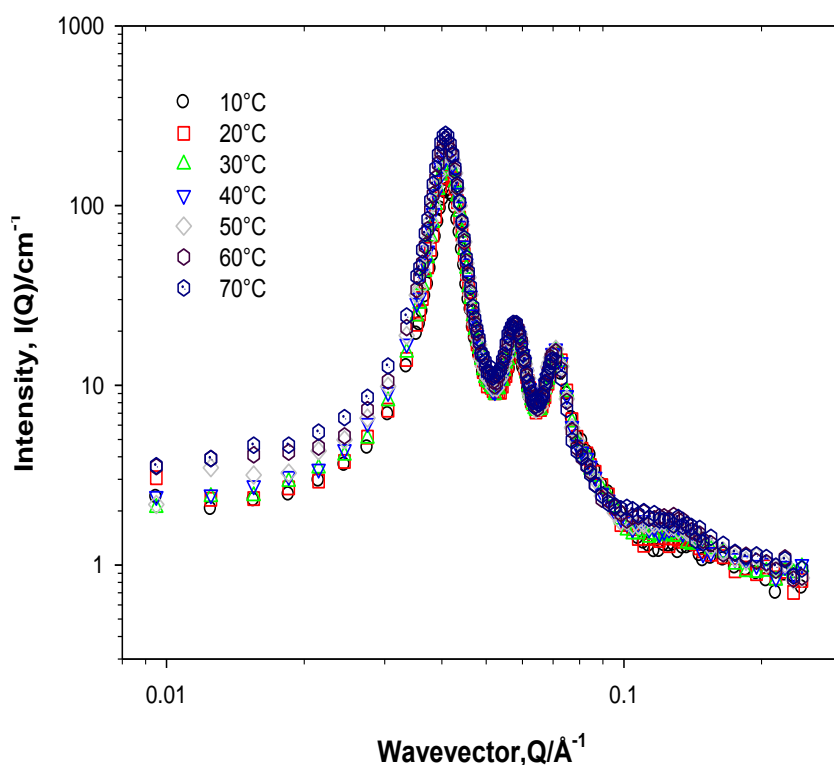
Figure 3.8 SANS from 40 wt% F108 as a function of temperature in D$_2$O.

System	a (Å)	Volume(x 10^6 Å^3)	D_{HS} (Å)
20 wt%, 30°C	238	13.8	206
20 wt%, 40°C	242	14.1	210
20 wt%, 50°C	242	14.1	210
20 wt%, 60°C	245	14.7	213
20 wt%, 70°C	220	10.6	193
30 wt%, 30°C	220	10.6	193
30 wt%, 70°C	220	10.6	193
40 wt%, 30°C	215	9.90	186
40 wt%, 70°C	217	10.2	189

Table 3.3 Structure parameters of bcc gels from F108 at different concentrations and temperatures in D₂O.
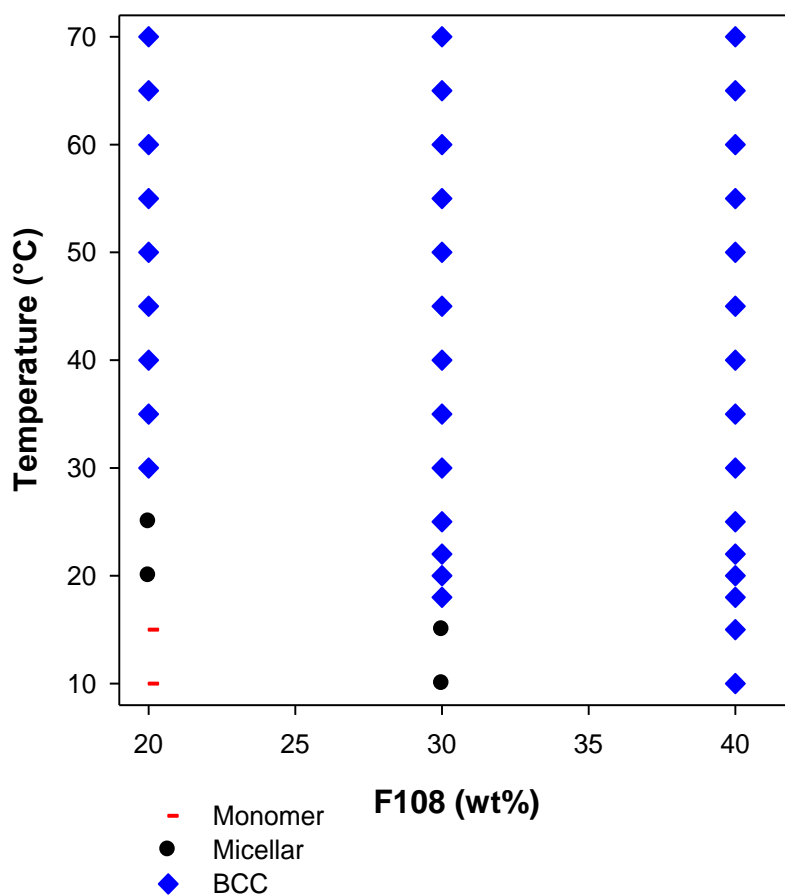
Figure 3.9 Phase diagram of Pluronic F108.

3.4.6 P123/F108 mixtures in D_2O

3.4.6.1 Phase behaviour of Hybrid 1(H1), P123:F108 (75:25) at 20 wt% and 30 wt%

Figure 3.10 shows the scattering from the mixed micelles at 20 wt% at different temperatures, and as the majority of the system is comprised of P123 (75%), the similarities between the scattering behaviour from H1 and P123 at the same concentration are not unexpected. These systems also exhibit a strong structure factor peak indicating significant inter-particle interactions.

At 30 wt% Hybrid 1 (H1), Figure 3.11, the scattering shows similar micellar behaviour as in the 20 wt% H1 case, Figure 3.10. This differs from the scattering from P123 at the same concentrations. Indeed, the P123 concentration in the mixture is at 22.5 wt%, but one would still expect the overall polymer concentration to induce gelation and ordering.
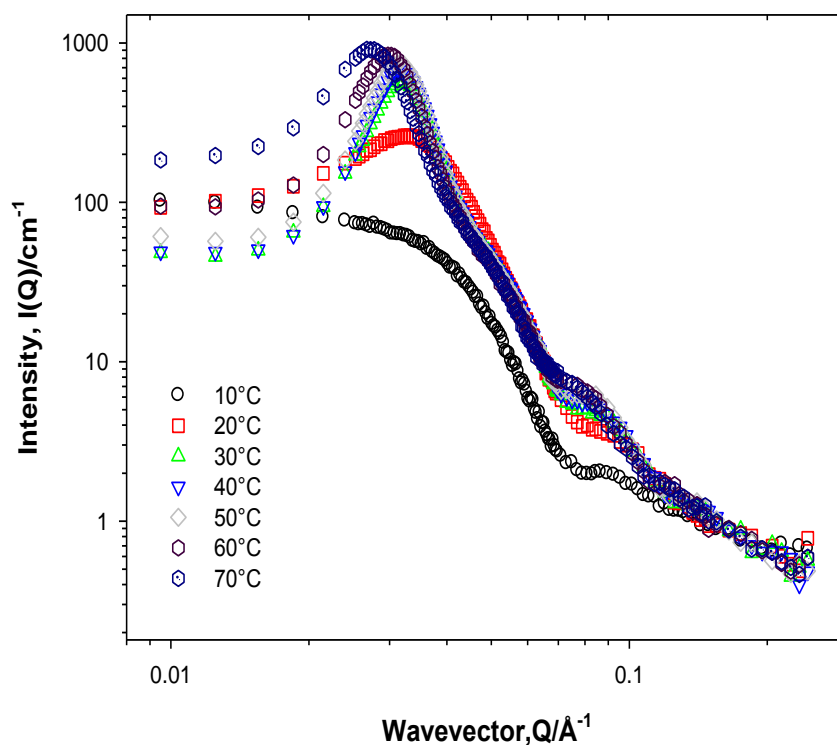
Figure 3.10 SANS from 20 wt% H1 as a function of temperature in D_2O.
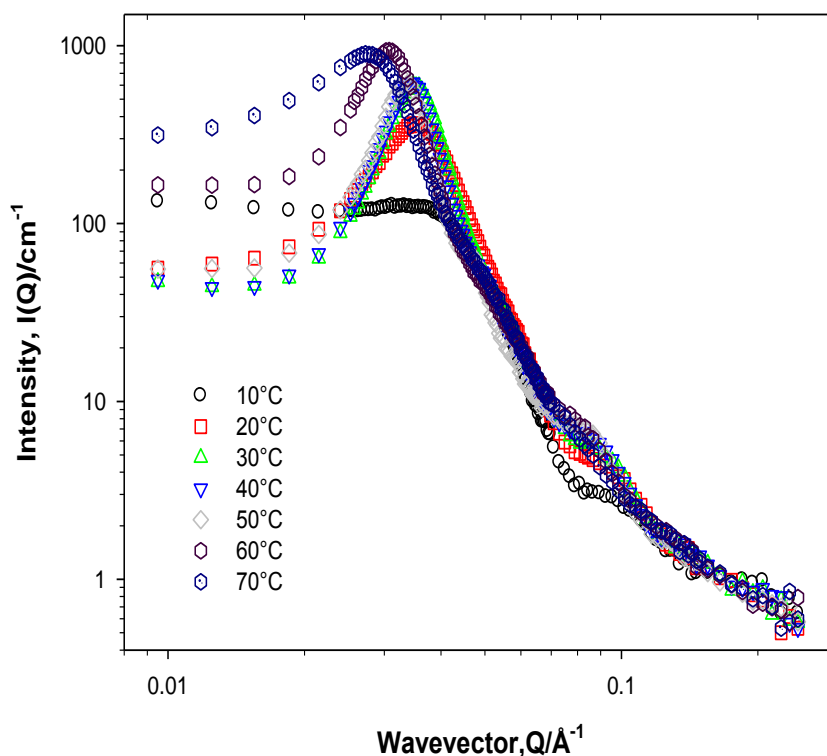
Figure 3.11 SANS from 30 wt% H1 as a function of temperature in D$_2$O.

3.4.6.2 Phase behaviour of Hybrid 1(H1), P123:F108 (75:25) at 40 wt%

The effect of F108 on the system is more significant in this case than the lower concentrations. If we draw a detailed comparison between the scattering behaviour from 30 wt% P123 and this hybrid, sharp changes in the crystalline structures are observed. These changes are presented, Figure 3.12 and in the phase diagram, Figure 3.13. As previously mentioned, the 30 wt% P123 phase behaviour was micellar only at 10°C, above this temperature, gelation occurred. At 15-22°C, a multiple phase and bcc were observed, but at higher temperatures, the structure was interchanging between what seemed to be largely multiphasic and lamellar structures.

The scattering behaviour from this hybrid is dominated by the presence of micelles up to 22°C (CGT increased), as the temperature increases (>22°C), a hcp structure presence is strongly evident, and this structure up to 65°C.

At 70°C, a loss of the ordering is observed, again, indicating some thermal breakdown of the gel structure. These observations show that the addition of small amounts of Pluronic with similar PPO but longer PEO chains (F108) contributed to the increase in the critical gelation temperature. This was accompanied by the destabilisation of the P123 lamellar structures (in both cases, 30 and 40 wt %) in favour of the hcp. This is possibly due to the steric constraints induced by the longer PEO chain leading to softer interactions between the micelles.
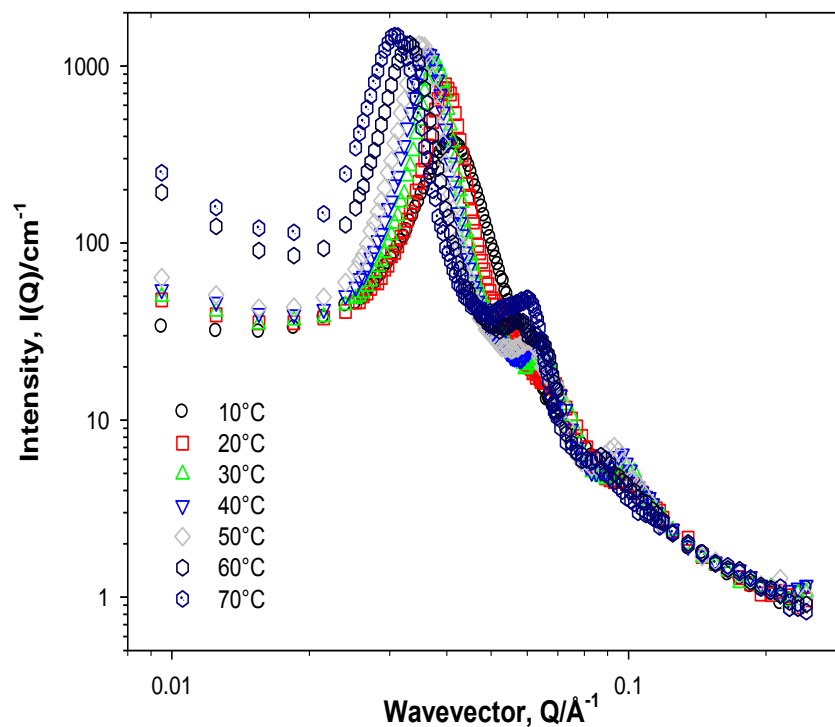
Figure 3.12 SANS from 40 wt% H1 as a function of temperature in D$_2$O.
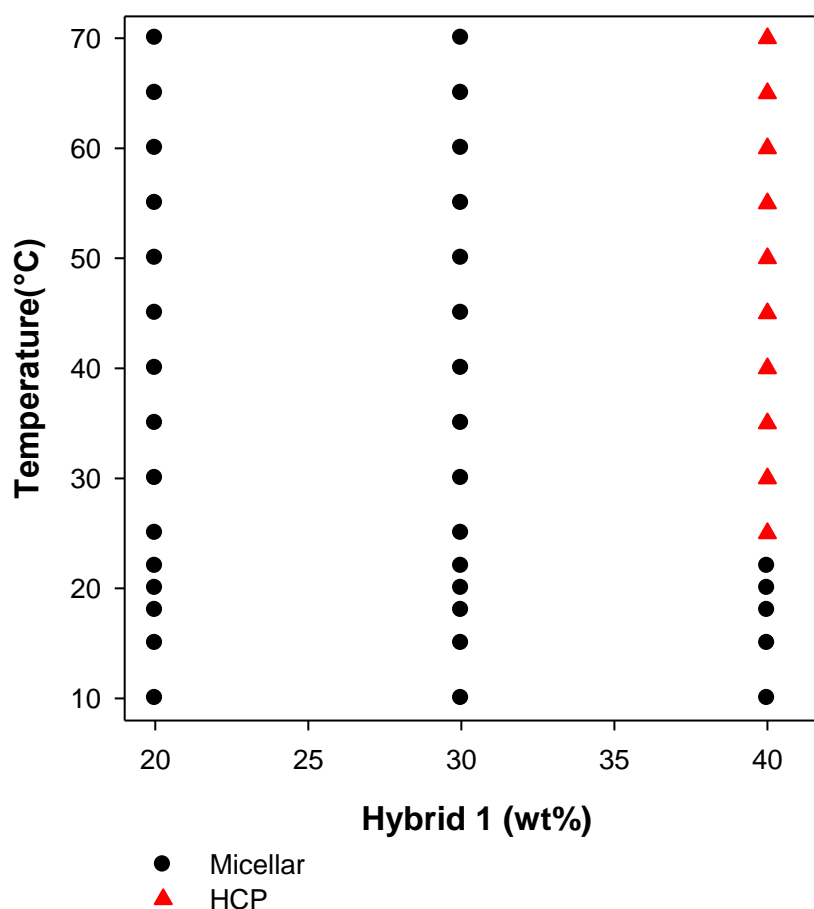
Figure 3.13 Phase diagram of Hybrid 1, P123:F108 (75:25)

3.4.6.3 Phase behaviour of Hybrid 2 (H2); P123:F108 (50:50) at 20 wt%

Of main interest here is the emergence of fcc structure relative peaks at 0.0298 $Å^{-1}$, 0.048 $Å^{-1}$ and 0.0548 $Å^{-1}$ in the SANS data, Figure 3.14, at temperatures above 20°C. This is a rather interesting observation, given that neither 10 wt% P123 nor 10 wt% F108 (at least at low to medium temperatures) has shown to form any gels previously, these observation are indeed as a result of the overall concentration of the polymer, rather than an individual control of the structure by one of the two polymers as was the case in Hybrid 1. These previous observations are strongly suggesting that the difference in the PEO chain between both P123 and F108 is the reason behind the formation of the fcc structures. The structure showed minimal sensitivity to the temperature and the lattice parameter remained unchanged as the temperature increased; *d*-spacing of 215 Å and *a* of 375 Å. Figure 3.15 shows the phase diagram obtained with H2 at 20 wt%, where the critical gelation temperature is > 20°C.

One would expect that a structure favouring an fcc arrangement, would be of micelles with a large PPO core and a short PEO shell, behaving like a polymer brush, exhibiting a short range repulsion. This is not the case here, as the shell is expected to comprise both long and short PEO chains. Further investigations are needed to obtain a detailed structure of both the core and shell to deduce the dynamics behind the fcc structure formation in gels from this specific hybrid.
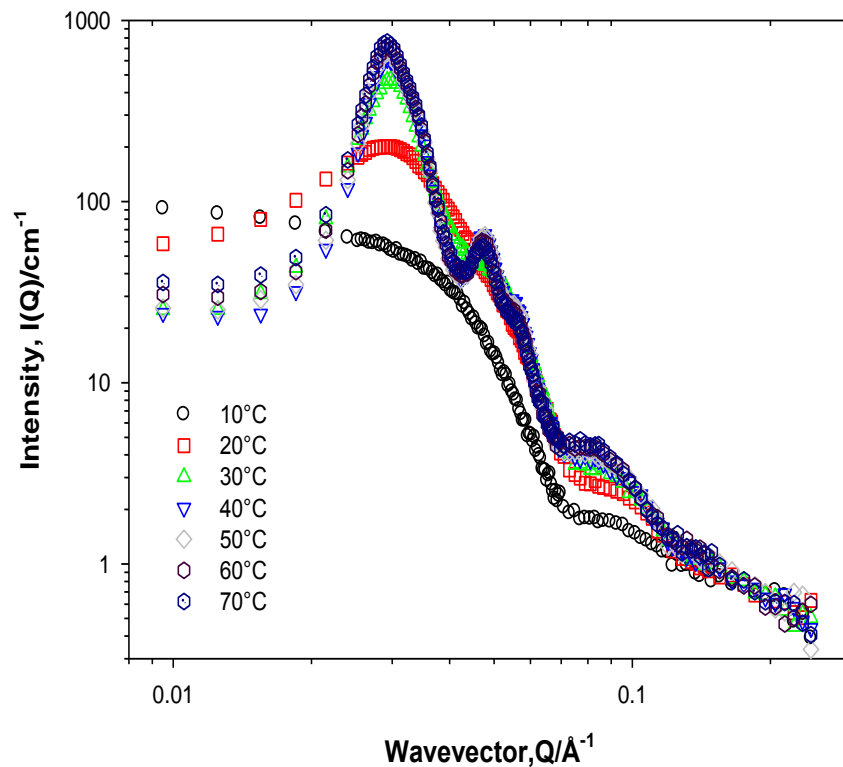
Figure 3.14 SANS from 20 wt% H2 as a function of temperature in D$_2$O.
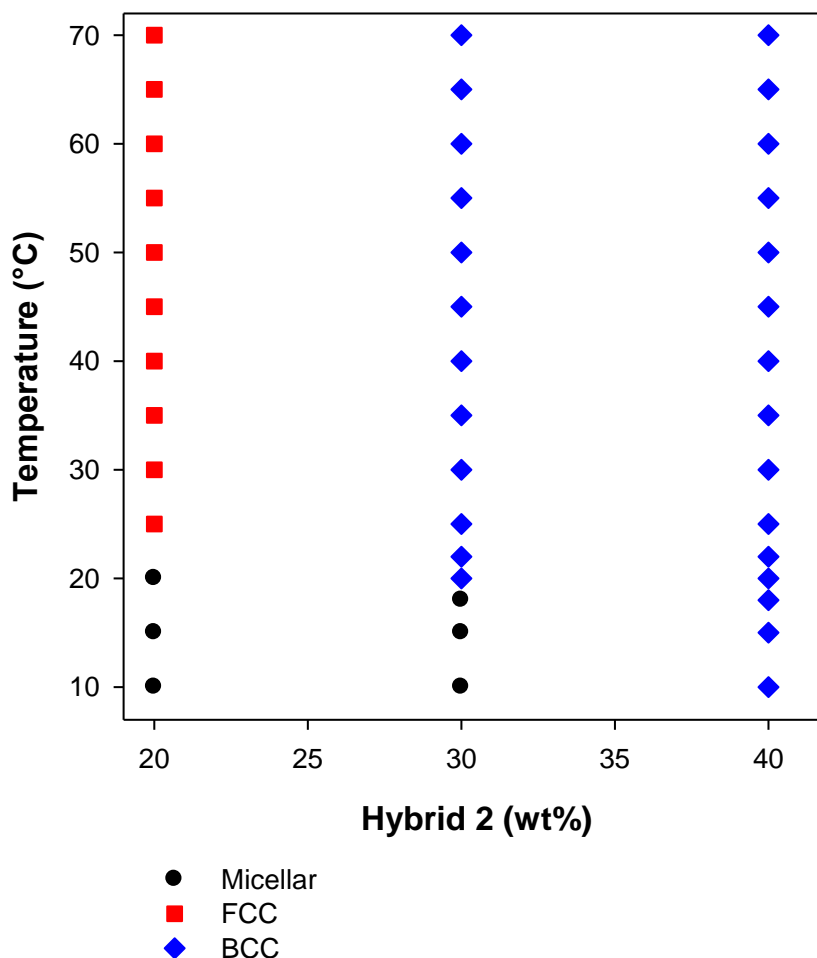
Figure 3.15 Phase diagram of Hybrid 2, P123:F108 (50:50)

3.4.6.4 Phase behaviour of Hybrid 2 (H2); P123:F108 (50:50) at 30 and 40 wt%

Similarly to Hybrid 3 (Figures 3.17 and 3.18), Hybrid 2 at 30 and 40 wt% gel structure seems to be largely cubic. This is very similar to F108 behaviour only at all temperatures. This highlights the dominant effect of F108 on the overall structure even at a 50:50 polymer ratio. However, a more interesting observation is that at these higher polymer concentration, the structure is now of a bcc nature not an fcc as in the 20 wt% case. The lattice parameters, Table 3.4, shows the same trend of pure F108 systems with bcc structures.

System	a (Å)	Volume($\times 10^6$ Å^3)	D_{HS} (Å)
30 wt%, 30°C	255	16.5	220
30 wt%, 70°C	260	17.5	225
40 wt%, 30°C	240	13.8	205
40 wt%, 65°C	250	15.6	220

Table 3.4 bcc structure parameters of H2 gels as a function of concentration and temperature in D$_2$O.

This fcc to bcc transition is most probably due to the changes in the packing efficiency as the concentration and the temperature increases, with a subsequent space constraint in the arrangement of the micelles. This is again similar to the features observed for pure F108 systems. fcc to bcc transitions have been previously reported by Liu *et al.* for F127/B20-5000 (EO$_{45}$BO$_{14}$EO$_{45}$)[26] and for polystyrene-polyisoprene (PS-PI) block copolymers by McConnell *et al.*[36] These authors have noted that the transition depend greatly on which morphology yield the most stable cubic phase. This was found to be determined by the repulsive force between the solvated chains that forms the micellar corona.

3.4.6.5 Phase behaviour of Hybrid 3 (H3); P123:F108 (25:75)

At 20 wt%, Hybrid 3 exhibited similar structure behaviour to Hybrid 2 at the same concentration, Figure 3.16, where the only noticeable difference is the increase in the CGT (25°C) if compared to the Hybrid 2 case (20°C). At 20 wt% at temperatures above the CGT (*e.g.* at 30°C) we still observe the fcc structure, $a \approx 350$ Å. This is also very similar to the lattice parameters from the fcc structure observed in the 20 wt% H2 case at the same temperature.

These general observations regarding the change in the CGT and the similarities in the gel structure could be extended to the 30 and the 40 wt% case. For 30 wt%, the CGT has been lowered from ≈18°C in Hybrid 2 to ≈10°C in Hybrid 3. While for 40 wt%, gelation was observed at temperatures as low as 10°C, in a very similar behaviour as 40 wt% Hybrid 2. In regards to the gel structure, it also remained bcc, insensitive to the overall concentration and temperatures. SANS data and the phase diagram are shown in Figures 3.18 and 3.19.
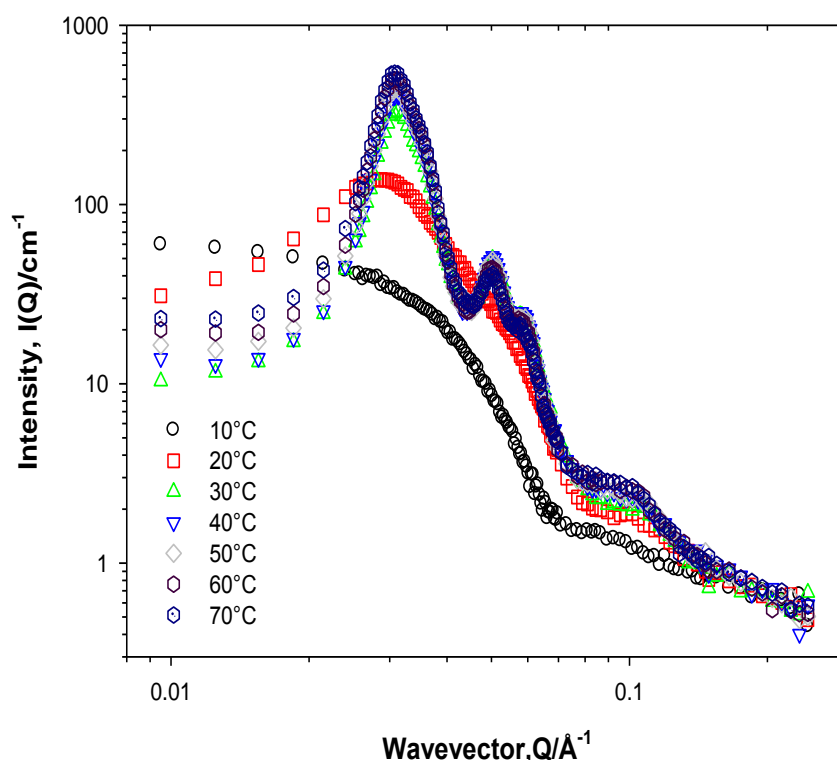
Figure 3.16 SANS from 20 wt% H3 as a function of temperature in D_2O.
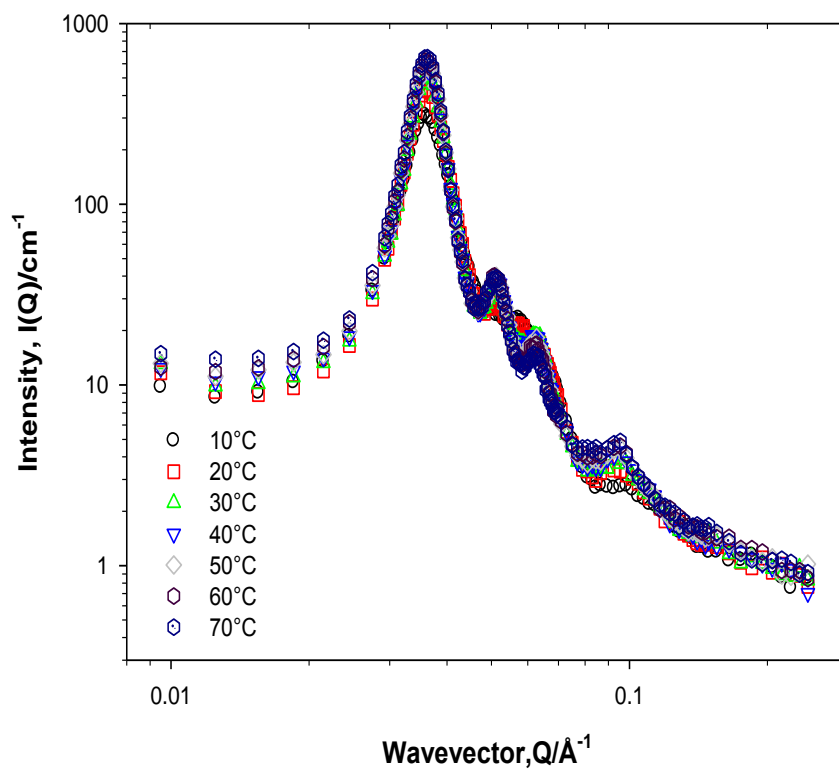
Figure 3.17 SANS from 30 wt% H3 as a function of temperature in D$_2$O.
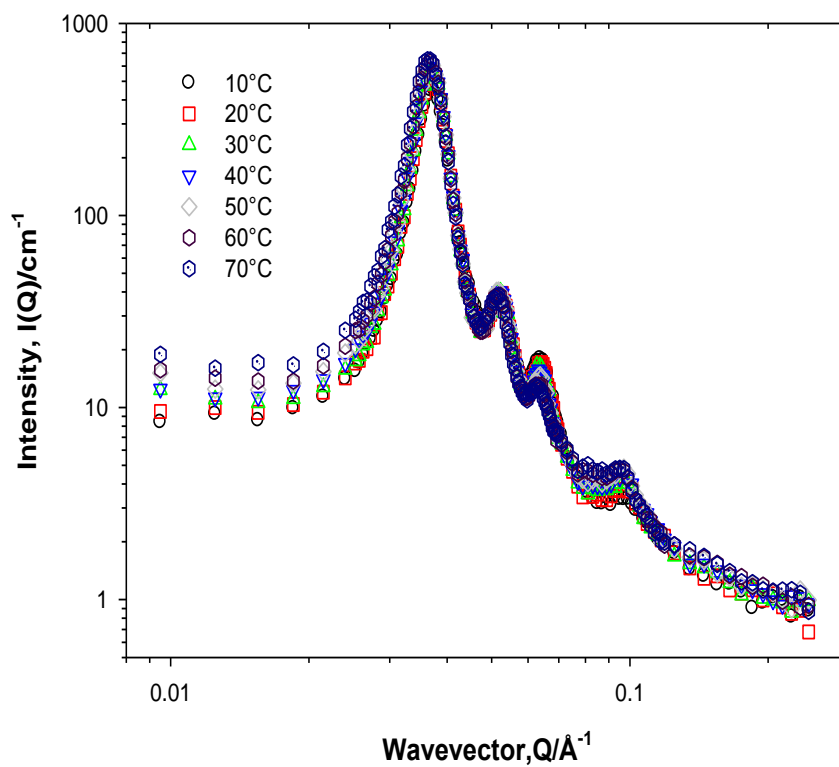
Figure 3.18 SANS from 40 wt% H3 as a function of temperature in D$_2$O
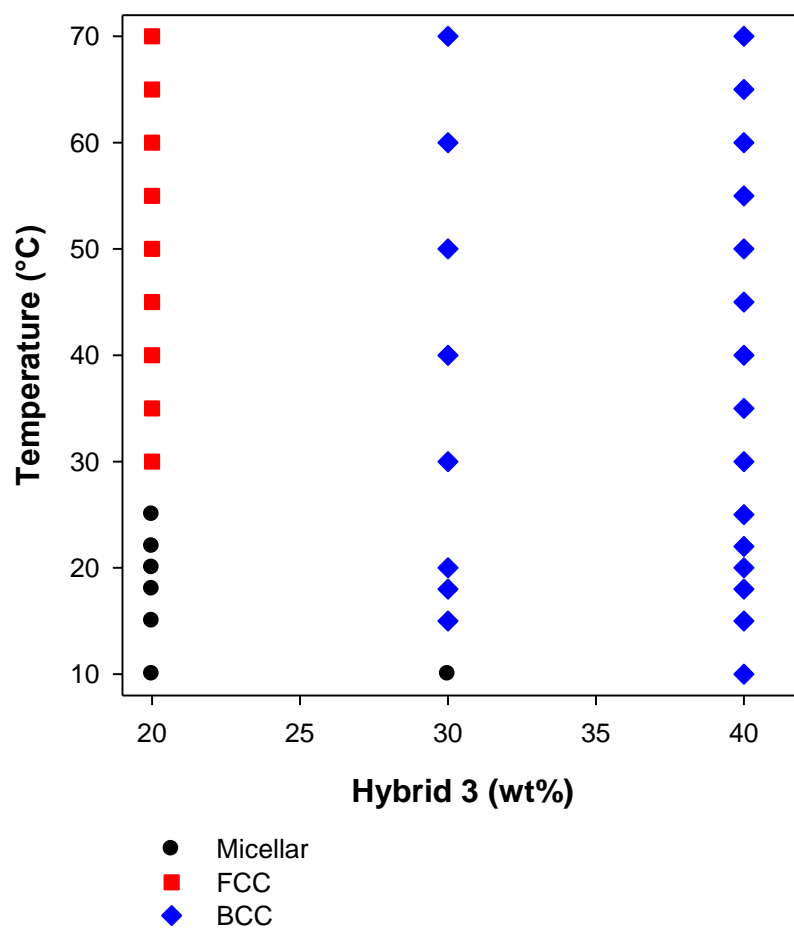
Figure 3.19 Phase diagram of Hybrid 3, P123:F108 (25:75)

Chapter 3. Temperature and concentration induced gelation of triblock copolymers as viewed by SANS

3.5 Conclusions

Small-angle neutron scattering has been used to probe the local structures of solutions and gels from Pluronic P123, F108 and their mixtures. The data from gels showed strong Bragg peaks (reflections) with up to three orders and this data was analysed with respect to peak positions. It was found that heating the samples induced different structural arrangements in almost all the samples and gelation was observed. In gels formed with low polymer concentrations, at low temperatures, spherical micelles were observed. As the temperature increased, these micelles tended to form cubic and hexagonal crystals. This transition in the structure depended significantly on the composition of the micelle.

Pure P123 systems, at low concentrations (20 wt%) did not show gelation at any temperature. However, at higher concentrations (30 and 40 wt%), gelation was observed and the structure transitioned from micellar to cubic (only in 30 wt%) to hexagonal and then finally to lamellar. For pure F108 systems, the structure was micellar at low temperatures and concentrations, but largely of bcc nature when the concentration and the temperature increased.

Investigating the structures obtained from mixed Pluronic systems revealed that when P123 is the main component in the mixture, the scattering behaviour of the mixture is similar to the P123 on its own. However, in 40 wt% mixture, the data showed only micellar behaviour up to 25°C, in contrast to the P123 behaviour on its own at the same concentration in the mixture, where it showed a multiphase and bcc behaviour over a wide range of temperatures. The data also showed destabilisation of the lamellar phase of pure P123 systems, and hcp structures were favoured instead. Interestingly, in mixtures of 50:50 P123:F108 gels, the data showed that the structure seems to be dominated by F108, where it showed an fcc structure for lower concentrations and bcc dominated systems at higher ones. This behaviour was also observed in mixtures of 25:75 P123:F108 gels.

In conclusion, this work shows that adding P123 to F108 systems did not show any destabilisation of the cubic phase as was reported before with F127 and P123.[24] However, the cubic phase only transitioned from fcc to bcc as a function of the overall polymer concentration. These observations helped us draw up ways in which the structural behaviour of the gels could be controlled and modified, eventually leading to controlling the rheological properties of the gels.

Chapter 3. Temperature and concentration induced gelation of triblock copolymers as viewed by SANS

Bibliography

(1) Escobar-Chávez, J. J.; López-Cervantes, M.; Naïk, A.; Kalia, Y. N.; Quintanar-Guerrero, D.; Ganem-Quintanar, A. Applications of Thermo-Reversible Pluronic F-127 Gels in Pharmaceutical Formulations. *J. Pharm. Pharm. Sci.* **2006**, *9*, 339–358.

(2) Pitto-Barry, A.; Barry, N. P. E. Pluronic® Block-Copolymers in Medicine: From Chemical and Biological Versatility to Rationalisation and Clinical Advances. *Polym. Chem.* **2014**, *5*, 3291–3297.

(3) Kabanov, A. V.; Lemieux, P.; Vinogradov, S.; Alakhov, V. Pluronic® Block Copolymers: Novel Functional Molecules for Gene Therapy. *Adv. Drug Deliv. Rev.* **2002**, *54*, 223–233.

(4) Kabanov, A. V.; Batrakova, E. V.; Alakhov, V. Y. Pluronic® Block Copolymers as Novel Polymer Therapeutics for Drug and Gene Delivery. *J. Control. Release* **2002**, *82*, 189–212.

(5) Sarkar, B.; Ravi, V.; Alexandridis, P. Micellization of Amphiphilic Block Copolymers in Binary and Ternary Solvent Mixtures. *J. Colloid Interface Sci.* **2013**, *390*, 137–146.

(6) Alexandridis, P.; Hatton, T. A. Block Copolymer Surfactants in Aqueous Solutions and at Interface: Thermodynamics, Structure, Dynamics and Modeling. *Colloids Surfaces A Physicochem. Eng. Asp.* **1995**, *96*, 1–46.

(7) Alexandridis, P.; Holzwarthf, J. F.; Hatton, T. A. Micellization of Poly (Ethylene Oxide) -Poly (Propylene Oxide) -Poly (Ethylene Oxide) Triblock Copolymers in Aqueous Solutions: Thermodynamics of Copolymer Association. *Macromolecules* **1994**, *27*, 2414–2425.

(8) Jangher, A.; Griffiths, P. C.; Paul, A.; King, S. M.; Heenan, R. K.; Schweins, R. Polymeric Micelle Disruption by Cosolvents and Anionic Surfactants. *Colloids Surfaces A Physicochem. Eng. Asp.* **2011**, *391*, 88–94.

(9) Mansour, O. T.; Cattoz, B.; Heenan, R. K.; King, S. M.; Griffiths, P. C. Probing Competitive Interactions in Quaternary Formulations. *J. Colloid Interface Sci.* **2015**, *454*, 35–43.

(10) Bercea, M.; Darie, R. N.; Nita, L. E.; Morariu, S. Temperature Responsive Gels Based on Pluronic F127 and Poly(vinyl Alcohol). *Ind. Eng. Chem. Res.* **2011**, *50*, 4199–4206.

(11) Molino, F. R.; Berret, J. F.; Porte, G.; Diat, O.; Lindner, P. Identification of Flow Mechanisms for a Soft Crystal. *Eur. Phys. J. B* **1998**, *3*, 59–72.

(12) Newby, G. E.; Watkins, E. B.; Merino, D. H.; Staniec, P. A.; Bikondoa, O. In Situ Rheo-GISANS of Triblock Copolymers: Gelation and Shear Effects on Quasi-Crystalline Structures at Interfaces. *RSC Adv.* **2015**, *5*, 104164–104171.

(13) Newby, G. E.; Hamley, I. W.; King, S. M.; Martin, C. M.; Terrill, N. J. Structure, Rheology and Shear Alignment of Pluronic Block Copolymer Mixtures. *J. Colloid Interface Sci.* **2009**, *329*, 54–61.

(14) Wolff, N.; Gerth, S.; Gutfreund, P.; Wolff, M. Temperature Dependent Cubic and Hexagonal Close Packing in Micellar Structures. *Soft Matter* **2014**, *10*, 8420–8426.

(15) Pandey, M.; Belgamwar, V.; Gattani, S.; Surana, S.; Tekade, A. Pluronic Lecithin Organogel as a Topical Drug Delivery System. *Drug Deliv.* **2010**, *17*, 38–47.

(16) Gilbert, J. C.; Hadgraft, J.; Bye, A.; Brookes, L. G. Drug Release from Pluronic F-127 Gels. *Int. J. Pharm.* **1986**, *32*, 223–228.

(17) Jiang, J.; Burger, C.; Li, C.; Li, J.; Lin, M. Y.; Colby, R. H.; Rafailovich, M. H.; Sokolov, J. C. Shear-Induced Layered Structure of Polymeric Micelles by SANS. *Macromolecules* **2007**, *40*, 4016–4022.

(18) Artzner, F.; Geiger, S.; Olivier, A.; Allais, C.; Finet, S.; Agnely, F. Interactions between Poloxamers in Aqueous Solutions: Micellization and Gelation Studied by Differential Scanning Calorimetry, Small Angle X-Ray Scattering, and Rheology. *Langmuir* **2007**, *23*, 5085–5092.

(19) Farrugia, M.; Morgan, S. P.; Alexander, C.; Mather, M. L. Ultrasonic Monitoring of Drug Loaded Pluronic F127 Micellular Hydrogel Phase Behaviour. *Mater. Sci. Eng. C* **2014**, *34*, 280–286.

(20)   Pragatheeswaran, A. M.; Chen, S. B. Effect of Chain Length of PEO on the Gelation and Micellization of the Pluronic F127 Copolymer Aqueous System. *Langmuir* **2013**, *29*, 9694–9701.

(21)   Gilbert, J. C.; Richardson, J. L.; Davies, M. C.; Palin, K. J.; Hadgraft, J. The Effect of Solutes and Polymers on the Gelation Properties of Pluronic F-127 Solutions for Controlled Drug Delivery. *J. Control. Release* **1987**, *5*, 113–118.

(22)   Jiang, J.; Li, C.; Lombardi, J.; Colby, R. H.; Rigas, B.; Rafailovich, M. H.; Sokolov, J. C. The Effect of Physiologically Relevant Additives on the Rheological Properties of Concentrated Pluronic Copolymer Gels. *Polymer (Guildf).* **2008**, *49*, 3561–3567.

(23)   Ulrich, K.; Galvosas, P.; Kärger, J.; Grinberg, F. "Pore-Like" Effects of Super-Molecular Self-Assembly on Molecular Diffusion of Poly(Ethylene Oxide)-Poly(Propylene Oxide)-Poly(Ethylene Oxide) in Water. *Materials (Basel).* **2012**, *5*, 966–984.

(24)   Chaibundit, C.; Ricardo, N. M. P. S.; Costa, F. D. M. L. L.; Yeates, S. G.; Booth, C. Micellization and Gelation of Mixed Copolymers P123 and F127 in Aqueous Solution. *Langmuir* **2007**, *23*, 9229–9236.

(25)   Oshiro, A.; Silva, D. C.; Mello, J. C. De; Moraes, V. W. R. De; Cavalcanti, L. P.; Franco, M. K. K. D.; Alkschbirs, M. I.; Fraceto, L. F.; Yokaichiya, F.; Rodrigues, T. Pluronics F127/L81 Binary Hydrogels as Drug-Delivery Systems: Influence of Physicochemical Aspects on Release Kinetics and Cytotoxicity. *Langmuir* **2014**, *30*, 13689–13698.

(26)   Liu, T.; Chu, B. Formation of Homogeneous Gel-like Phases by Mixed Triblock Copolymer Micelles in Aqueous Solution: FCC to BCC Phase Transition. *J. Appl. Crystallogr.* **2000**, *33*, 727–730.

(27)   Pozzo, D. C.; Walker, L. M. Small-Angle Neutron Scattering of Silica Nanoparticles Templated in PEO-PPO-PEO Cubic Crystals. *Colloids Surfaces A Physicochem. Eng. Asp.* **2007**, *294*, 117–129.

(28) Goldmints, I.; Gottberg, F. K. Von; Smith, K. A.; Hatton, T. A. Small-Angle Neutron Scattering Study of PEO - PPO - PEO Micelle Structure in the Unimer-to-Micelle Transition Region. *Langmuir* **1997**, *7463*, 3659–3664.

(29) Foster, B.; Cosgrove, T.; Hammouda, B. Pluronic Triblock Copolymer Systems and Their Interactions with Ibuprofen. *Langmuir* **2009**, *25*, 6760–6766.

(30) Lettow, J. S.; Lancaster, T. M.; Glinka, C. J.; Ying, J. Y. Small-Angle Neutron Scattering and Theoretical Investigation of Poly (Ethylene Oxide)- Poly (Propylene Oxide) - Poly(Ethylene Oxide) Stabilized Oil-in-Water Microemulsions. *Langmuir* **2005**, 5738–5746.

(31) Alexander, S.; Cosgrove, T.; Castle, T. C.; Grillo, I.; Prescott, S. W. Effect of Temperature, Cosolvent ,and Added Drug on Pluronic − Flurbiprofen Micellization. *J. Phys. Chem. B* **2012**, *116*, 11545–11551.

(32) Mortensen, K.; Brown, W. Poly(ethylene Oxide)-Poly(propylene Oxide)-Poly(ethylene Oxide) Triblock Copolymers in Aqueous Solution. The Influence of Relative Block Size. *Macromolecules* **1993**, *26*, 4128–4135.

(33) Wanka, G.; Hoffmann, H.; Ulbricht, W. Phase Diagrams and Aggregation Behavior of Poly(oxyethylene)-Poly(oxypropylene)-Poly(oxyethylene) Triblock Copolymers in Aqueous Solutions. *Macromolecules* **1994**, *27*, 4145–4159.

(34) Svensson, M.; Alexandridis, P.; Linse, P. Phase Behavior and Microstructure in Binary Block Copolymer / Selective Solvent Systems : Experiments and Theory. *Macromolecules* **1999**, *32*, 637–645.

(35) Mortensen, K.; Batsberg, W.; Hvid, S. Effects of PEO-PPO Diblock Impurities on the Cubic Structure of Aqueous PEO-PPO-PEO Pluronics Micelles: Fee and Bcc Ordered Structures in F127. *Macromolecules* **2008**, *41*, 1720–1727.

(36) McConnell, G. A.; Lin, M. Y.; Gast, A. P. Long-Range Order in Polymeric Micelles Under Steady Shear. *Macromolelcules* **1995**, *28*, 6754–6764.

Chapter 4

4. Probing the interfacial structure of small molecule surfactants stabilised air-in-water foams

4.1 Abstract

Small-angle neutron scattering has been used to probe the interfacial structure of foams stabilised by small molecule surfactants at concentrations well below their critical micelle concentration. The data for wet foams showed a pronounced Q^{-4} dependence at low Q and noticeable inflexions over the mid Q range. These features were found to be dependent on the surfactant structure (mainly the alkyl chain length) with inflexions changing position along the measured Q range. Foams stabilised by sodium dodecylsulfate were allowed to drain and the induced changes in the scattering intensity and peak positions were recorded. Characteristic features in the data such as new peaks attributed to the formation of micellar structure were observed, the position of which varied with the level of drainage. These inflexions suggests a novel interfacial structure at the air/water interface, and the data was successfully fitted to a model consisting of paracrystalline stacks of adsorbed surfactant layers, a structure that we believe is induced by the foams interface.

Chapter 4. Probing the interfacial structure of small molecule surfactants stabilised air-in-water foams

4.1 Introduction

Foams are systems comprising concentrated dispersions of gas bubbles in a continuous aqueous phase, and are widely encountered as precursors in a number of applications, *e.g.* medical,[1,2] insulation materials,[3] cosmetic[4] and firefighting.[5] There has also been a recent growing interest in these systems for their applications in food industries.[6,7] For the majority of foams, the aqueous phases contain surfactants or proteins, which act as stabilisers. Of main interest here is the structure and performance of these foams and their dependence on the assembly of small molecule surfactants at the air-liquid interface.

Physicochemical properties of the foams such as ionic strength, pH, and temperature significantly affect the interfacial behaviour of the foaming agents or stabilisers (surfactants). It is well established that surfactants and their blends are of crucial importance to foam formulations.[8–10] In the absence of surfactants, a foam will catastrophically coalesce and collapse,[11,12] whereas in their presence, the interface is efficiently stabilised by the monomer adsorption at the air-water interface as evidenced by changes to the surface tension, surface shear viscosity and surface elasticity.[13]

Foams, like any other lyophobic systems are thermodynamically unstable due to their high interfacial energy. This energy promotes processes that eventually lead to foam coarsening and destruction. Foam destruction can occur via a number of processes: bubble coalescence as a result of drainage and film thinning; Ostwald ripening driven by the diffusion of gas across thin films from smaller to larger bubbles; and by drainage due to gravity or surface tension gradients.[14]

It is well-established that surfactants form micelles in the bulk above their critical micelle concentration (CMC), above which there are substantial changes in solution properties.[15–18] In the case of foams, Petkova *et al.*[12] have determined a "transitional concentration" above which, foams were found to be stable, these concentrations being 10-30 times below the CMC for the surfactants studied (sodium dodecylsulfate, dodecyltrimethylammonium bromide and Brij 35).

Chapter 4. Probing the interfacial structure of small molecule surfactants stabilised air-in-water foams

Partially hydrophobic colloidal silica particles have also been shown to adsorb at the air-water interface where it was found that these particles form a "colloidal armour" at the interface that stabilises the foams for durations up to months.[19,20] Most of the recent studies have focused on the process of foaming and foam stabilization using traditional measurements (foam half-life, bubble size measurement, *etc.*), but far fewer studies have investigated the complex interfacial structure formed by these molecules, within macroscopic foam and/or single foam films.

Neutron and X-ray reflectivity have been used extensively to quantify the gas-liquid interface, but on planar interfaces, and not under dynamic conditions relevant to the foam.[21,22] There also have been a number of small angle scattering studies on foams, [23–25] illustrating the viability of the technique, but the conclusions have been largely qualitative and are yet to improve the understanding of the assembly of stabiliser at the air-water interface.

Axelos *et al.*[24] studied a series of wet and dry foams generated with a series of surfactants with varying concentrations using SANS. Under steady state foaming conditions, a pronounced Q^{-4} dependence was observed with a number of peaks varying in shape and position depending on the drainage conditions. These peaks were attributed to the surfactant in the liquid in the walls for the wet foams (the systems studied were above the CMC) and to parallel air/water interfaces for dry foams.

Ropers *et al*[25] along with the previous authors studied hexadecyltrimethylammonium bromide (CTAB), and polysaccharide/CTAB complex stabilised free draining foams by SANS. A different approach towards data interpretation was used and the data were analysed from both scattering and reflectivity points of view. They concluded that the polysaccharide addition yields a shift in the peak position towards lower Q values attributed to the film thickness. It was also postulated that this shift is insensitive to the drainage duration and that the emergence of another peak was the result of a thicker liquid film.

Chapter 4. Probing the interfacial structure of small molecule surfactants stabilised air-in-water foams

Micheau *et al.*[26] have investigated foams from the pH sensitive nonaoxyethylene oleylether carboxylic acid, where their modelling and analysis was shaped by the work of Axelos and co-workers. Similar SANS data features were observed and they concluded that the oscillations in the data originates from the reflectivity of neutrons from the thin liquid films within the foam. The thickness of these liquid films was found to be sensitive to pH and surface charge. However, it was not entirely clear how the contribution of micelles and lamellar structures on the observed scattering was taken into account. The concentration of surfactant in the samples under investigation being well above the CMC, such structures (micelles and foam-induced surfactant lamellae) are expected to be present and would give rise to significant scattering in the Q region where those features are discussed. In addition, the dynamics behind the presence of two parallel air/liquid interfaces remains unclear.

Fameau *et al.*[27] have studied a series of foams stabilised by thermo-sensitive fatty acids (12-hydroxy-stearic acid, 12-HSA) using SANS amongst other techniques, where they compared scattering data from bulk solution and the foams (wet and dry). A series of Bragg peaks were observed at different Q positions, which they attributed to the presence of multilamellar tubular arrangement of the fatty acid bilayers in the foam. They have also studied these systems at different H_2O/D_2O compositions from both scattering and reflectivity points of view, utilising contrast variation. They found that for a reflectivity experiment, as the H_2O content increases, the position of the peaks shift, and for a SANS experiment, when the H_2O content increases, no shift in the peaks were observed but only a decrease in the scattering intensity was recorded. Based on these findings, the authors have demonstrated that the SANS signal originates from tubes present in the liquid foam and eliminated the possibility of the signal originating from the reflectivity of neutrons at the air/water interface.

Hurcom *et al.*[28] have previously successfully used small-angle neutron scattering to study air-in-water foams stabilised by a series of Pluronic block copolymers at different concentrations below and above the CMC.

Chapter 4. Probing the interfacial structure of small molecule surfactants stabilised air-in-water foams

Similar SANS features were observed for all the foams for all systems. The data below the CMC was interpreted and modelled as a paracrsytalline stack of polymeric surfactant lamellae at the air/water interface. The thickness of these layers was found to be dependent on the EO and PO block characteristics and the overall molecular weight of the polymer.

The quantity and the stability of foams stabilised by surfactants have been proven to be closely linked to the surfactant alkyl chain length as this introduces a balance between the solubility and surface activity.[29,30] Against this background, this work has been performed to extend the study to different amphiphilic molecules, comprising two homologous series of small molecule surfactants (SMS); alkyl sulfates ($C_nH_{2n+1}SO_4Na$) and alkyl bromides ($C_nH_{2n+1}TABr$). The study was carried out at half their CMC measured by surface tension, Figure C.1, C.2 (Appendix C), Table 4.1 and 4.2, (in excellent agreement with literature[31,32]), the surfactant concentrations within the water films is hence assumed too dilute to contain any micelles.

4.2 Experimental

4.2.1 Materials

Homologous series of ionic surfactants were used as received, as listed in Tables 4.1 and 4.2. Solutions for SANS experiments were prepared in deuterated water (99.9%, Sigma Aldrich). Deuterated sodium dodecylsulfate (d-SDS or d-$C_{12}SO_4$), dodecyltrimethylammonium bromide (d-C_{12}h-TAB), were synthesised by ISIS deuteration facility and have been used as received. Regarding materials purity, there was no evidence of any impurity in surface tension data (manifest as pre-CMC minima or incorrect CMC values).

SMS description	Chemical formula	MW (gmol^{-1})	CMC (mM)	Presented as
Sodium n-octylsulfate	$CH_3(CH_2)_7OSO_3Na$	232.3	100	C_8SO_4Na
Sodium decylsulfate	$CH_3(CH_2)_9OSO_3Na$	260.3	32.0	$C_{10}SO_4Na$
Sodium dodecylsulfate	$CH_3(CH_2)_{11}OSO_3Na$	288.4	7.90	$C_{12}SO_4Na$
Sodium tetradecylsulfate	$CH_3(CH_2)_{13}OSO_3Na$	316.4	2.20	$C_{14}SO_4Na$
Sodium hexadecylsulfate	$CH_3(CH_2)_{15}OSO_3Na$	344.5	0.90	$C_{16}SO_4Na$

Table 4.1 Chemical formula, approximate molecular weight and the measured CMC values of alkyl sulfate small molecule surfactants used in this work.

SMS description	Chemical formula	MW (gmol^{-1})	CMC (mM)	Presented as
Trimethyloctylammonium bromide	$CH_3(CH_2)_7N(CH_3)_3Br$	252.3	145	C_8TAB
Decyltrimethylammonium bromide	$CH_3(CH_2)_9N(CH_3)_3Br$	280.3	59.0	$C_{10}TAB$
Dodecyltrimethylammonium bromide	$CH_3(CH_2)_{11}N(CH_3)_3Br$	308.3	14.5	$C_{12}TAB$
Tetradecyltrimethylammonium bromide	$CH_3(CH_2)_{13}N(CH_3)_3Br$	336.4	3.70	$C_{14}TAB$
Hexadecyltrimethylammonium bromide	$CH_3(CH_2)_{15}N(CH_3)_3Br$	364.4	1.10	$C_{16}TAB$

Table 4.2 Chemical formula, approximate molecular weight and the measured CMC values of alkyl bromide small molecule surfactants used in this work.

4.2.2 Methods

4.2.2.1 Tensiometry

Surface tension measurements were carried out using a maximum bubble pressure tensiometer (SITA science on-line t60, Germany), calibrated by reference to de-ionized water. Surface tension was recorded at a bubble lifetimes of 10 seconds. All measurements were taken at 25 ± 1°C.

4.2.2.2 Small-angle neutron scattering (SANS):

In all the experiments, the foam was generated by pushing nitrogen gas through a 20 µm frit (A) at the base of a Perspex column (height of 25 cm, diameter of 4.6 cm) which contains approximately 50 ml of the surfactant solution. A 2 cm wide groove has been removed and covered with aluminium foil to allow the neutrons to cross the sample. The neutron beam impinges on the aluminium foil between (B) and (C) behind which the Perspex has been partially removed. For stable foams, the reservoir (D) collects the foam sample and returns it to the base via the plastic tube at (E). The cell could also be equipped with controlled heating set up (heating jacket) at (F) and (G), however it has not been used in this study. The wet foams were studied in which continuous airflow (0.4 L/hour) produces constantly regenerated foam. As such, the bubbles appear spherical and are separated by thick lamella walls. All experiments were performed at room temperature.

Chapter 4. Probing the interfacial structure of small molecule surfactants stabilised air-in-water foams

SANS experiments were performed on either (i) the time of flight (a) LOQ and (b) SANS2d diffractometers at the ISIS pulsed spallation neutron source, Rutherford Appleton Laboratory, Didcot, UK. A range defined by $Q= (4\pi/\lambda) \sin (\theta/2)$ between 0.009 and $\geq$ 0.5 Å^{-1} (LOQ) and 0.005 and $\geq$ 0.3 Å^{-1} (SANS2d) was obtained by using neutron wavelengths (λ) spanning 2.2 to 10.0 Å with a fixed detector distance of 4 m (LOQ) and 1.75 to 16.5 Å with a fixed detector distance of 4 m (SANS2d), or (ii) steady-state reactor sources at (a) D11 diffractometer at the ILL, Grenoble where a Q range is selected by choosing three instrument settings at a constant neutron wavelength (λ) of 8 Å (ILL) and sample detector distance of 1.2, 8 and 39 m and (b) KWS-1 diffractometer at the Jülich Centre for Neutron Science at FRM II, Garching, using three detector distances (2, 8 and 20 m) and a neutron wavelength of 5 Å.

Experimental measurement times were between 5-10 minutes (LOQ and SANS2d) and between 20-30 minutes (MLZ and ILL, this was a little longer as three detector distances were used with no hysteresis). All scattering data were (a) normalized for the sample transmission, (b) background corrected using the empty foam cell and, (c) corrected for the linearity and efficiency of the detector response using the instrument specific software package and the scattering from a polystyrene blend taped to the front of the foam cell, Figure 4.1.
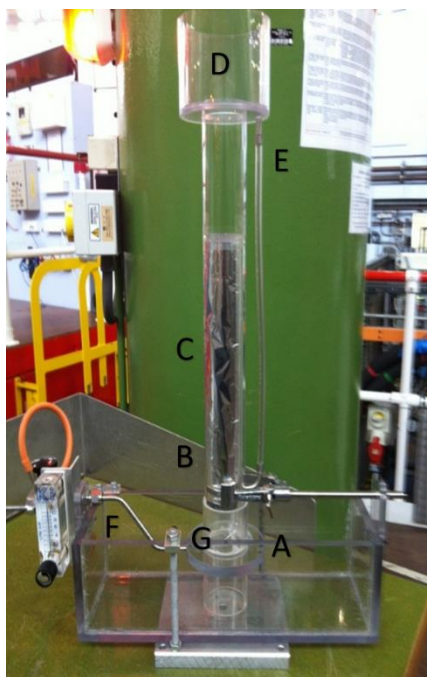
Figure 4.1 SANS sample environment for studying foams.[28]

4.3 Results and Discussion

4.3.1 SANS from foams stabilised by small molecule surfactants

The scattering in these systems may arise from (a) any structure normal to the air/water interface, which would follow an approximate Q^{-4} dependence given that these interfaces are not perfectly flat, (b) any in plane structure normal to the interface, (c) fluctuations in the composition of the interfaces parallel to the beam, (d) structures that would be present in the liquid junctions between the bubbles, this may resemble the 'bulk solutions' at appropriate concentration, and (e) in the aged polyhedral foams, the long almost cylindrical regions at the junction of bubbles associated with the plateau borders.

Representative data are presented in Figure 4.2 (recorded on D11) from continually generated foams from SMS. The data shows a number of features; the pronounced Q^{-4} dependence at low Q, characteristic of the Porod scattering from a smooth surface with a large radius. Over the mid Q range, there are noticeable inflexions or "bumps" around 0.0365 Å^{-1} for $C_{12}SO_4Na$ corresponding to d-spacing ($2\pi/Q_{peak}$) of 170 Å, whilst for the $C_{12}TAB$ case, the inflexion occurs at 0.035 Å^{-1} corresponding to a spacing of 195 Å.

At high Q, the data decays into an incoherent background scattering that varies from one system to another depending on the amount of the sample in the beam. It is worth mentioning that the SANS data were obtained reproducibly for the $C_{12}SO_4Na$ foam from all the four different diffractometers used in this study, and were all in excellent agreement in terms of features and peak positions, (Appendix C, Figures C.3 and C.4).

It should also be stressed again that the systems studied here are at concentrations significantly below their CMC, thus no (solution like) micelles are present, and the peaks do not arise from the micellar form factor. The scattering arising from $C_{12}SO_4Na$ solution above the CMC is shown in Figure 4.3.
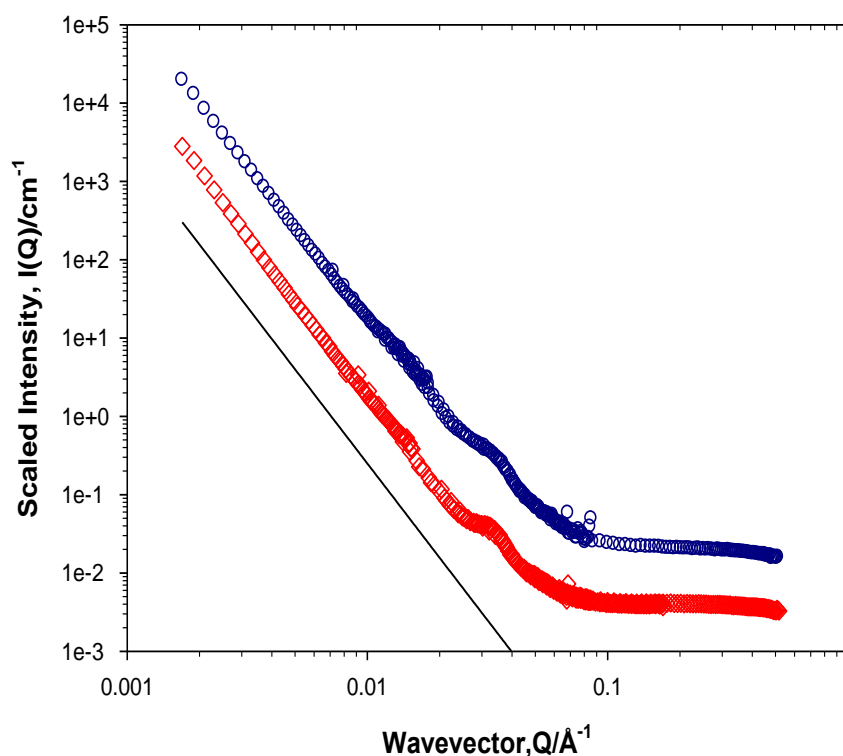
Figure 4.2 SANS from foams stabilised with 4 mM $C_{12}SO_4Na$ 'SDS', (circles) and 7 mM $C_{12}TAB$ (diamonds) in D_2O. Typical Q^{-4} dependence is presented as a solid line. Data have been shifted vertically for clarity.

4.3.2 SANS from draining and drained foams

We have also performed neutron scattering experiments to investigate foams stabilised by $C_{12}SO_4Na$ at three different drainage conditions, as shown in Figure 4.3 (recorded on D11). Upon draining, very well defined peaks emerge with maxima at Q ≈ 0.015 Å^{-1} and 0.042 Å^{-1}.

At low Q, one could interpret the maxima at Q ≈ 0.015 Å^{-1} as indicating the presence of a lamellar ordering of the $C_{12}SO_4Na$ between the walls, and postulate that it is foam induced. There are significant similarities in the foam scattering and the solution scattering where C > CMC, as shown in Table 4.3 and Figure C.6. Therefore, the scattering is dominated by the solution in the film borders.

System Description	Q_{peak} 1 (Å^{-1})	Q_{peak} 2 (Å^{-1})
4 mM $C_{12}SO_4Na$ (foam)	--	0.038
$C_{12}SO_4Na$ – draining	0.016	0.042
$C_{12}SO_4Na$ – drained	0.018	0.045
10 mM $C_{12}SO_4Na$ (foam)	0.017	0.044
10 mM $C_{12}SO_4Na$ (solution)	0.040	--
15 mM $C_{12}SO_4Na$	0.040	--
20 mM $C_{12}SO_4Na$	0.045	--
30 mM $C_{12}SO_4Na$	0.047	--

Table 4.3 Positions of first and second maxima in the scattering data from $C_{12}SO_4Na$ foams at different air flow conditions/concentrations, and correlation peak positions from $C_{12}SO_4Na$ micelles in solution at different concentrations.

Lamellar Bragg peaks have been previously reported for emulsions stabilised by Pluronic L92,[33] and recently in foams as discussed earlier by Fameau *et al.*[27,34], where these peaks were noted but not discussed. Ederth *et al.*[35] used neutron reflectivity (NR) to monitor aerosol-OT (AOT) the structure of draining foam films. The authors observed weak Bragg peaks, which have been attributed to a lamellar structure of AOT bilayers in the foam films. This weak intensity profile of the Bragg peaks has been related to the small number of layers of AOT that contributes to the scattering in the films, films inhomogeneities and the presence of other structures such as disk like micelles or discontinuous bilayers.

Chapter 4. Probing the interfacial structure of small molecule surfactants stabilised air-in-water foams

Micellar layering in films stabilised by $C_{12}SO_4Na$ at concentrations above the CMC has been studied previously by Lee *et al.*[36] using a white (polychromatic) reflected light. Layer transitions were observed based on $C_{12}SO_4Na$ concentration as a function of draining time, where the highest $C_{12}SO_4Na$ concentration (0.06 M) underwent a three micellar layer to two micellar layer transition. The lowest studied concentration (0.03 M), transitioned from one micellar layer to a film without any micelles. This agrees with our observations *i.e.* there is a significant contribution to the overall scattering from the surfactant micelles in the aqueous film forming the lamellae of the bubble (in both free drainage foams and foams stabilised by $C_{12}SO_4Na$ above the CMC). These findings are in good agreement with those of Fameau and co-authors[27] and with what we have observed previously for polymeric surfactant stabilised foams.[28]
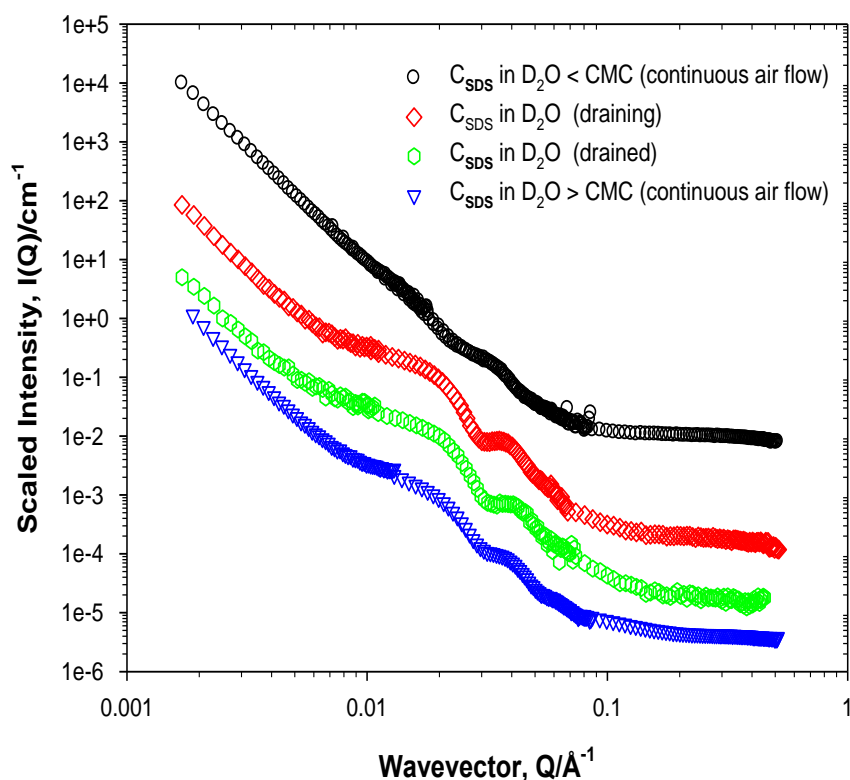
Figure 4.3 SANS from foams stabilised by $C_{12}SO_4Na$ at different air flow conditions compared to foams stabilised by 10 mM $C_{12}SO_4Na$ (above the CMC). Data have been shifted vertically for clarity.

As the foam drains, we observe significant changes in the scattering patterns, Figure C.7. The emergence of the asymmetric scattering "spikes" on the right is a signature of the transition from spherical (curved bubble walls) to polyhedral bubbles (flat single films[26,37]) as the liquid fraction in the foam decreases. These drainage conditions also explain the observed weaker scattering intensity at the low Q region.

The inflexions observed in Figures 4.2 and 4.3 indicate the presence of regular structures. We propose these are not related to the total film thickness as suggested by Axelos[24] or most recently Micheau *et al.*[26] The *d*-spacing values are too small to represent the thickness of the films as the foams studied here are in wet conditions; continuously generated and the bubble lamellae is expected to be of micrometer size. This assumption represents a major difference between our analysis and those of the French groups.[24,26,37] It is also worth mentioning, that the SANS behaviour was recorded from the $C_{12}SO_4Na$ foams at different airflow conditions and heights in the Prespex column, and no significant change in the scattering behaviour was recorded.

4.3.3 SANS data analysis and modelling

A simple approach to adopt towards the visualization of data with a strong Q^{-4} is Porod plots; $Q^4 I(Q)$ *vs. Q,* Figure C.4. This entirely removes the Q^{-4} dependence from the data and emphasises any other features observed in the data, *i.e.* the peaks. However, such approach only emphasises the existing peaks and their dimensions without providing any further detailed structure information, hence a more evolved approach towards the analysis was devised.

We employed a model of the air/water interface that comprises a paracrystalline stack of *M* thin surfactant/water layers (number of stacks), of thickness *L,* separation *D* and diffuseness *T* (the variation in interface structure perpendicular to the interface; an ideal interface will have zero diffuseness).[38,39] To this, a Q^n term is added to account for the scattering from the smooth air/water interface*.* To limit the functionality of the fit, the diffuseness *T* has been constrained to 0.01.
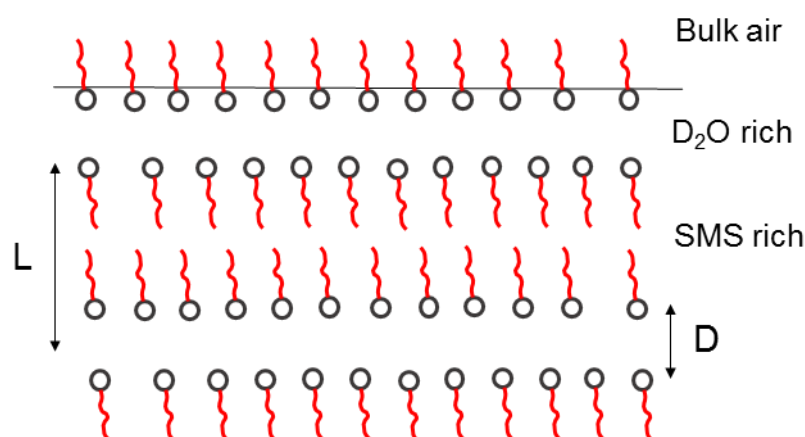
Figure 4.4 Cartoon of the paracrystalline stack model of the adsorbed SMS layers at the air/water interface. *L* is the layer thickness and *D* defines the separation.

Typical starting values for the heterogeneity of *L* and *D* are $\sigma(L)/L$ and $\sigma(D)/D = 0.2$, though these values have shown to have a negligible effect on the overall quality of the fit within reasonable bounds. The scattering length densities (contrast) of the various materials is such that in D_2O, the scattering arises equally from the air–D_2O and surfactant–D_2O interfaces, and any further deconvolution of the data is not feasible, at least in these systems.

To explore the validity of our assumptions, the paracrystalline stack model[38,39] has also been used to define the nature of the peaks around mid Q. By neglecting any contribution from solution surface scattering, the model adopts a thin layer of water of thickness L parallel to the air/water interface, one can simulate the expected oscillations from such layers from a neutron scattering perspective *via* ($\sin^2(QL/2)/Q^4$ *vs* Q), which are very similar to the cos (QL) Kiessig fringes observed by neutron reflectivity from thin interfaces.[40]

A range of film thicknesses was employed and for clarity purposes, exemplar data only have been presented in Figure 4.5, (the full simulations have been presented in Figure C.8). The simulations have been generated for heterogeneous film thicknesses (averaged over a thickness of 50-150 Å and 180-220 Å with steps of 10 Å).

The form of the data, and the maxima observed in the foam scattering data, clearly does not correspond to any of the features or the peak positions observed in the scattering behaviour in Figure 4.2, contrary to the observations recorded by Ropers *et al.*, where there was an overlap between the reflectivity simulated peaks and the peaks from the liquid films in their drained foams.
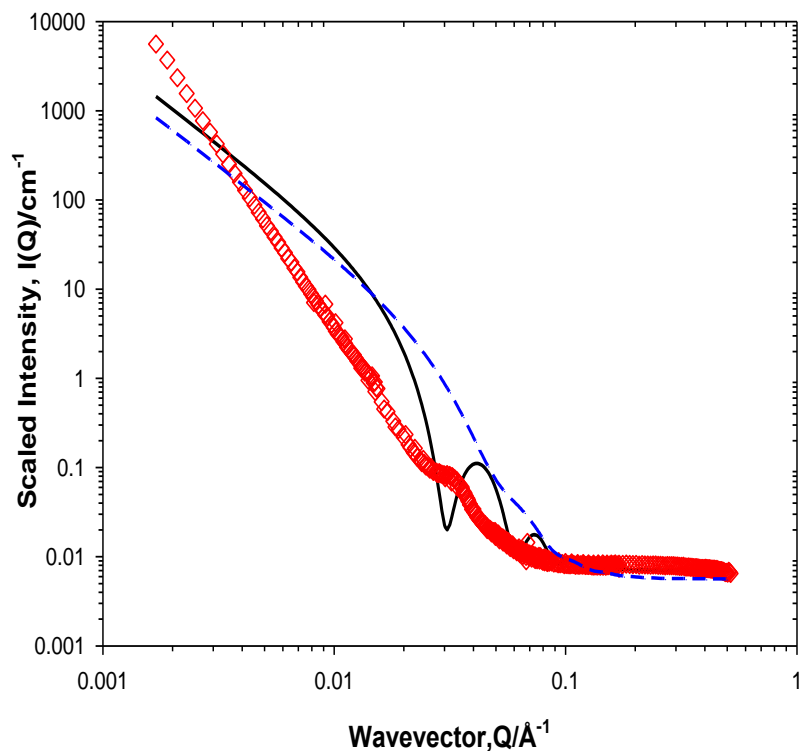
Figure 4.5 Simulated SANS from films of thickness (50-150 Å) with 10 Å increments (dashed line), from films of thickness (180-220 Å) with 10 Å increments (solid line) using the paracrystalline model, and SANS from foam stabilised with 7 mM $C_{12}TAB$ (diamonds) in D_2O for comparison. Data have been shifted vertically for clarity.

Chapter 4. Probing the interfacial structure of small molecule surfactants stabilised air-in-water foams

4.3.4 Effect of chain length on peak positions

As the small molecule surfactant hydrophobic chain length increases, subtle changes in the peak positions towards higher Q can be observed. This could be seen in both Figures 4.6 (alkyl sulfate series) and 4.7 (alkyl bromide series). As shown in these figures, the paracrystalline stack model seems to fit the data very well. The changes observed in the scattering data, mainly the subtle shift of the peak position towards higher Q was found to be sensitive to thickness L and the molecular structure of the small molecule surfactant. The thickness L (bilayer of surfactant) value was estimated by calculating the critical chain length (Å) of the surfactant ($1.5 + (1.26 \times N_c) \times 2)$), where N_c is the number of carbon atoms in the alkyl chain. The value of M (number of layers) was found to produce suitable fits at small values (~5), while larger values did not significantly improve the quality of the fit. Significant parameters from the fit are presented in Table 4.4.

System Description	L (Å) ±2	M	D (Å) ±5	Q_{peak} (Å^{-1})	d-spacing (Å)
50 mM C$_8$SO$_4$Na	26	5	185	0.033	190
16 mM C$_{10}$SO$_4$ Na	30	5	180	0.035	180
4 mM C$_{12}$SO$_4$Na	36	5	185	0.038	165
72 mM C$_8$TAB	26	5	185	0.034	187
29 mM C$_{10}$TAB	30	5	180	0.035	185
7 mM C$_{12}$TAB	40	5	185	0.037	180
1.8 mM C$_{14}$TAB	50	5	185	0.038	175

Table 4.4 Fit parameters to the scattering from small molecule surfactant stabilised foams at different concentrations below their CMC.

The relationship between the separation, D, from the model and the d-spacing does not seem to be straightforward. One would expect a closer agreement between both values, however, the d-spacing appears to be more sensitive to the chain length; as the chain length increases, the spacing between the layer decreases. The most compelling explanation is that the separation does not strictly correspond to the value of the spacing between the surfactant layers, but to a value that seems to include the dimensions from the surfactant structure as well. The SANS data from the alkyl bromides series also shows similar features as the alkyl sulfates, however, the changes in the peak position as a function of the chain length, seems to be more obvious in this case when compared to the alkyl sulfates.

As for the validity and sensitivity of model parameters, fitting one set of data with the parameters from another did not yield any suitable fits. For example, Figure 4.7 shows the SANS data and fits from trimethyloctylammonium bromide (C_8TAB) and dodecyltrimethylammonium bromide (C_{12}TAB), where the parameters used to fit the data from C_8TAB does not suitably fit the data from C_{12}TAB and *vice versa*.
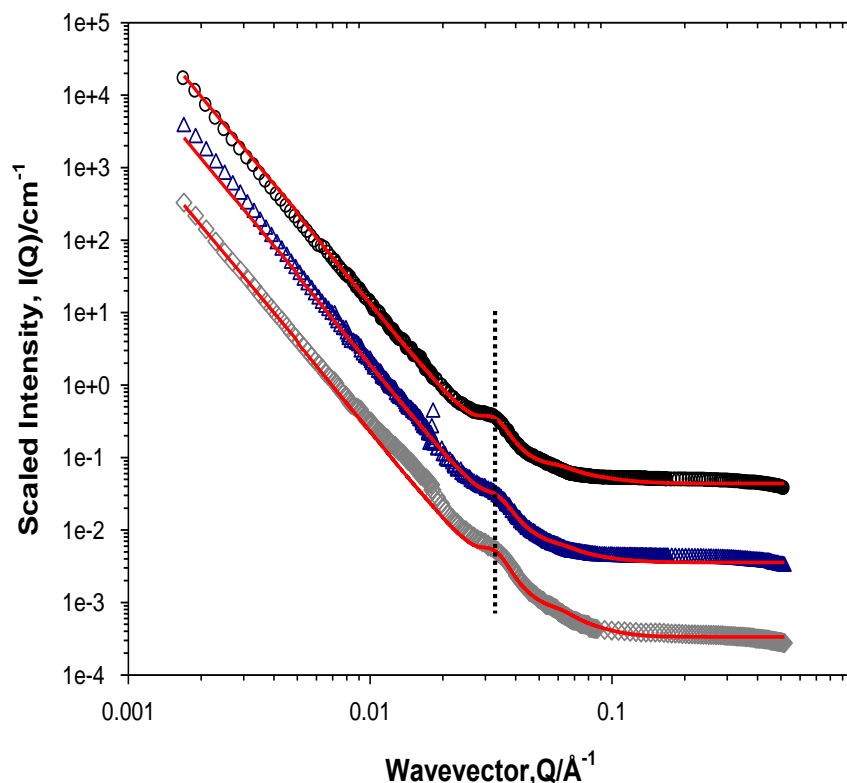
Figure 4.6 SANS from foams stabilised with 50 mM C_8SO_4Na (circles), 16 mM $C_{10}SO_4Na$ (triangles) and 4 mM $C_{12}SO_4Na$ (diamonds). Solid lines are fits to the paracystalline model described in the text. Data have been shifted vertically for clarity. Dotted lines are a guide to the eye.

Figure 4.7 SANS from foams stabilised with 72 mM C$_8$TAB (circles), 29 mM C$_{10}$TAB (triangles) and 7 mM C$_{12}$TAB (diamonds) and 1.8 mM C$_{14}$TAB (hexagons) in D$_2$O. Solid lines are fits to the paracrystalline model described in the text. Data have been shifted vertically for clarity. Dotted lines are a guide to the eye.
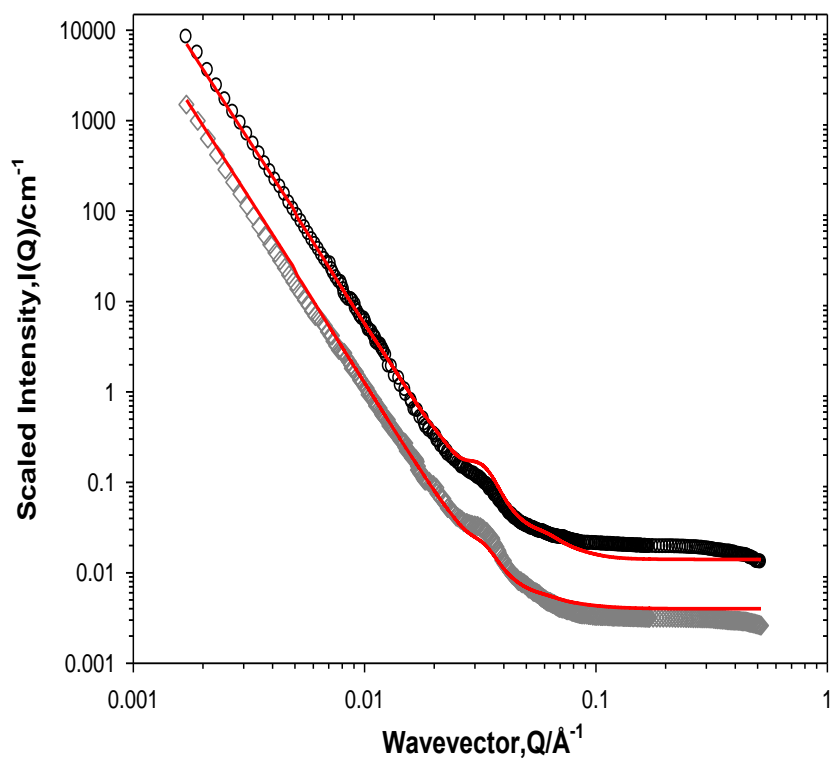
Figure 4.8 SANS from foams stabilised with 72 mM C$_8$TAB (circles) and 7 mM C$_{12}$TAB (diamonds). Solid lines are fits to the paracystalline model described in the text. Data have been shifted vertically for clarity.

4.4 Conclusions

Wet foams stabilised by small molecule surfactants have been characterised using small-angle neutron scattering. The data showed a strong Q^{-4} dependence and a series of inflexions over the mid Q range which was interpreted as a paracrystalline stack of small molecule surfactant layers. Data fitting revealed that the thickness of the stacks, L, was sensitive to the surfactant chain length. However, other parameters such as the separation, D showed limited sensitivity to the surfactant chain length and in most of the cases was estimated to be ≈ 185 Å. When comparing both the D value and the d-spacing value, one can establish that D is a term (at least for these systems) that includes the contributions from the surfactant structure and does not corresponds to a discreet, defined water film between the surfactant layers.

There is still a debate as to whether these inflexions arise from the film thickness of the bubbles (160-180 Å). However, in this work, wet foams were studied and were continually generated; hence, the bubble lamellae were estimated to be of micrometres in size and clearly visible to the eye. Moreover, previous neutron reflectivity (NR) experiments has shown the presence of lamellar ordering of aerosol-OT at the foam air/water interface.[35] Furthermore, SANS simulations, in a very similar approach to NR, were generated for films of varying thickness. The form of the data and the position of the inflexions was found not to match the scattering behaviour of the foams investigated here.

Chapter 4. Probing the interfacial structure of small molecule surfactants stabilised air-in-water foams

Bibliography

(1)   Prieto, E. M.; Page, J. M.; Harmata, A. J.; Guelcher, S. A. Injectable Foams for Regenerative Medicine. *Wiley Interdiscip. Rev. Nanomedicine Nanobiotechnology* **2014**, *6*, 136–154.

(2)   Dowling, M. B.; MacIntire, I. C.; White, J. C.; Narayan, M.; Duggan, M. J.; King, D. R.; Raghavan, S. R. Sprayable Foams Based on an Amphiphilic Biopolymer for Control of Hemorrhage Without Compression. *ACS Biomater. Sci. Eng.* **2015**, *1*, 440–447.

(3)   Wicklein, B.; Kocjan, A.; Salazar-Alvarez, G.; Carosio, F.; Camino, G.; Antonietti, M.; Bergström, L. Thermally Insulating and Fire-Retardant Lightweight Anisotropic Foams Based on Nanocellulose and Graphene Oxide. *Nat. Nanotechnol.* **2015**, *10*, 277–283.

(4)   Bureiko, A.; Trybala, A.; Kovalchuk, N.; Starov, V. Current Applications of Foams Formed from Mixed Surfactant-Polymer Solutions. *Adv. Colloid Interface Sci.* **2014**, *222*, 670–677.

(5)   Vinogradov, A. V.; Kuprin, D. S.; Abduragimov, I. M.; Kuprin, G. N.; Serebriyakov, E.; Vinogradov, V. V. Silica Foams for Fire Prevention and Firefighting. *ACS Appl. Mater. Interfaces* **2016**, 294–301.

(6)   Green, A. J.; Littlejohn, K. A.; Hooley, P.; Cox, P. W. Formation and Stability of Food Foams and Aerated Emulsions: Hydrophobins as Novel Functional Ingredients. *Curr. Opin. Colloid Interface Sci.* **2013**, *18*, 292–301.

(7)   Daugelaite, D.; Guillermic, R.; Scanlon, M. G.; Page, J. H. Quantifying Liquid Drainage in Egg-White Sucrose Foams by Resistivity Measurements. *Colloids Surfaces A Physicochem. Eng. Asp.* **2016**, *489*, 241–248.

(8)   Mansour, O. T.; Cattoz, B.; Heenan, R. K.; King, S. M.; Griffiths, P. C. Probing Competitive Interactions in Quaternary Formulations. *J. Colloid Interface Sci.* **2015**, *454*, 35–43.

(9)   Griffiths, P. C.; Hirst, N.; Paul, A.; King, S. M. Effect of Ethanol on the Interaction between Poly (Vinylpyrrolidone) and Sodium Dodecyl Sulfate. *Langmuir* **2004**, *20*, 6904–6913.

(10)   Griffiths, P. C.; Paul, A.; Stilbs, P.; Pettersson, E. Binding in Mixed Surfactant Systems. *Langmuir* **2003**, *19*, 8605–8607.

(11)   Petkova, R.; Tcholakova, S.; Denkov, N. D. Role of Polymer–surfactant Interactions in Foams: Effects of pH and Surfactant Head Group for Cationic Polyvinylamine and Anionic Surfactants. *Colloids Surfaces A Physicochem. Eng. Asp.* **2013**, 1–12.

(12)   Petkova, R.; Tcholakova, S.; Denkov, N. D. Foaming and Foam Stability for Mixed Polymer-Surfactant Solutions: Effects of Surfactant Type and Polymer Charge. *Langmuir* **2012**, *28*, 4996–5009.

(13)   Lioumbas, J. S.; Georgiou, E.; Kostoglou, M.; Karapantsios, T. D. Foam Free Drainage and Bubbles Size for Surfactant Concentrations below the CMC. *Colloids Surfaces A Physicochem. Eng. Asp.* **2015**, *487*, 92–103.

(14)   Exerowa, D. K.; Kruglyakov, P. M. *Foam and Foams Films*; Elsevier Science: Chennai, 1998.

(15)   Griffiths, P. C.; Paul, A.; Hirst, N. Electrophoretic NMR Studies of Polymer and Surfactant Systems. *Chem. Soc. Rev.* **2006**, *35*, 134–145.

(16)   Hecht, E.; Mortensen, K. Interaction of ABA Block Copolymers with Ionic Surfactants: Influence on Micellization and Gelation. *J. Phys. Chem. B* **1995**, *88*, 4866–4874.

(17)   Patel, V.; Dey, J.; Ganguly, R.; Kumar, S.; Nath, S.; Aswal, V. K.; Bahadur, P. Solubilization of Hydrophobic Alcohols in Aqueous Pluronic Solutions: Investigating the Role of Dehydration of the Micellar Core in Tuning the Restructuring and Growth of Pluronic Micelles. *Soft Matter* **2013**, *9*, 7583–7591.

(18)   Alexandridis, P.; Hatton, T. A. Block Copolymer Surfactants in Aqueous Solutions and at Interface: Thermodynamics, Structure, Dynamics and Modeling. *Colloids Surfaces A Physicochem. Eng. Asp.* **1995**, *96*, 1–46.

(19)   Stocco, A.; Rio, E.; Binks, B. P.; Langevin, D. Aqueous Foams Stabilized Solely by Particles. *Soft Matter* **2011**, *7*, 1260–1267.

(20) Du, Z.; Bilbao-Montoya, M. P.; Binks, B. P.; Dickinson, E.; Ettelaie, R.; Murray, B. S. Outstanding Stability of Particle-Stabilized Bubbles. *Langmuir* **2003**, *19*, 3106–3108.

(21) Howse, J. R.; Steitz, R.; Pannek, M.; Simon, P.; Schubert, D. W.; Findenegg, G. H. Adsorbed Surfactant Layers at Polymer/liquid Interfaces. A Neutron Reflectivity Study. *Phys. Chem. Chem. Phys.* **2001**, *3*, 4044–4051.

(22) Liu, X.; Dedinaite, A.; Nylander, T.; Dabkowska, A. P.; Skoda, M.; Makuska, R.; Claesson, P. M. Association of Anionic Surfactant and Physisorbed Branched Brush Layers Probed by Neutron and Optical Reflectometry. *J. Colloid Interface Sci.* **2015**, *440*, 245–252.

(23) Schmidt, I.; Novales, B.; Boué, F.; Axelos, M. Foaming Properties of Protein/pectin Electrostatic Complexes and Foam Structure at Nanoscale. *J. Colloid Interface Sci.* **2010**, *345*, 316–324.

(24) Axelos, M.; Boué, F. Foams as Viewed by Small-Angle Neutron Scattering. *Langmuir* **2003**, *19*, 6598–6604.

(25) Ropers, M. H.; Novales, B.; Boué, F.; Axelos, M. Polysaccharide/Surfactant Complexes at the Air-Water Interface - Effect of the Charge Density on Interfacial and Foaming Behaviors. *Langmuir* **2008**, *24*, 12849–12857.

(26) Micheau, C.; Bauduin, P.; Diat, O.; Faure, S. Specific Salt and pH Effects on Foam Film of a pH Sensitive Surfactant. *Langmuir* **2013**, *29*, 8472–8481.

(27) Fameau, A. L.; Saint-Jalmes, A.; Cousin, F.; Houinsou Houssou, B.; Novales, B.; Navailles, L.; Nallet, F.; Gaillard, C.; Boué, F.; Douliez, J. P. Smart Foams: Switching Reversibly between Ultrastable and Unstable Foams. *Angew. Chemie - Int. Ed.* **2011**, *50*, 8264–8269.

(28) Hurcom, J.; Paul, A.; Heenan, R. K.; Davies, A.; Woodman, N.; Schweins, R.; Griffiths, P. C. The Interfacial Structure of Polymeric Surfactant Stabilised Air-in-Water Foams. *Soft Matter* **2014**, *10*, 3003–3008.

(29) Garrett, P. R.; Moore, P. R. Foam and Dynamic Surface Properties of Micellar Alkyl Benzene Sulphonates. *J. Colloid Interface Sci.* **1993**, *159*, 214–225.

(30) Denkov, N. D.; Tcholakova, S.; Golemanov, K.; Ananthpadmanabhan, K. P.; Lips, A. The Role of Surfactant Type and Bubble Surface Mobility in Foam Rheology. *Soft Matter* **2009**, *5*, 3389–3408.

(31) Rosen, M. J.; Kunjappu, J. T. *Surfactants and Interfacial Phenomena: Fourth Edition*; John Wiley and Sons: New Jersey, 2012.

(32) Holmberg, K.; Jonsson, B.; Kronberg, B.; Lindman, B. *Surfactants And Polymers In Aqueous Solutions: Second Edition*; John Wiley and Sons: Chichester, 1998; Vol. 14.

(33) Zank, J.; Reynolds, P. A.; Jackson, A. J.; Baranyai, K. J.; Perriman, A. W.; Barker, J. G.; Kim, M. H.; White, J. W. Aggregation in a High Internal Phase Emulsion Observed by SANS and USANS. *Phys. B Condens. Matter* **2006**, *385–386*, 776–779.

(34) Fameau, A. L.; Salonen, A. Effect of Particles and Aggregated Structures on the Foam Stability and Aging. *Comptes Rendus Phys.* **2014**, *15*, 748–760.

(35) Ederth, T.; Thomas, R. K. A Neutron Reflectivity Study of Drainage and Stratification of AOT Foam Films. *Langmuir* **2003**, *19*, 7727–7733.

(36) Lee, J.; Nikolov, A.; Wasan, D. Foam Stability: The Importance of Film Size and the Micellar Structuring Phenomenon. *Can. J. Chem. Eng.* **2014**, *92*, 2039–2045.

(37) Etrillard, J.; Axelos, M. A. V; Cantat, I.; Artzner, F.; Renault, A.; Weiss, T.; Delannay, R. In Situ Investigations on Organic Foam Films Using Neutron and Synchrotron Radiation. *Langmuir* **2005**, *21*, 2229–2234.

(38) Shibayama, M.; Hashimoto, T. Small-Angle X-Ray Scattering Analyses of Lamellar Microdomains Based on a Model of One-Dimensional Paracrystal with Uniaxial Orientation. *Macromolecules* **1986**, *19*, 740–749.

(39) Kotlarchyk, M.; Ritzau, S. M. Paracrystal Model of the High-Temperature Lamellar Phase of a Ternary Microemulsion System. *J. Appl. Crystallogr.* **1991**, *24*, 753–758.

(40) Sinha, S. K. Small-Angle and Surface Scattering from Porous and Fractal Materials. In *Complementarity Between Neutron and Synchrotron X-Ray Scattering*; World Scientific: Singapore, 1998; pp. 251–281.

Chapter 5

5. The interfacial structure of air-in-water foams stabilised by polymer and small molecule surfactants mixtures

5.1 Abstract

Small-angle neutron scattering has been used to investigate foams stabilised by polymer-small molecule surfactant (alkyl sulfates and alkyl bromides) mixtures below the critical micelle concentration. The data showed a typical Q^{-4} dependence, along with a series of inflexions at mid Q that has been attributed to paracrystalline stack of the polymer and surfactant at the foam air/water interface. The strength of the interactions between the polymers and the small molecule surfactants was shown to control the thickness of these layers. For weakly interacting systems, *e.g.* P123 and $C_{12}TAB$, there were no changes observed in the dimensions of the surfactant layers. For systems showing strong interactions, *e.g.* P123 and $C_{12}SO_4Na$, the surfactant layers became thinner and the spacing between the surfactant layers increased. Mixtures of the homopolymer PVP and $C_{12}SO_4Na$ were also investigated, and it was demonstrated that the presence of the PVP did not affect the $C_{12}SO_4Na$ interfacial structure.

5.2 Introduction

Polymer-surfactant stabilised foams are of growing interest for a wide range of products in different industries, such as paper, foodstuffs, home, personal care and pharmaceutical industries either because the foam is an end product (foodstuffs) or encountered during the manufacturing process (*e.g.* paper).[1–4] The ability to understand and control the interactions between the polymers and the surfactants provides new insights into controlling the foaming properties of these systems, and eventually, optimizing the performance of the formulation. The interactions between polymers and surfactants in the bulk solutions have been extensively investigated and are relatively well understood.[5–10] But far less is known of how these interactions affect the foam properties (foamability, foam stability, *etc.*) and interfacial structures.

In general, binary mixtures of polymers and surfactants have been investigated and discussed in terms of the strength of the interactions between the surfactant and the polymer chains. Numerous reviews exist on this topic.[11–15] These interactions are hydrophobic or electrostatic in nature, depending on the chemical composition of the two components. The surfactant structure in these complexes could be of monomeric or micellar nature depending on several factors such as the surfactant/polymer concentration, the presence of any additives and the conditions of the solution being studied. Prasad *et al.*[16] have investigated a series of samples comprising the homopolymer polyvinypyrrolidone (PVP, molecular weight of 40,000 gmol^{-1}) and the anionic surfactant sodium dodecylsulfate ($C_{12}SO_4Na$ or SDS) using tensiometry, conductometry, microcalorimetry and dynamic light scattering (DLS). The authors concluded that the presence of PVP impacted the surfactant self-aggregation behavior at concentrations lower than its aqueous critical micelle concentration (CMC) demonstrating the presence of interactions between the polymer and the surfactant. The polymer is "saturated" when the prevailing unimer concentration exceeds the CMC, and free micelles form in solution.

The interactions between polyethylene oxide (PEO) and $C_{12}SO_4Na$ in the bulk have been studied by Barbosa and coauthors[17] as a function of different simple ionic cosolutes, such as, NaCl, Na_2SO_4 and Li_2SO_4 and more complex ones as $Na_2[Fe(CN_3)NO]$ and $Na_3[Co(NO)_6]$ using isothermal titration calorimetry (ITC) and small-angle X-ray scattering (SAXS).

The authors showed that at low surfactant concentrations, there are no significant interactions between the surfactant and the polymer. This was not the case at higher surfactant concentrations, where it was shown that the interactions yielded more stable micelles in which the EO groups are solubilized in the headgroup region of the micelle. The addition the simple cosolutes had no impact on the interactions, however, the addition of the more complex ones lead to the absence of any interactions between the polymer and the surfactant.

Most of these recent studies on polymer and/or surfactant complexes, have been performed under static conditions,[18–23] postulating about the composition and the structure of these adsorbed layers at the interface. Also, most of these studies have investigated these systems at conditions close to equilibrium, where in a practical application, these systems are often used at conditions that are far from equilibrium. Far fewer of these studies have investigated foams stabilised by these complexes, where the conclusions were largely qualitative and a detailed understanding of the foam induced interface is yet to be drawn.

Generally speaking, the interactions between polymers and surfactants in the bulk are expected to drive the structure and the composition of the layers adsorbed at the air/water interface. Few studies have focused on the relationship between such adsorbed layers and the foam's stability (time taken for the foam to collapse) and "foaminess" (measured height of the foam). Petkova *et al.*[24] have investigated the interactions between the cationic poly(vinylamine) PVA, the non-ionic poly(*N*-vinyl-formamide) PVFA and the anionic $C_{12}SO_4Na$, the cationic dodecyltrimethylammonium bromide ($C_{12}TAB$) and the non-ionic Brij 35 ($C_{12}EO_{23}$). The authors demonstrated that systems comprising $C_{12}SO_4Na$ and PVA showed strong interactions illustrated by a remarkable decrease in the foamability but higher foam stability when compared to the $C_{12}SO_4Na$ foam on its own. This decrease in foamability was related to the synergistic interactions between the polymer and the surfactant which resulted in a decrease in the concentration of the unbound $C_{12}SO_4Na$ monomer, due to its strong binding to the polymer.

The weakly interacting systems of $C_{12}SO_4Na$ + PVFA, $C_{12}TAB$ + PVA and $C_{12}TAB$ + PVFA showed enhanced foamability and foaminess. This was attributed to a combination of mechanisms; the fast surfactant adsorption on the solution surface promoting foaming, and the strong steric repulsion by the surface active surfactant-polymer complex formed in the static foams, stabilising them.

Neutron techniques have a proven ability to probe the adsorption of molecules at interfaces, and have contributed significantly to the understanding of the structure-activity relationships of interfacially bound species. In the case of foam related systems, neutron and X-ray reflectivity have been used extensively to quantify the gas-liquid interface, but quasi-exclusively on planar interfaces, and not under conditions relevant to the foam.[18,20,25]

The most recent work by Angus-Smyth *et al.*[25] on the dynamic adsorption of weakly interacting polymer/surfactant mixtures at the air/water interface provided detailed insights about the composition of the adsorbed layers. These mixtures comprised PEO, $C_{12}SO_4Na$ and tetradecyltrimethylammonium bromide ($C_{14}TAB$) and were studied using ellipsometry and neutron reflectivity (NR). The authors created the dynamic conditions by using an overflowing cylinder, where the liquid containing the polymer and surfactant mixtures was forced up the inner cylinder by a gravity feed, the overflow was collected in the outer cylinder and recirculated by a pump. The authors co-modeled the NR and ellipsometry data to elucidate the mechanism by which the polymer, the surfactants and their mixtures adsorb at the air/water interface. It was concluded that for PEO/$C_{14}TAB$ systems, the polymer adsorption drops significantly (to zero) over a narrow range of $C_{14}TAB$, while for PEO/$C_{12}SO_4Na$ systems, the inhibition of the polymer adsorption was more gradual.

NR has been used by Ederth *et al.*[26] to monitor the structure of draining Aerosol-OT (AOT) foam films. The authors have observed weak Bragg peaks which have been attributed to a lamellar structure of AOT bilayers in the foam films. This weak intensity profile of the Bragg peaks has been related to the small number of layers of AOT that contributes to the scattering in the films, films inhomogeneities and the presence of other structures such like micelles or discontinuous bilayers.

Chapter 5. The interfacial structure of air-in-water foams stabilised by polymer and small molecule surfactants mixtures

These conclusions were in very good agreement with the results from our previous study on polymeric surfactant stabilised foams using small-angle neutron scattering (SANS) [27] and with the studies on small molecule surfactants (SMS) stabilised foams in Chapter 4.

In that latter study, we investigated foams stabilised by SMS below their CMC, the data showed a pronounced Q^{-4} dependence and a series of inflexions over the mid Q range. These inflexions were attributed to a paracrystalline stack of SMS bilayers, where the position of these inflexions was found to be sensitive to the surfactant structure (headgroup size and chain length). Data fitted to a model of paracrystalline stack of surfactants in which the thickness of the surfactant layer, spacing between the layers and the number of these layers were taken into account (Chapter 4, Figure 4.5). Upon draining these foams, micellar like scattering was observed which was attributed to the presence of solution like micelles in the foam films, this was postulated to occur due to the sensitivity of the paracrystalline stacks to the water content within the foam films.

In this Chapter, we extend our study on the interfacial structure of polymers and SMS stabilised foams using tensiometry and SANS. The systems investigated here comprised the following: (a) pure surfactant systems of the anionic sodium octylsufalte (C_8SO_4Na) and sodium dodecyl sulfate ($C_{12}SO_4Na$) ,the cationic trimethyloctylammonium bromide (C_8TAB) and dodecyltrimethylammonium bromide ($C_{12}TAB$) and the non-ionic polymeric surfactant Pluronic® P123, (b) mixtures of P123 + C_8SO_4Na, P123 + C_8TAB and P123 + $C_{12}SO_4Na$, P123 + $C_{12}TAB$ and (c) mixtures of $C_{12}SO_4Na$ and PVP-40, at concentrations below the respective CMC or critical aggregation concentration (CAC), and all with relatively similar surface activity. To our knowledge, this is the first time that the interfacial structure of foams stabilised by mixtures of polymers and surfactants have been extensively studied by SANS.

5.3 Experimental

5.3.1 Materials

The small molecule surfactant sodium octylsulfate (C_8SO_4Na, 99 %) was purchased from Alfa-Aesar and was used as received. Trimethyloctylammonium bromide (C_8TAB, 98 %), dodecyltrimethylammonium bromide ($C_{12}TAB$, 99 %), sodium dodecylsulfate (SDS, $C_{12}SO_4Na$, 98 %), polyvinylpyrrolidone (PVP-40, average mol wt. 40,000 g mol^{-1}) and Pluronic® P123 (mol wt. 5800 g mol^{-1}) were all purchased from Sigma Aldrich (UK) and were all used as received. For the SANS experiments, the samples were prepared in deuterium oxide (99.9 %, Sigma Aldrich). All the polymers and surfactants used in this work were protonated.

5.3.2 Methods

5.3.2.1 Tensiometry

Surface tension measurements were carried out using a maximum bubble pressure tensiometer (SITA science on-line t60, Germany), calibrated by reference to de-ionized water. Surface tension was recorded at a bubble lifetimes of 10 seconds. All measurements were taken at 25 ± 1°C.

5.3.2.2 SANS

In all the experiments, the foam was generated by pushing nitrogen gas through a frit at the base of a Perspex column (height of 25 cm) which contains approximately 50 ml of the surfactant solution. A 2 cm wide groove has been removed and covered with aluminium foil to allow the neutrons to cross the sample (detailed description of the foam cell components has been included in Chapter 4).

SANS experiments were performed on either (i) the time of flight SANS2d diffractometer at the ISIS pulsed spallation neutron source, Rutherford Appleton Laboratory, Didcot, UK. A Q range defined by $Q= (4\pi/\lambda) \sin (\theta/2)$ between 0.004 and ≥ 0.6 Å^{-1} was obtained by using neutron wavelengths (λ) spanning 1.75 to 16.5 Å with a fixed detector distance of 4 m, or (ii) at the D11 diffractometer at the steady state reactor source, ILL, Grenoble where a Q range is selected by choosing three instrument settings at a constant neutron wavelength (λ) of 8 Å and sample detector distance of 1.2, 8 and 39 m.

All scattering data were (a) normalized for the sample transmission, (b) background corrected using the empty foam cell and (c) corrected for the linearity and efficiency of the detector response using the instrument specific software package and the scattering from a polystyrene blend taped to the front of the foam cell.

5.4 Results and Discussion

5.4.1 Surface properties

Surface properties of the SMS, P123 and their mixtures have been characterised by measuring their surface tension. In Figure 5.1, the data shows surface tension *vs.* concentration for the pure systems of C_8SO_4Na and $C_{12}SO_4Na$. The data exhibits a typical surface tension behaviour for pure surfactants, where by increasing the surfactant concentration, the surface tension is lowered, as the systems goes from a surface tension of ≈ 71 mN/m to a system where the interface is saturated with the surfactant (≈ 35 mN/m) along with the formation of the micelles in bulk. An important feature of this transition is presented as a "break point", indicative of the surfactant CMC. The data from this group also shows a similar surface activity behaviour, for example, at concentrations half their CMC (50 mM for C_8SO_4Na) and (4 mM $C_{12}SO_4Na$), Table 5.1 and 5.2, the surface tension value is almost of equal value of $\approx$ 40 mN/m. Similar features were observed from C_8TAB and $C_{12}TAB$ systems, Figure 5.2, where the position of the break point also varied significantly with hydrocarbon chain length, however, the surface activity shows a different behaviour, *i.e.* $C_{12}TAB$ is more surface active.
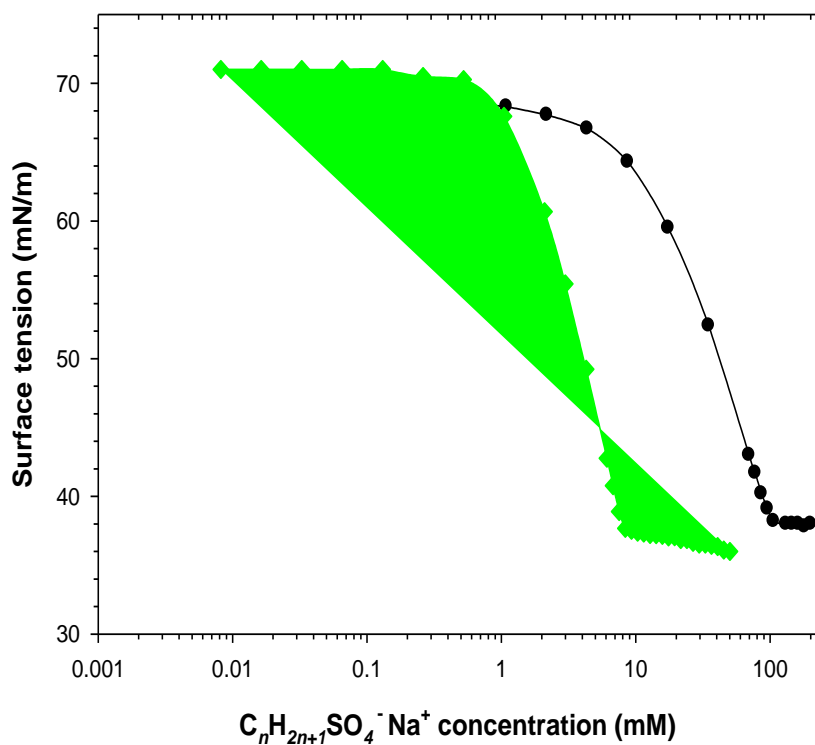
Figure 5.1 Surface tension as a function of C$_8$SO$_4$Na (circles) and C$_{12}$SO$_4$Na (diamonds) concentration in water.
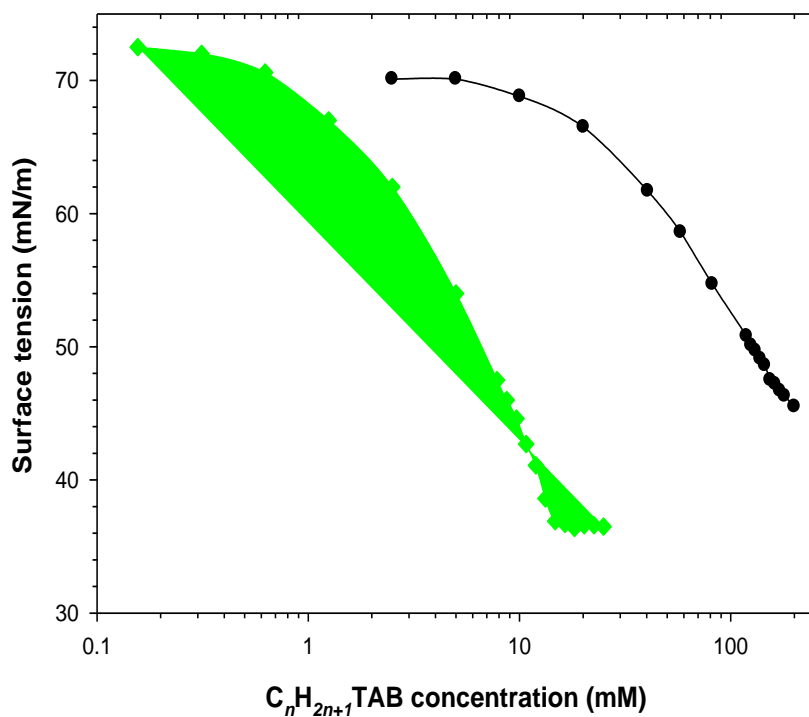
Figure 5.2 Surface tension as a function of C$_8$TAB (circles) and C$_{12}$TAB (diamonds) concentration in water.

This could possibly be attributed to the large size of the headgroup (if compared to the size of sulfate group) and its effect on the degree of counterion binding which eventually affects the surfactant's surface activity profile.

Surfactant	CMC (mM)	CMC from literature (mM)
C_8SO_4Na	100	110[28]
$C_{12}SO_4Na$	7.9	8.0[29–31]

Table 5.1 Critical micelle concentration from C_8 and C_{12} alkyl sulfate surfactants in water.

Surfactant	CMC (mM)	CMC from literature (mM)
C_8TAB	145	140[28,32]
$C_{12}TAB$	14.5	15.5[28,33–35]

Table 5.2 Critical micelle concentration from C_8 and C_{12} alkyl bromide surfactants in water.

5.4.1.1 Surface tension from SMS and P123 mixtures in water

Moving to the binary mixture cases, a far more interesting surface behaviour in comparison with the single surfactant systems can be observed. Figure 5.3 and 5.4, shows the surface tension data from C_8SO_4Na, $C_{12}SO_4Na$ and C_8TAB, $C_{12}TAB$ respectively in the presence of 0.025 wt% P123 (below the CMC, ≈ 0.05 wt%) in water. These interesting features includes the appearance of maxima in the surface tension data. The P123 + C_8SO_4Na system (Figure 5.3) at low SMS concentration, the data shows a plateau where the system in this region is dominated by the P123 monomers, as the SMS concentration increases, the surface tension decreases (between 40 and 60 mM), indicating the formation of species more surface active than P123.

With higher SMS concentration, the data now shows a maxima, indicating that the surface is now stripped of the more surface active species, and replaced again by less surface active species. At concentrations higher than 120 mM, the data shows a plateau again, but in this region, it is dominated by the SMS.
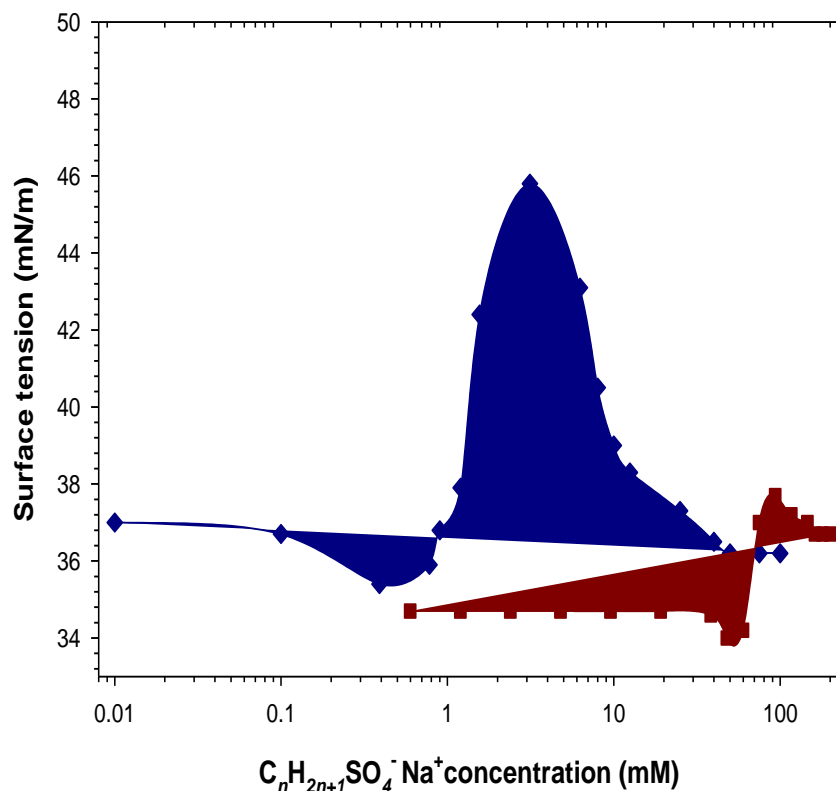
Figure 5.3 Surface tension as a function of C₈SO₄Na (squares) and C₁₂SO₄Na (diamonds) concentration in 0.025 wt% P123 and water.

In the P123 + $C_{12}SO_4Na$ case, the data follows the same trend, however some differences are observed, for example, the concentration range at which the maxima is observed is now between 1 and 11 mM of $C_{12}SO_4Na$ in comparison with 65 and 105 mM for the C_8SO_4Na case. The surface tension at the maximum is ≈ 46 mN/m in comparison to ≈ 38 mN/m in the P123 + C_8SO_4Na.

These are very interesting observations, especially when considering that both C_8SO_4Na and $C_{12}SO_4Na$ show a similar surface behaviour, ± 2.0 mN/m, at the concentrations in which the surface tension was measured without the presence of any P123.

Surface tension is a measure of the surface properties, hence it is difficult to design an experiment that investigates both the surface and the bulk characteristics. Hence, relating these changes observed earlier in the surface tension behaviour to the nature of the interactions, whether synergistic or antagonistic, between P123 and the SMS, is not that straightforward, especially when both are surface active.

In the P123 + C$_n$TAB case, abrupt changes in surface tension are only observed in the C$_{12}$ case, where only one minimum in the surface tension, ≈ 31 mN/m, is observed. As the C$_{12}$TAB concentration increases, the interface is being replaced by more surface active complex as the SMS concentration increases. The data shows again a plateau as the SMS dominates the interface. For the P123 + C$_8$TAB case, the surface tension data does not show such abrupt changes, but behaves in a similar fashion to the pure C$_8$TAB. In all cases, the concentration at which the surface tension begins to show these features, has been identified here as the critical aggregate concentration (CAC) and summarised in Table 5.3 and 5.4. For clarity, the CMC values of pure SMS have been also included in Table 5.3.
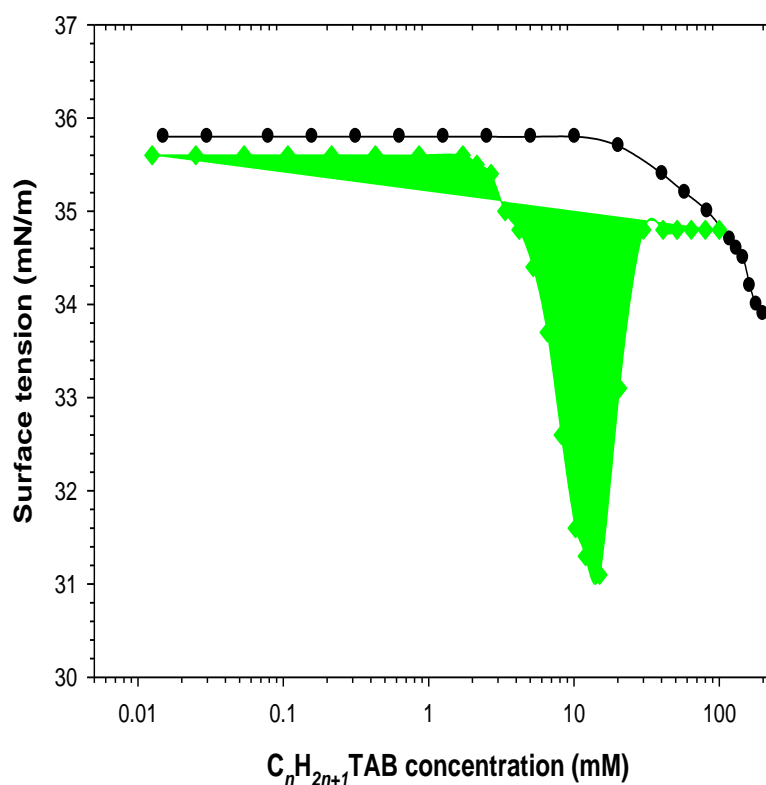
Figure 5.4 Surface tension as a function of C$_8$TAB (circles) and C$_{12}$TAB (diamonds) in 0.025 wt% P123 and water.

System description	CMC (mM)	Surface tension (mN/m)
C_8SO_4Na	100	38.6
$C_{12}SO_4Na$	7.90	39.0
C_8TAB	145	48.6
$C_{12}TAB$	14.5	37.7

Table 5.3 Critical micelle concentration (CMC), and the surface tension of SMS at the CMC in water.

System description	CAC (mM)	Surface tension (mN/m)
P123 + C_8SO_4Na	35	34.6
P123 + $C_{12}SO_4Na$	0.2	36.0
P123 + C_8TAB	25	35.8
P123 + $C_{12}TAB$	2.0	35.5

Table 5.4 Critical aggregation concentration (CAC) and the surface tension of SMS with 0.025 wt% P123 at the CAC in water.

As stated earlier, the interactions between P123 and SMS have been studied before, (this also includes the work in chapter 2), where generally, the modelling was largely applied on systems where mixed micelles were present. To our knowledge, no studies have investigated P123-SMS complexes below the CAC or the CMC_{mixed}, where only surfactant monomers are expected to be present. Here, we extend the study described in Chapter 2 on mixed micellar systems, where P123 was found to interact strongly with $C_{12}SO_4Na$ and P123 showed weak interactions with $C_{12}TAB$.

5.4.1.2 Surface tension from $C_{12}SO_4Na$ and PVP-40 mixtures in water

Surface tension profiles from PVP and $C_{12}SO_4Na$ mixtures are presented in Figure 5.5, where the surface behaviour of $C_{12}SO_4Na$ in the presence of three different concentrations of PVP (0.01, 0.1 and 1 wt%) was recorded. Interactions between PVP and $C_{12}SO_4Na$ have been reported before,[9,36–38] where at high enough polymer concentration (typically ≥ 0.5 wt%), two "break points" in the surface tension data were observed. These break points were related to the CAC of $C_{12}SO_4Na$ and the formation of free micelles in bulk.

In the absence of any polymers, the CMC of $C_{12}SO_4Na$ is 7.9 mM (Figure 5.1). In the presence of 0.01 and 0.1 wt% PVP, we can only observe one break point for the surfactant at 10 mM and 11 mM, respectively. This change in the CMC/CAC signals the presence of strong interactions between the polymer and the surfactant. A better understanding of the changes occurring in the interface and the bulk in the PVP-$C_{12}SO_4Na$ systems could be derived in the presence of 1 wt% PVP. There are now more than one break point as has been reported before in the 0.5 wt% PVP case. The first break point CAC (1) is at 2 mM. This break point is believed to be related to the CAC of the $C_{12}SO_4Na$ where it forms polymer-surfactant aggregates in the bulk and at the interface. As the concentration of the surfactant increases, the surface tension decreases as the system becomes dominated by the surfactant, another break point CAC (2) is observed at 45 mM, where free $C_{12}SO_4Na$ micelles start to from in solution along with the surfactant monomers saturating the interface.[16,37]
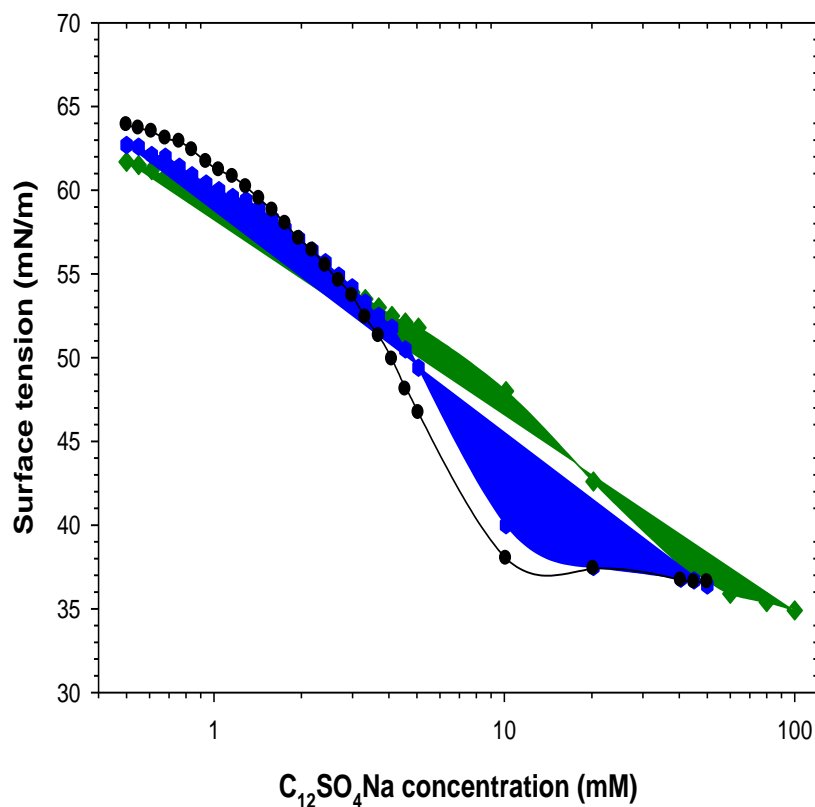
Figure 5.5 Surface tension as a function of $C_{12}SO_4Na$ in 0.01 wt% PVP (circles), 0.1 wt% PVP (hexagons) and 1 wt% PVP (diamonds) in water.

Several previous studies have studied the relationship between the foamability, foam stability and the surface behaviour of polymer surfactant mixtures.[24,39–41] Here, the technique is used to compliment to the SANS measurements. Surface tension has helped identify some peculiar surface tension behaviour and also CMC and CAC. This dictated the samples to be studied by SANS, at concentrations well below (half) the CAC of each mixture, so no solution-like micelles would be present in the foam films.

5.4.2 SANS from air-in-water foams stabilised by P123-SMS

5.4.2.1 Foams stabilised by P123 – C_8 SMS

The scattering in these systems may arise from: (a) any structure normal to the air/water interface, which would follow an approximate Q^{-4} dependence given that these interfaces are not perfectly flat; (b) any in plane structure normal to the interface; (c) fluctuations in the composition of the interfaces parallel to the beam; (d) structures that would be present in the liquid junctions between the bubbles, this may resemble the 'bulk solutions' at appropriate concentration; and (e) in the aged polyhedral foams, the long almost cylindrical regions at the junction of bubbles associated with the plateau borders.

SANS data (recorded on D11) from foams stabilised by 0.025 wt% P123, 50 mM C_8SO_4Na and their mixture; P123 + C_8SO_4Na at concentrations below the CAC (0.025 wt% P123 and 15 mM C_8SO_4Na) are shown in Figure 5.6. The data shows the same pronounced Q^{-4} dependence observed previously from foams stabilised by polymeric surfactants[27] and small molecule surfactants (chapter 4).

For the P123, at mid Q, the data show an inflexion at $Q \approx 0.0357$ Å^{-1} corresponding to a d-spacing *(2π/Q)* of 178 Å ± 5. In the C_8SO_4Na case, the inflexion is present at $Q \approx$ 0.0330 Å^{-1} which corresponds to a d-spacing of 195 Å ± 5. In the mixture case, the d-spacing is of an intermediate value (185 Å ± 5). These inflexions could be highlighted through plotting the data in Porod plot, I(Q)*Q^4 *vs Q,* Figure 5.7. In Chapter 4, it was shown that these peaks observed at mid Q corresponds to a multi-layer structure of the SMS at the air/water interface. This is a structure that we believe to be induced at the air/water interface by the foam.
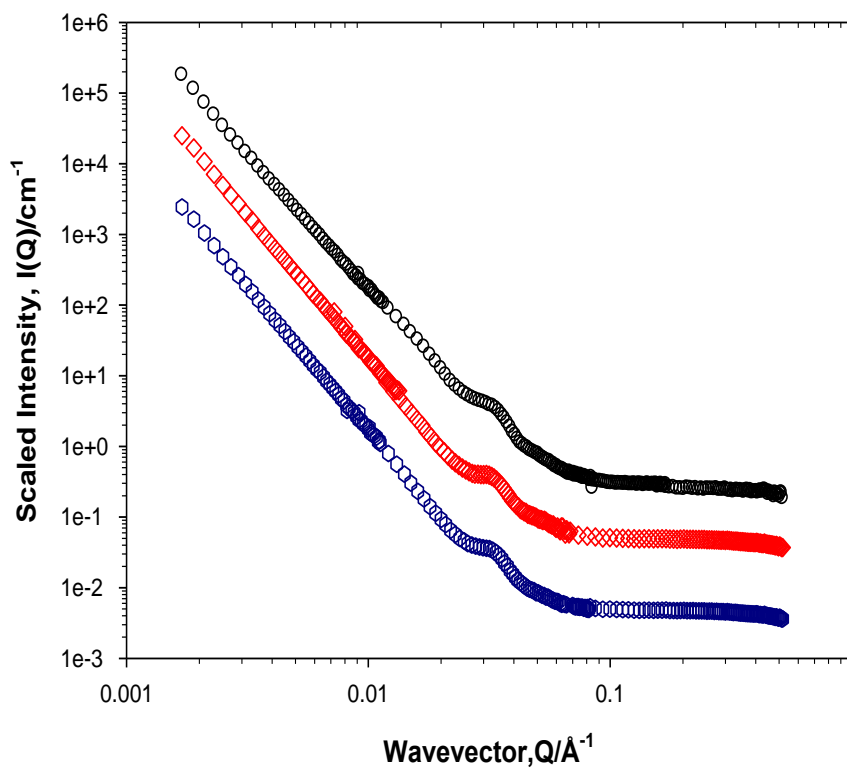
Figure 5.6 SANS from foams stabilised by 0.025 wt% P123 (circles), 50 mM C$_8$SO$_4$Na (diamonds) and 0.025 wt% P123 + 15 mM C$_8$SO$_4$Na (hexagons). Data have been shifted vertically for clarity.
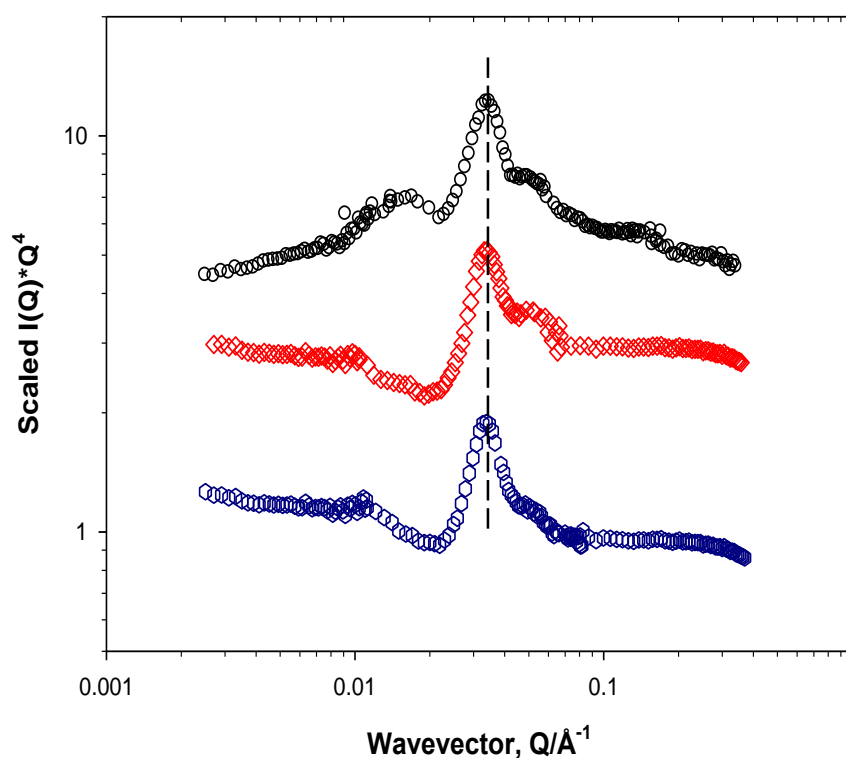
Figure 5.7 Plot of I(Q^4) *vs*. Q for foams stabilised by 0.025 wt% P123 (circles), 50 mM C_8SO_4Na (diamonds) and 0.025 wt% P123 + 15 mM C_8SO_4Na (hexagons). Data have been shifted vertically for clarity. Dashed lines are a guide to the eye.

The Porod plot, Figure 5.7, also highlights the presence of a higher order inflexion for the P123 at lower Q, ≈ 0.017 Å^{-1}. This higher order peak corresponds to a *d*-spacing value of ≈ 370 Å. This value is almost double the value of the second order inflexion observed at $Q \approx 0.0357$ Å^{-1}. This might be related to the arrangement of the multilayers in a quite possibly discontinued or heterogeneous lamellar fashion. For a perfectly lamellar structure, one would expect to see a regular reflection (*n*=1, *n*=2, *n*=3), however, the differences observed in the peak positions implies that the structure is not perfectly lamellar. This small change observed in the peak position from the foam stabilised by P123 + C_8SO_4Na mixture indicates that there are weak interactions between the polymer and the surfactant. This suggests that the multilayer is formed mainly of the P123 (given its high molecular weight) with coexisting C_8SO_4Na monomers, without changing any of the P123 layers dimensions.

A similar conclusion maybe derived from the P123, C_8TAB and their mixture. As presented in Figures 5.8 and 5.9, the data adopts similar features, where the peak positions from foams stabilised by the P123 + C_8TAB - at concentrations below the CAC (0.025 wt% P123 + 15 mM C_8TAB) ,corresponds to a *d*-spacing value of 180 Å. This is also an intermediate value if compared to the pure C_8TAB (185 Å) and P123 (178 Å) systems. By following the same assumption that the layers are mainly comprised of P123 layers, one can come to a similar conclusion in which the interactions between P123 and C_8TAB are weak and that the C_8TAB monomers are embedded in the P123 layers without changing its dimensions.
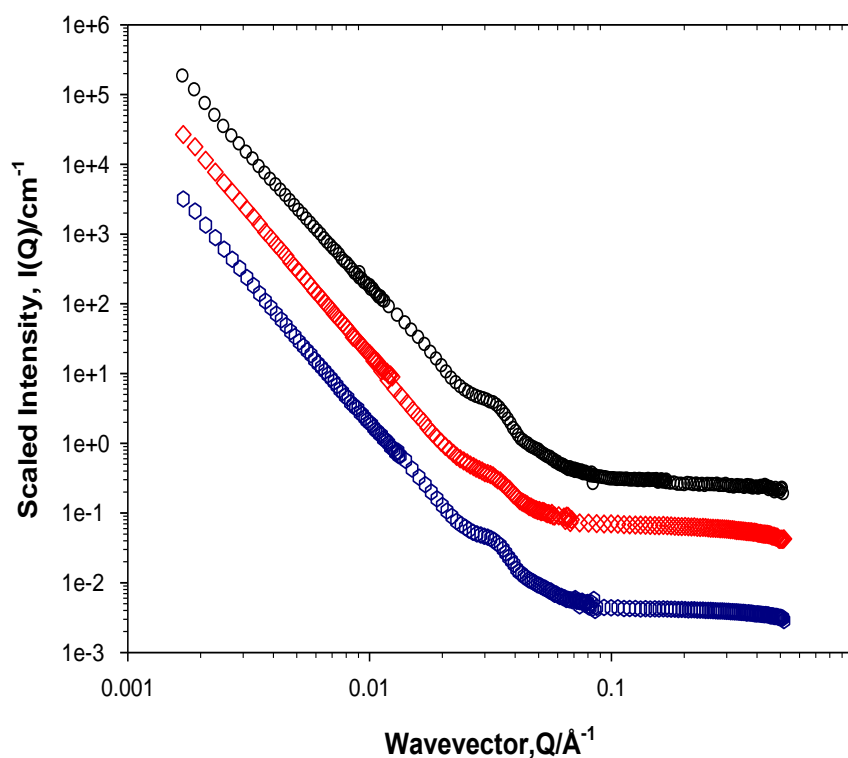
Figure 5.8 SANS from foams stabilised by 0.025 wt% P123 (circles), 72 mM C_8TAB (diamonds) and 0.025 wt% P123 + 15 mM C_8TAB (hexagons). Data have been shifted vertically for clarity.
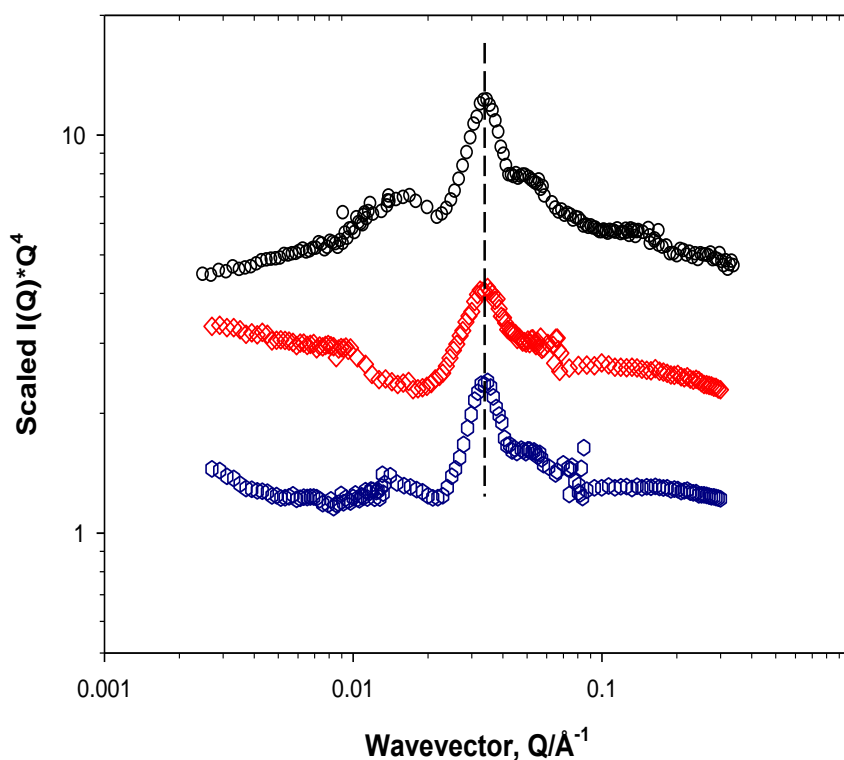
Figure 5.9 Plot of I(Q^4) *vs. Q* for foams stabilised by 0.025 wt% P123 (circles), 72 mM C$_8$TAB (diamonds) and 0.025 wt% P123 + 15 mM C$_8$TAB (hexagons). Data have been shifted vertically for clarity. Dashed lines are a guide to the eye.

5.4.2.2 SANS from foams stabilised by P123-C$_{12}$ SMS

The effect of the strength of the interactions between P123 and C$_{12}$-based SMS on the foam interfacial structure is more evident here if compared with the C$_8$ case. Figure 5.10 presents the SANS data (SANS2d) from foams stabilised by 0.025 wt% P123, 4 mM C$_{12}$SO$_4$Na and their mixture at concentrations below the CAC (0.025 wt% P123 + 0.1 mM C$_{12}$SO$_4$Na). The data recorded from P123 on SANS2d shows the same features as the data recorded for the same polymer at the same concentration, 0.025 wt% on D11. The peak positions obtained from both diffractometers are also in good agreement. The P123 from SANS2d showed the higher order peak at $\approx$ 0.0180 Å^{-1} corresponding to a *d*-spacing value of $\approx$ 350 Å (370 Å, D11) and the second order peak at *Q $\approx$ 0.0332* Å^{-1} corresponding to a *d*-spacing value of $\approx$ 185 Å (175 Å ,D11).

120
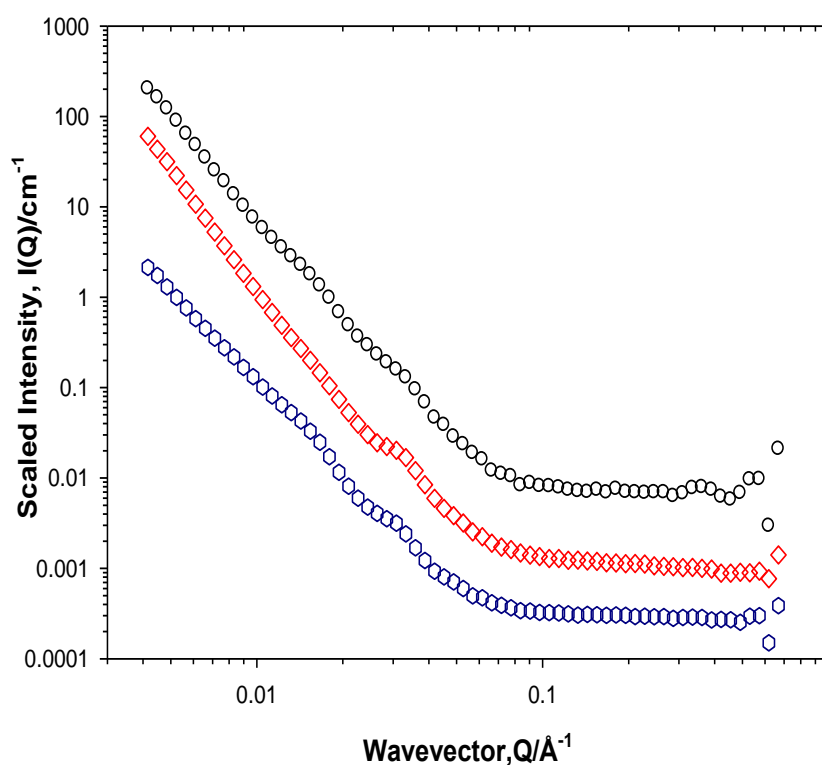
Figure 5.10 SANS from foams stabilised by 0.025 wt% P123 (circles), 4 mM C$_{12}$SO$_4$Na (diamonds) and 0.025 wt% P123 + 0.1 mM C$_{12}$SO$_4$Na (hexagons). Data have been shifted vertically for clarity.

Data recorded for 4 mM C$_{12}$SO$_4$Na foams, showed one peak at mid Q (0.0340 Å^{-1}, d-spacing of 185 Å). Whilst adding C$_{12}$SO$_4$Na, even at concentrations as low as 0.1 mM, has shown a significant impact on the P123 peaks positions. For example, the peak at low Q, now corresponds to a d-spacing value of ≈ 380 Å, where the peak at mid Q corresponds to a d-spacing value of ≈ 205 Å.

Using our previous knowledge of the strong interactions between the P123 and C$_{12}$SO$_4$Na, this increase in both d-spacing values suggests the formation of a new polymer-surfactant structure at the air/water interface, in which the surfactant is adsorbed on the PPO monomers of the P123, forming a thinner mixed surfactant layer, resulting in a larger spacing between these layer. The same approach for data presentation has been followed as before and Porod plots have been used to highlight the peaks at low and mid Q, Figure 5.11.
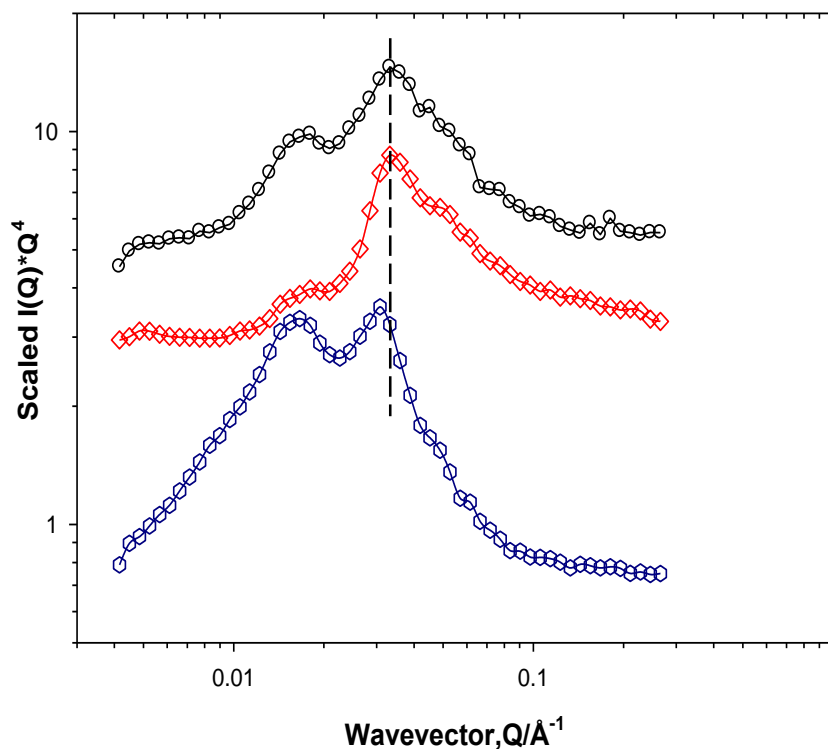
Figure 5.11 Plot of I(Q^4) *vs. Q* for foams stabilised by 0.025 wt% P123 (circles), 4 mM $C_{12}SO_4Na$ (diamonds) and 0.025 wt% P123 + 0.1 mM $C_{12}SO_4Na$ (hexagons). Lines are a guide to the eye. Data have been shifted vertically for clarity. Dashed lines are a guide to the eye.

On the other hand, in the 7 mM $C_{12}TAB$ case, the peak position corresponds to a *d*-spacing value of ≈ 185 Å, whereas for the foams from systems comprising P123 and $C_{12}TAB$, Figure 5.12 and 5.13, P123 peaks at low and mid *Q* remains at the same position after the addition of 0.1 mM $C_{12}TAB$. This finding follows the observations noted from the P123 + C_8TAB case, in which no changes in the P123 peak positions was observed after adding up to 15 mM of C_8TAB. This also indicates that the P123 multi-layers thickness remains unchanged in the presence of the $C_{12}TAB$ due to the weak interactions between both components. These weak interactions between the polymer and the surfactant could be attributed to the electrostatic repulsion as a result of a slight positive charge present on the polymer, originating from the protonation of the ether oxygen in the PEO chains.[42,43] A summary of the peak positions and *d*-spacing values are presented in Table 5.3.
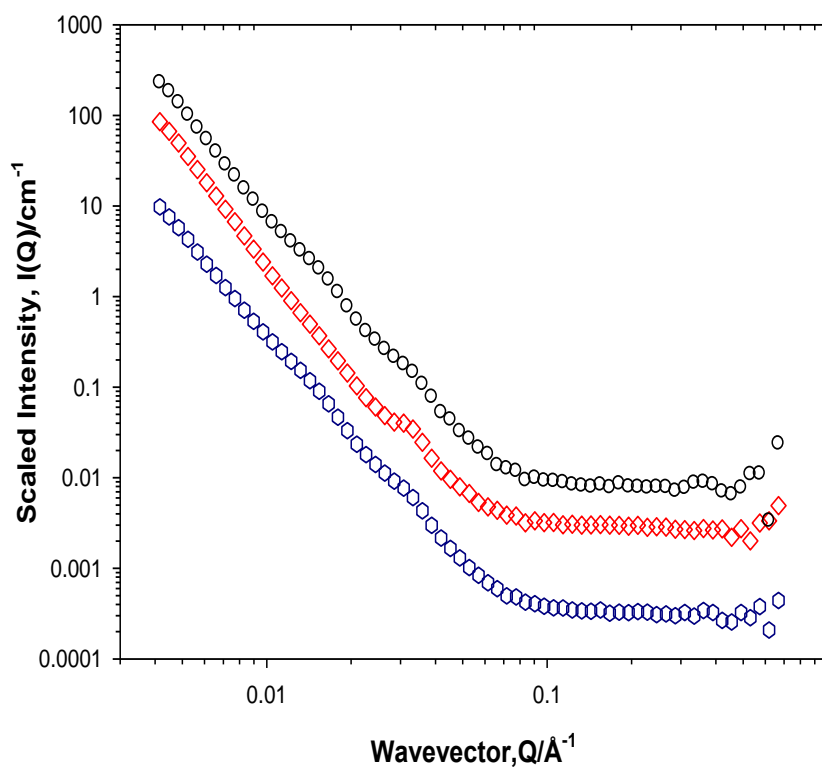
Figure 5.12 SANS from foams stabilised by 0.025 wt% P123 (circles), 7 mM C$_{12}$TAB (diamonds) and 0.025 wt% P123 + 0.1 mM C$_{12}$TAB (hexagons).
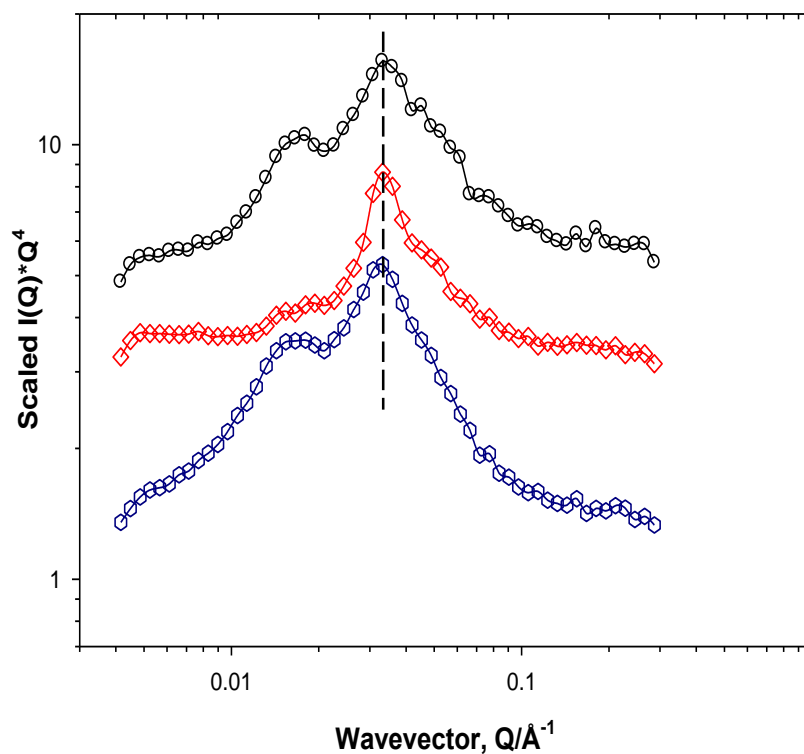

Figure 5.13 Plot of I(Q^4) *vs. Q* for foams stabilised by 0.025 wt% P123 (circles), 7 mM C$_{12}$TAB (diamonds) and 0.025 wt% P123 + 0.1 mM C$_{12}$TAB (hexagons). Lines are a guide to the eye. Data have been shifted vertically for clarity.

System description	d-spacing, ± 5 (Å)	
0.025 wt% P123 (D11)	378	178
50 mM C_8SO_4Na	195	
0.025 wt% P123 + 15 mM C_8SO_4Na	185	
72 mM C_8TAB	185	
0.025 wt% P123 + 15 mM C_8TAB	180	
0.025 wt% P123 (SANS2d)	350	185
4 mM $C_{12}SO_4Na$	185	
0.025 wt% P123 + 0.1 mM $C_{12}SO_4Na$	205	
7 mM $C_{12}TAB$	185	
0.025 wt% P123 + 0.1 mM $C_{12}TAB$	185	

Table 5.5 *d*-spacing values (Å) from SANS as a function of P123 and SMS peaks at mid *Q*. For pure P123 systems (from ILL and SANS2d), both orders of spacing are presented. *d*-spacing values from the mixtures corresponds to the mid *Q* peaks attributed to the P123 multilayers.

5.4.2.3 SANS from foams stabilised by PVP-$C_{12}SO_4Na$

The findings from the surface tension data of PVP-$C_{12}SO_4Na$ allowed us to extend the SANS study to include further systems including these mixtures at concentrations above the CAC (1); 2 mM (at least for the 1 wt% PVP system). We have investigated the interfacial structure of foams stabilised by 4 mM $C_{12}SO_4Na$ and 0.01 wt%, 0.1 wt% and 1 wt% PVP. The scattering behaviour (SANS2d) is presented in Figure 5.14. There are several features to be highlighted in the data: (a) the peak position of the $C_{12}SO_4Na$; being the surface active component, seems to be insensitive to the PVP presence at all the concentrations studied; (b) as the concentration of the polymer increases, there is a significant contribution of the polymer in solution (present in the foam films) to the scattering. This is obvious in the *Q* range of 0.05 Å^{-1} – 0.15 Å^{-1} in the Porod plots, Figure 5.15. This agrees with previous observations from foams stabilised by a high concentration of Pluronics.[27]
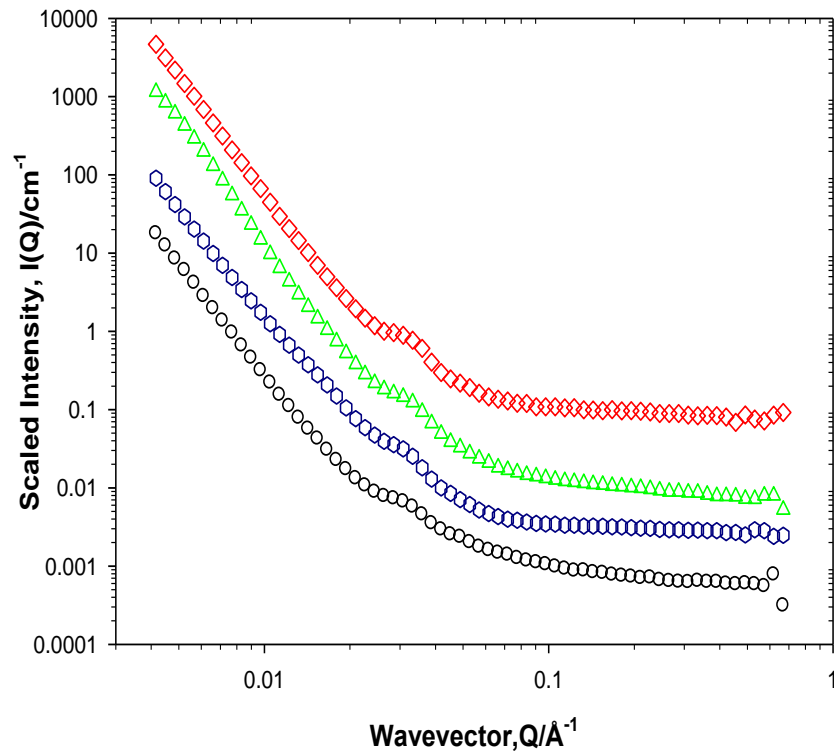
Figure 5.14 SANS from foams stabilised by 4 mM C$_{12}$SO$_4$Na (diamonds), 4 mM C$_{12}$SO$_4$Na + 0.01 wt% PVP (triangles), 0.1 wt% PVP (hexagons) and 1 wt% PVP (circles). Data have been shifted vertically for clarity.
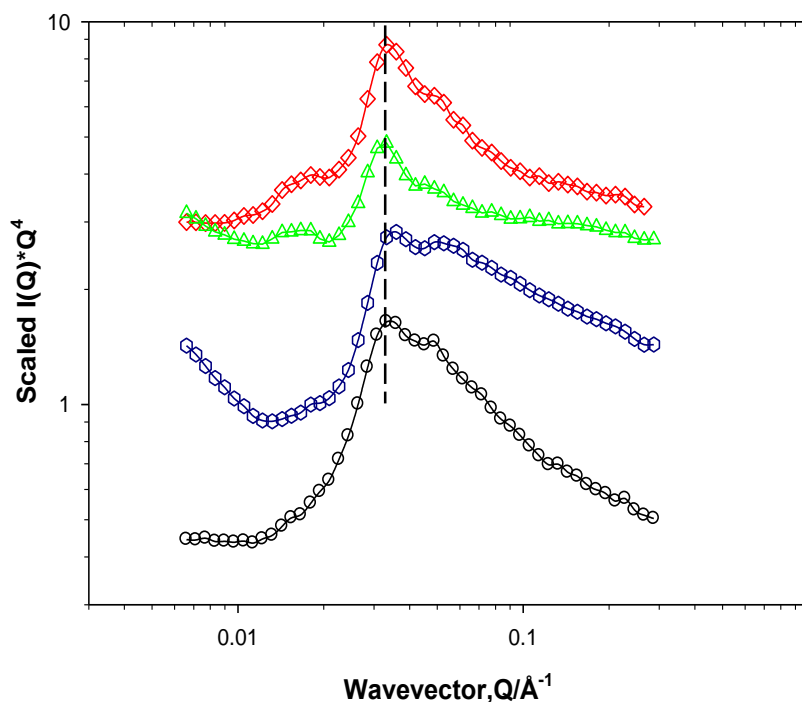
Figure 5.15 **Plot of I(Q^4)** *vs.* **Q for foams stabilised by 4 mM $C_{12}SO_4Na$ (diamonds), 4 mM $C_{12}SO_4Na$ + 0.01 wt% PVP (triangles), 0.1 wt% PVP (hexagons) and 1 wt% PVP (circles). Lines are a guide to the eye. Data have been shifted vertically for clarity. Dashed lines are a guide to the eye.**

The absence of changes in peak position of the $C_{12}SO_4Na$ in the presence of PVP, indicates that there are no changes to the surfactant structure at the air/water interface. This agrees well with the observations recorded by Prucell *et al.*[44] where they have used NR to study PVP-$C_{12}SO_4Na$ structure at the air/water interface. The authors concluded that there was no substantial effect from the PVP on the thickness of the $C_{12}SO_4Na$ interfacial layer at any polymer concentration.

The explanation behind this could be derived again from the system's behaviour in bulk and its effect on the structure at the air/water interface. Prasad *et al.*[16] have observed three break points in the surface tension data, in which one of them was attributed to the interface being stripped of both the PVP and the $C_{12}SO_4Na$, up to a point where the binding of the $C_{12}SO_4Na$ to the PVP is complete.

5.5 Conclusions

A series of foams stabilised by polymer-surfactant mixtures have been investigated by small-angle neutron scattering. The data revealed the presence of an interfacial structure of multi-layers of polymer + surfactant presented by a series of inflexions at mid Q. It was shown that the nature of the interactions between the polymers and the surfactants had control over the dimensions of these multi-layers. There were only weak interactions observed between Pluronic P123 and C_8SO_4Na, C_8TAB and $C_{12}TAB$ at concentrations below the critical aggregate concentration (CAC). This was reflected on the foam SANS data by the absence of any significant change in the positions of the inflexions across the Q range.

In the strongly interacting system of P123 + $C_{12}SO_4Na$, there was a noticeable shift in the inflexions position towards lower Q, indicating a change in the interfacial structure (mainly the thickness), presented by an increase of the d-spacing value from P123 system (185 Å to 205 Å). This is believed to occur as result of strong interactions between P123 and $C_{12}SO_4Na$, in which the small molecule surfactant adsorbs onto the P123 monomer, reducing its dimensions. We hypothesize that this will also reduce the thickness of the surfactant layers observed by SANS at the foam air/water interface, hence the increase in the d-spacing values.

Foams comprising PVP and $C_{12}SO_4Na$ were also investigated by SANS and tensiometry. The surface tension data revealed CAC that shown dependence on the amount of the polymer present in the system. Systems comprising the polymer and surfactant at concentrations above the CAC (1) were then studied by SANS. The peak positions from $C_{12}SO_4Na$ did not show any sensitivity to the presence of the PVP in the system, and the peak observed from the mixture remained in the same position as the peak from the surfactant on its own. Whereas, at high polymer concentrations, there was a noticeable contribution of the polymer in solution (in the foam films) to the scattering.

Bibliography

(1)   Arzhavitina, A.; Steckel, H. Foams for Pharmaceutical and Cosmetic Application. *Int. J. Pharm.* **2010**, *394*, 1–17.

(2)   Prudon, C.H., Haigh, J.M., Surber, C., Smith, E. Foam Drug Delivery in Dermatology. Beyond the Scalp. Am. J. **2003**, *Drug Deliv*, 71–75.

(3)   Rodríguez Patino, J. M.; Carrera Sánchez, C.; Rodríguez Niño, M. R. Implications of Interfacial Characteristics of Food Foaming Agents in Foam Formulations. *Adv. Colloid Interface Sci.* **2008**, *140*, 95–113.

(4)   Kralova, I.; Sjöblom, J. Surfactants Used in Food Industry: A Review. *J. Dispers. Sci. Technol.* **2009**, *30*, 1363–1383.

(5)   Goddard, E. D. Polymer—surfactant Interaction Part I. Uncharged Water-Soluble Polymers and Charged Surfactants. *Colloids and Surfaces* **1986**, *19*, 255–300.

(6)   Goddard, E. D. Polymer/Surfactant Interaction: Interfacial Aspects. *J. Colloid Interface Sci.* **2002**, *256*, 228–235.

(7)   Bain, C. D.; Claesson, P. M.; Langevin, D.; Meszaros, R.; Nylander, T.; Stubenrauch, C.; Titmuss, S.; von Klitzing, R. Complexes of Surfactants with Oppositely Charged Polymers at Surfaces and in Bulk. *Adv. Colloid Interface Sci.* **2010**, *155*, 32–49.

(8)   Anthony, O.; Zana, R. Interactions between Water-Soluble Polymers and Surfactants: Effect of the Polymer Hydrophobicity. 1. Hydrophilic Polyelectrolytes. *Langmuir* **1996**, *12*, 1967–1975.

(9)   Griffiths, P. C.; Cheung, A. Y. F.; Farley, C.; Paul, A.; Heenan, R. K.; King, S. M.; Pettersson, E.; Stilbs, P.; Ranganathan, R. Small-Angle Neutron Scattering, Electron Paramagnetic Resonance, Electrophoretic NMR, and Time-Resolved Fluorescence Quenching Studies of Sodium Dodecyl Sulfate and Tetra(ethylene Oxide) Dodecyl Ether Mixed Surfactant Micelles. *J. Phys. Chem. B* **2004**, *108*, 1351–1356.

(10)   Griffiths, P. C.; Hirst, N.; Paul, A.; King, S. M. Effect of Ethanol on the Interaction between Poly (Vinylpyrrolidone) and Sodium Dodecyl Sulfate. *Langmuir* **2004**, *20*, 6904–6913.

(11)   Jaber, R.; Wasbrough, M. J.; Holdaway, J. A.; Edler, K. J. Interactions between Quaternary Ammonium Surfactants and Polyethylenimine at High pH in Film Forming Systems. *J. Colloid Interface Sci.* **2015**, *449*, 286–296.

(12)   Negm, N. A.; Mohamed, A. S.; Ahmed, S. M.; El-Raouf, M. A. Polymer-Cationic Surfactant Interaction: 1. Surface and Physicochemical Properties of Polyvinyl Alcohol (PVA)-S-Alkyl Isothiouronium Bromide Surfactant Mixed Systems. *J. Surfactants Deterg.* **2015**, *18*, 245–250.

(13)   Banerjee, S.; Cazeneuve, C.; Baghdadli, N.; Ringeissen, S.; Leermakers, F. A. M.; Luengo, G. S. Surfactant-Polymer Interactions: Molecular Architecture Does Matter. *Soft Matter* **2015**, *11*, 2504–2511.

(14)   Rehman, N.; Khan, A.; Bibi, I.; Bica, C. I. D.; Siddiq, M. Intermolecular Interactions of Polymer/Surfactants Mixture in Aqueous Solution Investigated by Various Techniques. *J. Dispers. Sci. Technol.* **2013**, *34*, 1202–1210.

(15)   Mészaros, R.; Varga, I.; Gilanyi, T. Effect of Polymer Molecular Weight on the Polymer/surfactant Interaction. *J. Phys. Chem. B* **2005**, *109*, 13538–13544.

(16)   Prasad, M.; Palepu, R.; Moulik, S. P. Interaction between Sodium Dodecyl Sulfate (SDS) and Polyvinylpyrrolidone (PVP) Investigated with Forward and Reverse Component Addition Protocols Employing Tensiometric, Conductometric, Microcalorimetric, Electrokinetic, and DLS Techniques. *Colloid Polym. Sci.* **2006**, *284*, 871–878.

(17)   Barbosa, A. M.; Santos, I. J. B.; Ferreira, G. M. D.; Hespanhol Da Silva, M. D. C.; Teixeira, Á. V. N. D. C.; Da Silva, L. H. M. Microcalorimetric and SAXS Determination of PEO-SDS Interactions: The Effect of Cosolutes Formed by Ions. *J. Phys. Chem. B* **2010**, *114*, 11967–11974.

(18) Halacheva, S. S.; Penfold, J.; Thomas, R. K. Adsorption of the Linear Poly(ethyleneimine) Precursor Poly(2-Ethyl-2-Oxazoline) and Sodium Dodecyl Sulfate Mixtures at the Air − Water Interface: The Impact of Modification of the Poly(ethyleneimine) Functionality. *Langmuir* **2012**, *28*, 17331–17338.

(19) Halacheva, S. S.; Penfold, J.; Thomas, R. K.; Webster, J. R. P. Solution pH and Oligoamine Molecular Weight Dependence of the Transition from Monolayer to Multilayer Adsorption at the Air-Water Interface from Sodium Dodecyl Sulfate/oligoamine Mixtures. *Langmuir* **2013**, *29*, 5832–5840.

(20) Tucker, I. M.; Petkov, J. T.; Jones, C.; Penfold, J.; Thomas, R. K.; Rogers, S. E.; Terry, a E.; Heenan, R. K.; Grillo, I. Adsorption of Polymer Surfactant Mixtures at the Oil Water Interface. *Langmuir* **2012**, *28*, 14974–14982.

(21) Staples, E.; Tucker, I.; Penfold, J.; Warren, N.; Thomas, R. K.; Taylor, D. J. F. Organization of Polymer - Surfactant Mixtures at the Air - Water Interface : Sodium Dodecyl Sulfate and Poly (Dimethyldiallylammonium Chloride). *Langmuir* **2002**, *18*, 5147–5153.

(22) Zhang, X. L.; Taylor, D. J. F.; Thomas, R. K.; Penfold, J. Adsorption of Polyelectrolyte / Surfactant Mixtures at the Air - Water Interface : Modified Poly (Ethyleneimine) and Sodium Dodecyl Sulfate. *Langmuir* **2011**, *27*, 2601–2612.

(23) Vongsetskul, T.; Taylor, D. J. F.; Zhang, J.; Li, P. X.; Thomas, R. K.; Penfold, J. Interaction of a Cationic Gemini Surfactant with DNA and with Sodium Poly(styrene Sulphonate) at the Air/water Interface: A Neutron Reflectometry Study. *Langmuir* **2009**, *25*, 4027–4035.

(24) Petkova, R.; Tcholakova, S.; Denkov, N. D. Foaming and Foam Stability for Mixed Polymer-Surfactant Solutions: Effects of Surfactant Type and Polymer Charge. *Langmuir* **2012**, *28*, 4996–5009.

(25) Angus-Smyth, A.; Campbell, R. A.; Bain, C. D. Dynamic Adsorption of Weakly Interacting Polymer/surfactant Mixtures at the Air/water Interface. *Langmuir* **2012**, *28*, 12479–12492.

(26) Ederth, T.; Thomas, R. K. A Neutron Reflectivity Study of Drainage and Stratification of AOT Foam Films. *Langmuir* **2003**, *19*, 7727–7733.

(27)   Hurcom, J.; Paul, A.; Heenan, R. K.; Davies, A.; Woodman, N.; Schweins, R.; Griffiths, P. C. The Interfacial Structure of Polymeric Surfactant Stabilised Air-in-Water Foams. *Soft Matter* **2014**, *10*, 3003–3008.

(28)   Rosen, M. J.; Kunjappu, J. T. *Surfactants and Interfacial Phenomena: Fourth Edition*; John Wiley and Sons: New Jersey, **2012**.

(29)   Liu, X.; Dedinaite, A.; Nylander, T.; Dabkowska, A. P.; Skoda, M.; Makuska, R.; Claesson, P. M. Association of Anionic Surfactant and Physisorbed Branched Brush Layers Probed by Neutron and Optical Reflectometry. *J. Colloid Interface Sci.* **2015**, *440*, 245–252.

(30)   Safarpour, M. A.; Rafati, A. A.; Gharibi, H.; Rezaie Sameti, M. Influence of Short-Chain Alcohols on the Micellization Parameters of Sodium Dodecyl Sulfate (SDS). *J. Chinese Chem. Soc.* **1999**, *46*, 983–991.

(31)   Valente, A. J. M.; Burrows, H. D.; Cruz, S. M. A.; Pereira, R. F. P.; Ribeiro, A. C. F.; Lobo, V. M. M. Aggregation and Micellization of Sodium Dodecyl Sulfate in the Presence of Ce(III) at Different Temperatures: A Conductometric Study. *J. Colloid Interface Sci.* **2008**, *323*, 141–145.

(32)   D'Errico, G.; Ortona, O.; Paduano, L.; Tedeschi, A.; Vitagliano, V. Mixed Micellar Aggregates of Cationic and Nonionic Surfactants with Short Hydrophobic Tails. An Intradiffusion Study. *Phys. Chem. Chem. Phys.* **2002**, *4*, 5317–5324.

(33)   Bales, B. L.; Zana, R. Characterization of Micelles of Quaternary Ammonium Surfactants as Reaction Media I: Dodeclytrimethylammonium Bromide and Chloride. *J. Phys. Chem. B* **2002**, *106*, 1926–1939.

(34)   Bergstrom, M.; Pedersen, J. S. Structure of Pure SDS and DTAB Micelles in Brine Determined by Small-Angle Neutron Scattering (SANS). *Phys. Chem. Chem. Phys.* **1999**, *1*, 4437–4446.

(35)   Hooshyar, H.; Sadeghi, R. Influence of Sodium Salts on the Micellization and Interfacial Behavior of Cationic Surfactant Dodecyltrimethylammonium Bromide in Aqueous Solution. *J. Chem. Eng. Data* **2015**, *60*, 983–992.

(36)   Persi, L.; La Mesa, C.; D'Aprano, A. Dynamic and Thermodynamic Aspects of Polymer-Surfactant Interactions: The SDS-PVP-Water System. *Berichte Der Bunsen-Gesellschaft-Physical Chem. Chem. Phys.* **1997**, *101*, 1949–1956.

(37)   Misselyn-Bauduin, A.-M.; Thibaut, A.; Grandjean, J.; Broze, G.; Jérôme, R. Investigation of the Interactions of Polyvinylpyrrolidone with Mixtures of Anionic and Nonionic Surfactants or Anionic and Zwitterionic Surfactants by Pulsed Field Gradient NMR. *J. Colloid Interface Sci.* **2001**, *238*, 1–7.

(38)   Mesa, C. La; Persi, L.; Aprano, A. D. Polymer-Surfactant Interactions : Non Ionic Polymers with SDS and DTABr. *Berichte der Bunsengesellschaft für Phys. Chemie* **1998**, *102*, 1459–1466.

(39)   Petkova, R.; Tcholakova, S.; Denkov, N. D. Role of Polymer–surfactant Interactions in Foams: Effects of pH and Surfactant Head Group for Cationic Polyvinylamine and Anionic Surfactants. *Colloids Surfaces A Physicochem. Eng. Asp.* **2013**, 1–12.

(40)   Kristen-hochrein, N.; Fauser, H.; Schelero, N.; Klitzing, R. Von. Oppositely Charged Polyelectrolyte / Surfactant Mixtures in Foam Films : Effect of Molecular Weight. *Colloids Surfaces A Physicochem. Eng. Asp.* **2011**, *382*, 165–173.

(41)   Kristen, N.; Simulescu, V.; Vüllings, A.; Laschewsky, A.; Miller, R.; Von Klitzing, R. No Charge Reversal at Foam Film Surfaces after Addition of Oppositely Charged Polyelectrolytes? *J. Phys. Chem. B* **2009**, *113*, 7986–7990.

(42)   Schwuger, M. J. Mechanism of Interaction between Ionic Surfactants and Polyglycol Ethers in Water. *J. Colloid Interface Sci.* **1973**, *43*, 491–498.

(43)   Mata, J.; Joshi, T.; Varade, D.; Ghosh, G.; Bahadur, P. Aggregation Behavior of a PEO–PPO–PEO Block Copolymer + Ionic Surfactants Mixed Systems in Water and Aqueous Salt Solutions. *Colloids Surfaces A Physicochem. Eng. Asp.* **2004**, *247*, 1–7.

(44) Purcell, I. P.; Lu, J. R.; Thomas, R. K.; Howe, A. M.; Penfold, J. Adsorption of Sodium Dodecyl Sulfate at the Surface of Aqueous Solutions of Poly(vinylpyrrolidone) Studied by Neutron Reflection. *Langmuir* **1998**, *14*, 1637–1648.

Chapter 6

6. Summary and recommendations for further work

6.1 Summary

Solutions, gels and foams comprising polymers, small molecules and their mixtures have been investigated. Our primary focus was on foams stabilised by small molecule surfactants (SMS), but their study necessitated the characterisation of solution interactions first, Chapter 2.

In Chapter 2, the experiments focused on the interactions present in aqueous mixtures of Pluronic P123, (SMS) and alcohols (short, medium and long chain). Tensiometry, PGSE-NMR and SANS were used to characterise these systems. Tensiometry provided an insight into the surface properties and behaviour of these systems while self-diffusion coefficients from PGSE-NMR allowed us to estimate the partitioning of the alcohols in the P123 micelles, which eventually helped us understand the role of the alcohols in driving the interactions between P123 and SMS. Ethanol was found to partition mainly in the shell of the micelle forming smaller micelles, while both hexanol and decanol partitioned in the core.

Adding SMS such as $C_{12}SO_4Na$, $C_{12}TAB$ and Brij 35 to P123 has caused a disruption in the P123 micelle structures, yielding smaller mixed micelles as confirmed by SANS. $C_{12}SO_4Na$ was found to have the strongest interaction with P123, followed by Brij 35 then $C_{12}TAB$. Using contrast variation in SANS experiments, the presence of the alcohols in the mixed surfactant systems was shown to impact the strength of the interactions for P123 and $C_{12}TAB$, the $C_{12}TAB$ micelle mole fraction increases for all cases of alcohol, indicative of a weaker interaction between the SMS and the Pluronic (consistent with the relative changes in CMC). No significant changes in the fraction of $C_{12}SO_4Na$ in the mixed system were observed in the P123 + $C_{12}SO_4Na$ case in the presence of alcohols, this is indicative of the strong interactions between both. This analysis was not possible to perform on P123 + Brij 35 due to the unavailability of a deuterated form of Brij 35.

While studying the solution interactions, some interesting behaviour from P123 at high concentrations was observed. We then decided to extend the study to include the investigation of gels from Pluronic P123, F108 and their mixtures, Chapter 3. Of main interest here was the microstructure of the gels and the changes observed in the microstructure as a function of temperature and Pluronic concentrations.

Chapter 6. Conclusions and recommendations for further work

The investigations were performed using SANS, where a series of Bragg peaks were recorded indicative of micellar ordering. P123 showed different gel structures (hexagonally close packed (hcp), body-centred cubic (bcc), lamellar and multiphase) by changing concentration and temperature.

Whilst for F108 gels, only bcc was observed and it showed insensitivity to both the concentration and temperature changes. Gels from P123/F108 mixtures showed a very interesting behaviour, where P123 did not destabilise the cubic structure as observed before for P123/F127 gels. The structures observed from the mixture cases were largely cubic (bcc and face-centred cubic, fcc) and hcp. These transitions were suggested to be closely related to the micelle composition, especially the PEO chain length and its effect on the packing of the micelles.

Chapter 4 involved investigating foams stabilised by a range of SMS (C_nSO_4Na and C_nTAB) using tensiometry and SANS. In this study, wet and dry foams were studied. Wet foams stabilised by surfactants below the CMC showed a pronounced Q^{-4} dependence, with a series of inflexions at mid Q. Data analysis and modelling was pursued and the results suggested that the inflexions at mid Q corresponds to an interface comprising multi-layered structure of SMS rich and water rich layers. Investigating dry foams allowed us to study the changes in the multi-layer structure, inflexions with different features and positions across the wavevector appeared in the data. This was attributed to the strong presence of micelles and discontinuous layers of surfactants in the film. Comparing the dry foam SANS data with wet foams stabilised with SMS at concentrations above the CMC supports this conclusion, given that the features are largely similar in both cases.

Finally, foam from mixtures of PVP-40, P123 and SMS (C_8SO_4Na, C_8TAB, $C_{12}SO_4Na$ and $C_{12}TAB$) were investigated, Chapter 5. Tensiometry and SANS were once more employed. Using our previous knowledge of the interactions between these polymers and surfactants along with the previous data interpretation of foams stabilised by SMS on their own, it was possible to correlate between the interactions occurring in the polymer-surfactant systems in bulk and the multi-layered structure observed at the foam air/water interface. In the weakly interacting systems (P123 + C_8TAB, P123 + C_8SO_4Na and P123 + $C_{12}TAB$), no change in the inflexion position at mid Q was observed.

The strongly interacting system (P123+ $C_{12}SO_4Na$) showed a noticeable shift in the inflexion position towards lower Q, indicating the presence of larger spacing between the multi-layers, *i.e.* the formation of thinner surfactant layers.

Neutron reflectivity (NR) was previously used to investigate the widely studied system; PVP-40 and $C_{12}SO_4Na$ at equilibrium. The experiments have not revealed any interesting structures at the air/water interface. This is a very similar conclusion to ours (in terms of the changes observed in the surfactant multi-layered structure as the polymer concentration increased). Where SANS was used to study foams stabilised by the same systems, and no change in the position of the inflexion was observed, but instead, as the polymer concentration increased, there was an expected significant contribution to the scattering from the polymer in the foam films (solution scattering).

6.2 Recommendations for further work

The main focus of this thesis was to try to understand and control the interactions between polymers and small molecules in order eventually to reach a robust formulation. The systems investigated here mainly comprised three or four components, where in real-life formulations, the number of components is far more than three or four. However, understanding the fundamentals of the interactions on a smaller scale has always shown to be of crucial importance in any pre-formulation process.

The investigations of mixed systems in solution in this thesis have focused exclusively on the interactions between P123, SMS in the presence of alcohols. An area of further work would be to start introducing or replacing components to the systems. Micellization of Pluronic in the presence of several NSAIDS (non-steroidal anti-inflammatory drugs) has been investigated, but the encapsulation efficiency, release profile and mechanisms in the presence of physiologically relevant media remains not very well understood. Another area worth pursuing would be the possibility of using a well-controlled system like P123-SMS-alcohols to stabilise and optimise more complex systems such as emulsions, gels, paints, *etc.*

When Pluronic gels in this thesis were investigated, this was mainly focused on understanding the microstructure of the gels using SANS. It will be of definite interest to study the rheological, physicochemical properties of the single components and their mixtures. Understanding these properties along with a detailed understanding of the gels microstructures is expected to assist any further work, especially in biomedical applications and drug delivery, where the latter could be investigated using the techniques used in this thesis such as PGSE-NMR and SANS.

The interfacial structure of the foams was shown to be influenced by the surfactant architecture and the nature of the interactions between the polymers and surfactants. This could be extended to include investigating more challenging systems, such as particle stabilised foams, where the particles arrangement at the interface will be very interesting to probe. The possibility of using SANS to study these systems has been validated, however another approach towards the sample environment design was realised.

Particle stabilised foams are most stable and reproducible when prepared by strong mixing rather than pushing air through the sample as in the case of surfactant stabilised foams. The new sample environment should then have an airflow supply (to prevent any drainage if wet foams are of interest) and also a very powerful mixer to generate stable foams. Designing a new foam cell with these features, is indeed feasible, but will be very challenging.

Foaming of denatured proteins is an area of increasing interest due to its wide applications in food industry (*e.g.* beer foams and meringue from egg whites). The mechanism by which these foams are stabilised is widely accepted to be related to either the high hydrophobicity or the increased viscosity of the denatured protein. A better and detailed understanding of these mechanisms would be an area worth pursuing. SANS will also be a very powerful technique to probe the local protein structure at the interface, which will eventually help have better control over these foams.

Appendix A

The following graphs are in support of the data presented and discussed in Chapter 2 (p.7).

1. Determination of CMC by surface tension data:

Surface tension data for surfactants mixtures in ethanol were presented in Chapter 2, please see Figure 2.1 and Tables 2.1 and 2.2, here we present a collective representation of the surface tension data in hexanol and decanol, Figure A.1 and A.2. The behaviour of the P123-SDS systems in hexanol shows a different surface behaviour due the nature of the hexanol surface activity. This can be shown by how the surface tension changes while going from a pure SDS/hexanol system to a mixed system of P123/SDS/hexanol in water system, or, by having a constant hexanol in water concentration and diluting pure SDS or pure P123 systems, where below the CMC of both surfactants, the mixture phase separates.
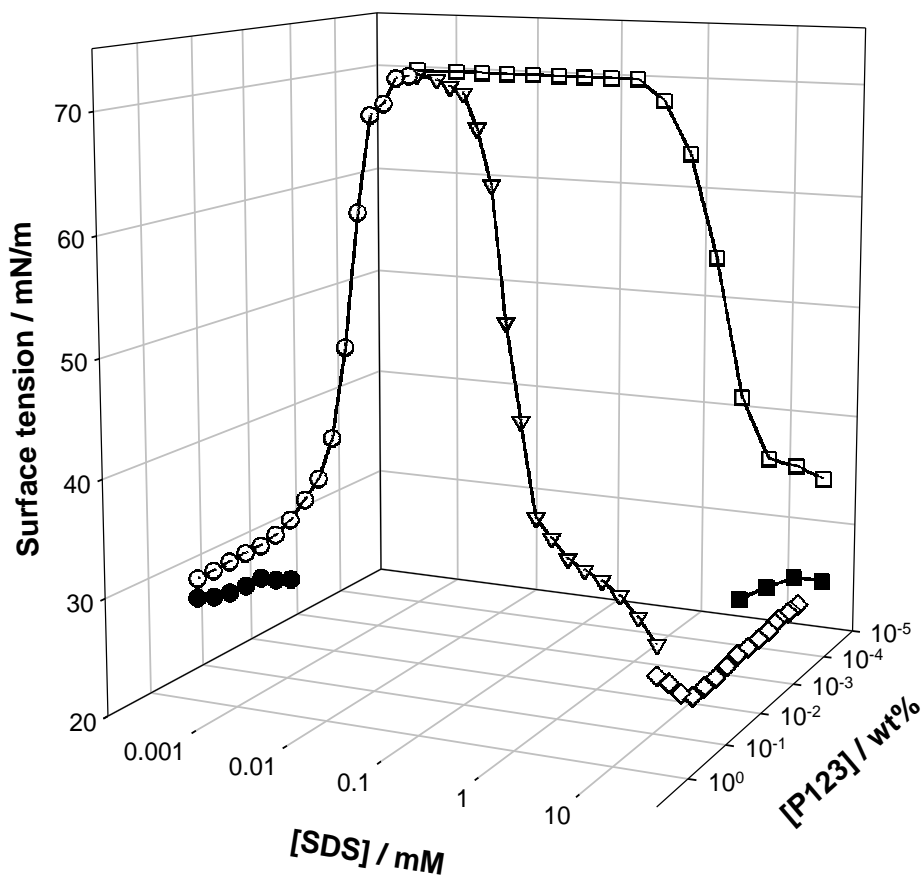
Figure A.1 Surface tension as a function of surfactant concentration: open squares = [SDS/water], filled squares = [SDS + constant hexanol concentration of 1 wt% in water].

Open diamonds = [P123 + constant SDS and hexanol concentration of 50 mM & 1 wt% in water].

Open triangles = [P123 + SDS in water], open circles = [P123/water], filled circles = [P123 + constant hexanol concentration of 1 wt% in water].
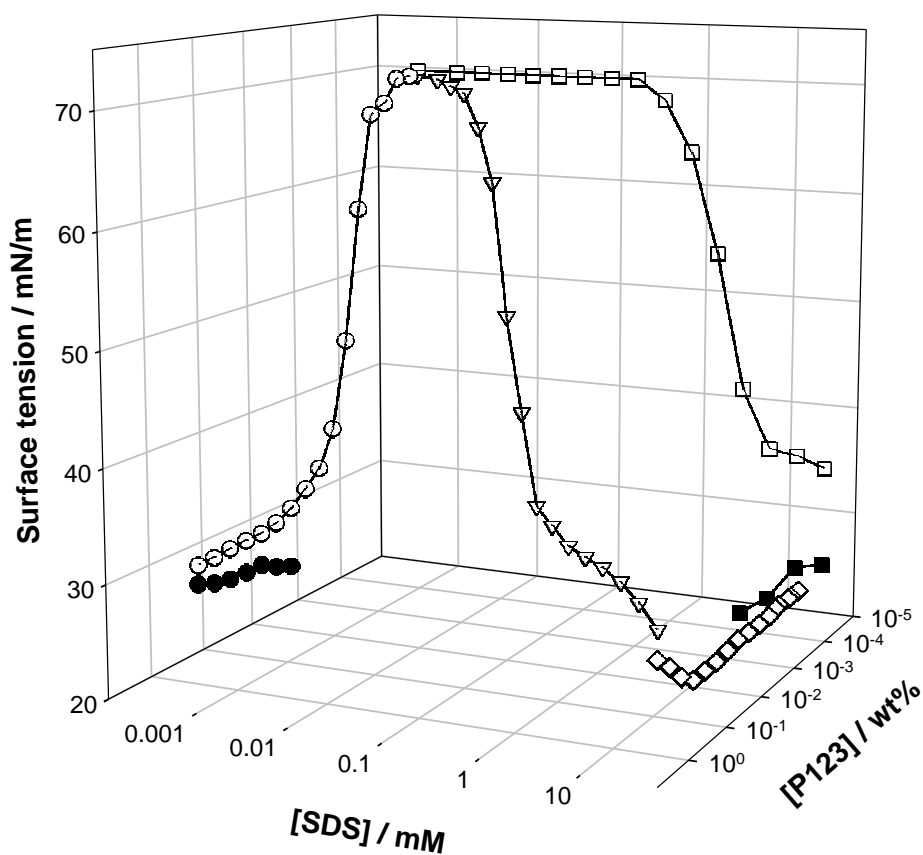
Figure A.2 Surface tension as a function of surfactant concentration: open squares = [SDS/water], filled squares = [SDS + constant decanol concentration of 0.1 wt% in water].

Open diamonds = [P123 + constant SDS and decanol concentration of 50 mM & 0.1 wt% in water].

Open triangles = [P123 + SDS in water], open circles = [P123/water], filled circles = [P123 + constant decanol concentration of 0.1 wt% in water].

2. Investigating micelle structure using SANS:

The material balance equations helps in understanding the details of the probed structures by SANS. The micelle is considered as a model formed of a core containing PO and a fraction, f, of the EO chains, and the shell contains the remaining fractions of the EO (1-f). Moreover, we can assume that the D_2O is present in the core and in the shell to hydrate the EO blocks. If we can also assume that there are y_A D_2O molecules per EO monomer in the core (region A) and y_B D_2O molecules per EO monomer in the shell (region B). The aggregation number, N_{agg}, is defined as the number of P123 molecules per micelle and note that there are 70 PO monomers per block and 40 EO monomers per macromolecule. Results are shown in Figure A.3.
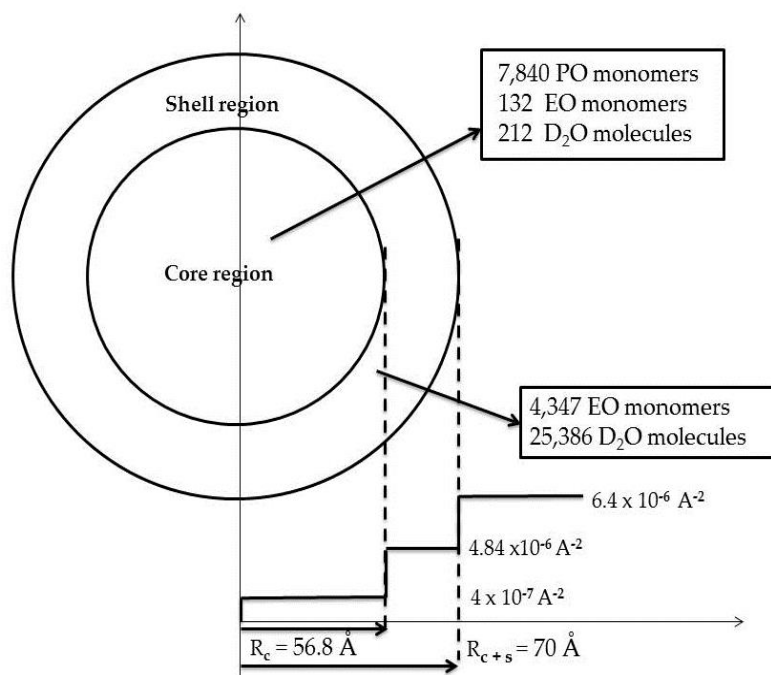
Figure A.1 P123 core-shell density model for SANS
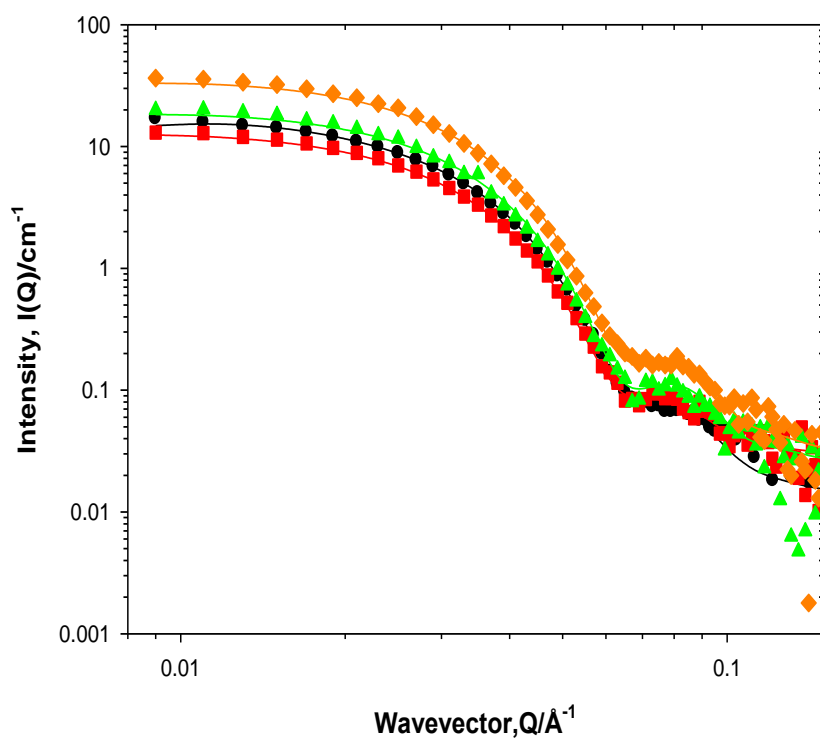
Figure A.2 SANS from 0.5 wt% P123 solutions as a function of alcohol concentration; circles [alcohol] = 0 wt%, squares [ethanol] = 1 wt%, triangles [hexanol] = 0.1 wt% and diamonds [decanol] = 0.01 wt%. Solid lines are fits to the core-shell model, see Table A.1. Error bars have been removed for clarity.

Alcohol concentration (wt%)	0 wt%	1 wt% Ethanol	0.1 wt% hexanol	0.01 wt% decanol
Core radius (±0.5, Å)	57	50	59	59
Shell thickness (±1, Å)	17	13	11	14
Volume fraction of hard spheres (±0.001)	0.005	0.004	0.005	0.005
Volume of the micelles (nm^3), V_{mic}	1500	1300	1430	1650
Micelles number density, n, 10^{15} cm^{-3}	3.3	4.6	3.5	3.0

Table A.1 SANS parameters for 0.5 wt% P123 as a function of alcohol concentration at 25°C.
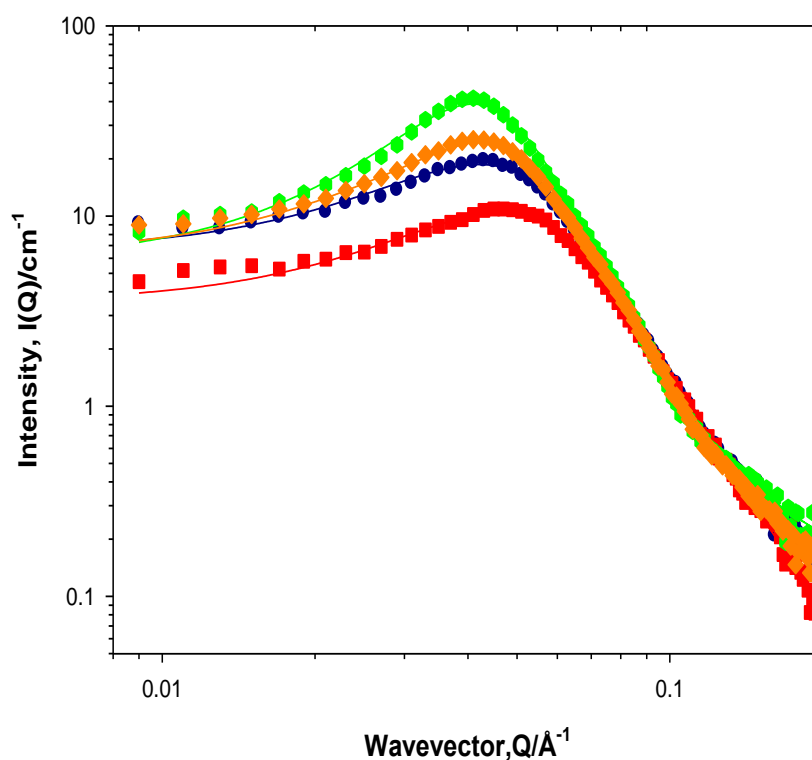
Figure A.3 SANS from 5 wt% P123 solutions + 50 mM h-C$_{12}$TAB as a function of alcohol chain length; circles [alcohol] = 0 wt%, squares [ethanol] = 10 wt%, hexagons [hexanol] = 1 wt% and diamonds [decanol] = 0.1 wt%. Solid lines correspond to model fits as discussed in the text. Error bars have been removed for clarity.

Alcohol concentration (wt%)	0 wt%	10 wt% Ethanol	1 wt% hexanol	0.1 wt% decanol
Radius A (±1, Å)	23	20	30	27
Radius B (±1, Å)	49	45	52	48
Volume fraction of hard spheres (±0.001)	0.06	0.05	0.06	0.06
Volume of the micelles (nm^3), V_{mic}	195	169	339	260
Micelles number density, n, 10^{17} cm^{-3}	3.1	3.0	1.7	2.3
Mixed micelle aggregation number, (±5)	20	17	35	26

Table A.2 SANS parameters for 5 wt% P123- 50 mM h-C$_{12}$TAB as a function of alcohol concentration at 25°C.
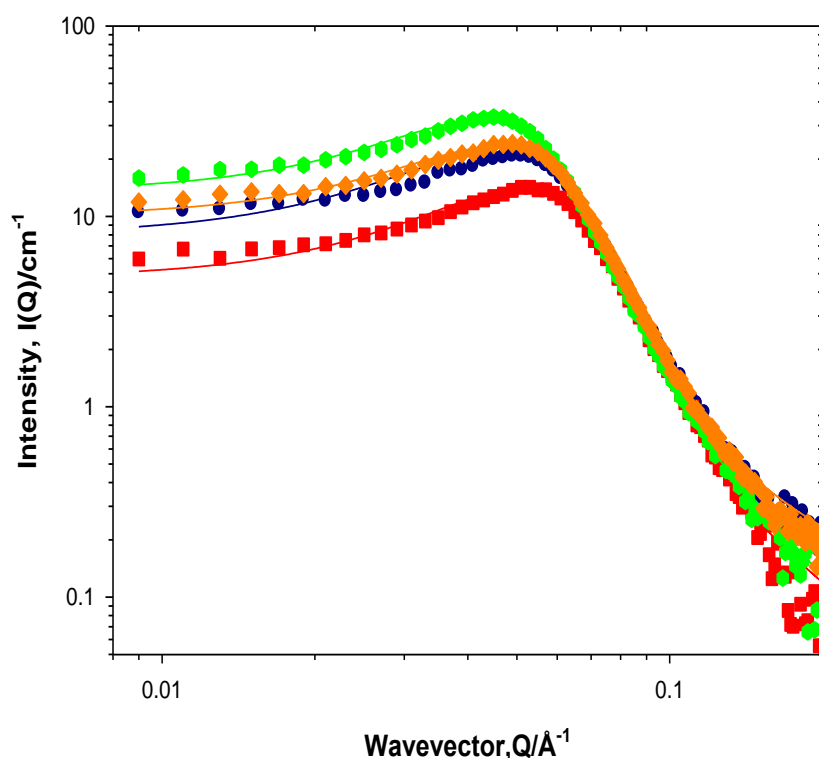
Figure A.4 SANS from 5 wt% P123 solutions + 50 mM Brij 35 as a function of alcohol chain length; circles [alcohol] = 0 wt%, squares [ethanol] = 10 wt%, hexagons [hexanol] = 1 wt% and diamonds [decanol] = 0.1 wt%. Solid lines correspond to model fits as discussed in the text. Error bars have been removed for clarity.

Alcohol concentration (wt%)	0 wt%	10 wt% Ethanol	1 wt% hexanol	0.1 wt% decanol
Radius A (±1, Å)	24	24	30	27
Radius B (±1, Å)	44	40	47	46
Volume fraction of hard spheres (±0.001)	0.10	0.09	0.10	0.10
Volume of the micelles (nm³) , V_{mic}	210	170	270	220
Micelles number density, n, 10^{17} cm⁻³	4.3	5.2	3.3	4.1
Mixed micelle aggregation number, (±5)	25	15	30	30

Table A.3 SANS parameters for 5 wt% P123 - 50 mM Brij 35 as a function of alcohol concentration at 25°C.
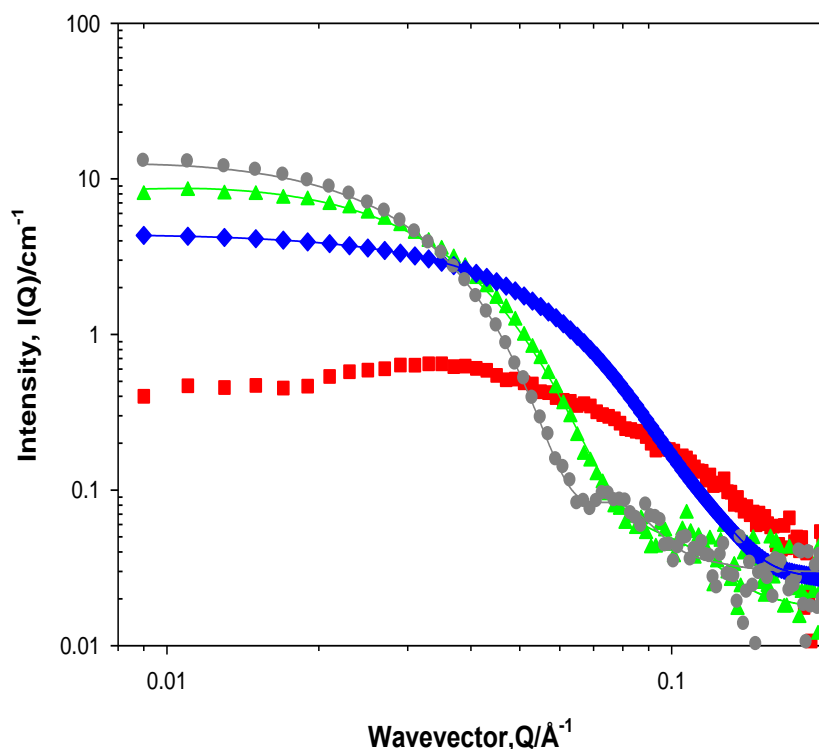
Figure A.5 SANS from 0.5 wt% P123 solutions and 1 wt% ethanol as a function of small molecule surfactant head group size; circles [surfactant] = 0 mM, squares [h-SDS] = 5 mM, triangles [h-C_{12}TAB] = 5 mM, and diamonds [Brij 35] = 5 mM. Error bars have been removed for clarity.

Surfactant	h-C_{12}TAB	Brij 35
Radius A (±1, Å)	40	25
Thickness/Radius B (±1, Å)	10	50
Volume fraction of hard spheres (±0.001)	0.005	0.010
Volume of the micelles (nm³), V_{mic}	525	230
Micelles number density, n, 10^{16} cm^{-3}	1.9	4.2
Mixed micelle aggregation number (±5)	80	25

Table A.4 SANS parameters for 0.5 wt% P123 as a function of 5 mM h-surfactants in 1 wt% ethanol and D_2O at 25°C.
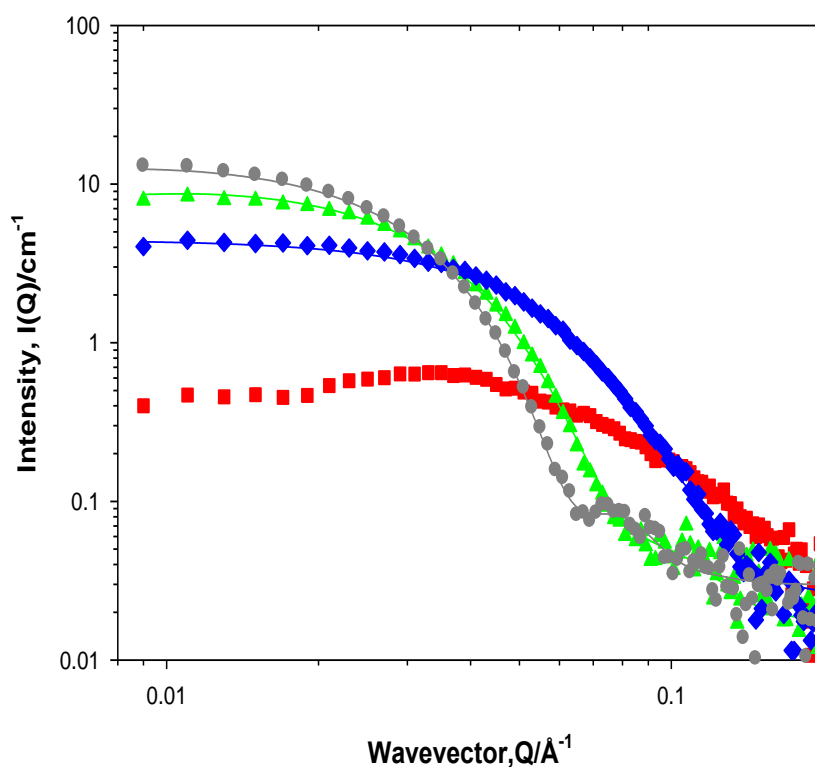
Figure A.6 SANS from 0.5 wt% P123 solutions and 0.1 wt% hexanol as a function of small molecule surfactant head group size; circles [surfactant] = 0 mM, squares [h-SDS] = 5 mM, triangles [h-C₁₂TAB] = 5 mM, and diamonds [Brij 35] = 5 mM. Error bars have been removed for clarity.

Surfactant	h-C_{12}TAB	Brij 35
Radius A (±1, Å)	48	23
Thickness/Radius B (±1, Å)	13	53
Volume fraction of hard spheres (±0.001)	0.006	0.010
Volume of the micelles (nm³), V_{mic}	950	270
Micelles number density, n, 10^{16} cm⁻³	0.6	3.7
Mixed micelle aggregation number (±5)	95	30

Table A.5 SANS parameters for 0.5 wt% P123 as a function of 5 mM h-surfactants in 0.1 wt% hexanol and D_2O 25°C.

Figure A.7 SANS from 0.5 wt% P123 solutions and 0.01 wt% decanol as a function of small molecule surfactant head group size; circles [surfactant] = 0 mM, squares [h-SDS] = 5mM, triangles [h-C$_{12}$TAB] = 5 mM, and diamonds [Brij 35] = 5 mM. Error bars have been removed for clarity.

Surfactant	h-C$_{12}$TAB	Brij 35
Radius A (±1, Å)	50	24
Thickness/Radius B (±1, Å)	10	51
Volume fraction of hard spheres (±0.001)	0.006	0.01
Volume of the micelles (nm^3), V_{mic}	905	260
Micelles number density,n,10^{16} cm^{-3}	0.6	3.8
Mixed micelle aggregation number (±5)	90	27

Table A.6 SANS parameters for 0.5 wt% P123 as a function of 5 mM h-surfactants in 0.01 wt% decanol and D$_2$O 25°C.

Appendix B.

The following graph is in support of the data presented and discussed in Chapter 3 (p.37)
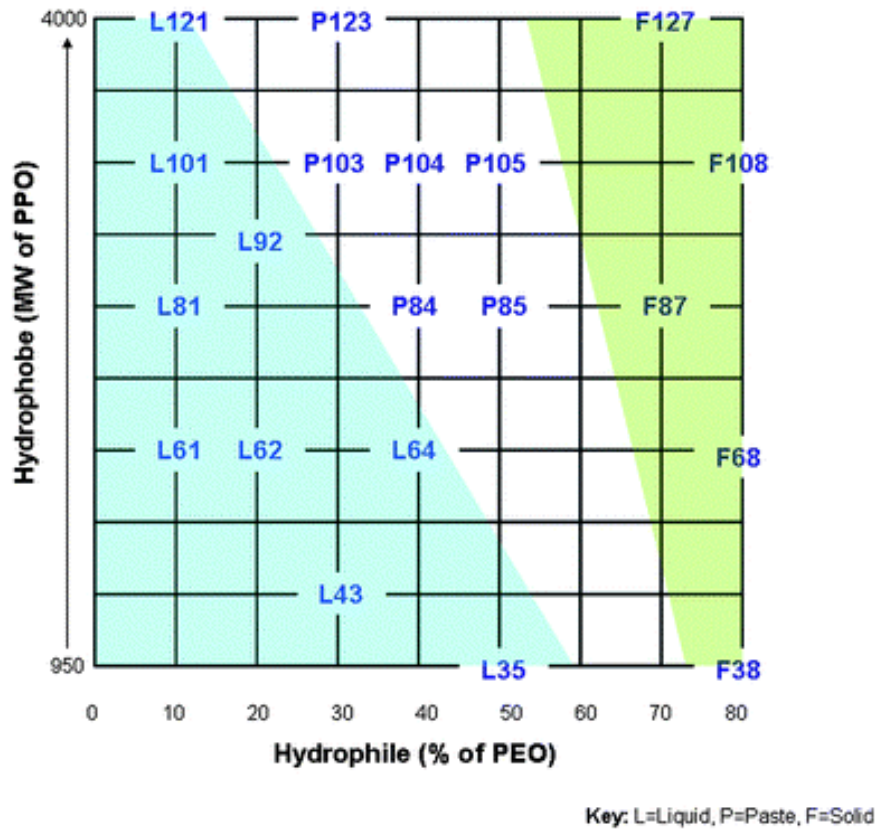
Figure B.1 Molecular weight ranges of the hydrophobe vs. the percentage of hydrophile of the block copolymer. Adapted from Alexandridis et al.[1]

Appendix B.

Bibliography

(1)   Alexandridis, P.; Hatton, T. A. Block Copolymer Surfactants in Aqueous Solutions and at Interface: Thermodynamics , Structure , Dynamics , and Modeling. *Colloids Surfaces A Physicochem. Eng. Asp.* **1995**, *96*, 1–46.

Appendix C

The following graphs are in support of the data presented and discussed in Chapter 4 (p.71)
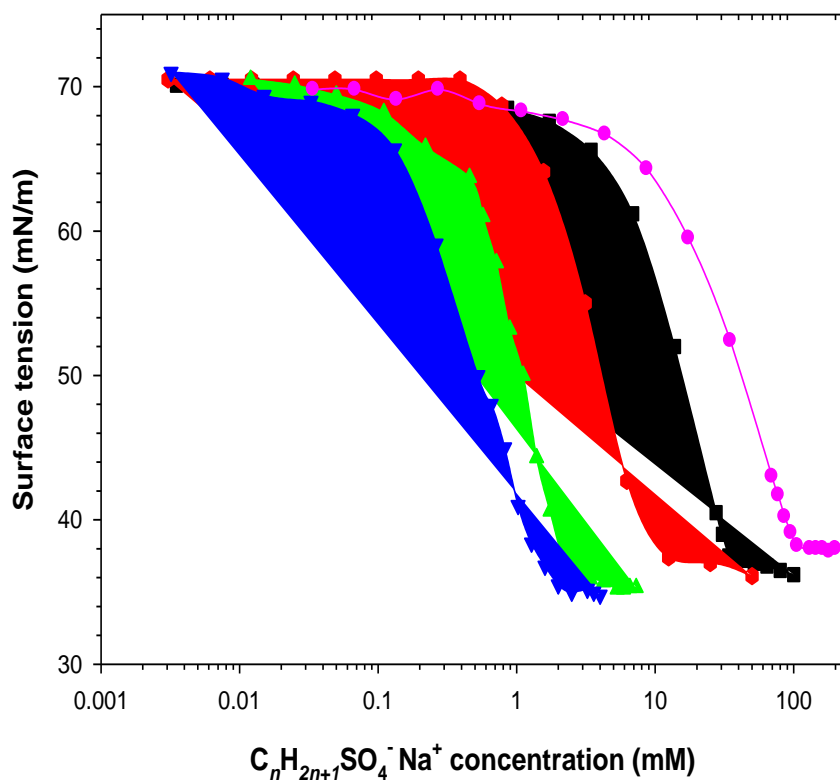
Figure C.1 Surface tension as a function of $C_nH_{2n+1}SO_4^-Na^+$ concentration in water; C_8 [circles], C_{10} [squares], C_{12} [hexagons], C_{14} [triangles up] and C_{16} [triangles down].
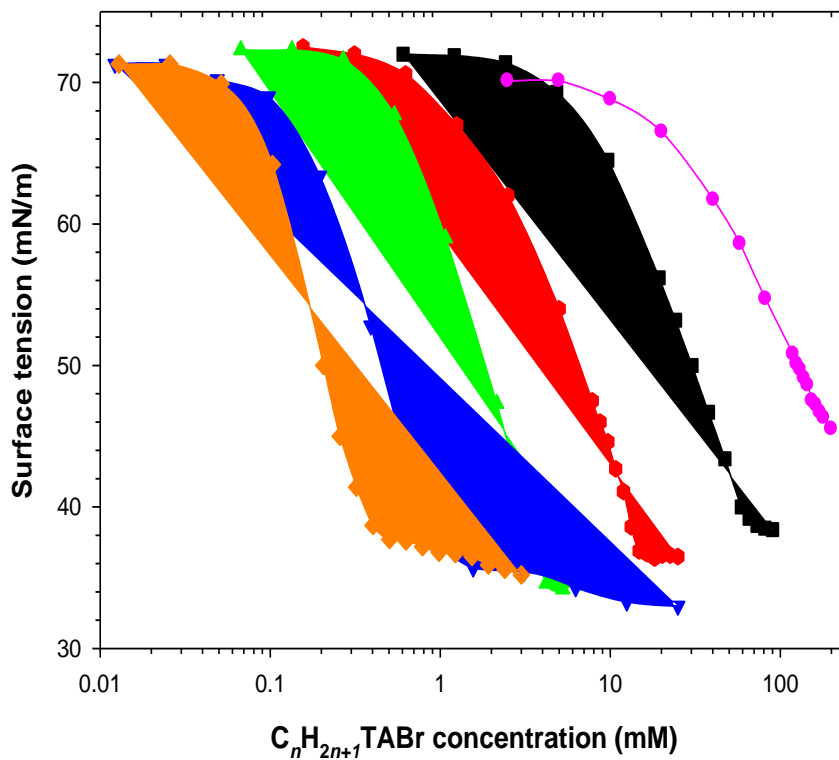
Figure C.2 Surface tension as a function of C$_n$H$_{2n+1}$TAB concentration in water; C$_8$ [circles], C$_{10}$ [squares], C$_{12}$ [hexagons], C$_{14}$ [triangles up], C$_{16}$ [triangles down] and C$_{18}$ [diamonds].
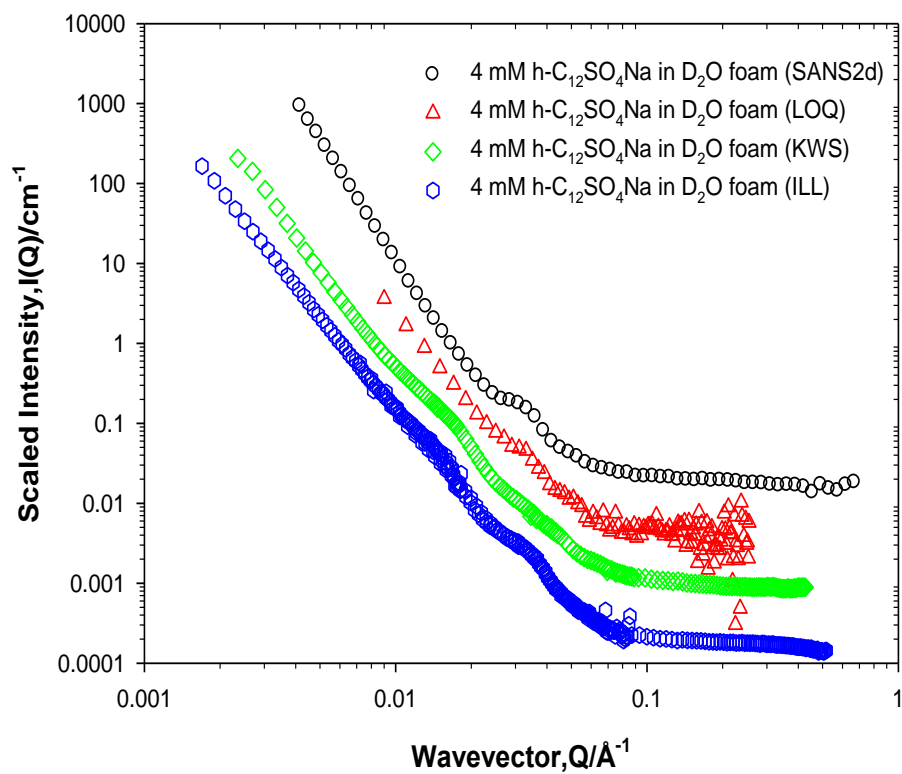
Figure C.3 SANS from foams stabilised with 4 mM h-SDS in D₂O recorded from different diffractometers. Data have been shifted vertically for clarity.
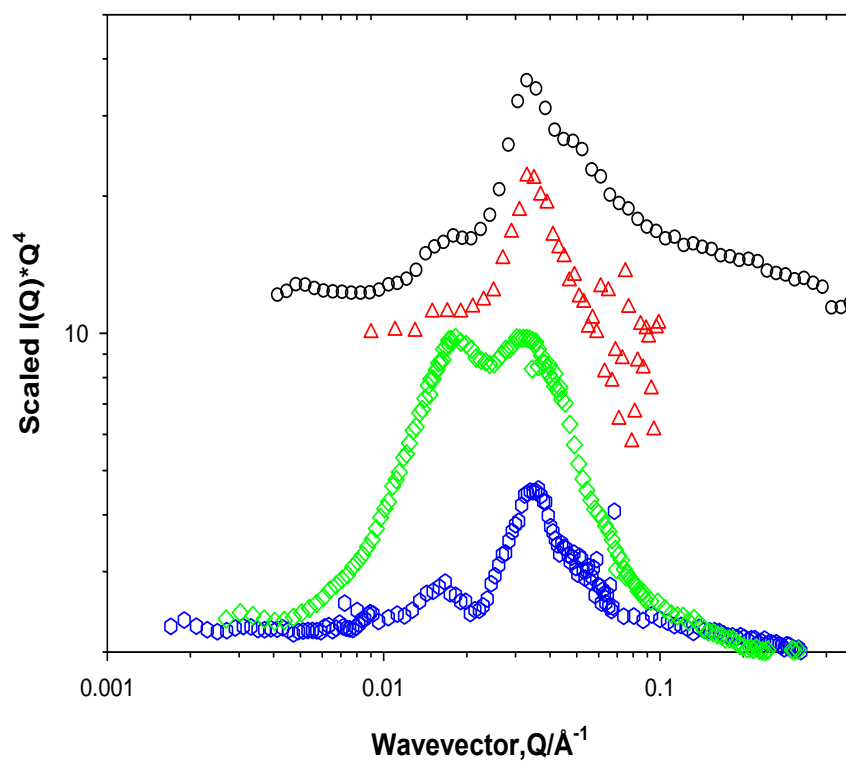
Figure C.4 Plot of *I(Q⁴) vs. Q* for foams stabilised with 4 mM h-SDS in D$_2$O recorded from different diffractometers, following the same order of instruments labelling as in Figure C.3. Data have been shifted vertically for clarity.
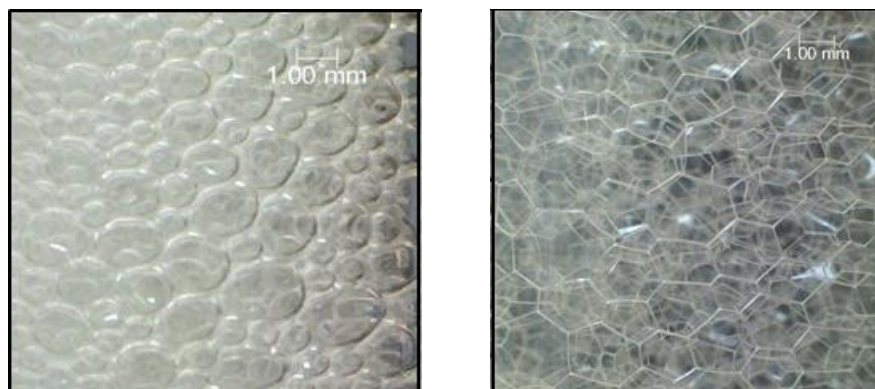
Figure C.5 Transition in the foam structure from spherical (left) to polyhedral (right) as a function of time
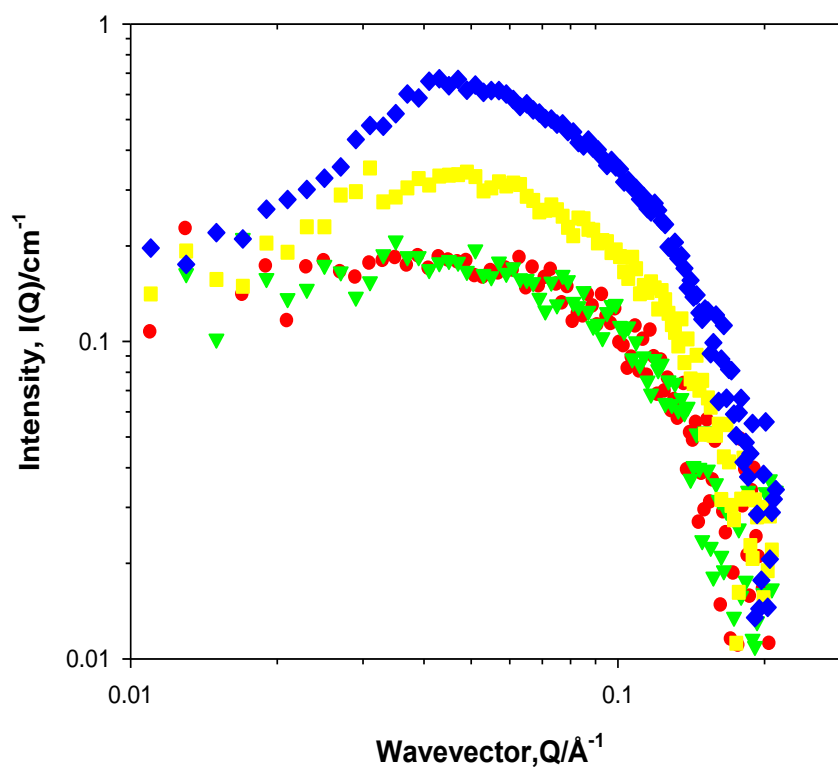
Figure C.6 SANS as a function of C$_{12}$SO$_4$Na concentration in D$_2$O; 10 mM (circles), 15 mM (triangles), 20 mM (squares) and 30 mM (diamonds).
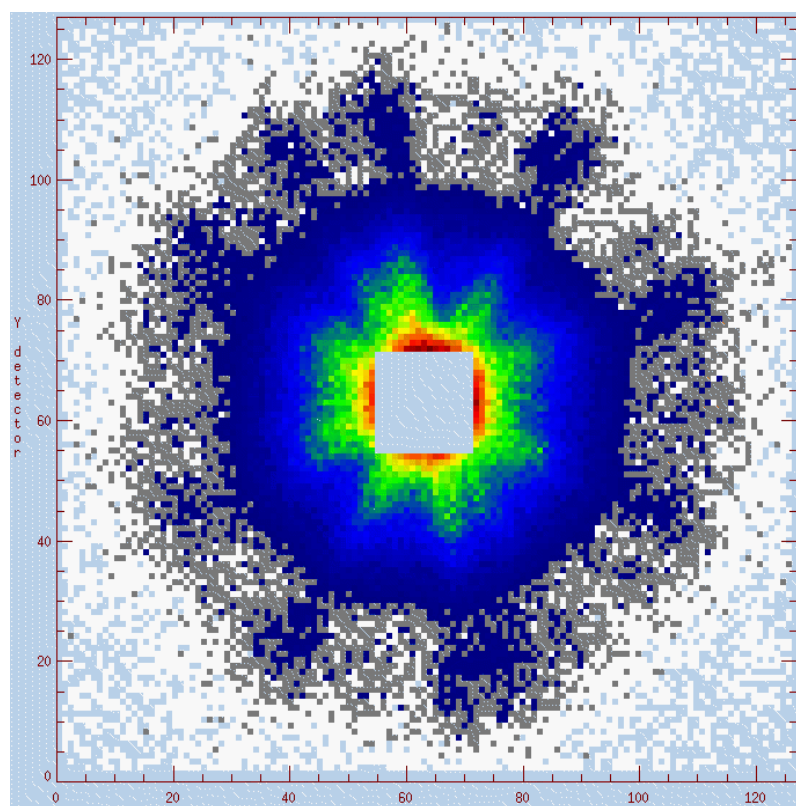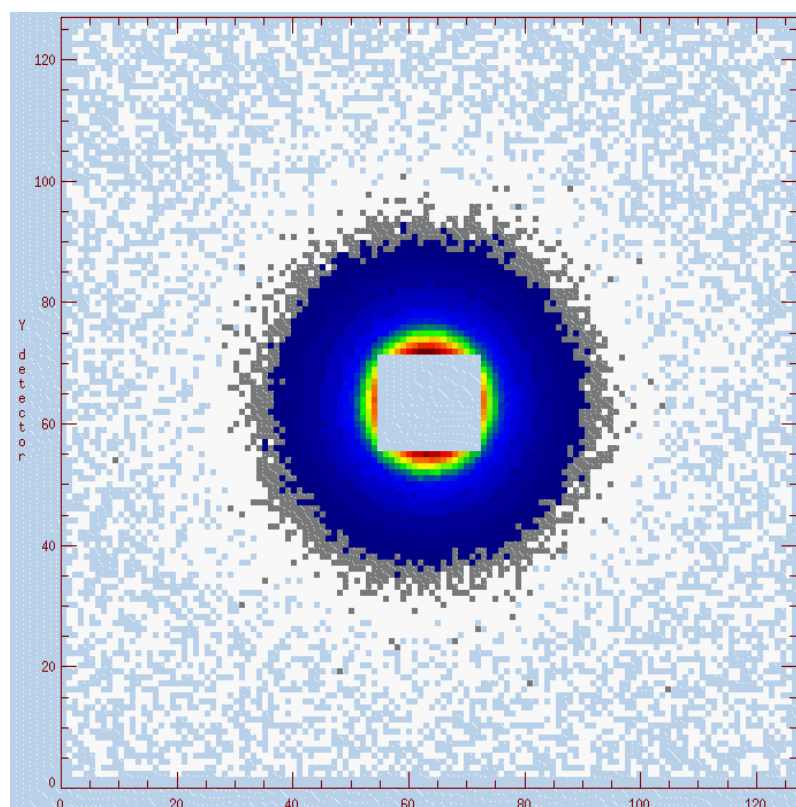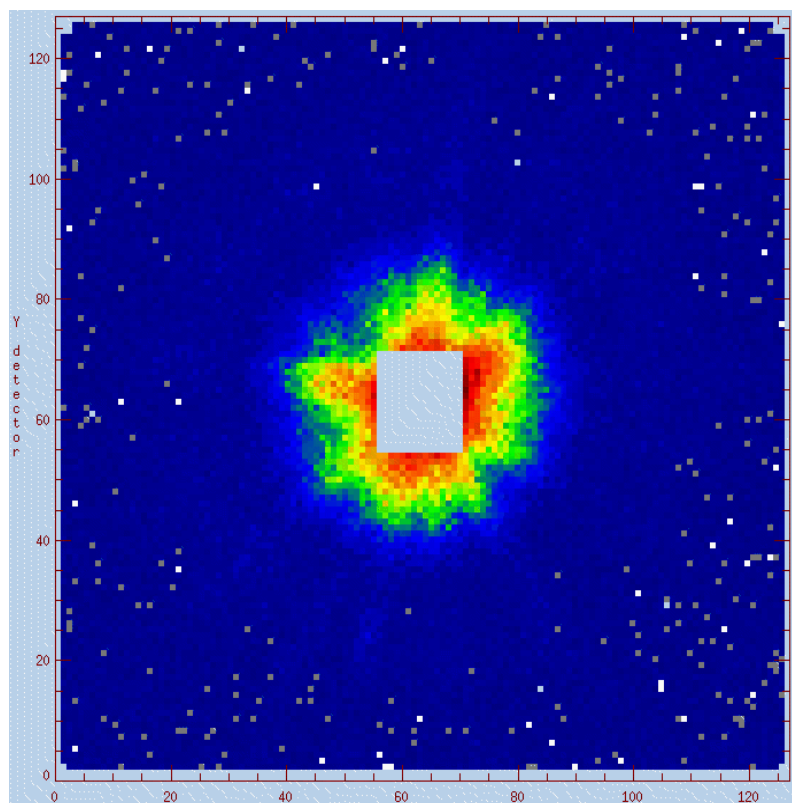
Figure C.7 SANS patterns as foam stabilised by C$_{12}$SO$_4$Na at different drainage conditions evolves from wet to dry (top to bottom). All patterns presented are from the data collected in the Q range between 0.007 Å^{-1} and 0.07 Å^{-1}.
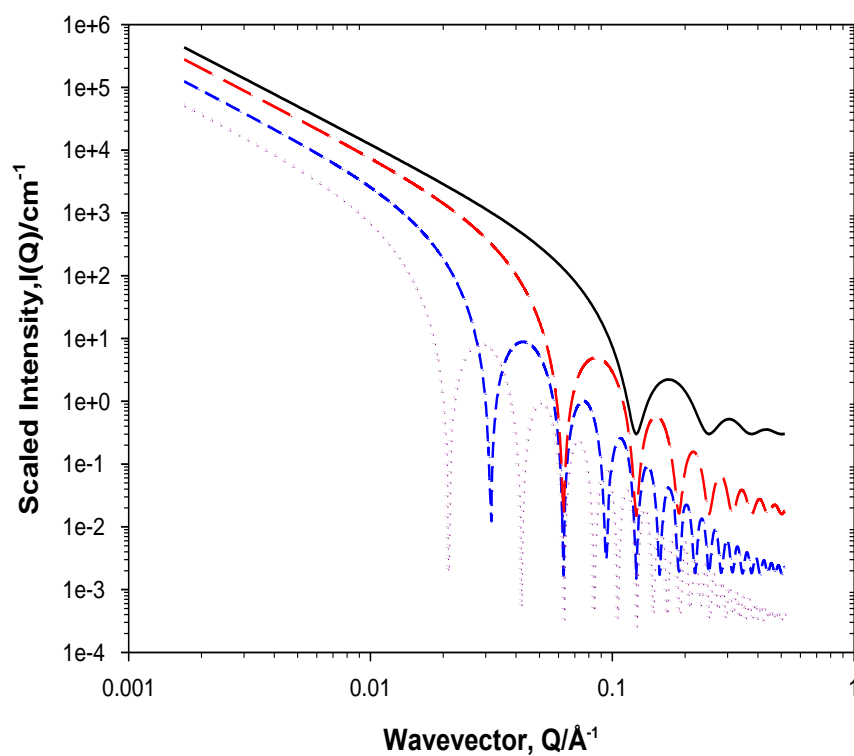
Figure C.8 Simulated SANS from films of thickness; 50 Å (sold lines), 100 Å (long dashed line), 200 Å (short dashed line) and 300 Å (dotted line).
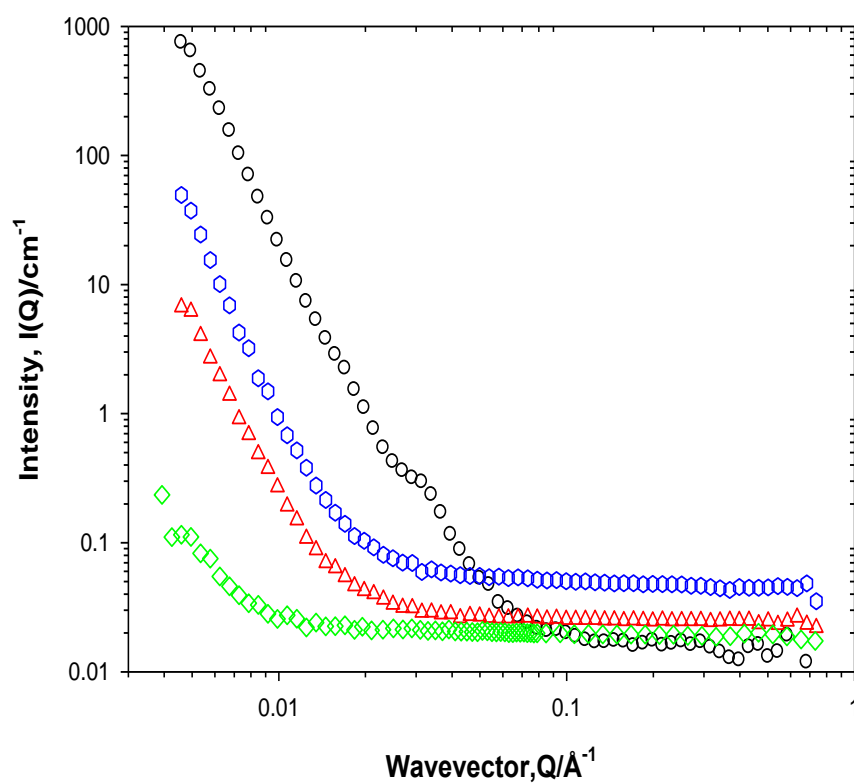
Figure C.9 SANS from foams stabilised with 4 mM h-$C_{12}SO_4Na$ (circles) in D_2O, 4 mM h-$C_{12}SO_4Na$ in 50:50 D_2O:H_2O (hexagons), 4 mM d- $C_{12}SO_4Na$ in 50:50 D_2O:H_2O (triangles) and 4 mM d- $C_{12}SO_4Na$ in null reflecting water (NRW). The h-$C_{12}SO_4Na$ in D_2O data have been shifted vertically by a factor of 4 for clarity.

Appendix D

Experimental Techniques

D.1 Maximum bubble pressure tensiometry

Maximum bubble pressure is a very useful way to measure the surface tension. The bubble pressure tensiometer produces air bubbles at a constant controlled rate through a capillary with a known radius. When the air bubble is produced in the sample at the tip of the capillary, the curvature initially increases, to the point where a maximum in the pressure is observed, then the bubble curvature increases exponentially with time and the pressure inside decreases. Finally, the bubble is removed from the capillary and another cycle starts. At the maximum pressure, the radius of the bubble's curvature is equal to the radius of the capillary and surface tension (σ) could be calculated from the Young-Laplace equation:

$$\sigma = \frac{(\rho_{max} - \rho_o)r}{2} \tag{D.1}$$

Where ρ_{max} is the maximum pressure inside the bubble, ρ_o is the hydrostatic pressure at the tip of the capillary and r is the radius of the capillary.

Appendix D. Experimental techniques

D.2 Pulsed-gradient spin echo nuclear magnetic resonance, PGSE-NMR

NMR spectroscopy is a widely studied technique and several textbooks offer detailed description of the theory and the technique,[1] only selected theory and experimental methods that are relevant to this thesis are covered. The NMR principle is based on the spin of the atomic nuclei in an external magnetic field. When a nuclei possess an odd number of protons and/or neutrons, a magnetic dipole is generated along the spin axis, its intrinsic magnitude is called the nuclear magnetic moment, μ. After the application of an external magnetic field, B, magnetic moments precess around the z-axis. The z-axis is defined in the direction of the magnetic field. The energy, E, of a magnetic dipole in the magnetic field is:

$$E = -\mu B \tag{D.1}$$

Diffusion of a molecule occurs as a result of its random movement in a medium controlled by thermal fluctuations. Measuring diffusion coefficients is very important in studying multicomponent systems as the interactions between two molecules in solution will lead to a correlation between the diffusion rates. Several factors may affect the diffusion of molecules and particles in solution, including molecular weight, viscosity and temperature. The diffusion coefficient, D, of a particle in solution could be related to the factors above using the Stokes–Einstein equation:

$$D = \frac{k_B T}{f_T} \tag{D.2}$$

Where k_B is the Boltzmann constant, T is the temperature and f_T is the friction factor. The friction factor for a spherical particle is given by:

$$f_T = 6\pi\eta R_H \tag{D.3}$$

Where η is the solvent viscosity and R_H is the particle's hydrodynamic radius.

PSGE-NMR[2–4] was used to measure the diffusion coefficients of Pluronic and its mixed micelles in this thesis. The spin echo sequence is shown in Figure D.1.
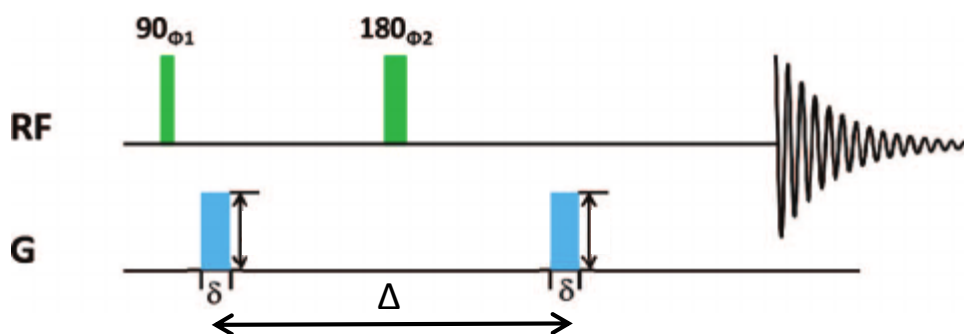
Figure D.1 Schematic of the pulsed-gradient spin echo (PGSE) NMR. Adapted from Zhang *et al.*[5]

This PGSE sequence combines a series of radiofrequency (RF) pulses and magnetic field gradients that contains spatial information. As shown in Figure D.1, the magnetisation is tipped into the *xy* plane by a 90° RF pulse. A field gradient pulse is then applied to disperse the magnetisation (by inducing a phase shift in the spin states), this dispersion depends on the strength (G) and duration (δ) of the pulse. After a period of time, $\Delta/2$, (Δ being the period in which the spins are assumed to diffuse) a 180° RF pulse is applied to invert the dispersed magnetisation such that after a period of Δ, the magnetisation is the negative of what it was following the gradient pulse. At this point, a second field gradient pulse is applied to refocus the signal.

This refocusing will only be achieved for the spin nuclei who were static during the measurement, and in this case, the intensity of the spin echo will not change. On the other hand, if the nuclei were diffusing during the measurement, refocusing of the spin nuclei will not be achieved by the second gradient pulse and the intensity of the spin echo will decrease.

The PGSE-NMR data was fitted and analysed using CORE.[6,7] The program relies on the assumptions that (i) the band shape for each specific component in the sample will be the same throughout a pulsed field gradient experiment and (ii) the band shape will attenuate by the same relative amount as the field gradient pulse parameters are changed. Thus, CORE evaluates the experimental data in two dimensions by a global least-squares fit, yielding band shapes and estimations of the diffusion coefficients for each species in the sample, Figure D.2.
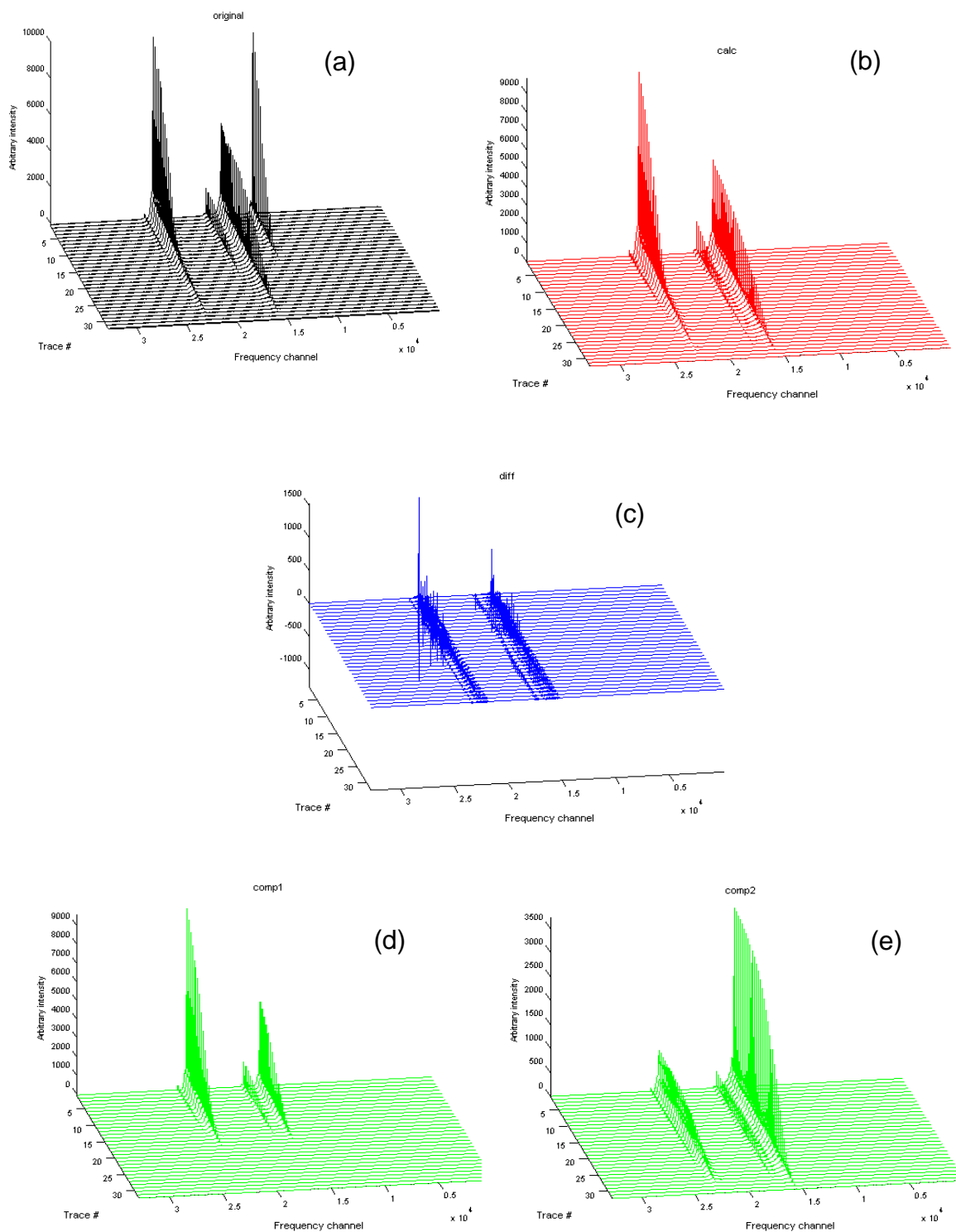
Figure D.2 : COmponent REsolved (CORE) analysis of the diffusion of 5wt% Pluronic P123+50 mM h-C$_{12}$TAB in D$_2$O at 25°C; (a) original spectrum (b) calculated fit after masking HOD peak (c) residuals (d) SMS rich component + P123, (e) P123 rich component + SMS. The HOD has been "edited out" of the analysis protocol, leaving just two components, Pluronic and the SMS.

D.3 Small Angle Neutron Scattering (SANS)

Neutrons are about 10^5 times smaller than the average distance between nuclei, they are uncharged particles that are scattering by short-range repulsive interactions with atomic nuclei. This renders them with very good penetration of most material without causing any damage to their structure. Hence, SANS is a very powerful technique to probe the structure and properties of a wide range of systems, including colloids and polymers.

A schematic representation of a SANS experiment is presented in Figure D.3. The scattering vector, Q, is a very important term in SANS. Q is the difference between the incident (k_i) and scattered (k_s) wave vectors:

$$Q = |Q| = |k_s - k_i| = \frac{4\pi}{\lambda} n sin\left(\frac{\theta}{2}\right)$$ (D.4)

Where n is the neutron refractive index, which is approximately equal to unity, and θ is the scattering angle.
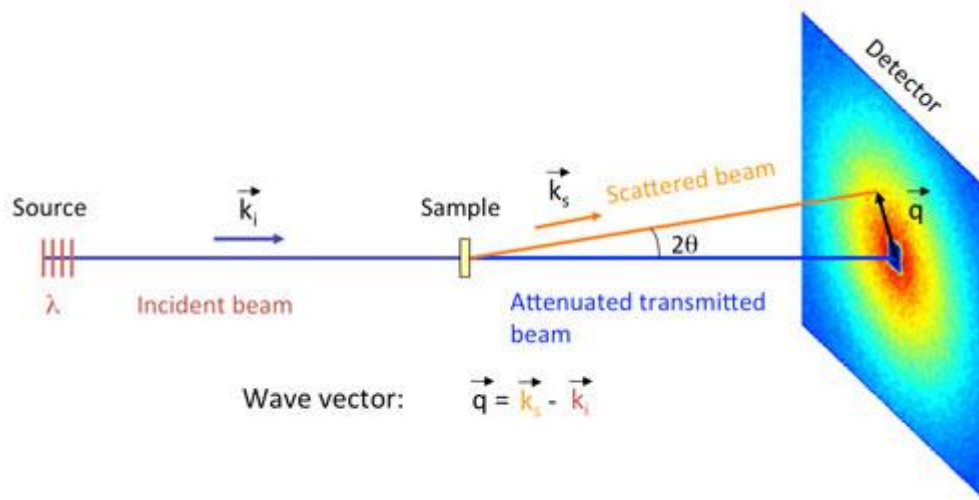
Figure D.3 Schematic of a scattering experiment. Adapted from Grillo *et al.* [8]

Appendix D. Experimental techniques

During a SANS experiment, the intensity of scattering is recorded as a function of the wavevector. For homogenous isotropic scatterers, e.g. spherical particles, the intensity, I(Q) could be given as:

$$I(Q) = NV^2(\Delta\rho)^2 P(Q)S(Q) + B_{inc} \qquad (D.5)$$

where N is the number of particles per unit volume, V is the volume of the particles, $\Delta\rho$ is the contrast in the scattering length density between a particle and the solvent, $P(Q)$ is the form factor and $S(Q)$ is the structure factor and B_{inc} is the incoherent background scattering.

The interactions between neutron and the nucleus controls the way the neutrons scatters. The strength of these interactions is given by the neutron scattering length of a nucleus, b. The calculation of b is not trivial and its values are determined and calculated experimentally. The scattering power of a substance defines a very important term, the scattering length density (SLD), this is a key parameter that determines whether or not this substance will be visible to the neutrons. The SLD from a molecule, ρ_N, can be calculated:

$$\rho_N = \frac{\delta N_A}{M}\sum b_i \qquad (D.6)$$

where δ is the bulk density of the molecule, N_A is the Avogadros number, M is the molecular weight of the molecule and b_i is the coherent neutron scattering length of the nucleus i.

A particular powerful approach in SANS experiments is contrast variation. This uses the significant difference in the SLD between hydrogen (^{1}H) and deuterium (^{2}D), where if possible, the hydrogen in a molecule is substituted with deuterium. Therefore, it is possible to change the SLD of the molecule in a multi-component system so it matches that of its surrounding medium, making it "invisible" to the neutrons, Figure D.4.
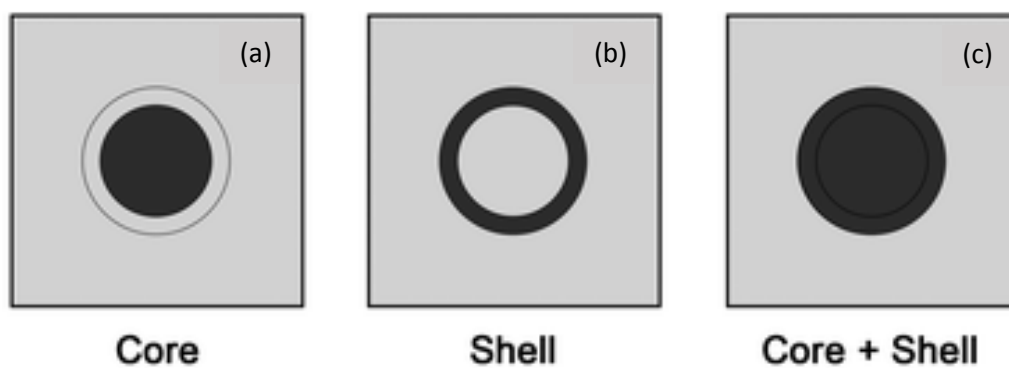
Figure D.4 An example of contrast variation in a core-shell system: (a) h-core, d-shell and d-solvent, (b): d-core, h-shell and d-solvent and (c): h-core, h-shell and d-solvent. Adapted from Hollamby et al.[9]

Appendix D. Experimental techniques

Bibliography

(1)   Farrar, T.; Becker, E. *Pulse and Fourier Transform NMR: Introduction to Theory and Methods*; Academic Press: New York, **1971**.

(2)   Griffiths, P.; Stilbs, P. NMR Self-Diffusion Studies of Polymeric Surfactants. *Curr. Opin. Colloid Interface Sci.* **2002**, *7*, 249–252.

(3)   Matsukawa, S.; Yasunaga, H.; Zhao, C.; Kuroki, S.; Kurosu, H.; Ando, I. Diffusion Processes in Polymer Gels as Studied by Pulsed Field-Gradient Spin-Echo NMR Spectroscopy. *Prog. Polym. Sci.* **1999**, *24*, 995–1044.

(4)   Stilbs, P. Micellar Breakdown by Short-Chain Alcohols. A Multicomponent FT-PGSE-NMR Self-Diffusion Study. *J. Colloid Interface Sci.* **1982**, *89*, 547–554.

(5)   Zhang, Z.; Madsen, L. A. Observation of Separate Cation and Anion Electrophoretic Mobilities in Pure Ionic Liquids. *J. Chem. Phys.* **2014**, *140*, 084201–084210.

(6)   Stilbs, P.; Paulsen, K.; Griffiths, P. C. Global Least-Squares Analysis of Large, Correlated Spectral Data Sets: Application to Component-Resolved FT-PGSE NMR Spectroscopy. *J. Phys. Chem. B* **1996**, *3654*, 8180–8189.

(7)   Östlund, J.; Nydén, M.; Stilbs, P. Component-Resolved Diffusion in Multicomponent Mixtures. A Case Study of High-Field PGSE-NMR Self-Diffusion Measurements in Asphaltene/naphthenic Acid/solvent. *Energy & fuels* **2004**, 531–538.

(8)   Grillo, I. Small-Angle Neutron Scattering and Applications in Soft Matter. In *Soft matter characterization*; Springer: Amsterdam, **2008**; pp. 707–759.

(9)   Hollamby, M. J. Practical Applications of Small-Angle Neutron Scattering. *Phys. Chem. Chem. Phys.* **2013**, *15*, 10566–10579.
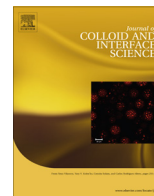
Probing competitive interactions in quaternary formulations

Omar T. Mansour [a], Beatrice Cattoz [a], Richard K. Heenan [b], Stephen M. King [b], Peter C. Griffiths [a],*

[a] Faculty of Science and Engineering, University of Greenwich, Medway Campus, Central Avenue, Chatham Maritime, Kent ME4 4TB, UK
[b] Science and Technology Facilities Council, ISIS Facility, Rutherford Appleton Laboratory, Didcot, Oxfordshire OX11 0QX, UK

GRAPHICAL ABSTRACT
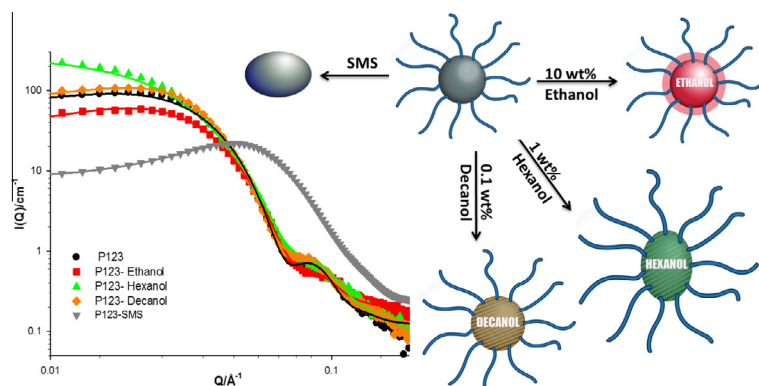
ARTICLE INFO

ABSTRACT

Hypothesis: The interaction of amphiphilic block copolymers of the poly(ethylene oxide)–poly(propylene oxide)–poly(ethylene oxide) (PEO–PPO–PEO) group with small molecule surfactants may be "tuned" by the presence of selected alcohols, with strong interactions leading to substantial changes in (mixed) micelle morphology, whilst weaker interactions lead to coexisting micelle types.

Experiments: The nature and the strength of the interactions between Pluronic P123 ($EO_{20}PO_{70}EO_{20}$) and small molecule surfactants (anionic sodium dodecylsulfate, SDS, $C_{12}SO_4Na$), (cationic dodecyltrimethylammonium bromide, $C_{12}TAB$) and (non-ionic polyoxyethylene(23)lauryl ether, Brij 35, $C_{12}EO_{23}OH$) is expected to depend on the partitioning of the short, medium and long chain alcohols (ethanol, hexanol and decanol respectively) and was probed using tensiometry, pulsed-gradient spin-echo nuclear magnetic resonance (PGSE-NMR) and small-angle neutron scattering (SANS).

Findings: The SANS data for aqueous P123 solutions with added alcohols were well described by a charged spherical core/shell model for the micelle morphology. The addition of the surfactants led to significantly smaller, oblate elliptical mixed micelles in the absence of alcohols. Addition of ethanol to these systems led to a decrease in the micelle size, whereas larger micelles were observed upon addition of the longer chain alcohols. NMR studies provided complementary estimates of the micelle composition, and the partitioning of the various components into the micelle.

© 2015 Elsevier Inc. All rights reserved.

---

* Corresponding author.
  E-mail address: p.griffiths@greenwich.ac.uk (P.C. Griffiths).

1. Introduction

Amphiphilic molecules, commonly known as surfactants, form discrete aggregates, called micelles above the critical micelle concentration (CMC). A widely studied and practically relevant series of surfactants is the water soluble triblock copolymer group made up of poly(ethylene oxide) (PEO) and poly(propylene oxide) (PPO), denoted as (PEO$_n$-PPO$_m$-PEO$_n$), commercially known as Pluronic (BASF), Synperonic (Croda) or Poloxamers (ICI) [1–7]. The CMC is sensitive to the chemical composition of the Pluronic and various grades are available. It has been well established that Pluronics form temperature sensitive micelles that adopt a core–shell morphology, where the more hydrophobic domain (PPO) forms the core and the hydrophilic domain (PEO) forms the hydrophilic corona, i.e. the shell [8–12].

In practical applications, it is usual that polymer–surfactant mixtures are employed as these often have improved properties derived by complex formulation; the addition of ionic/non-ionic surfactants to such polymeric surfactant solutions. The improvement in performance arises due to the synergistic or antagonistic interactions between the various surfactants [13]. A considerable number of studies have focused on determining the onset of the micellization process and the composition/morphology of the mixed micelles formed [9,14–16], though theoretical modelling is limited to systems that are considerably more simple than generally encountered in 'real-life' formulations [17,18] .

The interactions of small molecule surfactants with Pluronic are of relevance to their numerous pharmaceutical, domestic, technological and industrial applications. Mixtures of small molecules surfactant with Pluronic have previously been examined [6,19,20] as has the effect of alcohols [11,13,21]. To our knowledge, there have been far fewer studies of the quaternary systems, Pluronic/small molecule surfactants/alcohol/water, at least in non (micro) emulsion systems.

Previously, we quantified the interaction between the homopolymer polyvinylpyrrolidone (PVP) and SDS in the presence of ethanol [13], and subsequently Pluronic P123 and sodium dodecylsulfate (SDS) in the presence of ethanol [11]. A range of techniques were employed including small-angle neutron scattering (SANS), surface tension and spectrofluorometry. Synergistic interactions between the SDS and P123 were observed, these interactions were characterised by the adsorption of the SDS into the PPO core. It was also observed that addition of ethanol to both P123 and SDS solubilised the PPO core, increasing the CMC of P123, and that reducing the dielectric constant of the solvent led to the formation of smaller micelles in both cases [6,11,19].

Against this background, the present study was undertaken to quantify the effect of short (ethanol), medium (hexanol) and long (decanol) chain alcohols, ionic/non-ionic surfactants comprising dodecyl chain and different head group sizes (anionic SDS, cationic C$_{12}$TAB and non-ionic Brij 35) on the micellar structure of one specific Pluronic, P123. These effects were investigated using SANS, pulsed-gradient spin-echo nuclear magnetic resonance spectroscopy (PGSE-NMR) and surface tension measurements. The aim is to quantify the interactions between the Pluronic and the small molecule and to elaborate the dependence on the presence of the added alcohol, and demonstrate how the partitioning of the alcohol will drive the interaction between the surfactants.

2. Experimental

2.1. Materials

Pluronic P123, PEO$_{20}$-PPO$_{70}$-PEO$_{20}$, average $M_n \sim 5800$ g mol^{-1} (Aldrich) was used as received. Sodium dodecylsulfate (SDS)

(Aldrich, purity 98.5%), dodecyltrimethylammonium bromide (C$_{12}$TAB) (Aldrich, purity 98%), polyoxyethylene (23) lauryl ether (Brij 35) (Aldrich) were all used as received. Deuterated SDS (d-SDS) and C$_{12}$TAB (d-C$_{12}$TAB) for SANS experiments were purchased from Aldrich (99.9%) and used as received. Ethanol, hexanol and decanol, all protonated (Fisher Scientific), deuterium oxide (Aldrich, 99.9%) were used as received.

2.2. Methods

2.2.1. Surface tension

The surface tension measurements of pure and the mixed systems were carried out using a maximum bubble pressure tensiometer (SITA science on-line t60, Germany), calibrated by reference to de-ionised water. Surface tension was recorded at a bubble life time of value 10 s. All measurements were taken at 25 ± 1 °C.

2.2.2. Small-angle neutron scattering

SANS measurements were performed at 25 °C on the fixed-geometry, time of flight LOQ diffractometer (ISIS Spallation Neutron Source, Oxfordshire, UK). Neutron wavelengths spanning 2.2–10 Å were used to access a Q range $(Q = 4\pi \sin(\theta/2)/\lambda)$ of approximately 0.008–0.25 Å^{-1} (25 Hz), with a fixed sample-detector distance of 4.1 m.

The samples were contained in 1 mm path length, UV-spectrophotometer grade, quartz cuvettes (Hellma) and mounted in aluminium holders on top of an enclosed, computer-controlled, sample chamber. Temperature control was achieved through the use of a thermostatted circulating bath pumping fluid through the base of the sample chamber. Under these conditions a temperature stability of better than ±0.5 °C can be achieved. Experimental measuring times were approximately 40 min.

All scattering data were normalised for the sample transmission and the incident wavelength distribution, corrected for instrumental and sample backgrounds using a quartz cell filled with D$_2$O (this also removes the incoherent instrumental background arising from vacuum windows, etc.), and corrected for the linearity and efficiency of the detector response using the instrument specific software package. The data were put onto an absolute scale using a well characterised partially deuterated polystyrene blend standard sample.

The intensity of the scattered radiation, $I(Q)$, as a function of the wave vector, Q, is given by:

$$I(Q) = N_m V_m^2 (\Delta\rho)^2 P(Q) S(Q) + B_{inc.} \tag{1}$$

where $P(Q)$ describes the morphology of the scattering species, $S(Q)$ describes the spatial arrangement of the micelles in solution, N_m is the number of micelles per unit volume, V_m is the volume of the micelle, $\Delta\rho$ is the difference between the neutron scattering length density of the micelle and the solvent and B_{inc} is the incoherent background scattering.

Assuming there are three discrete regions; core, shell and the continuous solvent, the macroscopic scattering cross section is given as the particle number density multiplied by the square of the single-particle form factor, $P(Q)$:

$$P(Q) = N\left[(\rho_A - \rho_C)V_A \frac{3j_1(QR_A)}{QR_A} + (\rho_B - \rho_C)V_{A+B}\left(\frac{3j_1(QR_B)}{QR_B} - \frac{3j_1(QR_A)}{QR_A}\right)\right]^2 \tag{2}$$

where N is the number of core–shell particles per unit volume of solution, ρ_A is the scattering length density for the core, ρ_B is the scattering length density for the shell, ρ_C is the scattering length density for the solvent, V_A is the specific volume in the core, V_B is

the specific volume in the shell and V_{A+B} is the volumes of the core and that of the shell [22].

The first part of the equation is the contribution to the differential cross section from the core with the relevant scattering length density difference that between the core and the solvent. The second part of the equation is the shell contribution (R_A and R_B) to the scattering (j_1 is the first order spherical bessel function of the first kind) [22].

The $S(Q)$ used in the fitting routine is the rescaled mean spherical approximation (RMSA) provided by Hayter et al. [23,24] for spheres of given micellar concentration, charge and ionic strength, incorporating refinements for low-volume fractions and a penetrating ionic background.

The data were fitted using the SasView analysis program [25]. The software is open source and has been developed by major neutron scattering facilities; ISIS, ILL and NIST. The morphology of the micelle adopted for P123 here follows a model for that of a charged particle with core shell morphology. The shell may also contain solvent and/or the added surfactant or alcohol, so an intermediate scattering length density (SLD) between that of the core and solvent could be used. In some cases e.g., P123/small molecule surfactant mixed micelles, we invoke a slightly simpler model of a charged solid ellipsoidal micelle (i.e. no shell) as there are no signature of the shell (a bump at high Q) in the data. A detailed structure of the core–shell micelle is not required as it will be difficult to extract meaningful information without over parameterising the fit. It should be also noted that for anisotropic particles such as ellipsoids, there is a numerical integration over the particle orientation. Given that Pluronic micelles are known to be slightly polydisperse [26,27], a polydispersity parameter was included in the fitting routine and for most of the samples, it was set at 0.15.

The mixed micelle has been treated as a two component (P123 and small molecule surfactant, SMS) surfactant system [28]. The volume of this mixed micelle having aggregation number, N, is calculated by:

$$V_m = N(x_1 v_{SMS} + (1 - x_1)v_{P123}) \tag{3}$$

where x_1 is the mole fraction of SMS in the mixed micelle. v_{SMS} and v_{P123} are the molecular volumes of SMS and P123 respectively. The micelle composition was extracted from the SANS data without any data fitting [6], from the ratio of the intensities of scattering $R(Q)$ obtained with h- and d-SMS at the same composition via:

$$Vf_{SMS} = \left(\frac{(\sqrt{R(Q)} - 1)(\rho_{P123} - \rho_{D2O})}{(\rho_{h-SMS} - \rho_{P123}) - \sqrt{R(Q)}(\rho_{d-SMS} - \rho_{P123})} \right) \tag{4}$$

where

$$R(Q) = \frac{I(Q)^{h-SMS.P123} - B_{inc.}^{h-SMS.P123}}{I(Q)^{d-SMS.P123} - B_{inc.}^{d-SMS.P123}}$$

For the P123-Brij 35 mixed micelles, the micelle composition was not extracted using the same method as it was not possible to obtain deuterated Brij 35.

2.2.3. Pulsed-Gradient Spin Echo Nuclear Magnetic Resonance (PGSE-NMR)

PGSE-NMR (diffusion NMR) experiments were carried out at 25 °C on a 400 MHz Bruker FT NMR spectrometer. The gradient pulse duration (δ) was set to 1 ms and the magnetic field gradient (G) was varied from 5 to 500 G/cm. The diffusion time (Δ) was set to 300 ms. Further information on PGSE-NMR may be found in reference [29]. 8 scans were accumulated over 16 gradient steps. The self-diffusion coefficient was extracted by using CORE [30].

The partitioning of the alcohol and small molecule surfactant may be easily quantified by NMR diffusion measurements since the measured self-diffusion coefficient is an average value

containing contributions from the monomeric and micellized surfactant, weighted by the respective concentrations. This is equivalent to the fractional time spent by each molecule in a given environment, and is frequently expressed in terms of the fractional micelle composition, $p_{micelle}^{P123}$ [31]:

$$\overline{D}^{P123} = p_{micelle}^{P123} D_{micelle}^{P123} + (1 - p_{micelle}^{P123})D_{monomer}^{P123} \tag{5}$$

where $\overline{D}^{P123}$ is the measured self-diffusion coefficient, $D_{micelle}^{P123}$ is the micelle self-diffusion coefficient and $D_{monomer}^{P123}$ is the self-diffusion coefficient of P123 monomers.

A similar analysis [31] to extract the partitioning of the alcohol (p_{free}^{R-OH}) and the small molecule surfactant, may be conducted as shown in Eq. (6), where $D_{micelle}$ is the measured self-diffusion coefficient, $D_{micelle}^{R-OH}$ is the micelle self-diffusion coefficient after alcohol solubilisation and D_{free}^{R-OH} is the free alcohol self-diffusion coefficient.

$$p_{free}^{R-OH} = \frac{D_{free}^{R-OH} - D_{micelle}^{R-OH}}{D_{free}^{R-OH} - D_{micelle}} \tag{6}$$

Hence from a single PGSE-NMR measurement, p_{free}^{R-OH} and $p_{micelle}^{P123}$ can be obtained.

3. Results and discussion

3.1. Onset of micellization

Surface tension is a particularly convenient experimental technique to determine the onset of micellization. However, for complex systems e.g. mixtures of surfactants/water, the discontinuities in the surface tension may be at least initially counterintuitive. For example, when one dilutes a binary surfactant/water system through its CMC, does the experimental design maintain a fixed ratio of two surfactants or a fixed concentration of one of the materials. The surface tension curves would be quite different, as the system would evolve from mixed micelles to none or mixed to pure. This is especially important when there is a hydrophobic component present. It also should be noted that surface tension is a measure of the surface properties, hence, the difficulty of designing an experiment investigating bulk characteristics and competitive interactions. Accordingly, selections of behaviours are presented in Fig. 1.

Fig. 1, compiles several approaches we have used to design surface tension experiments. Focusing on the SDS case, which is more interesting, if we dilute P123 in simple aqueous solvent (open circles), there is clearly one break point in the curve yielding CMC ∼0.1 wt%. In the presence of SDS, keeping [P123] = 0.5 wt% (filled grey circles), several behaviours that are insensitive to the ethanol presence can be noticed. Three different SDS concentration regions can be distinguished, for low SDS concentrations, up to 1 mM, the surface tension remains unaffected by the SDS and remains dominantly controlled by the P123; over an intermediate SDS concentration, up to 10 mM, the surface tension increases sharply to a plateau, upon further increase of SDS concentration, the surface tension again decreases.

As outlined in Table 1a, the CMC of pure SDS (empty squares) is 7.9 mM which agrees well with earlier reported data [32–34]. In the presence of 0.5 wt% of the polymer, the CMC of SDS is lowered significantly from 7.9 mM to 1.2 mM, such decrease in the CMC could be understood as the aggregation of the SDS on the polymer (See Table 1b).

In the presence of ethanol, the CMC and the surface tension of SDS (filled squares) is also remarkably reduced, confirming that the micellization is promoted by the presence of ethanol- the
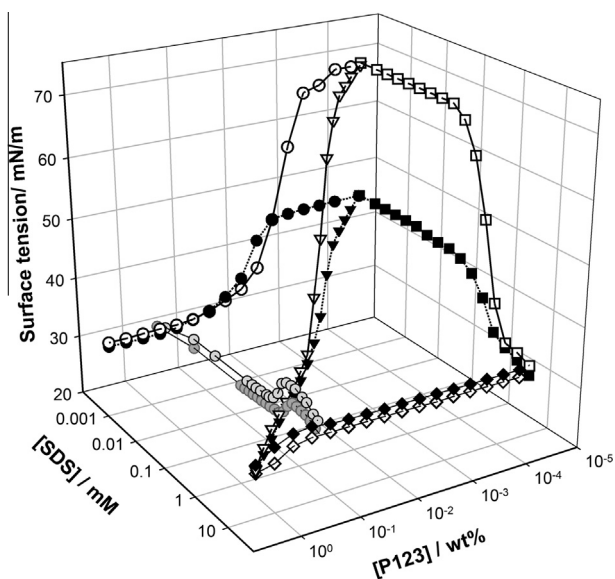
Fig. 1. Surface tension as a function of surfactant concentration: open squares, □ = [SDS/water], filled squares, ■ = [SDS + constant ethanol concentration, 10 wt% in water], open diamonds, ◇ = [P123 + constant SDS and ethanol concentration, 50 mM & 10 wt% in water], filled diamonds, ◆ = [P123 + constant SDS concentration, 50 mM in water], open triangles, △ = [P123 + SDS in water], filled triangles, ▲ = [P123 + SDS + constant ethanol concentration, 10 wt% in water], grey open circles across the SDS axis, ◕ = [SDS + constant P123 concentration, 0.5 wt% in water]/grey filled circles across the SDS axis, ◑ = [SDS + constant P123 and ethanol concentration, 0.5 wt% & 10 wt% ethanol in water], open circles, ○ = [P123/water], filled circles, ● = [P123 + constant ethanol concentration, 10 wt% in water].

Table 1a
Surface tension derived CMC/critical aggregate concentration (CAC) values as a function of P123, SDS and ethanol concentration in water.

System	CMC or CAC
SDS/water	7.9 mM
SDS/0.5 wt% P123-water	1.2 mM
SDS/10 wt% ethanol	4.5 mM
P123/water	0.1 wt%
P123/10 wt% ethanol	0.6 wt%
P123/50 mM SDS-water	0.3 wt%
P123/50 mM SDS-10 wt% ethanol	0.6 wt%

Table 1b
Surface tension derived CMC/critical aggregate concentration (CAC) values as a function of P123, $C_{12}TAB$ and ethanol concentration in water.

System	CMC or CAC
$C_{12}TAB$/water	15 mM
$C_{12}TAB$/0.5 wt% P123-water	3.7 mM
$C_{12}TAB$/10 wt% ethanol	12 mM
P123/water	0.1 wt%
P123/10 wt% ethanol	0.6 wt%
P123/50 mM $C_{12}TAB$-water	0.04 wt%
P123/50 mM $C_{12}TAB$-10 wt% ethanol	0.1 wt%

cosurfactant effect. In the presence of 10 wt% ethanol, the P123 surface tension curve (filled circles), shows one break in the curve yielding a CMC of ∼0.6 wt%, which in comparison to the CMC of the simpler P123 solution, ∼0.1 wt%, confirms that the micellization process is unfavoured (the CMC increases) as the solvent is less hydrophobic.

When a fixed concentration of SDS/ethanol is kept (open diamonds), a decrease in surface tension is observed by increasing the P123 concentration as the less surface active species (small molecule surfactant and ethanol) are being stripped from the

surface and it is being replaced with more active ones, P123. Whilst if we keep a fixed SDS/hexanol concentration, the surface tension increases by increasing the P123 concentration as it has a lower surface activity compared to the SDS/hexanol and water mixture (Supplementary material).

Changes in the system along the concentration range of ternary mixtures of P123 or small molecule surfactant and the hydrophobic alcohols (hexanol and decanol) in water, where the alcohol is kept constant, are quite significant. Below the CMC, where surfactant monomers only are present, the alcohol solubilisation is lower and the alcohol phase separates out of the solution. This phase behaviour and the maximum solubilisation of the alcohol, within the context of previously published SANS data [11,35,36] were the defining rules for alcohol concentration selection in the aqueous P123 and P123-small molecule surfactant mixtures.

The interactions contributing to the formation of the mixed micelles can be described as synergistic or antagonistic in terms of the change in the CMC. We use the terms in a more general sense. In these quaternary systems investigated, interactions with varying strengths between the surfactants were observed for SDS-P123, $C_{12}TAB$-P123 and Brij 35-P123 in water and water/alcohol mixtures. These interactions are observed as the small surfactant molecules are being included in between the Pluronic molecules. The size and shape of the self-assembled structure is dictated by these interactions. SANS has been used to quantify these structures, and again illustrative data are presented.

3.2. Effect of alcohols on the pluronic micelle structure

Scattering profiles for 5 wt% Pluronic P123 above the CMC are shown in Fig. 2. The scattering profile of 5 wt% P123 in D_2O yields considerable scattering intensity with a noticeable "bump" around $Q = 0.09$ Å^{-1}, reflecting a sharp discontinuity in the scattering length density profile across the micelle indicative of the well-defined core and corona regions. Fitting the data to the core–shell model described earlier shows that the P123 micelles are slightly polydisperse with a spherical core of 57 Å ± 1 and corona 14 Å ± 0.5 with the latter adopting Gaussian statistics [26].

Given that the CMC of P123 increases in the presence of ethanol, it is more likely that this decreasing intensity at low Q after the

Fig. 2. SANS from 5 wt% P123 solutions as a function of alcohol concentration; black circles, ●, [alcohol] = 0 wt%, red squares, ■, [ethanol] = 10 wt%, green triangles, ▲, [hexanol] = 1 wt% and orange diamonds, ◆, [decanol] = 0.1 wt%. The inset shows the structure factor $S(Q)$ extracted from the fit of the same data in the same colouring order of the main graph. Solid lines are fits to the core–shell model, see Table 2. (For interpretation of the references to colour in this figure legend, the reader is referred to the web version of this article.)

addition of 10 wt% ethanol, Fig. 2, is due to the reduction of the number and/or the volume of the micelle and/or a change in the interaction between the micelles via the structure factor. This could be simply attributed to the fact that the ethanol/water mixture solubilises the hydrophobic PPO core more than pure water [36,37], changing the effective HLB of the surfactant. Support (albeit indirect) arises from an interpretation of the micellar volume fraction parameter extracted from the Hayter–Penfold fit, in that all attempts to describe the data with a volume fraction greater than 0.05 (in essence, the mass fractions of the Pluronic plus the solubilised alcohol) led to poor fits. It was concluded therefore, that the ethanol displaces the water in the EO-rich shell, thereby not significantly increasing the fraction of the micelle bounded material.

By contrast, in the case of 1 wt% hexanol and 0.1 wt% decanol, the scattering intensity at low Q increases reflecting the presence of more and/or larger micelles as the hydrophobic alcohol is incorporated into the micellar core. Making the reasonable assumption that the hydroxyl group is present at the core/corona interface to maintain its hydration, the modelling shows that this drives the formation of a larger micelle. The slight shift of the structure factor, extracted from the fit (inset in Fig. 2) towards higher Q values is indicative of the decreasing distance between the micelles associated with the increase in the micelle size. The key parameters, extracted from the fitting, are listed in Table 2.

The SLD for the solvent (D_2O) was kept constant in the fitting routine for most of the samples at $6.39 \times 10^{-6}\,\text{Å}^{-2}$, but was adjusted accordingly using the partitioning values extracted from PGSE-NMR data analysis. For example, the samples containing 10 wt% ethanol, where PGSE-NMR has shown that 2.5% only remains unbound in the solvent, the SLD of the solvent (D_2O and some fraction of the h-ethanol) and the core (PPO and the remaining fraction of h-ethanol) were included in the fitting routine based on some simple assumptions; (i) all the ethanol partitions into the core, (ii) all the ethanol partitions into the shell, (iii) some distribution of the ethanol between the core and the shell. For each simulation, the SLD of the appropriate region was estimated based on the composition, and this value is used as an input parameter ("guess") or occasionally held constant in the fitting routine. Based on this analysis, we conclude that the majority of the ethanol is located in the shell of the micelle. PGSE-NMR has also shown that both hexanol and decanol partition into the micelle, but in these cases, due to their low concentration, the change in the solvent SLD was negligible.

Fig. 2 also shows the effect of hexanol on the aggregation behaviour of the P123 micelle. Addition of 1wt% hexanol resulted in a large increase in the scattering intensity at low Q. The linearity observed in the low Q region is suggestive of the ellipsoidal micelles [35,38]. Data fitting suggests the formation of prolate ellipsoidal micelles with major axis of 160 Å and a minor axis of 55 Å. Key fitting parameters are listed in Table 2.

The material-balance equations, described by Slawecki et al. [39] allow us to quantify the composition of the core and shell of the P123 micelle in D_2O using the SANS data. There were 5–6 D_2O molecules per EO monomer in the shell. The aggregation number, 110 ± 5, is in good agreement with other reported values from data previously fitted to the Pedersen model for Pluronics in solution [40] at the same polymer concentration and temperature, 5 wt% [11,36]. Percentage of EO monomers inside the PO core was found to be 2.96% which agrees with the simple understanding of a core shell model, where both regions are well defined.

Self-diffusion coefficients obtained by PGSE-NMR were used to determine values of p^{OH}_{free}, (free fraction of alcohol not solubilised the micelles) as shown in Eq. (6). Applying the values obtained for p^{OH}_{free} to the mass balance equation, one may correct to a first assumption that 50%, 15% and 3% of these micelle volumes are the solubilised alcohols, giving an estimate of the aggregation number of 60, 200 and 160 for micelles with ethanol, hexanol and decanol respectively. These estimates of the aggregation numbers are entirely consistent with the measured P123 diffusion rates.

Significant changes in micelle morphology are observed when small molecule surfactants are added to the P123/alcohol systems. Take for example the SDS case, on addition of 50 mM SDS to the 5 wt% P123 aqueous and alcohol/aqueous solutions, Fig. 3, SANS data show significant loss in the scattering intensity and the emergence of correlation peaks at higher Q values which together indicates the formation of smaller, mixed, charged micelles.

Adding the SDS has resulted in the loss of the "bump" at $\sim 0.09\,\text{Å}^{-1}$. The addition of the ethanol to the P123/SDS mixed micelle led to a slight decrease in the scattering intensity with no significant change in the position of the correlation peak. As shown previously in Fig. 2, the hydrophobicity of the micellar core

Table 2
Fitting parameters for 5 wt% P123 as a function of alcohol concentration at 25 °C (from SANS and PGSE-NMR).

Alcohol concentration (wt%)	0 wt%	10 wt% Ethanol	1 wt% Hexanol	0.1 wt% Decanol
Core radius (±1, Å)	57	50	a: 160/ b:55	60
Shell thickness (±0.5, Å)	14	13.5	–	13
Volume fraction of hard spheres(±0.001)	0.05	0.05	0.05	0.05
Volume of the micelles (nm³), V_{mic}	1500	1100	2100	1600
Free alcohol fraction,p^{OH}_{free}, from NMR	–	0.25	0.03	0
Aggregation number, N_{agg} (±5),	110	60[a]	200	160
Micelles number density,n, $10^{16}\,\text{cm}^{-3}$	3.5[b]	4.7	2.0	3.2

[a] Similar aggregation numbers for P123 with ethanol have been reported by Jangher et al. [11], Alexander et al. [36] and Soni et al. [41].
[b] Micelles number density value is in good agreement with the values reported by Manet et al. [42].

Fig. 3. SANS from 5 wt% P123 solutions + 50 mM h-SDS as a function of alcohol chain length; black circles, ●, [alcohol] = 0 wt% and [h-SDS]=0 mM, red squares, ■, [alcohol] = 0 wt%, green triangles, ▲, [ethanol] = 10 wt%, orange diamonds, ◆, [hexanol] = 1 wt% and blue hexagons, ⬡, [decanol] = 0.1 wt%. Solid lines correspond to model fits as discussed in the text. Data above Q = 0.15 Å⁻¹ have been omitted for clarity. (For interpretation of the references to colour in this figure legend, the reader is referred to the web version of this article.)

increases by increasing the hydrophobicity of the alcohols, evident by the increase in the scattering intensity, along with a shift in the correlation peak towards the lower Q region indicating the formation of larger aggregates, Table 3. The scattering from these mixed micelles were fitted using a form factor describing the micelle as an oblate ellipsoid with a charged structure factor as calculated by Hayter and Penfold. The key parameters are listed in Table 3.

It is widely accepted that SDS absorbs into the PPO core as the interaction between SDS and the hydrophobic PPO block of P123 is stronger than that between SDS and the hydrophilic PEO block where it renders the core less hydrophobic [15,16]. Jansson et al. [43] showed that at low SDS/P123 mol ratios, the principle structure is a P123 micelle with co-micellised SDS. At higher SDS/P123 mol ratios, P123 micelles are broken up, forming SDS-rich micelles co-micellised with few P123 molecules.

One could envisage a situation where the bulkiness of the head group of the small molecule or its charge density would control the size and the hydration level of the mixed micelle, Table 4. SANS data, Fig. 4 shows the effect of the head group size on the scattering intensity. The mixed micelle aggregation number shows variations with changing the small molecule surfactant charge. For the P123/SDS system, the aggregation number decreases after adding SDS to the block copolymer (Nagg = 12 ± 5) [11,15,16,44], which is expected as the head group (SO_4Na^+) is forming small curved surfaces, whereas in the P123/C_{12}TAB system, the C_{12}TAB ($N(CH_3)_3Br^-$) is likely to be less charged where the degree of counter-ion dissociation is less, hence the decrease in the curvature and the formation of larger structures (Nagg = 20 ± 5). Upon introducing a non-ionic surfactant, Brij 35, there is a further decrease in the charge which forms even bigger structures (Nagg = 25 ± 5). For comparison, the dimensions expressed in terms of the volume of the pure component micelles are; SDS–35 nm³ [19], C_{12}TAB–40 nm³ [45]; Brij–275 nm³ [46] whilst P123–1500 nm³) (see Table 5).

Fig. 5 shows the variations in the scattering data at lower P123 and small molecule surfactant concentrations but at identical P123/surfactant ratio and above CMC_{mixed}. Studying these systems at lower concentrations yields more insight about the shape of the aggregates formed and the nature of the interactions between the surfactants. At low SDS concentrations, 5 mM, there is significantly

Fig. 4. SANS from 5 wt% P123 solutions as a function of small molecule surfactant head group size; black circles, ●, [surfactant] = 0 mM, red squares, ■, [h-SDS] = 50 mM, green triangles, ▲, [h-C_{12}TAB] = 50 mM, orange diamonds, ◆, [Brij 35] = 50 mM. (For interpretation of the references to colour in this figure legend, the reader is referred to the web version of this article.)

Table 5
SANS parameters for 0.5 wt% P123 as a function of 5 mM h-surfactants in D₂O.

Surfactant	No SMS added	C_{12}TAB	Brij 35
Radius A (±1, Å)	57	42	23
Thickness/Radius B (±1, Å)	17	12	51
Volume fraction of hard spheres (±0.001)	0.005	0.005	0.01
Volume of the micelles (nm³)	1500	860	250
Micelles number density, n, 10^{15} cm⁻³	3.3	5.8	40
Mixed micelle aggregation number (±5)	130[a]	88	26

[a] Result is in good agreement with Jangher et al. [11] and Bhattacharjee et al. [26].
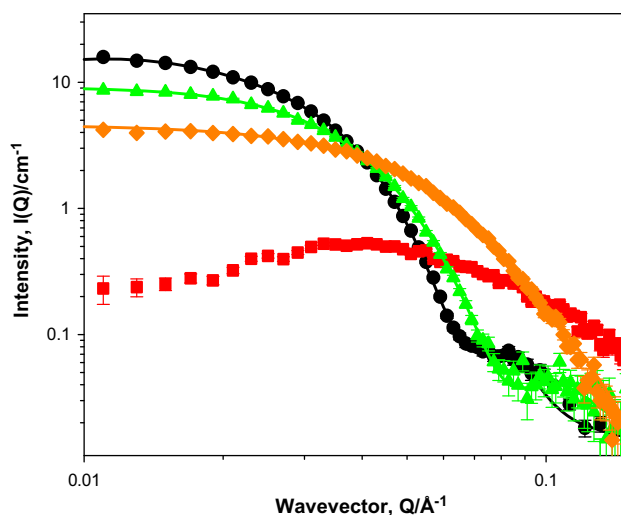
Fig. 5. SANS from 0.5 wt% P123 solutions as a function small molecule surfactant head group size; black circles, ●, [surfactant] = 0 mM, red squares, ■, [h-SDS] = 5 mM, green triangles, ▲, [h-C_{12}TAB] = 5 mM, orange diamonds, ◆, [Brij 35] = 5 mM. (For interpretation of the references to colour in this figure legend, the reader is referred to the web version of this article.)

less scattering intensity indicating the presence of small, charged micelles as a result of the strong adsorption of the SDS into the PPO core and the synergistic interaction between SDS and P123.

Table 3
SANS parameters for 5 wt% P123–50 mM h-SDS as a function of alcohol concentration.

Alcohol concentration (wt%/v)	0 wt%	10 wt% Ethanol	1 wt% Hexanol	0.1 wt% Decanol
Radius A, polar (±0.5, Å)	17	17	21	19
Radius B, equatorial (±1, Å)	39	37	46	39
Volume fraction of hard spheres (±0.001)	0.06	0.05	0.06	0.06
Volume of the micelles (nm³)	110	95	185	120
Mixed micelle aggregation number (±5)	12	10	20	13
Micelles number density, n, 10^{17} cm⁻³	5.9	5.2	3.2	5.0

Table 4
SANS parameters for 5 wt% P123 as a function of 50 mM h-surfactants in D₂O.

Surfactant	SDS	C_{12}TAB	Brij 35
Radius A, polar (±0.5, Å)	17	23	26
Radius B, equatorial (±1, Å)	39	45	45
Volume fraction of hard spheres (±0.001)	0.06	0.06	0.09
Volume of the micelles (nm³)	110	195	210
Mixed micelle aggregation number, ±5	12	20	25
Micelles number density, n, 10^{17} cm⁻³	5.9	3.1	4.3

On increasing the head group size of the surfactant, i.e. $C_{12}TAB$, the scattering intensity is recovered where the micelle also regains its core–shell morphology demonstrating antagonistic interactions between both surfactants. Upon a further increase in the head group size; Brij 35, the scattering pattern adopts a slope of -2 at high Q confirming the formation of a mixed oblate elliptical micelle. The synergistic interactions between P123 and Brij 35 as reported in earlier reports [47,48], occurs as both surfactants have hydrated EO chains when in contact with water, which results in a full miscibility of both surfactants in the mixed micelle. The antagonistic interactions between P123 and $C_{12}TAB$ could be related to two possible explanations. The first being the large size of the head group where it shields the hydrophobic core, and suppress the presence of the polymer at the hydrocarbon–water interface. The second explanation is related to the electrostatic repulsion as a result of a slight positive charge present on the polymer, originating from the protonation of the ether oxygen in the PEO chains [49,50].

3.3. Determination of the micelle composition

Contrast variation experiments have also been used to separate the scattering from the P123 and the small molecule surfactants; the use of d-surfactants in D_2O renders them invisible. In the case of h-P123/d-SDS/D_2O, Fig. 6a, SDS is invisible and the scattering intensity observed arises predominantly from P123. In the h-P123/h-SDS/D_2O case, both surfactants are visible and hence the stronger scattering intensity observed. h-P123/h-$C_{12}TAB$/D_2O system, Fig. 6b, shows a higher intensity profiles than the h-SDS case and a signature of a structure adopting core–shell morphology.

A crude estimate of the SDS and $C_{12}TAB$ fraction (Vf_{SMS}) presented as α, within the aggregate could be extracted from the SANS measurements without any data fitting from the ratio of the scattering intensities, $R(Q)$, obtained with h and d-surfactants at the same composition, Eq. (4). For 0.5 wt% P123–5 mM SDS, $\alpha(SDS) = 31$ (±5)% [11], and for 0.5 wt% P123–5 mM $C_{12}TAB$, $\alpha(C_{12}TAB) = 11$ (±5)%.

These findings agree with the data extracted from the fitting where SDS had the strongest interaction with P123 as discussed earlier, and it forms up to 30% of the mixed micelle structure, where in the weakest interaction case (P123–$C_{12}TAB$), the small molecule surfactant makes up 11% only of the mixed micelle structure.
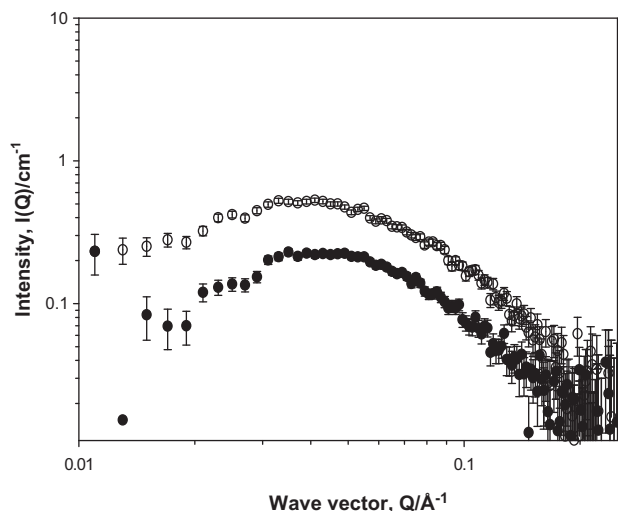

Fig. 6a. SANS from 0.5 wt% P123 and [5 mM h-SDS] = empty circles (○), [5 mM d-SDS] = filled circles (●) in D_2O.
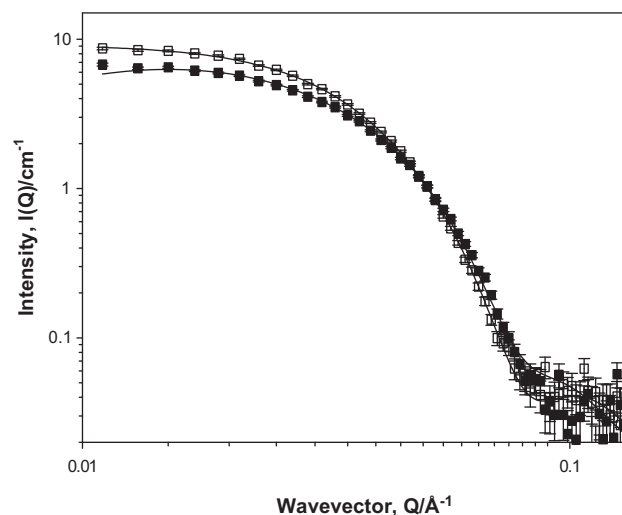
Fig. 6b. SANS from 0.5 wt% P123 and [5 mM h-$C_{12}TAB$] = empty squares (□), [5 mM d-$C_{12}TAB$] = filled squares (■) in D_2O.

Drawing the same analysis to these systems in the presence of alcohols, provides a further understanding to the role of the solvent partitioning in controlling the interactions, Table 6. When 1 wt% ethanol is added to the mixed system of $C_{12}TAB$ and P123, the subtle effect of ethanol becomes greater, yielding a higher $C_{12}TAB$ fraction ($\alpha(C_{12}TAB) = 35(\pm5)$%) in comparison to the P123 + $C_{12}TAB$ in D_2O case, $\alpha(C_{12}TAB) = 11(\pm5)$%.

Adding ethanol with the same concentration to the P123 + SDS system, ($\alpha(SDS) = 28(\pm5)$%), the P123 + SDS effect wins over the effect of the ethanol, without showing any significant changes in the SDS fraction.

The P123 + SDS effect still wins over the further increase in the hydrophobicity of the alcohol, as the fraction of SDS does not change significantly. However, the alcohols effect still wins over the P123 + $C_{12}TAB$ effect, where the fraction of $C_{12}TAB$ shows a noticeable change, Table 6.

The model developed by Nagarajan [51] and Nikas et al. [52] for mixed, charged surfactant micelles allows us to frame the discussion on the effect of the added alcohol on the mechanisms driving the interactions in these systems. The model states that the free energy of formation for mixed aggregates has a number of contributing terms - the deformation of the surfactant tail as it conforms to packing requirements within the micellar core, the energy of forming the aggregate core/solvent interface which depends on the aggregation number and the presence of any alcohol, and a term that accounts for the headgroup interactions over the micellar surface, again defined by the composition of this region. Further terms must be included to account for the free energy of the polymer, including any change in entropy induced by the different packing of the polymer within the mixed micelle compared to the pure micelle, plus any changes induced in the interfacial energy terms due to the displacement of solvent by polymer in the micellar shell.

Table 6
Mixed micelle composition in terms of small molecule surfactant fraction, α (±5)%, as a function of alcohol concentration.

System description	0 wt% alcohol	1 wt% ethanol	0.1 wt% hexanol	0.01 wt% decanol
0.5 wt% P123/5 mM SDS	31	28	30	31
0.5 wt% P123/5 mM $C_{12}TAB$	11	35	21	14

Making the assumption that the interfacial tension of the aggregate core/continuous phase follows the same trend as the surface tension of the bulk solution, the energy required to produce the interface decreases on addition of alcohol, favouring micelle formation – the CMCs of SDS and $C_{12}TAB$ decrease with added alcohols. The term which considers the ionic headgroup interactions is a complex one, which cannot be estimated simply. A number of factors come into play in determining the energies of the headgroup interactions, including the dielectric constant, Debye length, the radius of the micelle and the presence of the polymer. For instance, the dielectric constant of the solution decreases in the presence of alcohol, which in turn influences the various charge effects such as counterion dissociation (hence the size and shape of the micelle), changes in the level of hydration of the ethylene oxide (EO) groups, as well as composition dependent micelle/solvent interfacial tension. Work is on-going to identify and model the magnitudes of these various effects, but a first step in this process is the determination of the polymer/small molecule surfactant micelle dimensions. It is hoped that this paper will stimulate further effort on this area.

4. Conclusions

The effect of small molecule surfactants and alcohols on the aggregation behaviour of Pluronic P123 has been widely studied due to their extensive use in industry [1–7]. Aqueous/alcohol mixtures comprising the polymeric (Pluronic) surfactant P123, anionic SDS, cationic $C_{12}TAB$ and non-ionic Brij 35 have been characterised by using tensiometry, PGSE-NMR and SANS. The results are presented firstly in terms of the ternary systems, (i) Interaction between P123 in the presence of alcohols; (ii) Interaction P123 in the presence of surfactants and (iii) The quaternary system.

4.1. Interaction between P123 in the presence of alcohols

The partitioning in the micelle has been quantified by PGSE-NMR where it also shows that larger aggregates with slow diffusion rates were formed after adding hexanol and decanol and faster diffusing aggregates were formed after the addition of ethanol. The partitioning is in good agreement with the literature values [35,41].

The micelle size decreases with the addition of ethanol, but increases with both hexanol and decanol. The micelle shape is spherical in the absence of any alcohol, and interestingly, remains so in the presence of ethanol and decanol, but forms prolate micelles in the presence of hexanol. We suggest this is a balance between the site and degree of alcohol solubilisation – ethanol is located in the outer shell of the Pluronic micelle, the more hydrophobic hexanol and decanol are solubilised into the core.

4.2. Interaction between P123 in the presence of surfactants

The scattering data clearly report on micelle disruption by the small molecule surfactants. By comparing the relative changes in the scattering profiles, we found that SDS has the strongest interaction with P123 [11,43], followed by Brij 35 and then $C_{12}TAB$ which showed the weakest interaction [49,50].

4.3. Interaction between P123 in the presence of both alcohols and surfactants

The addition of the alcohols to the Pluronic/small molecule surfactant solution has introduced further changes to the mixed micelle composition. The effects of the alcohol have been compared with the effect of mixing the pure surfactants, in terms of the micelle composition. For (the dilute) Pluronic/SDS cases, adding the different alcohols has little effect on the micelle composition, suggesting that there is a strong interaction between SDS and P123. For systems comprising P123 and $C_{12}TAB$, the $C_{12}TAB$ micelle mole fraction increases for all cases of alcohol, indicative of a weaker interaction between the small molecule surfactant and the Pluronic (consistent with the relative changes in CMC).

This work has allowed us to extend our understanding of the interactions between different surfactants and will direct the design of further experiments where more complex systems will be investigated.

Appendix A. Supplementary material

Supplementary data associated with this article can be found, in the online version, at http://dx.doi.org/10.1016/j.jcis.2015.04.068.

References

[1] R. Kaur, S. Kumar, V.K. Aswal, R.K. Mahajan, Langmuir 29 (2013) (1833), http://dx.doi.org/10.1021/la401864p. 11821-11821.
[2] C. Booth, D. Attwood, Macromol. Rapid Commun. 527 (2000) 501–527, http://dx.doi.org/10.1002/1521-3927(20000601)21:9<501::AID-MARC501>3.0.CO;2-R.
[3] P. Alexandridis, J.F. Holzwarthf, T.A. Hatton, Macromolecules 27 (1994) 2414–2425, http://dx.doi.org/10.1016/j.jcis.2012.09.028.
[4] G. Marinov, B. Michels, R. Zana, Langmuir 14 (1998) 2639–2644, http://dx.doi.org/10.1021/la971069w.
[5] P. Alexandridis, T.A. Hatton, Colloids Surf. A Physicochem. Eng. Asp. 96 (1995) 1–46, http://dx.doi.org/10.1016/0927-7757(94)03028-X.
[6] P.C. Griffiths, A.Y.F. Cheung, G.J. Finney, C. Farley, S.M. King, R.K. Heenan, B.L. Bales, Langmuir 18 (2002) 1065–1072, http://dx.doi.org/10.1021/la011163j.
[7] J. Nambam, J. Philip, J. Phys. Chem. B 116 (2012) 1499–1507, http://dx.doi.org/10.1021/jp208902a.
[8] Y. Li, R. Xu, D.M. Bloor, J.F. Holzwarth, E. Wyn-Jones, S. Couderc, Langmuir 16 (2000) 10515–10520, http://dx.doi.org/10.1021/la000899y.
[9] R. Ivanova, B. Lindman, P. Alexandridis, Adv. Colloid Interf. Sci. 89–90 (2001) 351–382, http://dx.doi.org/10.1016/S0001-8686(00)00049-X.
[10] A. Kabanov, E. Batrakova, V. Alakhov, J. Control. Release 82 (2002) 189–212, http://dx.doi.org/10.1016/S0168-3659(02)00009-3.
[11] A. Jangher, P.C. Griffiths, A. Paul, S.M. King, R.K. Heenan, R. Schweins, Colloids Surf. A Physicochem. Eng. Asp. 391 (2011) 88–94, http://dx.doi.org/10.1016/j.colsurfa.2011.08.006.
[12] P. Linse, M. Malmsten, Macromolecules 25 (1992) 5434–5439, http://dx.doi.org/10.1021/ma00046a048.
[13] P. Griffiths, N. Hirst, A. Paul, S. King, Langmuir 20 (2004) 6904–6913, http://dx.doi.org/10.1021/la049348o.
[14] K. Nakashima, P. Bahadur, Adv. Colloid Interf. Sci. 123–126 (2006) 75–96, http://dx.doi.org/10.1016/j.cis.2006.05.016.
[15] R. Ganguly, V. Aswal, Langmuir 20 (2006) 9843–9849, http://dx.doi.org/10.1021/jp0607061.
[16] E. Hecht, K. Mortensen, J. Phys. Chem. B 88 (1995) 4866–4874, http://dx.doi.org/10.1021/j100013a068.
[17] C. Sarmoria, S. Puvvada, D. Blankschtein, Langmuir 8 (1992) 2690–2697, http://dx.doi.org/10.1021/la00047a019.
[18] S.B. Puvvada, Surfactants Solut. 11 (1991) 95–111.
[19] P. Griffiths, A. Paul, R. Heenan, J. Phys. Chem. B 108 (2004) 3810–3816, http://dx.doi.org/10.1021/jp0371478.
[20] P. Desai, N. Jain, R. Sharma, P. Bahadur, Colloids Surf. A Physicochem. Eng. Asp. 178 (2001) 57–69, http://dx.doi.org/10.1016/S0927-7757(00)00493-3.
[21] B. Sarkar, V. Ravi, P. Alexandridis, J. Colloid Interf. Sci. 390 (2013) 137–146, http://dx.doi.org/10.1016/j.jcis.2012.09.028.
[22] B. Hammouda, Eur. Polym. J. 46 (2010) 2275–2281, http://dx.doi.org/10.1016/j.eurpolymj.2010.10.012.
[23] J. Hansen, J.B. Hayter, Mol. Phys. 42 (1981) 109–118, http://dx.doi.org/10.1080/00268978100100091.
[24] J. Hansen, J.B. Hayter, Mol. Phys. 46 (1982) 651–656, http://dx.doi.org/10.1080/00268978200101471.

[25] SasView, http://www.sasview.org/ version 2.1.
[26] J. Bhattacharjee, G. Verma, V.K. Aswal, V. Patravale, P.A. Hassan, RSC Adv. 3 (2013) 23080–23089, http://dx.doi.org/10.1039/c3ra44983a.
[27] B. Foster, T. Cosgrove, B. Hammouda, Langmuir 25 (2009) 6760–6766, http://dx.doi.org/10.1021/la900298m.
[28] J. Joshi, V. Aswal, P. Goyal, Pramana 71 (2008) 1039–1043, http://dx.doi.org/10.1007/s12043-008-0220-z.
[29] P. Occhipinti, P.C. Griffiths, Adv. Drug Deliv. Rev. 60 (2008) 1570–1582, http://dx.doi.org/10.1016/j.addr.2008.08.006.
[30] P. Stilbs, K. Paulsen, P. Griffiths, J. Phys. Chem. B 3654 (1996) 8180–8189, http://dx.doi.org/10.1021/jp9535607.
[31] P. Stilbs, J. Colloid Interf. Sci. 89 (1982) 547–554, http://dx.doi.org/10.1016/0021-9797(82)90206-5.
[32] A. Cifuentes, J. Bernal, J. Diez-Masa, Anal. Chem. 69 (1997) 4271–4274, http://dx.doi.org/10.1021/ac970696n.
[33] S. Lin, Y. Lin, E. Chen, C. Hsu, C. Kwan, Langmuir 15 (1999) 4370–4376, http://dx.doi.org/10.1021/la001075j.
[34] B.D. Flockhart, J. Colloid Interf. Sci. 565 (1957) 557–565.
[35] V. Patel, J. Dey, R. Ganguly, S. Kumar, S. Nath, V.K. Aswal, P. Bahadur, Soft Matter. 9 (2013) 7583, http://dx.doi.org/10.1039/c3sm50600b.
[36] S. Alexander, T. Cosgrove, T.C. Castle, I. Grillo, S.W. Prescott, J. Phys. Chem. B 116 (2012) 11545–11551, http://dx.doi.org/10.1021/jp303185m.
[37] P. Alexandridis, L. Yang, Macromolecules 33 (2000) 5574–5587, http://dx.doi.org/10.1021/ma000332o.
[38] S. Kumar, V.K. Aswal, J. Phys. Condens. Matter. 23 (2011) 035101, http://dx.doi.org/10.1088/0953-8984/23/3/035101.
[39] T. Slawecki, C. Glinka, B. Hammouda, Phys. Rev. E 58 (1998) 4084–4087. doi:10.1103/PhysRevE.58.R4084.
[40] J. Pedersen, C. Svaneborg, Curr. Opin. Colloid Interf. Sci. 7 (2002) 158–166. doi:10.1016/S1359-0294(02)00044-4.
[41] S. Soni, G. Brotons, J. Phys. Chem. B 110 (2006) 15157–15165, http://dx.doi.org/10.1021/jp062159p.
[42] S. Manet, A. Lecchi, J. Phys. Chem. B 115 (2011) 11318–11329, http://dx.doi.org/10.1021/jp200212g.
[43] J. Jansson, K. Schillén, J. Phys. Chem. B 109 (2005) 7073–7083, http://dx.doi.org/10.1021/jp0468354.
[44] E. Hecht, H. Hoffmann, Langmuir 14 (1994) 86–91, http://dx.doi.org/10.1021/la00013a013.
[45] B.L. Bales, R. Zana, J. Phys. Chem. B 106 (2002) 1926–1939, http://dx.doi.org/10.1021/jp013813y.
[46] M. Tomšič, M. Bešter-Rogač, A. Jamnik, W. Kunz, D. Touraud, A. Bergmann, O. Glatter, J. Colloid Interf. Sci. 294 (2006) 194–211, http://dx.doi.org/10.1016/j.jcis.2005.06.088.
[47] S. Couderc, Y. Li, D.M. Bloor, J.F. Holzwarth, Langmuir 77 (2001) 4818–4824, http://dx.doi.org/10.1021/la0104267.
[48] D. Löf, M. Tomšič, J. Phys. Chem. B 113 (2009) 5478–5486. doi:abs/10.1021/jp808442d.
[49] M. Schwuger, J. Colloid Interf. Sci. 43 (1973), http://dx.doi.org/10.1016/0021-9797(73)90395-0.
[50] J. Mata, T. Joshi, D. Varade, G. Ghosh, P. Bahadur, Colloids Surfaces A Physicochem. Eng. Asp. 247 (2004) 1–7, http://dx.doi.org/10.1016/j.colsurfa.2004.07.011.
[51] R. Nagarajan, in: Structure–Performance Relationships in Surfactants, MarcelDekker, New York, 1997, p. Chapters 1 and 12.
[52] Y. Nikas, D. Blankschtein, Langmuir 10 (1994) 3512–3528, http://dx.doi.org/10.1021/la00022a026.
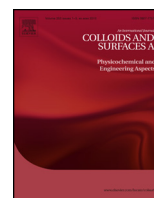
Quantifying the micellar structure formed from hydrocarbon-fluorocarbon surfactants

Zaineb O. Et-Tarhouni [a,*], Emma Carter [a], Damien M. Murphy [a], Peter C. Griffiths [b], Omar T. Mansour [b], Stephen M. King [c], Alison Paul [a,**]

[a] School of Chemistry, Cardiff University, Main Building, Park Place, Cardiff CF10 3TB, UK
[b] Department of Pharmaceutical, Chemical and Environmental Sciences, Faculty of Engineering and Science, University of Greenwich, Medway Campus, Central Avenue, Chatham Maritime, Kent, ME4 4TB, UK
[c] Rutherford Appleton Laboratory, Science and Technology Facilities Council, Didcot, Oxfordshire, OX11 0QX, UK

HIGHLIGHTS

- Unusual micellisation process occurs in the system $C_{16}TAB$/FSN-100 mixture solutions.
- FSN-100 forms disc-like micelles with aggregation number of 65.
- $C_{16}TAB$ forms globular, charged micelles with a larger aggregation number than FSN-100.

GRAPHICAL ABSTRACT
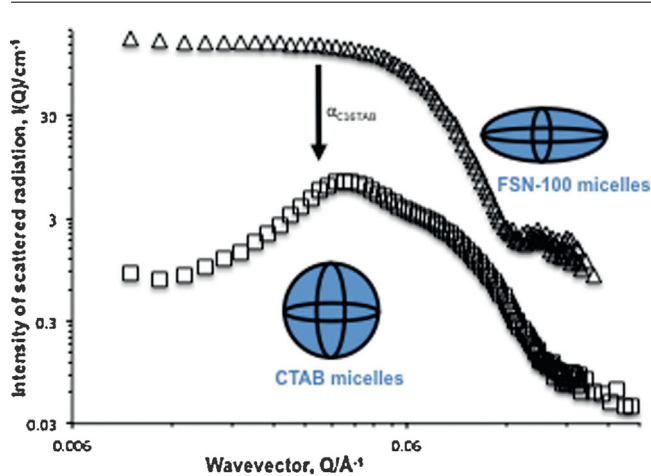
ARTICLE INFO

ABSTRACT

Many technological formulations contain mixtures of surfactants, each contributing some distinct property. Characteristics of each surfactant are often modulated in the mixture, based on the interactions between the various components present. Here, the mixing of the hydrocarbon surfactant cetyltrimethyl ammonium bromide ($C_{16}TAB$) and the fluorocarbon surfactant, Zonyl-FSN-100 with average chemical structure of $C_8F_{17}C_2H_4 (OC_2H_4)_9OH$, is quantified, in particular, the size and shape of the micelles and their critical micelle concentration (CMC). The CMC data suggest there are specific interactions between the two components which are strongly antagonistic. Small-angle neutron scattering (SANS) has been used to quantify the size and shape of the micelle, and these data indicate that the single component FSN-100 forms disc-like micelles with a small aggregation number (~65) and the $C_{16}TAB$ forms globular, charged micelles with a larger aggregation number (135). The aggregation number of the mixed micelle is substantially greater than either of the pure species. Overall, a detailed study of CTAB, FSN-100 and their mixture systems will be presented in this paper.

© 2015 Elsevier B.V. All rights reserved.

* Corresponding author.
** Corresponding author.
E-mail addresses: zeltarhouni@yahoo.com (Z.O. Et-Tarhouni), paula3@cardiff.ac.uk (A. Paul).

1. Introduction

Surfactant solutions have been a subject of many investigations [1–7]. Surfactants self-assemble in aqueous solutions to form a wide variety of aggregated structures and many techniques have been developed to study these structures, most based on determining the shape/size of the micelles formed, and their critical micelle concentration. The latter gives an idea of the strength and nature of the interaction between the surfactants in the solution. Here, surface tension, fluorescence, small-angle neutron scattering (SANS), pulsed-gradient spin-echo NMR (PGSE-NMR) spectroscopy and electron paramagnetic resonance spectroscopy (EPR) have been employed to provide a detailed insight into one interesting system, a mixture of a charged, hydrocarbon surfactant and a non-charged, fluorocarbon surfactant.

Hydrocarbon surfactant micelle systems have been extensively studied [3–6], however there are far fewer studies on fluorinated and partially fluorinated surfactant micelles, even though the latter material possess many unique features, especially increased surface activity and hydrophobicity [7–10]. The miscibility of fluorocarbon and hydrocarbon surfactants often presents a challenge to formulation. In this study, we are concerned with the
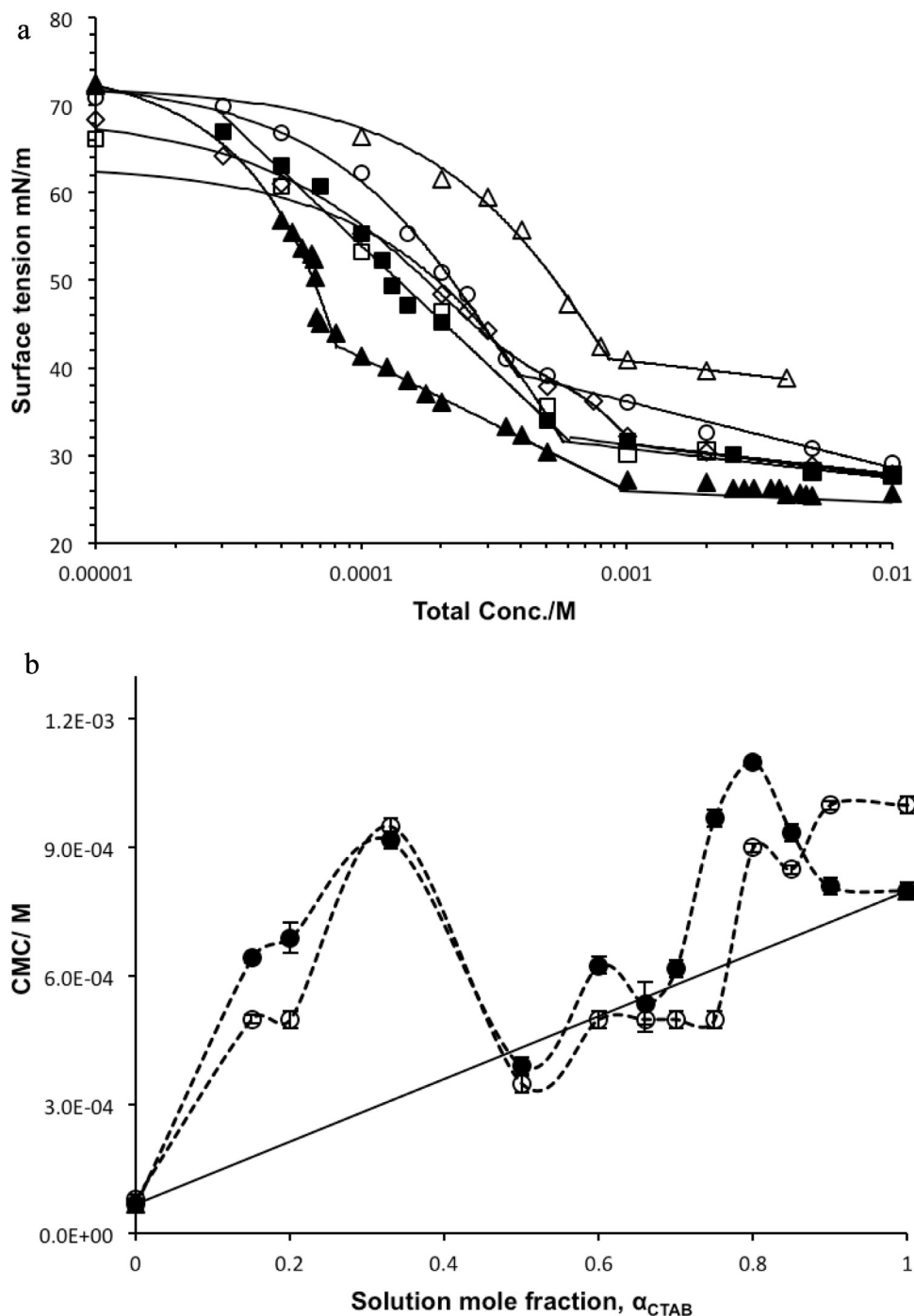
Fig. 1. (a) Surface tension measurements as a function of total concentration for (open triangles) $\alpha_{C16TAB} = 1$, (closed triangles) $\alpha_{C16TAB} = 0$, (open squares) $\alpha_{C16TAB} = 0.15$, (open diamonds) $\alpha_{C16TAB} = 0.33$, (closed squares) $\alpha_{C16TAB} = 0.2$, and (open circles) $\alpha_{C16TAB} = 0.5$. (b) The critical micelle concentration, CMC, as a function of C_{16}TAB mole fraction determined by pyrene solubilisation (open circles) and surface tension (closed circles). Literature CMC values for the pure surfactants are also plotted, (open triangles).
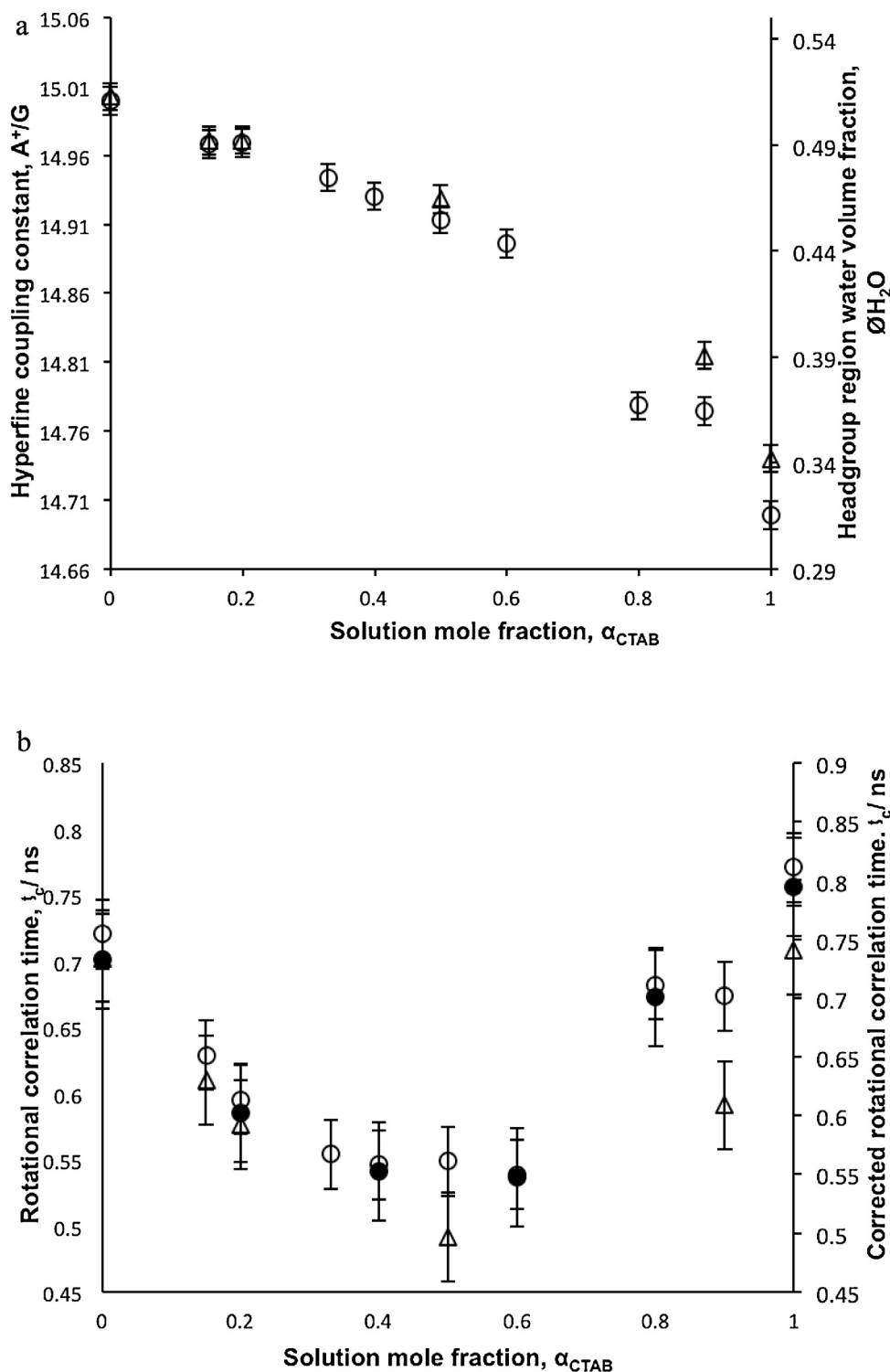
Fig. 2. (a) Hyperfine coupling constant of $C_{16}TAB$/FSN-100 mixtures, as a function of $C_{16}TAB$ solution mole fraction at a total surfactant concentration of 20 mM (open triangles) and 50 mM (open circles). The corresponding volume fraction of water in the headgroup region is indicated on the secondary axis. (b) Rotational correlation time of 16-DSE in $C_{16}TAB$/FSN-100 mixtures, as a function of $C_{16}TAB$ solution mole fraction at a total surfactant concentration of 20 mM (open triangles) and 50 mM (open circles).

aggregation of $C_{16}TAB$ as the model hydrocarbon surfactant and FSN-100 as a model fluorocarbon surfactant; $C_{16}TAB$ has been well-characterised [3,11], whereas FSN-100 has been less well studied, but interestingly, it exhibits two CMC values in aqueous solution, indicating a rather more complex micellisation process [8,10].

2. Materials and methods

2.1. Materials

Cetyltrimethyl ammonium bromide ($C_{16}TAB$) and Zonyl FSN-100 fluorosurfactant, 16-doxyl stearic acid methyl ester (16-DSE)
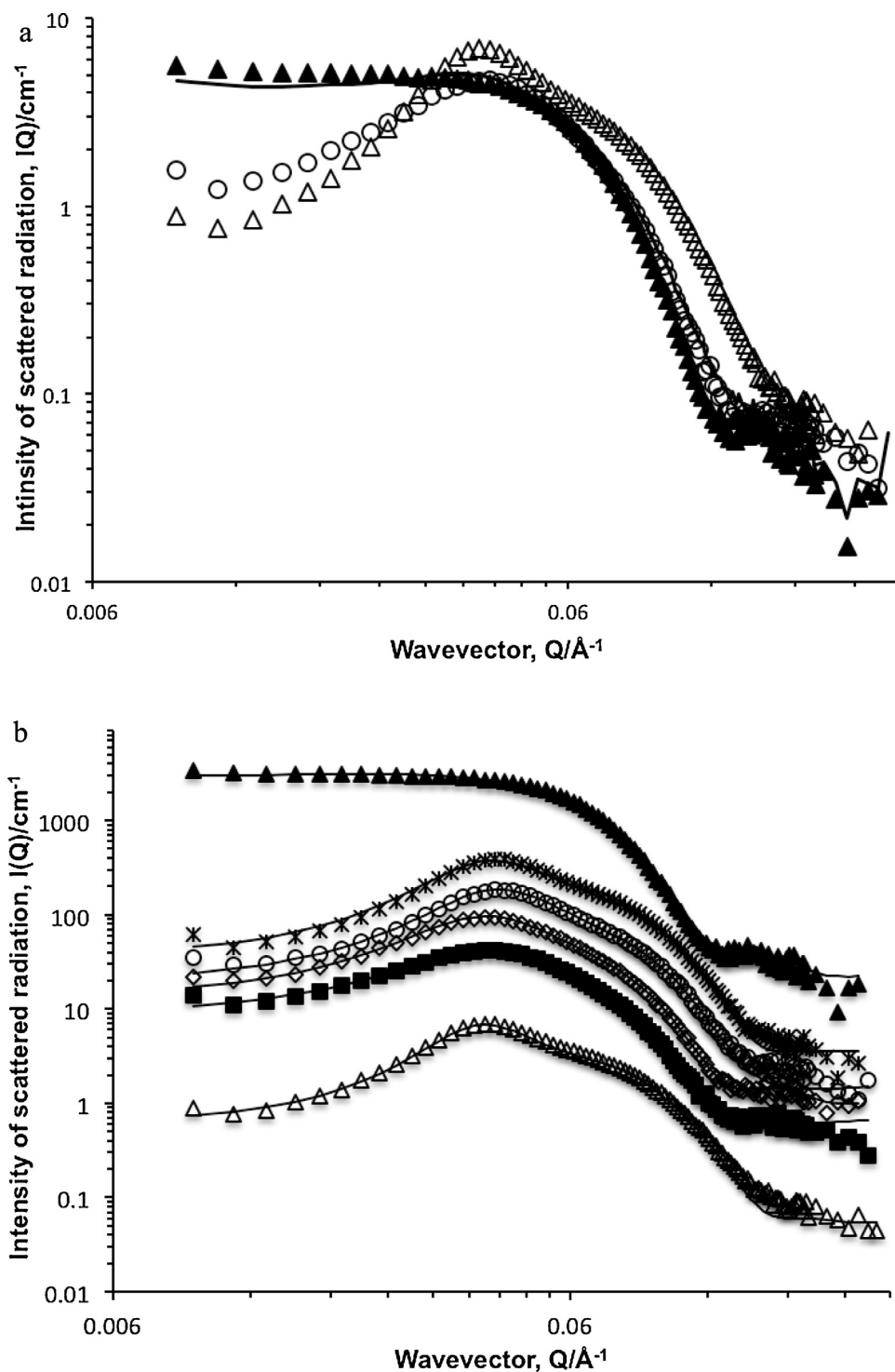
Fig. 3. (a) Small angle neutron scattering as a function of $C_{16}TAB$ mole fraction, (open triangles) $\alpha_{C16TAB} = 1$, (closed triangles) $\alpha_{C16TAB} = 0$, (open circles) $\alpha_{C16TAB} = 0.2$. The solid line represents the calculated numerical average of the two pure surfactant data sets, scaled to an appropriate concentration. (b) Small angle neutron scattering as a function of $C_{16}TAB$ mole fraction, (open triangles) $\alpha_{C16TAB} = 1$, (closed triangles) $\alpha_{C16TAB} = 0$, (closed squares) $\alpha_{C16TAB} = 0.2$, (open diamonds) $\alpha_{C16TAB} = 0.4$, (open circles) $\alpha_{C16TAB} = 0.6$, (stars) $\alpha_{C16TAB} = 0.8$. Fits are included as solid line. Data are offset by a factor of 3 for clarity.

spin-probe and pyrene fluorescent probe were purchased from Sigma-Aldrich and used as received. The solvent was D_2O in the SANS and PGSE-NMR, and deionized water in the surface tension, fluorescence and EPR measurements. Acetone (Aldrich) and ethanol (Aldrich) were used as solvents for the stock pyrene and 16-DSE solutions.

2.2. Surface tension

Surface tension measurements were carried out at room temperature and using LAUDA Drop Volume Tensiometer (TVT1). In this instrument, the volume of a drop that detaches from a capillary is determined. By increasing the volume of the drop, its weight increases until it reaches a critical value at which it cannot be coun-

Z.O. Et-Tarhouni et al. / Colloids and Surfaces A: Physicochem. Eng. Aspects 492 (2016) 255–262

259

terbalanced by the surface tension. The force balance at the drop results in the following relation for the surface tension, Eq. (1).

$$\sigma = Vg\Delta pF/2\pi r_{cap} \tag{1}$$

where σ = interfacial tension, V = drop volume, g = acceleration constant, Δp = difference of the densities of both adjacent phases, F = correlation factor, and r_{cap} = radius of the capillary.

2.3. Fluorescence

All solutions have been prepared from stock solutions by addition of surfactant stock solutions in distilled water to vials containing the pyrene probe. The pyrene concentration was kept constant at 2×10^{-6} M by addition of 0.01 ml of acetone containing pyrene stock solution to empty glass vials and subsequent evaporation of the acetone before addition of the aqueous surfactant solution. Photophysical data were obtained on a JobinYvon–Horiba Fluorolog spectrometer fitted with a JY TBX photodetection module. All spectra were recorded using an excitation wavelength of 340 nm. All samples have been measured at room temperature. CMCs were determined by the breakpoints in the concentration dependent ratio of the third to first vibronic peak, known as the I_3/I_1 ratio.

2.4. Small-angle neutron scattering

The SANS measurements were performed as detailed previously [12] on the fixed-geometry, time-of-flight LOQ diffractometer (ISIS Spallation Neutron Source, Oxfordshire, UK). All measurements were carried out at 25 °C. Experimental measuring times were between 40 and 80 min. All scattering data were normalised for the sample transmission and incident wavelength distribution, corrected for instrumental and sample backgrounds using an empty quartz cell, and for the linearity and efficiency of the detector response. The data were put onto an absolute scale using a well-characterised partially-deuterated polystyrene-blend standard sample.

2.4.1. SANS data fitting and analysis

The intensity of scattered radiation, $I(Q)$, as a function of the wave-vector, Q, is given by;

$$I_{sur.}(Q) = n\left[S(Q)|F(Q)|^2 + |F(Q)|^2 - |F(Q)|^2\right] + B_{inc} \tag{2}$$

where in the case of a core–shell morphology $F(Q)$ is represented as,

$F(Q) = V_1(\rho_1 - \rho_2)F_0(QR_1) + V_2(\rho_2 - \rho_0)F_0(QR_2)$. The first term represents the scattering from the core (subscript 1) and the second, the polar shell (subscript 2). $V_i = 4/3\pi R_i^3$ and $F_0(QR) = 3j_i(QR)/QR$, (j_i is the first-order spherical Bessel function). $S(Q)$ represents the spatial arrangement of the micelles in solution and n the micelle number density. ρ_i is the neutron scattering length density of the micellar core (subscript 1), the polar shell (subscript 2) and the solvent (subscript 0). These constants are combined into a single fittable parameter used to "scale" the model intensity to the absolute value. Post-fitting, this scalar is recalculated using the parameters describing the micelle morphology/composition and the molar concentration of micelles to validate the fit. The calculated and observed values should lie within ∼10%.

The model of the micelle adopted here is that of a charged particle with an elliptical core–shell morphology. In the model the average volume per headgroup average tail volume and their average scattering length densities are input as constants, calculated assuming the composition of the micelle is the same as the solution composition. For C_{16}TAB, $\rho_{C16TABhead} = 2.4 \times 10^{-6}$ Å^{-2} and

volume 412 Å^3. For the FSN-100, $\rho_{FSNhead} = 0.6 \times 10^{-6}$ Å^{-2} and volume 2000 Å^3. The bromide ion dissociation in the C_{16}TAB case does however, significantly affect the charge on the micelle and hence the structure factor S(Q), a point we return to later in the discussion. The average core scattering length density is also similarly calculated, with $\rho_{C16TABtail} = -0.4 \times 10^{-6}$ Å^{-2} and volume 460 Å^3 whereas $\rho_{FSNtail} = 2.0 \times 10^{-6}$ Å^{-2} and volume 295 Å^3.

The structure factor S(Q) was calculated using the Hayter and Penfold [13] for spheres of a given micellar concentration, charge and ionic strength, incorporating refinements for low volume fractions and a penetrating ionic background. Various approaches to parameterising the structure factor were adopted based on known or measured estimates of the micelle size and surfactant concentration to calculate the hard sphere volume fraction, charge and Debye length. We have shown that this method of calculating the structure factor, which assumes spherical particles, remains valid for dilute, isotropic samples of micelles with small degrees of ellipticity, as is the case here [14,15].

For the SANS analysis, the hard sphere volume fraction was fixed at 0.02, calculated from the total surfactant concentration (assuming a mass density of 1 g cm^{-3}). Starting values for the charge (20) and Debye length were estimated based on typical values for ionic surfactants [14], and scaled according to C_{16}TAB mole fraction. The S(Q) parameters were refined during the fitting process to obtain the best fit parameters for P(Q).

The fitting of SANS data is insensitive to the headgroup region, the shell comprising the various headgroups and associated water. The prevailing shell scattering length density is calculated from the average headgroup scattering length density and their hydration, given $\bar{\rho} = \varphi_{water}\rho_{water} + (1 - \varphi_{water})\bar{\rho}_{headgroups}$. Since $\varphi_{water} = V_{water}/V_{shell}$, the parameters V_{water} and V_{shell} are strongly coupled and not amenable to fitting. We adopt the approach of fixing φ_{water} at the EPR determined value that inter alia, defines the shell volume (thickness). The scattering length density of the hydrated shell region is then (re-) calculated within the analysis software, based on $\varphi_{water} f_{water}$. Hence, constraining this value eliminates the trial-and-error aspects required in previous work to find the overall "best fit" value of $\varphi_{water} f_{water}$ due to local minima in the least-squares fits [14].

2.5. PGSE-NMR spectroscopy

Pulsed-Gradient Spin-Echo (PGSE-) NMR measurements were performed on a Bruker AMX400 NMR spectrometer operating at 400 MHz (^{1}H) using a stimulated echo sequence. All the experiments were run at 25 °C using the standard heating/cooling system of the spectrometer to an accuracy of ±0.3 °C. All solutions were prepared from stock solutions using D$_2$O, and 0.6 ml were transferred to 5 mm o.d. NMR tubes (Willmad NMR tubes form Sigma–Aldrich).

The self-diffusion coefficient, D_s, was deduced by fitting the attenuation of the integral for a chosen peak to Eq. (3).

$$A(\delta, G, \Delta) = A_0 \exp(-k \times D_s) \tag{3}$$

where A is the signal intensity in the presence and absence (0) of the field gradients, and $k = -\gamma^2 G^2 \delta^2 (\Delta - \delta/3)$, where γ is the magnetogyric ratio, Δ the diffusion time, δ the gradient pulse length, and σ the ramp time, and G is the gradient field strength [16].

Association and complexation processes can both be extracted from an analysis of the self-diffusion coefficients D_s. In case of micellization studies, the attenuation function observed in the ^{1}H NMR spectra corresponded to the methylene resonance associated to –(CH$_2$)$_X$- of the inner part of the hydrocarbon chains related to the broad peak between d = 1.11–1.20 ppm and thus, reflects the time-average population-weighted average mobility of the monomeric

and micellized surfactant. In case of complexation, the attenuation function was recorded from the peak corresponding to the methylene in the spacer (singlet at $d = 5.36$ ppm) and again, reflected the time-average population-weighted average mobility of monomeric and micellised surfactant.

2.6. EPR spectroscopy

To prepare samples for EPR, 16-DSE (0.01 M) was prepared by dissolving the appropriate amount in 2 ml of ethanol and then 0.02 ml of the solution transferred into a separate glass vial. After allowing for ethanol evaporation, 1.0 ml of the sample was added to the vial and mixed for at least 1 h to give a final spin-probe concentration at 2×10^{-4} M and to ensure that the probe has been incorporated into the micelle solutions.

Experimental details for the EPR measurements are also identical to those described previously [15] and only brief details are repeated here. These non-degassed samples were sealed with a gas-oxygen torch into melting point capillaries, which were housed within a quartz EPR tube for the measurements. The temperature was controlled to ± 0.2 K by a Bruker Variable Temperature Unit BVT 2000. Five spectra were taken at X-band on a Bruker ESP-300 spectrometer.

2.6.1. EPR lineshape fitting and analysis

The lineshapes were fitted to a Voigt approximation to separate the Gaussian and Lorentzian components of the spectral lines and to locate the resonance fields of the three EPR lines arising from the nitroxide radical to a precision of a few mG. Rotational correlation times are computed from the overall linewidth of the centre line and the peak-to-peak heights of the three lines and corrected for inhomogeneous broadening using the procedure outlined by Bales [12,15].

The separation A+ of the low and centre lines ($M_I = +1$ and $M_I = 0$) is directly related to the polarity index H (25 °C), defined as the molar ratio of OH groups in a given volume relative to water (Eq. (4)). H (25 °C) therefore corresponds to the volume fraction of water in the polar shell, f_{water}, and may be used to constrain the SANS fitting.

$$H (25°C) = (A+ - 14.21) / 1.52 \tag{4}$$

3. Results and discussion

3.1. Critical micelle concentration (CMC) determinations

Surface tension measurements have been carried out for a range of solution compositions expressed as a function of C_{16}TAB (solution) mole fraction. The raw are included in Supplemental section (Figs. S1 and S2), but representative data are included in Fig. 1a. The two limits correspond to the single component species, for which our CMC values (C_{16}TAB = 0.8×10^{-4} M, FSN-100 = 6.8×10^{-5} M) are in excellent agreement with literature ones [6,8], (Supplemental Fig. S1). FSN-100 shows two break points (6.8×10^{-5} M, 1.0×10^{-3} M) again as observed previously [8], these have previously been ascribed to pre-association and micellization processes. As may be seen for FSN-100 rich mixtures, there are still two break points, but at higher α_{C16TAB}, only one prevails.

The CMC vs α_{C16TAB} behaviour in Fig. 1b shows a number of distinct features, in particular, significant regions where the CMC is greater than would be predicted by an ideal mixing approach. Therefore, there are specific interactions between the two molecules, and these are strongly antagonistic. What is surprising in this system is the presence of a region of apparent ideality around $0.5 > \alpha_{C16TAB} > 0.7$. Such increases in CMC, crucially to a concentration of one of the species to a value greater than its single

component CMC, as around $0.2 < \alpha_{C16TAB} < 0.4$ emphasises a loss of surfactant activity and the presence of a substantially different micellization process. Clearly, further analysis of the micelle composition and size/shape is warranted.

Surface tension detects changes in the surface composition, which generally reflects the prevailing solution structure. To provide a contrasting measure of the CMC, pyrene solubilisation has also been used. The two curves show remarkable similarity (Fig. 1b), indicating that there is indeed some unusual micellization process occurring in this system.

3.2. Electron paramagnetic resonance spectroscopy (EPR) measurements

In order to constrain various parameters in the analysis of the scattering data (the next section), EPR was used to quantify the hydration of the micelle headgroup region. The EPR technique introduces a very small amount of nitroxide free radical as a spin probe (in this case, 16-DSE) into the micelle and by measuring the hyperfine coupling constant, the micelle structure can be estimated. The data in this experiment were also recorded at two different total surfactant concentrations (20 mM and 50 mM) to assess whether the micelle structure undergoes a significant change with total concentration.

The hyperfine coupling constant from the EPR measurements are plotted versus C_{16}TAB mole fraction in Fig. 2a. It is obvious that there is a greater degree of water (52%) associated with the FSN-100 headgroup, presumably because of the larger headgroup providing a greater volume for water penetration. The C_{16}TAB is a smaller, spherical structure and the predicted value for ϕ_{H2O} at 50 mM would be calculated from Eq. (5) is 0.30, in fair agreement with the experimental value (0.32) (Table 1). Calculation of the estimate for FSN-100 is less precise due to the uncertainty in the headgroup structure, but again the calculated value (0.53) is in good agreement with the experimental one (0.52).

$$\phi_{H2O} = \frac{V_{shell} - V_{headgroups}}{V_{shell}} = \frac{\left(\frac{4}{3}\pi(R+\sigma)^3 X - \frac{4}{3}\pi R^3 X\right) - N_{agg}.V_{CTAB}}{\left(\frac{4}{3}\pi(R+\sigma)^3 X - \frac{4}{3}\pi R^3 X\right)} \tag{5}$$

The headgroup region of the cationic micelle is densely populated with the spherical, cationic headgroups and accordingly, the spin-probe will experience a relatively viscous environment (Fig. 2b). By contrast the non-ionic micelle headgroup region will be populated by fairly large, oligomeric sterically hindering headgroups and accordingly, the spin-probe will also experience a viscous environment. These features are not that sensitive to the aggregation number.

For each cationic molecule (C_{16}TAB) that is removed from the mixed headgroup region, by the mixing of the cationic and non-ionic headgroups, there will be a change in amount of water equivalent to the difference in the respective headgroup volumes, consistent with the change in aggregation number. This is seen as the largely linear dependence of hydration (Fig. 2a) as a function of CTAB mole fraction. Interestingly, the spin-probe experiences a more mobile, a less viscous environment (Fig. 2b), between the two single surfactant extremes, as evidenced by the minimum in the rotational correlation time, a minimum in the viscosity.

EPR experiment provides an additional characterisation of the micelle via the rotational correlation time (τ_c) which is a measure of the dynamics with the micelle and the micelle tumbling itself (Fig. 2b).

The two single component micelles have a similar microviscosity and there is a pronounced minimum in τ_c cross the entire mole fraction range, consistent with a decrease in local viscosity experienced by the probe.

It is customary to separate the dynamics of the spin probe within the micelle $\tau_{Relative}$ to that of the micelle itself $\tau_{micelle}$ in

Table 1
Experimental values for volume fraction of water in the polar shell (ϕH_2O) using EPR, in the single surfactant solutions and mixtures at two different total surfactant concentration.

$C_{16}TAB$/M	FSN-100/M	Exp.ϕ_{H2O}^{shell} 50 mM/($\pm$ 0.2)	Exp.ϕ_{H2O}^{shell} (20 mM/($\pm$ 0.2)
0	1	0.52	0.52
0.15	0.85	0.50	0.50
0.2	0.8	0.50	0.50
0.33	0.67	0.48	–
0.4	0.6	0.47	–
0.5	0.5	0.46	0.47
0.6	0.4	0.45	–
0.8	0.2	0.37	–
0.9	0.1	0.37	0.40
1	0	0.32	0.35

order to comment on the microviscosity of the headgroup region. We use the SANS estimate of the size to obtain $\tau_{micelle}$ to arrive at $\tau_{Relative}$, which is over-plotted in Fig. 2b, for selected data points [17]. Clearly, as expected, the $\tau_{corrected}$ has little impact on the appearance. There is still a pronounced minimum in microviscosity as a function of $C_{16}TAB$ mole fraction.

The microviscosity does not show any obvious dependence of N_{agg} as curvature, being largely defined by the numbers, and bulkiness of the headgroups, modulated by the prevailing degree of hydration. There is a clearly an opposite influence of the smaller TAB headgroup and the bulky, but hydrated ethylene oxide headgroup of the FSN-100.

3.3. Small- angle neutron scattering (SANS) studies

One mechanism by which apparent antagonistic micellization may occur is the coexistence of multiple types of micelles. Therefore, SANS was carried out to test this hypothesis and to quantify the size/shape of the micelles as a function of solution composition.

SANS measurements were performed on a single component $C_{16}TAB$ and FSN-100 as well as selected $C_{16}TAB$/FSN-100 mixtures at specific $C_{16}TAB$ mole fractions, in order to detect micelle shape and size corresponding to the features in the CMC plot. Fig. 3a illustrates the approach adopted to test the hypothesis that two micelle types coexist. The figure shows the data from $C_{16}TAB$ and FSN-100 alone, plus the measured data for α_{C16TAB} = 0.2, where the CMC shows a significant departure from ideality. The solid line represents the calculated numerical average of the two pure surfactant data sets, scaled to an appropriate concentration. As can be seen this calculated data set is not in agreement with the experimental data for α_{C16TAB} = 0.2. This clearly shows that we do not have two populations of FSN and $C_{16}TAB$ micelles, and therefore that mixed micelles must be present. This has been demonstrated for other sample compositions in Supplemental section (Figs. S3 and S4).

Fig. 3b shows the SANS data for the single components and four mixtures. The scattering curves are a composite of the form factor describing the size and the shape, and the structure factor describing the electrostatic interaction between micelles.

The scattering from ionic surfactant micelles possess an oscillatory structure factor which will lead to reduction in intensity at low Q and "bumps" at higher Q. These features are not expected in the scattering from a non-ionic micelle, at least at moderate concentrations. This simple interpretation accounts for many of the gross features in the data, in particular, the most striking difference in the curve from FSN-100 compared with all other mixtures. Expressed differently, once $C_{16}TAB$ is added to the solution, the micelles show less variance in structure, and more similarity with the pure $C_{16}TAB$. As predicted, the scattering intensity decreases at low Q as the $C_{16}TAB$ mole fraction increases, with shoulders around Q = 0.06 Å becoming more pronounced.

Therefore, we conclude that coexisting population of pure micelles do not exist, and the next challenge is to characterize, in detail, the structure of the mixed micelles formed.

Considering the fit for the single component surfactant solutions, the data have been fitted to a model describing the micelle morphology as globular, with a varying degree of ionic character. In both cases, constants have been applied to the analysis; specifically, using the known chemical structure, concentration molar volumes, dimensions and scattering length densities, in constraining with the known concentrations and the experimental values of the degree of hydration from EPR (Table 1). The fitting parameters that are allowed to freely float are the ellipticity, the charge and the incoherent background.

From Table 2, describing the fit for the single components and the mixtures parameters, reflect what is also evident from the data, namely that the mixtures are strongly characterised by the ionic $C_{16}TAB$ component. The aggregation numbers have been calculated via equation (6), the ratio of the core volume divided by a simple weighted value of the effective tail volume, this assumes that the micelle composition is identical to the solution one. In addition, the aggregation number of FSN-100 micelles is a little smaller than the literature value [10], whereas $C_{16}TAB$ micelle aggregation number is in a good agreement with the literature one [18].

$$N_{agg.} = \frac{V_{core}}{V_{tail}} = \frac{\frac{4}{3}\pi R_{core}^3 X}{\alpha_{CTAB}V_{CTAB}^{tail} + (1-\alpha)_{CTAB}V_{FSN-100}^{tail}} \quad (6)$$

where, $N_{agg.}$ Is the aggregation number, X is the ellipticity, R_{Core} is the core radius, V_{tail} is the surfactant tail volume, V_{Core} is the surfactant core volume.

The model assumes a single micelle type and the success of this approach in describing the data suggests that either a single micelle

Table 2
Parameters describing the fits of SANS data from $C_{16}TAB$, FSN-100, and their mixtures as a function of $C_{16}TAB$ mole fraction using a model that describes the micelle as a globular elliptical with some ionic character.

$C_{16}TAB$ mole fraction	R_{Core}/Å	Shell thickness ($\pm$5)/Å	Ellipticity, X	$V_{s(dry)}/V_{Core}$	N_{agg} ($\pm$)
0	13.3	24	1.5	0.8	65
0.2	27.8	12	1.1	0.9	310
0.4	27.8	11	1.0	0.9	250
0.6	26.2	10	1.0	0.9	190
0.8	21.6	10	1.1	1.0	140
1.0	25.8	8.0	0.85	0.9	135

type is indeed present or any coexisting population of micelles are not substantially different. As a complimentary approach, PGSE-NMR was employed to provide more information about micelle structures.

3.4. PGSE- NMR spectroscopy studies

In this experiment, the measured diffusion coefficient is a weighted value of the non-micellised and micellised components. One would expect that if a coexisting micelle population were present, coupled with varying levels of non-micellised surfactant, the diffusion coefficient of the $C_{16}TAB$ and FSN-100 would be quite different. Clearly, they are not (Supplemental Fig. S5), again, consistent with the SANS conclusion that these two surfactants mix, further, the diffusion coefficient values are mutually comparable consistent with the relative volumes of the respective micelles, also suggest that the solution composition is the same as the micellar one.

4. Conclusions

Mixed micelles of cationic $C_{16}TAB$ and non-ionic FSN-100 surfactants have been studied by various techniques. The data show that the two surfactants mix nonideally with CMCs higher than predicted for ideal mixtures whilst some concentrations show a degree of ideality. This behaviour confirms that there is a substantially different micellization process across a range of compositions. It is clear that from SANS data the mixed micelles are strongly characterised by the $C_{16}TAB$ component, and micelles have less variable in structure when different amount of $C_{16}TAB$ was added to the solution. With increasing $C_{16}TAB$ mole fraction, there is a reduction in the amount of water present in the headgroup region. Furthermore, combining resulted data from several techniques has been used to conduct a full picture of the micellar system of $C_{16}TAB$, FSN-100 and their mixtures.

Acknowledgments

Appendix A. Supplementary data

Supplementary data associated with this article can be found, in the online version, at http://dx.doi.org/10.1016/j.colsurfa.2015.12.015.

References

[1] H.B. de Aguiar, et al., Surface structure of sodium dodecyl sulfate surfactant and oil at the oil-in-water droplet liquid/liquid interface: a manifestation of a nonequilibrium surface state, J. Phys. Chem. B 115 (12) (2011) 2970–2978.

[2] N.C. Das, et al., Shape and size of highly concentrated micelles in CTAB/NaSal solutions by small angle neutron scattering (SANS), Langmuir 28 (33) (2012) 11962–11968.

[3] A.J. Mills, J. Wilkie, M.M. Britton, NMR and molecular dynamics study of the size, shape, and composition of reverse micelles in a cetyltrimethylammonium bromide (CTAB)/*n*-hexane/pentanol/water microemulsion, J. Phys. Chem. B 118 (36) (2014) 10767–10775.

[4] P.C. Griffiths, et al., Small-angle neutron scattering, electron paramagnetic resonance, electrophoretic NMR, and time-resolved fluorescence quenching studies of sodium dodecyl sulfate and tetra (ethylene oxide) dodecyl ether mixed surfactant micelles, J. Phys. Chem. B 108 (4) (2004) 1351–1356.

[5] P.C. Griffiths, et al., Role of counterion concentration in determining micelle aggregation: evaluation of the combination of constraints from small-angle neutron scattering, electron paramagnetic resonance, and time-resolved fluorescence quenching, J. Phys. Chem. B 108 (12) (2004) 3810–3816.

[6] J. Aguiar, et al., On the determination of the critical micelle concentration by the pyrene 1:3 ratio method, J. Colloid Interface Sci. 258 (1) (2003) 116–122.

[7] J. Eastoe, et al., Fluorinated nonionic surfactants bearing either CF3- or H-CF2-terminal groups: adsorption at the surface of aqueous solutions, Langmuir 17 (25) (2001) 7873–7878.

[8] K. Szymczyk, Behaviour of the fluorocarbon surfactants in the monolayer at the water–air interface and in the bulk phase, J. Fluorine Chem. 150 (2013) 109–116.

[9] K.V. Schubert, E.W. Kaler, Microemulsifying fluorinated oils with mixtures of fluorinated and hydrogenated surfactants, Colloids Surf. A: Physicochem. Eng. Aspects 84 (1) (1994) 97–106.

[10] J. Skvarla, et al., Micellization of Zonyl FSN-100 fluorosurfactant in aqueous solutions, Colloids Surf. A: Physicochem. Eng. Aspects 443 (2014) 209–215.

[11] M.A. Bahri, et al., Investigation of SDS, DTAB and CTAB micelle microviscosities by electron spin resonance, Colloids Surf. A: Physicochem. Eng. Aspects 290 (1–3) (2006) 206–212.

[12] B.L. Bales, C. Stenland, Statistical distributions and collision rates of additive molecules in compartmentalized liquids studied by Epr spectroscopy.1. Sodium dodecyl-sulfate micelles, 5-doxylstearic acid ester, and cobalt(Ii), J. Phys. Chem. 97 (13) (1993) 3418–3433.

[13] J.B. Hayter, J. Penfold, An analytic structure factor for macroion solutions, Mol. Phys. 42 (1) (1981) 109–118.

[14] B.L. Bales, et al., Precision relative aggregation number determinations of SDS micelles using a spin probe. A model of micelle surface hydration, J. Phys. Chem. B 102 (50) (1998) 10347–10358.

[15] B.L. Bales, Inhomogeneously broadened spin-label spectra, in biological magnetic resonance, Biol. Magnet. Reson. 8 (1989) 77.

[16] P.C. Griffiths, et al., FT-PGSE NMR study of mixed micellization of an anionic and a sugar-based nonionic surfactant, J. Phys. Chem. B 101 (6) (1997) 915–918.

[17] B.L. Bales, R. Ranganathan, P.C. Griffiths, Characterization of mixed micelles of SDS and a sugar-based nonionic surfactant as a variable reaction medium, J. Phys. Chem. B 105 (31) (2001) 7465–7473.

[18] J. Haldar, et al., Molecular modulation of surfactant aggregation in water: effect of the incorporation of multiple headgroups on micellar properties, Angew. Chem. Int. Ed. 40 (7) (2001), p. 1228-+.